

# THE JOURNAL OF PHYSICAL CHEMISTRY

(Registered in U. S. Patent Office)

## CONTENTS

### SYMPOSIUM ON THE PHOTOCHEMICAL STORAGE OF ENERGY, ENDICOTT HOUSE, DEDHAM, MASS., SEPTEMBER, 3-7, 1957

Lawrence J. Heidt, Robert S. Livingston, Eugene Rabinowitch and Farrington Daniels: Introduction to the Symposium on Photochemistry of Liquids and Solids.....	1
William Arnold and Helen Sherwood: Energy Storage in Chloroplasts.....	2
E. J. Bowen and J. Sahu: The Effect of Temperature on Fluorescence of Solutions.....	4
Jean T. DuBois: The Sensitized Fluorescence of $\beta$ -Naphthylamine, A Study in Transfer of Electronic Energy.....	8
J. Eggert: The Ignition of Explosives by Radiation.....	11
E. H. Gilmore and E. C. Lim: A Method for Evaluating Rate Constants in the Jablonski Model of Excited Species in Rigid Glasses.....	15
Otto S. Neuwirth: The Photolysis of Nitrosyl Chloride and the Storage of Solar Energy.....	17
Richard M. Noyes: Kinetic Complications Associated with Photochemical Storage of Energy.....	19
C. A. Parker and C. G. Hatchard: Photodecomposition of Complex Oxalates—Some Preliminary Experiments by Flash Photolysis.....	22
C. A. Parker: Photo-reduction of Methylene Blue—Some Preliminary Experiments by Flash Photolysis.....	26
J. W. Coleman and E. Rabinowitch: Evidence of Photoreduction of Chlorophyll <i>In Vivo</i> .....	30
C. Sivertz: Studies of the Photoinitiated Addition of Mercaptans to Olefins. IV. General Comments on the Kinetics of Mercaptan Addition Reactions to Olefins Including <i>cis-trans</i> Forms.....	34
J. B. Thomas and J. F. W. Nuboer: Fluorescence Induction Phenomena in Granular and Lamellate Chloroplasts.....	39
W. West and V. I. Saunders: Photochemical Processes in Thin Single Crystals of Silver Bromide: The Distribution and Behavior of Latent-Image and Photolytic Silver in Pure Crystals and in Crystals Containing Foreign Cations.....	45
.....	
W. T. Grubb: Ionic Migration in Ion-exchange Membranes.....	55
T. M. Reed, III, and T. E. Taylor: Viscosities of Liquid Mixtures.....	58
D. D. Williams, J. A. Grand and R. R. Miller: Determination of the Solubility of Oxygen Bearing Impurities in Sodium, Potassium and their Alloys.....	68
Philip L. Hanst and Jack G. Calvert: The Oxidation of Methyl Radicals at Room Temperature.....	71
Y. Marcus and Frederick Nelson: Anion-exchange Studies. XXV. The Rare Earth in Nitrate Solutions.....	77
Richard W. Laity: An Application of Irreversible Thermodynamics to the Study of Diffusion.....	80
William J. Schuele: Preparation of Fine Particles from Bi-Metal Oxalates.....	83
Peter J. Dunlop and Louis J. Gosting: Use of Diffusion and Thermodynamic Data to Test the Onsager Reciprocal Relation for Isothermal Diffusion in the System NaCl-KCl-H <sub>2</sub> O at 25°.....	86
Virginia D. Hogan and Saul Gordon: A Thermoanalytical Study of the Binary Oxidant System Barium Perchlorate-Potassium Nitrate.....	93
Osamu Asai, Michihiko Kishita and Masaji Kubo: Magnetic Susceptibilities of the Cupric Salts of Some $\alpha,\omega$ -Dicarboxylic Acids.....	96
Louis Watts Clark: The Mechanism of the Decomposition of Trichloroacetic Acid in Aromatic Amines.....	99
G. C. Hood, A. C. Jones and C. A. Reilley: Ionization of Strong Electrolytes. VII. Proton Magnetic Resonance and Raman Spectrum of Iodic Acid.....	101
Philip L. Hanst and Jack G. Calvert: The Thermal Decomposition of Dimethyl Peroxide: The Oxygen-Oxygen Bond Strength of Dialkyl Peroxides.....	104
Theodora P. Dirkse and Dale B. De Vries: The Effect of Continuously Changing Potential on the Silver Electrode in Alkaline Solutions.....	107
LeVerne P. Fernandez and Loren G. Hepler: Thermodynamics of Aqueous Benzoic Acid and the Entropy of Aqueous Benzoate Ion.....	110
C. E. Higgins, W. H. Baldwin and B. A. Soldano: Effects of Electrolytes and Temperature on the Solubility of Tributyl Phosphate in Water.....	113
W. H. Baldwin, C. E. Higgins and B. A. Soldano: The Distribution of Monovalent Electrolytes between Water and Tributyl Phosphate.....	118
.....	
NOTES	
W. J. Diamond: The Effect of Temperature on the Phase Equilibrium of Polyphosphates.....	123
H. R. Hunt and H. Taub: The Relative Acidity of H <sub>3</sub> O <sup>+</sup> and H <sub>2</sub> O <sup>+</sup> Coordinated to a Tripositive Ion.....	124
Evan Appleman, Michael Anbar and Henry Taube: Kinetics of Electron Transfer between Cobaltous and Cobaltic Ammines.....	126
John N. Blocher, Jr., and Elton H. Hall: Thermodynamics of the Mercury Reduction of Titanium Tetrafluoride.....	127

# THE JOURNAL OF PHYSICAL CHEMISTRY

(Registered in U. S. Patent Office)

W. ALBERT NOYES, JR., EDITOR

ALLEN D. BLISS

ASSISTANT EDITORS

A. B. F. DUNCAN

## EDITORIAL BOARD

C. E. H. BAWN

S. C. LIND

G. B. B. M. SUTHERLAND

R. W. DODSON

R. G. W. NORRISH

A. R. UBBELOHDE

JOHN D. FERRY

W. H. STOCKMAYER

E. R. VAN ARTSDALEN

G. D. HALSEY, JR.

EDGAR F. WESTRUM, JR.

Published monthly by the American Chemical Society at 20th and Northampton Sts., Easton, Pa.

Second-class mail privileges authorized at Easton, Pa.

The *Journal of Physical Chemistry* is devoted to the publication of selected symposia in the broad field of physical chemistry and to other contributed papers.

Manuscripts originating in the British Isles, Europe and Africa should be sent to F. C. Tompkins, The Faraday Society, 6 Gray's Inn Square, London W. C. 1, England.

Manuscripts originating elsewhere should be sent to W. Albert Noyes, Jr., Department of Chemistry, University of Rochester, Rochester 20, N. Y.

Correspondence regarding accepted papers, proofs and reprints should be directed to Assistant Editor, Allen D. Bliss, Department of Chemistry, Simmons College, 300 the Fenway, Boston 15, Mass.

Business Office: Alden H. Emery, Executive Secretary, American Chemical Society, 1155 Sixteenth St., N. W., Washington 6, D. C.

Advertising Office: Reinhold Publishing Corporation, 430 Park Avenue, New York 22, N. Y.

Articles must be submitted in duplicate, typed and double spaced. They should have at the beginning a brief Abstract, in no case exceeding 300 words. Original drawings should accompany the manuscript. Lettering at the sides of graphs (black on white or blue) may be pencilled in and will be typeset. Figures and tables should be held to a minimum consistent with adequate presentation of information. Photographs will not be printed on glossy paper except by special arrangement. All footnotes and references to the literature should be numbered consecutively and placed in the manuscript at the proper places. Initials of authors referred to in citations should be given. Nomenclature should conform to that used in *Chemical Abstracts*, mathematical characters marked for italic, Greek letters carefully made or annotated, and subscripts and superscripts clearly shown. Articles should be written as briefly as possible consistent with clarity and should avoid historical background unnecessary for specialists.

Notes describe fragmentary or incomplete studies but do not otherwise differ fundamentally from articles and are subjected to the same editorial appraisals as are articles. In their preparation particular attention should be paid to brevity and conciseness. Material included in Notes must be definitive and may not be republished subsequently.

Communications to the Editor are designed to afford prompt preliminary publication of observations or discoveries whose value to science is so great that immediate publication is

imperative. The appearance of related work from other laboratories is in itself not considered sufficient justification for the publication of a Communication, which must in addition meet special requirements of timeliness and significance. Their total length may in no case exceed 500 words or their equivalent. They differ from Articles and Notes in that their subject matter may be republished.

Symposium papers should be sent in all cases to Secretaries of Divisions sponsoring the symposium, who will be responsible for their transmittal to the Editor. The Secretary of the Division by agreement with the Editor will specify a time after which symposium papers cannot be accepted. The Editor reserves the right to refuse to publish symposium articles, for valid scientific reasons. Each symposium paper may not exceed four printed pages (about sixteen double spaced typewritten pages) in length except by prior arrangement with the Editor.

Remittances and orders for subscriptions and for single copies, notices of changes of address and new professional connections, and claims for missing numbers should be sent to the American Chemical Society, 1155 Sixteenth St., N. W., Washington 6, D. C. Changes of address for the *Journal of Physical Chemistry* must be received on or before the 30th of the preceding month.

Claims for missing numbers will not be allowed (1) if received more than sixty days from date of issue (because of delivery hazards, no claims can be honored from subscribers in Central Europe, Asia, or Pacific Islands other than Hawaii), (2) if loss was due to failure of notice of change of address to be received before the date specified in the preceding paragraph, or (3) if the reason for the claim is "missing from files."

Subscription Rates (1958): members of American Chemical Society, \$8.00 for 1 year; to non-members, \$16.00 for 1 year. Postage free to countries in the Pan American Union; Canada, \$0.40; all other countries, \$1.20. Single copies, current volume, \$1.35; foreign postage, \$0.15; Canadian postage \$0.05. Back volumes (Vol. 56-59) \$15.00 per volume; (starting with Vol. 60) \$18.00 per volume; foreign postage \$1.20, Canadian, \$0.40; \$1.75 per issue, foreign postage \$0.15, Canadian postage \$0.05.

The American Chemical Society and the Editors of the *Journal of Physical Chemistry* assume no responsibility for the statements and opinions advanced by contributors to THIS JOURNAL.

The American Chemical Society also publishes *Journal of the American Chemical Society*, *Chemical Abstracts*, *Industrial and Engineering Chemistry*, *Chemical and Engineering News*, *Analytical Chemistry*, *Journal of Agricultural and Food Chemistry* and *Journal of Organic Chemistry*. Rates on request.

---

---

# THE JOURNAL OF PHYSICAL CHEMISTRY

(Registered in U. S. Patent Office) (© Copyright, 1959, by the American Chemical Society)

VOLUME 63

JANUARY 23, 1959

NUMBER 1

---

---

## INTRODUCTION TO THE SYMPOSIUM ON PHOTOCHEMISTRY OF LIQUIDS AND SOLIDS

BY LAWRENCE J. HEIDT,<sup>1a</sup> ROBERT S. LIVINGSTON,<sup>1b</sup> EUGENE RABINOWITCH<sup>1c</sup> AND  
FARRINGTON DANIELS<sup>1d</sup>

*Received October 27, 1958*

A sub-committee of the National Academy of Sciences—National Research Council is charged with encouraging research which may ultimately lead to new ways of using solar energy directly as light, (*i.e.*, without preliminary conversion to heat). Photosynthesis and the growth of plants based on it are a remarkable and all-important example of such a utilization of sunlight. Are there no other photochemical reactions which could be used in this respect? There is no theoretical reason to exclude the possibility of energy storing photochemical reactions produced by sunlight, which would not require a living plant and a good agricultural soil.

The members of this committee are listed as authors in the title of this introduction. They met in October, 1956, to try to evaluate the possibilities of using sunlight through photochemical reactions. It was evident at once that much more fundamental research is needed, and so it was decided to call together world experts in this field, to exchange ideas and to decide which lines of research should be stimulated. Much of the fundamental research of photochemistry has been done on gases, but gaseous systems are too bulky for practical purposes; so it was decided to limit this symposium to fundamental research on the photochemistry of solids and liquids.

The plan of a symposium on the Photochemistry of Liquids and Solids was approved by the National Research Council, and the National Science Foundation made a substantial grant for its support. Professor Lawrence J. Heidt organized and conducted the Symposium, which was held in the Endicott House in Dedham, Massachusetts from September 3 to 7, 1957. There were twenty-six participants, including eight from Europe.

(1) (a) Massachusetts Institute of Technology; (b) University of Minnesota; (c) University of Illinois; (d) University of Wisconsin.

Although the committee was interested in encouraging photochemical research into practical utilization of solar energy and in getting new ideas which may eventually help to achieve this aim, the symposium carried no handicap of being restricted to matters directly related to such practical applications.

In addition to the twelve symposium papers, now published here in *THIS JOURNAL*, there were thirteen other papers, which were more in the nature of reviews. All twenty-five contributions will soon be published together as a monograph.

The contributions to basic photochemistry which follow may be grouped under four headings: (1) photochemical reactions in general, (2) fluorescence studies, (3) photochemical reactions involving chlorophyll, and (4) kinetic studies.

Of the five inorganic photochemical reactions described, the photodecomposition of nitrosyl chloride dissolved in carbon tetrachloride, described by Neuwirth, seems to be of special interest for solar energy utilization, because it is an endothermic reaction, produced by a wide range of wave lengths present in sunlight, and leading to products which can be separated, stored and recombined at a later time. Of the two products formed, the chlorine remains in solution, and the insoluble nitric oxide escapes. The two recombine later, when mixed, with the evolution of heat.

Parker reports on studies of flash photolysis of uranyl oxalate and cobalt oxalate in which long-lived intermediates were observed, and important information was gained concerning the efficiency of electron transfer reactions. In a second report, Parker describes two transient products formed in the flash photolysis of methylene blue.

Sivertz describes photochemical reactions between mercaptans and olefins and analyzes the role of free radicals in them.

West studies the formation of the latent image in silver bromide and the influence of impurities in the crystal lattice.

Eggert summarizes the influence of radiation on the ignition and detonation of explosives, and the transfer of energy in solids.

Fluorescence is a simpler phenomenon than photochemical reaction, and fundamental information about excited states can be obtained from its study. Bowen studies the effect of temperature on the fluorescence yields of substituted anthracenes in several solvents, particularly the activation energy required for quenching.

Dubois proposes a mechanism for the gas-phase fluorescence of  $\beta$ -naphthylamine, using benzene vapor at 150° as photosensitizer.

Chlorophyll is of special significance because it absorbs such a large fraction of sunlight and because it is necessary in biological photosynthesis. Thomas reports induction phenomena in fluorescence of different types of chloroplasts and correlates them with photosynthetic enzymes.

Arnold describes experiments on the thermoluminescence of dried and preilluminated chloroplast films which showed that five different activation energies may be involved.

Coleman and Rabinowitch report evidence of the photoreduction of chlorophyll *in vivo*, derived from observations of changes in the absorption spectrum which cells undergo during illumination.

R. M. Noyes presents general kinetic considerations applicable to reactions involved in the photochemical storage of energy.

## ENERGY STORAGE IN CHLOROPLASTS

BY WILLIAM ARNOLD AND HELEN SHERWOOD

*Biology Division, Oak Ridge National Laboratory,<sup>1</sup> Oak Ridge, Tennessee*

*Received July 11, 1958*

Dried chloroplast films that have been illuminated exhibit thermoluminescence. The glow curves have been analyzed to give the activation energies associated with this energy storage. The analysis shows that at least five different activation energies are involved: one at 0.93 e.v. represents a little less than half of the stored energy, another at 0.69 e.v. is a minor part, between these two there are two or three unresolved levels that represent the major fraction, finally, unilluminated samples always give a small signal corresponding to an activation energy higher than 0.93 e.v.

The phenomenon of energy storage in dried chloroplast films when illuminated was reported in a previous paper.<sup>2</sup> When the films are heated this energy is emitted as red light, showing that an activation energy is involved in the process. Evidence was given that not one but rather a distribution of activation energies was needed to explain the experiments. The present paper is a more detailed study of this distribution of activation energies.

### Materials and Methods

Chloroplasts were prepared and the films painted and dried on stainless steel disks as described in the previous paper.<sup>2</sup>

The glow curves (that is, the emitted light intensity as a function of the temperature or time as the sample was heated) were measured as before. However, two modifications in procedure were introduced. First each sample was heated only once. This change was made in response to sharp criticism on the part of the biochemists to the repeated heating of biological samples to 150°. Second, the rate of heating the sample was adjusted so as to make the reciprocal of the absolute temperature a linear function of time. A schedule of settings of the Variac, that controlled the heater, was made by trial and error. Figure 1 shows the heating curve used.

The exact mechanism whereby energy is stored in dried chloroplasts is not yet known. However two interpretations seem to be reasonable.

(1) The chloroplasts act like a semi-conductor and the energy is stored as trapped electrons. On heating these electrons are released and produce the light. An activation energy  $E$  is needed to transfer an electron from the trap to the conduction band.

(2) During illumination some high energy compound is

formed, that on heating decomposes by a first-order reaction, and emits light.  $E$  is the activation energy for the decomposition. Either case would be expected to follow the differential equation<sup>3</sup>

$$\frac{dN}{dt} = -NK e^{-E/kT} \quad (1)$$

where

- $N$  = the number of trapped electrons or high energy molecules
- $K$  = frequency factor
- $k$  = Boltzmann's constant
- $T$  = absolute temperature
- $t$  = time

It is assumed that the signal  $S$ , given by the photomultiplier used to measure the emitted light, is proportional to  $-dN/dt$ .

In the ordinary method of making a glow curve the sample is heated at a constant rate  $\beta$  so that  $T = T_0 + \beta t$  where  $T_0$  = the temperature at the beginning of the experiment and  $t$  = time from start of experiment. Using this expression for the temperature equation 1 can be integrated and written as

$$\ln N = - \int K e^{-E/k(T_0 + \beta t)} dt \quad (2)$$

The integral on the right leads to a series in which a great many terms must be used, making the comparison with experimental results very clumsy.

The equations describing glow curves made with the heating schedule shown in Fig. 1 take on a more tractable form using the relation

$$\frac{1}{T} = \frac{1}{T_0} - \gamma t$$

Equation 1 can now be integrated to give

$$N = N_0 e^{Q(1 - e^{\alpha t})} \quad (3)$$

where  $N_0$  = value of  $N$  at start of experiment

$$\alpha = \frac{E\gamma}{k}$$

(1) Operated by Union Carbide Nuclear Company for the U. S. Atomic Energy Commission.

(2) W. Arnold and H. K. Sherwood, *Proc. Nat. Acad. Sci.*, **43**, No. 1, 105 (1957).

(3) J. T. Randall and M. H. F. Wilkins, *Proc. Roy. Soc. (London)*, **184**, 372 (1945).

$$Q = \frac{Ke^{-E/kT_0}}{\alpha}$$

Since the signal  $S$  (the intensity of the emitted light) is proportional to  $-dN/dt$  we can write

$$S = -A \frac{dN}{dt} = AN_0\alpha Qe^{Q(1-e^{\alpha t}) + \alpha t}$$

where  $A$  = proportionality constant.  $S_m$  the maximum value of the signal will occur at the time  $t_m$  when

$$\frac{dS}{dt} = \alpha S(1 - Qe^{\alpha t}) = 0$$

so that  $t_m$  is given by

$$Qe^{\alpha t_m} = 1 \tag{4}$$

and

$$S_m = A\alpha N_0e^{Q(Q-1)}$$

The ratio of the signal at any time to the maximum signal

$$\frac{S}{S_m} = e^{(1+\alpha[t-t_m]) - e^{\alpha(t-t_m)}} \tag{5}$$

can be used to give the activation energy  $E$  and the frequency factor  $K$ .

The experimental data are plotted using  $S/S_m$  as the ordinate and time as the abscissa. The time of maximum signal  $t_m$  is determined by inspection. Equation 5 is then used to determine the value of  $\alpha$  that gives the best fit to the data. Knowing  $\alpha$  and  $t_m$  equation 4 gives the value of  $Q$ .  $E$  and  $K$  then are calculated from the values of  $\alpha$  and  $Q$ .

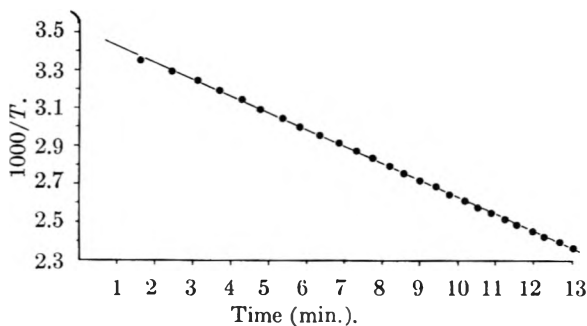


Fig. 1.

**Results**

Glow curves made on dried chloroplasts that have not been illuminated always show a small signal at the higher temperatures. The magnitude of this background signal is different from one batch of chloroplasts to another, but no treatment is known that reduces it to zero. In the following it is assumed that the effect of illumination is given by the difference between the glow curve made with an illuminated sample and one made on a sample held at the same temperature in the dark.

Glow curves made on samples of dried chloroplasts illuminated in air by neon light for 12 hours at 20° and corrected for background do not correspond to equation 5. The experimental curve is much wider than the calculated one, showing again that there are several activation energies involved. Partial heating before the experiment will anneal out that part of the stored energy that has the lower activation energy. Figure 2 gives data for an experiment made after both the illuminated and dark sample had been heated to 88° and slowly cooled down to 20°. The points are the experimental results and the solid line has been calculated by equation 5. The activation energy  $E$  is 0.93 e.v. and the frequency factor  $K$  is  $2.5 \times 10^9 \text{ sec.}^{-1}$ .

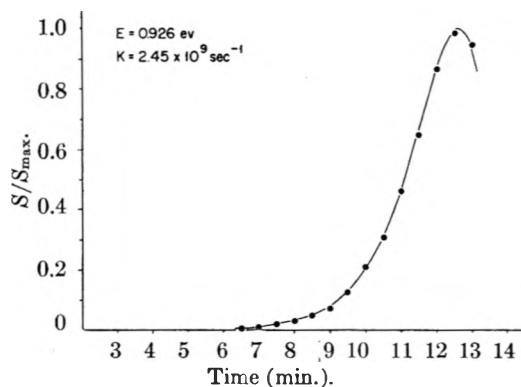


Fig. 2.

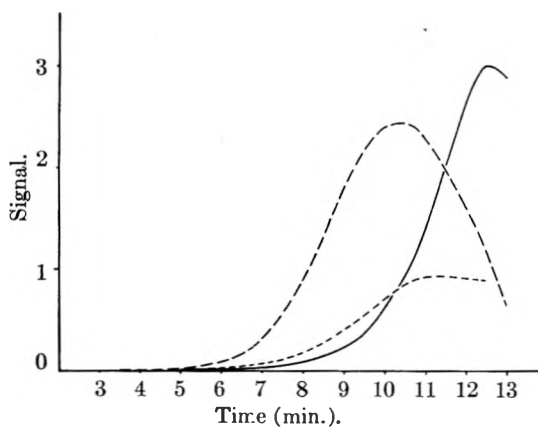


Fig. 3.

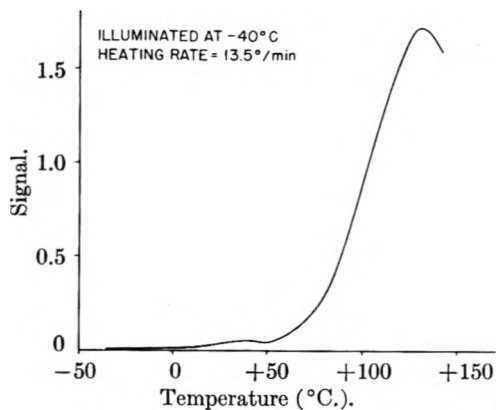


Fig. 4.

The glow curve for that part of the stored energy that is removed by annealing is shown in Fig. 3 as the dashed curve with a peak at 10 minutes. The curve is the difference between an illuminated sample and a sample illuminated and annealed. The curve can only be fitted to equation 5 by using two or three different activation energies, all somewhat smaller than the 0.93 e.v. found before. Figure 3 also gives as the solid line the data from Fig. 2 and the background signal from a dark sample. All three curves are plotted on the same scale. As can be seen the activation energy at 0.93 e.v. represents nearly one-half of all the light emitted.

Figure 4 gives a glow curve, made by heating at a constant rate, for a sample illuminated in dry air at -40°. The curve shows there is a small

peak at  $40^\circ$  that precedes the main light emission. The equations of Randall and Wilkins<sup>3</sup> with the value of  $K$  as  $2.5 \times 10^9 \text{ sec.}^{-1}$  give the activation energy for this peak as 0.69 e.v. Unless the sample is cooled this peak is largely annealed out during the illumination.

During the course of these experiments a number of qualitative observations were made that bear on the mechanism whereby dried chloroplasts store energy. They are summarized in the following statements. (1) The composition of the atmosphere surrounding the sample during the heating seems to have no effect on the glow curve. (2) Samples illuminated in air or  $\text{O}_2$  become charged, that is, store energy. (3) Samples illuminated in  $\text{N}_2$  or  $\text{SO}_2$  do not become charged. (4) Neither water vapor or  $\text{CO}_2$  seem to have any effect on the charging. (5) Air and  $\text{O}_2$  illuminated with short wave length ultraviolet light can charge the dried chloroplasts by flowing over the surface in the dark. (6) Nitrogen illuminated by ultraviolet does not charge the samples. (7) Air illuminated by ultraviolet and passed through a strong electric field to remove ions will still charge the samples.

#### Discussion

The two most reasonable explanations of the storage of energy in dried chloroplasts are the trap-

ping of electrons or the formation of some high energy chemical compound. The trapping of electrons is suggested by the following: (1) at least five different activation energies are involved in the glow curve. A multiplicity of electron trap levels is common in the storage of energy in crystals. (2) The spikes in electrical conduction shown in Fig. 4 and 5 of the previous paper<sup>2</sup> would seem to imply the freeing of electrons. (3) The value of the frequency factor  $K$  of  $2.5 \times 10^9 \text{ sec.}^{-1}$  is near to the  $10^8$ - $10^9 \text{ sec.}^{-1}$  suggested by Randall and Wilkins<sup>3</sup> as appropriate for the freeing of electrons.

On the other hand the chemical storage is suggested by: (1) oxygen is needed in order for the energy to be stored. If all that oxygen did was to trap an electron then  $\text{SO}_2$  would be expected to serve as well, and it does not. (2) The fact that air irradiated with ultraviolet light can be used to charge a chloroplast sample would indicate a chemical reaction.

Finally it might be argued that the storage represents a mixture of electron trapping and chemical compound formation. The occurrence of the spike in electrical conduction<sup>2</sup> at a temperature considerably below the temperature of maximum light emission may indicate that these two effects are different.

## THE EFFECT OF TEMPERATURE ON FLUORESCENCE OF SOLUTIONS

BY E. J. BOWEN AND J. SAHU

*Physical Chemistry Laboratory, Oxford University, England*

*Received May 19, 1968*

Measurements have been made of the effect of temperature on the fluorescence yields of substituted anthracenes dissolved in several solvents. 9-Substituted anthracenes show high yields and steep temperature dependencies, while side-substituted derivatives have low yields and small temperature variations. The results are interpreted in terms of the following concepts. There appear to be two processes of energy degradation of the excited molecules, a substantially temperature-independent one which probably is associated with the singlet-triplet conversion, and a temperature-dependent one having a heat of activation of degradation and a dependence on solvent viscosity which may be associated with a direct transition from excited to the ground state. Values also are given of fluorescence quenching constants of dissolved oxygen, bromobenzene and carbon tetrachloride for these anthracene derivatives.

Measurement of true temperature effects of the fluorescence of solutions is rendered difficult by the smallness of the changes and of the complications inherent in the estimation of the total light emitted. Previous attempts to obtain reliable results have been subject to uncertainties of magnitudes approaching those of the quantities measured. Apart from experimental errors due to instabilities of the apparatus, changes in the spatial distribution of the fluorescence caused by refractive index and polarization effects can occasion misleading interpretations of the results.<sup>1,2</sup> The correction to be applied for the refractive index effect can be assessed only roughly, as it depends on the detailed geometry of the apparatus, and it is sufficiently large in some instances to reverse the sign of the change of fluorescence with temperature. Measurements are here given which were made with a new form of apparatus designed par-

ticularly to minimize refractive index and polarization errors.

#### Experimental

Figure 1 shows the arrangement in section and in plan. A 5-liter glass flask was fitted with a tube A for evacuation, and with a tube B, reaching to the center, to contain the solution. The flask was lightly smoked internally with magnesium oxide and painted over the external surface with barium sulphate-Cellofas B mixture, except for holes to admit the exciting light and to observe the fluorescence. After evacuation the flask was thus both a Dewar vessel and an integrating sphere. A beam of filtered mercury 3660 Å. light was focussed by lens C on to the tube B, and the fluorescence collected from the flask wall at E allowed to fall on a spectrometer slit at D. The concentrations of the solutions were such as to give practically total light absorption in tube B, and the liquid level was above the top of the light beam to eliminate any effect from thermal expansion. This arrangement avoids errors due to changes in the spatial distribution of the fluorescence emitted from the solution, whether due to refractive index or to polarization effects.

The collected fluorescence light was dispersed by a Hürger D 246 spectrometer, with glass prism, to the exit slit of which was attached a 13 stage photo-multiplier connected

(1) E. J. Bowen and K. West, *J. Chem. Soc.*, 4394 (1955).

(2) E. J. Bowen and D. M. Stebbens, *ibid.*, 360 (1957).

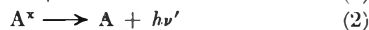
to a microammeter. The spectrometer-multiplier combination was calibrated by reference to a tungsten lamp of known color temperature so that fluorescence spectra could be plotted as relative quanta emitted per equal interval of wave number against the wave number. The areas of such curves are proportional to quantum yields of fluorescence. For the substances used in this work changes of band shape with temperature or solvent were slight, and it was usually sufficient to compare fluorescence emissions by measurement of the height of a band maximum. As a reference standard the quantum yield of a dilute, de-aerated benzene solution of anthracene was taken as 0.29.<sup>3</sup> The solutions contained in tube B, from which dissolved oxygen was removed by a fine stream of pure nitrogen, were heated or cooled by the temporary insertion of an inner glass tube, terminated by a closed copper-glass seal, into which hot water or liquid oxygen could be introduced. Temperatures were determined by a dipping thermo-junction.

The fluorescent solutes investigated were anthracene derivatives dissolved in several solvents. The concentrations necessary to give practically total light absorption were fortunately just low enough to make concentration quenching changes unimportant. Temperatures ranged downwards to  $-70^{\circ}$  for non-freezing solvents and upwards to  $+80^{\circ}$  for viscous paraffin.

### Results

Figure 2 shows the curves obtained for two methyl anthracenes, and Fig. 3 those for two dichloroanthracenes. It was found that all the 9-substituted anthracenes studied gave yields which tended close to unity at low temperatures and which fell off steeply at higher temperatures, except for the 9-cyano- and 9,10-diphenyl derivatives, which gave unit yields in all solvents over the whole temperature range. In contrast to this the side-substituted derivatives showed flattish yield-temperature curves whose zero extrapolations could not be determined, but which probably do not reach unity.

We may write for the 9-substituted derivatives the simple scheme



From this it follows that  $(1/F - 1) =$  the ratio of rates of processes 3 and 2, where  $F$  is the fluorescence yield. This ratio may be set equal to  $k \exp(-E/RT)$ , where  $E$  is the activation energy of process 3 and  $k$  is its pre-exponential constant multiplied by the mean life of process 2. Values of  $k$  and  $E$  (cal./mole) so determined are given in Table I.

For the derivatives where the curves are flattish and the course at lower temperatures uncertain, part of process 3 may be temperature independent and the equation may need to be of the form

$$1/F - K = k \exp(-E/RT)$$

As the experimental data are not accurate enough to determine  $K$  in this way the values of  $k$  and  $E$  given for them in Table I are evaluated on the simpler formula to serve merely as an empirical representation of the measurements.

The  $E$  values for the 9-substituted derivatives depend upon the nature of the anthracene molecule, and are greater for those of higher degree of electron delocalization. The variation with solvent is comparatively small, but when large changes are

(3) F. Weber and F. W. J. Teale, *Trans. Faraday Soc.*, **53**, 646 (1957).

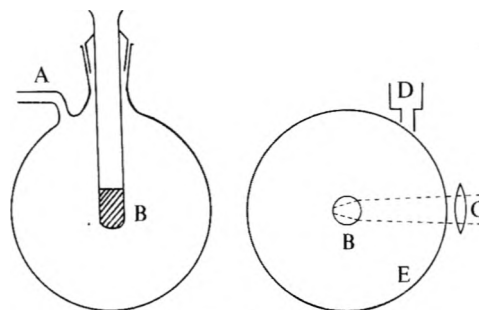


Fig. 1.

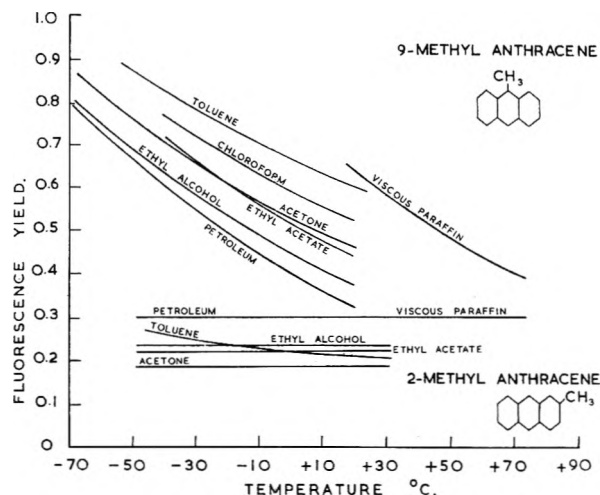


Fig. 2.

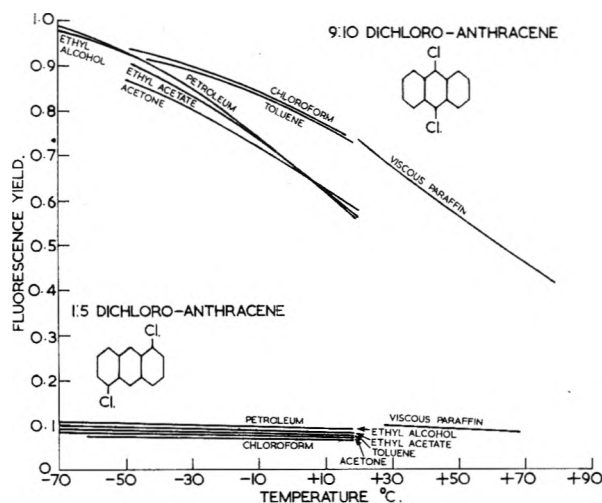


Fig. 3.

made in solvent viscosity there are appreciable variations in the constants  $k$  and  $E$ .

Table II gives the values obtained for paraffin solvents of widely different viscosities, A being viscous "Medicinal" paraffin, F a "petroleum ether," E kerosene, and B, C and D mixtures of A and F. The viscosity characteristics of these liquids were measured and are defined in Table III in terms of constants  $a$  and  $b$  in the equation:  $T/\eta = a \exp(-b/RT)$ , where  $T$  = absolute temperature and  $\eta$  = viscosity (poise). Approximate

TABLE I

Anthracene		Solvent					Chloro- form
		Petroleum ether	Ethyl alcohol	Ethyl acetate	Acetone	Toluene	
Unsubstituted	<i>k</i>	13	11	7	10.5	7	9.5
	<i>E</i>	1100	890	610	860	570	230
2-Methyl	<i>k</i>	2.24	3.24	3.54	4.7	10.7	
	<i>E</i>	Small	Small	Small	Small	570	
1-Chloro	<i>k</i>	11	13	9	10.5	16.5	12
	<i>E</i>	260	260	Small	Small	260	Small
1,5-Dichloro	<i>k</i>	24.5	26.5	21	22.5	24	5
	<i>E</i>	480	480	310	310	360	310
9-Methyl	<i>k</i>	253	91	100	90	23	31
	<i>E</i>	2840	2380	2580	2550	2120	2120
9-Ethyl	<i>k</i>	275.5	89	150		75	
	<i>E</i>	2920	2400	2830		2810	
9-Methoxy	<i>k</i>	14000	10200	5400	4780	3700	3260
	<i>E</i>	5310	4900	4500	4290	4850	4500
9-Phenyl	<i>k</i>	40.5	34.5	34.5	23.5	29	43
	<i>E</i>	2220	2140	2300	2000	2320	2480
9-Chloro	<i>k</i>	1980		1170	725	550	
	<i>E</i>	3370		3450	3250	3500	
9,10-Dichloro	<i>k</i>	842	842	404	104	96	134
	<i>E</i>	4100	4100	3730	2950	3300	3500
9-Cyano		Have a yield of unity in all the solvents					
9,10-Diphenyl		in the temperature range of $-70 + 20^\circ$					

TABLE II

Anthracene		Solvent					
		A	B	C	D	E	F
9-Methyl	<i>k</i>	430	420	342	340	335	253
	<i>E</i>	3900	3700	3380	3200	3160	2840
9-Ethyl	<i>k</i>	645	630	565	553	392	276
	<i>E</i>	4175	3950	3730	3580	3320	2920
9-Methoxy	<i>k</i>	47000	45000	42500	39200	37200	14000
	<i>E</i>	6450	6350	6200	6050	5950	5310
9-Phenyl	<i>k</i>	110	104	92	86	62	41
	<i>E</i>	3300	3140	2910	2810	2530	2220
9-Chloro	<i>k</i>	2000	2000	2000	2110	2110	1980
	<i>E</i>	3900	3700	3650	3600	3600	3370
9,10-Dichloro	<i>k</i>	1234	928	904	862	850	842
	<i>E</i>	4800	4500	4400	4250	4230	4100

TABLE III

Viscosity constants	Solvent					
	A	B	C	D	E	F
$a \times 10^{-6}$	57500	43.8	4.61	3.26	5.66	5.6
$b$ , cal./mole	9550	5360	3600	2780	3200	2560

TABLE IV

Anthracene derivative	<i>k</i>	<i>E</i> (cal./ mole)	<i>C</i>
9-Methyl	65	2000	$10^4$
9-Ethyl	50	1900	$10^4$
9-Methoxy	10,000	5000	$10^4$
9-Phenyl	2.4	1900	$4 \times 10^3$
9-Chloro	600	2600	$10^4$
9,10-Dichloro	270	3400	$7 \times 10^3$

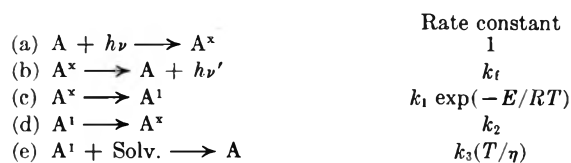
mate agreement with the measured fluorescence yields is given by the formula

$$1/F - 1 = k \exp(-E/RT) \times T/\eta / (C + T/\eta)$$

where  $C$  is a constant almost independent of the solvent.

Table IV gives numerical values of the constants.

This equation can be derived from the more elaborate scheme



which gives  $k = k_1/k_1$  and  $C = k_2/k_3$ . Process (c) represents an excited molecule  $A^x$ , stabilized by the solvent on its zero vibrational level, receiving thermal energy and reaching a "crossing

point" to a lower level on the potential energy surface; in process (d) it simply drops back to its zero vibrational level. In process (e) we imagine the molecule  $A^1$ , while executing vibrational movements at the crossing point, being trapped by inward diffusion of solvent molecules during one of its compression phases, so that it loses vibrational energy to the solvent and reverts electronically to the lower level.

The vapors of anthracene and of 9,10-diphenylanthracene have fluorescence yields of nearly unity, although the viscosity is exceedingly small.<sup>4</sup> This may be ascribed to a much smaller value of the constant  $k_3$  (which depends on collisional rate) for gases than for liquids.

(4) B. Stevens, *ibid.*, **51**, 610 (1955).



The expression given above covers relationships found by G. Oster and Y. Nishijima<sup>5</sup> for the fluorescence of diphenylmethane derivatives and by Porter and Windsor for the rate-constants of decay of the triplet level of anthracene in solution.<sup>6</sup>

Excited molecules may revert to a triplet level or directly to the ground level. It is likely that temperature-independent changes which appear to play a large part for side substituted anthracenes characterize the first of these, and that temperature-dependent ones of the kind discussed above relate to the second mode of deactivation.

Measurements also have been made of the quenching of the fluorescence of anthracenes by dissolved oxygen, bromobenzene and carbon tetrachloride. The Stern-Volmer constants were determined and the rate constants for the quenching process were evaluated in l. mole<sup>-1</sup> sec.<sup>-1</sup> units by dividing by the fluorescence yield and by the mean life of radiation, the latter value being taken as 10<sup>-8</sup> sec. in the absence of more precise data.<sup>7</sup> The constants for oxygen are given in Table V. For solvents of viscosities of those of Table II the La Mer theory<sup>8</sup> for the diffusion controlled bimolecular reaction predicts absolute rates of about 100 × 10<sup>8</sup>; the values found are much larger, and the discrepancy cannot be accounted for by lack of precision in the value assumed for the mean radiational life. It is probable that the excited oxygen molecule has a large range of effective action.

TABLE V  
O<sub>2</sub> QUENCHING CONSTANTS, L. MOLE<sup>-1</sup> SEC.<sup>-1</sup> × 10<sup>-8</sup>

Anthracene	Solvent					
	Petro- leum, 80-100°	Ethyl alco- hol	Ethyl acetate	Ace- tone	Tolu- ene	Chloro- form
Unsubst.	760	635	767	748	515	350
2-Methyl	585	454	670	715	640	
9-Methyl	460	545	573	785	607	485
9-Ethyl	658	510	660	620	550	393
9-Methoxy	680	515	655	765	515	440
9-Cyano	173	223	243		210	130
9-Phenyl	510	354	440	460	352	315
9,10-Diphenyl	350	320	355	380	271	226
1-Chloro	435	326	382	463	440	330
1,5-Dichloro	320	336	404	447	380	212
9-Chloro	480		525	555	400	286
9,10-Dichloro	271	345	415	477	390	268

Tables VI and VII give the constants for bromobenzene and carbon tetrachloride as quenching agents. The values are of comparable magnitude and about a hundred-fold lower than those for oxygen. Table VIII shows the effect of temperature. These bimolecular reactions lie just on the

(5) G. Oster and Y. Nishijima, *J. Am. Chem. Soc.*, **78**, 1581 (1956).

(6) G. Porter and M. W. Windsor, *Disc. Faraday Soc.*, **17**, 178 (1954).

(7) E. J. Bowen, *Trans. Faraday Soc.*, **50**, 97 (1954).

(8) J. Q. Umberger and V. K. La Mer, *J. Am. Chem. Soc.*, **67**, 1099 (1945).

TABLE VI  
C<sub>6</sub>H<sub>5</sub>Br QUENCHING CONSTANTS, L. MOLE<sup>-1</sup> SEC.<sup>-1</sup> × 10<sup>-8</sup>

Anthracene	Solvent					
	Petro- leum, 80-100°	Ethyl alco- hol	Ethyl ace- tate	Ace- tone	Tolu- ene	Chloro- form
Unsubst.	5.8	7.5	4.4	4.1	4.53	4.5
2-Methyl	6.4	7.5	5.7	8.3	7.3	
9-Methyl	2.2	2.48	1.45	1.25	0.4	0.8
9-Ethyl	1.5	1.74	0.76	0.56	0.38	0.29
9-Methoxy	0	0	0	0	0	0
9-Cyano	0	0	0	0	0	0
9-Phenyl	1.02	2.64	0.82	0.80	0.33	0.24
9,10-Diphenyl	0	0	0	0	0	0
1-Chloro	4.5	6.0	4.2	5.8	4.2	4.3
1,5-Dichloro	5.7	6.25	4.1	4.2	2.9	3.1
9,10-Dichloro	0	0	0	0	0	0

TABLE VII  
CCl<sub>4</sub> QUENCHING CONSTANTS, L. MOLE<sup>-1</sup> SEC.<sup>-1</sup> × 10<sup>-8</sup>

Anthracene	Solvent					
	Petro- leum, 80-100°	Ethyl alco- hol	Ethyl ace- tate	Ace- tone	Tolu- ene	Chloro- form
Unsubst.	3.4	66.0	45.4	68.3	18.9	12.8
2-Methyl	4.5	36.6	41.0	69.0	35.0	
9-Methyl	3.95	47.0	49.5	90.0	30.6	24.0
9-Ethyl	2.9	37.6	40.0	66.5	23.0	15.8
9-Methoxy	15.6	65.5	61.0	97.0	46.4	53.7
9-Cyano	0	0	0	0	0	0
9-Phenyl	1.68	20.2	18.0	31.0	8.0	8.8
9,10-Diphenyl	2.5	12.5	10.9	19.7	4.85	4.4
1-Chloro	0	2.5	6.5	13.8	2.2	1.65
1,5-Dichloro	0	0	0	1.8	0	0
9,10-Dichloro	0	0	0	0	0	0

TABLE VIII

EFFECT OF TEMPERATURE ON QUENCHING CONSTANTS <sup>a</sup>							
Solvent		-50	-30	-10	+20	+40	+60°
Petroleum,	B	5.8	5.9	5.8	5.9		
b.p. 80- 100°	C	1.4	1.9	2.6	3.4		
Kerosene	B				6.2	6.2	6.3
	C				2.3	3.4	5.1
Viscous	B				1.9	2.8	3.2
paraffin	C				3.4	3.9	4.8
Ethyl alco- hol	B	6.4	6.8	7.0	7.5		
	C	19	29	41	66		

<sup>a</sup> B = bromobenzene and C = carbon tetrachloride.

point where the controlling influence ceases to be diffusion. The bromobenzene constants are not very dependent on solvent or on temperature, in contrast with those for carbon tetrachloride. This would indicate that polarizability and the need for appreciable activation energy plays a larger part with the latter substance, and this may be correlated with the fact that bromobenzene quenching is a spin-reversal effect due to the heavy bromine atom while carbon tetrachloride quenching involves actual chemical reaction.<sup>9</sup>

(9) E. J. Bowen and K. K. Rohatgi, *Disc. Faraday Soc.*, **14**, 146 (1953).

# THE SENSITIZED FLUORESCENCE OF $\beta$ -NAPHTHYLAMINE. A STUDY IN TRANSFER OF ELECTRONIC ENERGY

BY JEAN T. DUBOIS

*Aeronautical Research Laboratory, Wright-Patterson Air Force Base, Ohio*

*Received July 11, 1958*

The gas phase sensitized fluorescence of  $\beta$ -naphthylamine was studied at 150° using benzene as photosensitizer. Amine pressures of 0.53 and 1.25 mm. were used. A kinetic mechanism for the transfer of electronic energy is proposed.

## Introduction

While studying the effect of foreign gases on the fluorescence of  $\beta$ -naphthylamine, Neporent<sup>1</sup> noticed that at a wave length of excitation  $\lambda 2537 \text{ \AA}$ . benzene enhances the vapor fluorescence of  $\beta$ -naphthylamine to an extent which cannot be accounted for on the sole basis of vibrational stabilization of the electronically excited amine (see Table I). Noting that benzene absorbs energy at  $\lambda 2537 \text{ \AA}$ . and that its internal filter effect would tend to diminish the fluorescence rather than increase it beyond the expected value, he ascribed the phenomenon to a transfer of electronic energy from the benzene. Thus benzene was sensitizing the fluorescence of  $\beta$ -naphthylamine (the measuring instrument being sensitive only to the amine fluorescence). At other wave lengths where the absorption by benzene is negligible, Neporent also showed that the presence of this gas merely removes the excess vibrational energy of the excited amine and that this effect is almost identical to that of pentane at the same wave length.

It is the purpose of this paper to confirm quantitatively Neporent's observations, to present new data on this system and to put forward a kinetic interpretation of the phenomenon.

## Experimental

**A. Materials.**— $\beta$ -Naphthylamine was supplied by the J. T. Baker Chemical Company and purified by sublimation at 110°. Benzene was a certified reagent from the Fisher Scientific Company and was further purified by distilling a middle-third fraction into a break-off seal.

TABLE I

NEPARENT'S RESULTS ON THE ENHANCEMENT OF THE VAPOR FLUORESCENCE OF  $\beta$ -NAPHTHYLAMINE IN THE PRESENCE OF BENZENE AT 150° AND  $\lambda 2537 \text{ \AA}$ .

Amine pressure = 0.53 mm.

$Z \times 10^{-8}$ , sec. <sup>-1</sup>	1	2	3	4	5	6	7
$F_z/F_0$	1.60	2.08	2.38	2.70	3.00	3.25	3.50

TABLE II

NEPARENT'S RESULTS ON THE ENHANCEMENT OF THE VAPOR FLUORESCENCE OF  $\beta$ -NAPHTHYLAMINE IN THE PRESENCE OF PENTANE AT 150° AND  $\lambda 2537 \text{ \AA}$ .

Amine pressure = 0.53 mm.

$Z \times 10^{-8}$ , sec. <sup>-1</sup>	1	2	3	4	5	6	7
$F_p/F_0$	1.12	1.33	1.50	1.70	1.85	2.08	2.25

**B. Apparatus.**—The benzene was stored and measured in a conventional manner as shown in Fig. 1; however, to prevent any contact with stopcock grease a special valve V was used. This simply consists of a fritted disk filter, each

side of which is connected to a mercury reservoir and to a branch of the system. The fritted disk is not penetrated by the liquid mercury but allows the gases to flow freely. The optical arrangement shown on the same diagram is also of conventional design. Filter F, used to remove the tail end of the fluorescence spectrum of benzene, consists of 5 ordinary microscope specimen-glass-slides. In this way the photomultiplier tube responded only to the amine fluorescence. Quartz lens L was positioned such that a complete image of the quartz cell was incident on the sensitive surface of the photomultiplier. This was done to eliminate effects on the signal, of the shifting of the center of absorption in the reaction cell, with increasing pressure of benzene. This problem can also be solved by using frontal illumination, instead of sighting the fluorescence at 90° to the exciting beam, providing that the fluorescence signal is not too weak. All of the electronic components were stabilized by a Stabiline 1E5102R Voltage Regulator. Furnace windings for the reaction cell, the amine supply and the all-metal valve were regulated by Sola Transformers. Temperatures at the reaction site, for the amine supply and at the all-metal valve were measured with iron-constantan thermocouples and a Leeds and Northrup Portable Precision Potentiometer No. 8662. The photomultiplier tube was operated at 1000 volts and the signal was fed to a Leeds and Northrup 69870 Speed-omax G Current Recorder.

**C. Procedure.**—The light source and all of the electronic equipment were turned on about one hour before measurements were made. During that period a vacuum of about  $10^{-3}$  mm. was established in the hot cell (*ca.* 150°). A first reading was made to establish a correction for small amounts of stray light. This was done by actuating a shutter in the path of the exciting beam. Valve K was closed and the amine supply temperature raised to obtain the desired pressure of the fluorescer. Allowing equilibrium to be established, a second reading was taken as before. This reading when properly corrected was recorded as  $F_0$ , the fluorescence intensity of the fluorescer at zero pressure of the sensitizer. Next, a pressure of benzene was introduced into the line, valve K was opened momentarily and after allowing time for equilibrium to be reached, a third reading was taken as previously. This reading, when corrected by the first was recorded as  $F$ , the fluorescence of the mixture at pressure  $p$  mm. of the sensitizer. For each fluorescence reading a simultaneous observation was made of the photomultiplier voltage, the temperature of the amine supply, the temperature of the reaction cell, and the pressure of sensitizer as read on a mercury manometer. It was imperative that the exciting beam be allowed to shine on the reaction cell only momentarily while taking a fluorescence reading, because of a photosensitized decomposition of benzene with excited mercury atoms, resulting in a decrease in the transparency of the cell windows. Small deposits on the windows can be pumped off in a few hours when the cell is hot. Thus it was thought preferable to cool the amine supply and pump on the hot cell after each fluorescence reading. In this way it was possible to obtain reproducible results.

## Results

The effect of benzene on the vapor fluorescence of  $\beta$ -naphthylamine at  $\lambda 2537 \text{ \AA}$ . was measured at *ca.* 150° for amine pressures of *ca.* 0.53 mm. and 1.25 mm. The experimental points, expressed as  $F/F_0$ , the ratio of the fluorescence of the amine at a pressure  $p$  mm. of benzene to that at zero pressure of benzene, are shown in Fig. 2. Smooth curve A in that figure also represents the average

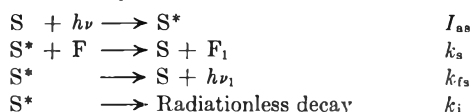
(1) B. S. Neporent, *Zhur. Fiz. Khim.*, **24**, 1219 (1950).

of Neporent's results at an amine pressure of 0.53 mm. It is noted that the scattering in the data is much less at the higher pressure of the amine. This is to be expected in view of the larger amount of fluorescence available at the higher pressure and also because of the reduction in the photo-sensitized decomposition of the benzene.

### Discussion

When  $\beta$ -naphthylamine absorbs radiation  $\lambda = 2537 \text{ \AA}$ . directly, it is raised to a high vibrational level of its first singlet excited electronic state. During the lifetime of the excited state the molecule may fluoresce or undergo a radiationless transition, the rate of which depends on the vibrational energy content of the molecule. In general, collisions with foreign gases which do not react with the excited amine and which are transparent to the exciting radiation remove vibrational energy from the excited state and increase the relative rate of fluorescence. This process is referred to as vibrational stabilization and has been submitted to kinetic analysis.<sup>2</sup>

Using this treatment for the vibrational stabilization of the amine and adding the following steps to take care of the simultaneous excitation of the fluorescer by sensitization with benzene



where  $S$  = sensitizer,  $S^*$  = excited sensitizer,  $F$  = fluorescer,  $F_1$  = high vibrational level of the electronically excited fluorescer, one arrives at the expression

$$\frac{F_2}{F_0} = \left\{ \frac{I_{af}}{(I_{af})_0} + \frac{I_{as}}{(I_{af})_0} \times \frac{K_s(F)}{K_s(F) + K_i + K_{fs}} \right\} V \quad (1)$$

In this equation  $I_{as}$  and  $I_{af}$  refer to the radiation absorbed by the sensitizer and by the fluorescer, respectively,  $(I_{af})_0$  refers to the absorption by the fluorescer at zero pressure of the sensitizer, and  $V$ , as derived in ref. 2, is

$$V = \frac{1}{1 + \tau_1 Z} \left\{ 1 + \frac{\tau_2 Z}{(1 + \tau_2 Z)} + \frac{\tau_2 \tau_3 Z^2}{(1 + \tau_2 Z)(1 + \tau_3 Z)} + \dots \frac{\tau_2 \tau_3 \dots \tau_n Z^{n-1}}{(1 + \tau_2 Z)(1 + \tau_3 Z) \dots (1 + \tau_{n-1} Z)} \right\} \quad (2)$$

where  $Z$  = number of collisions suffered per second by a naphthylamine molecule with benzene molecules and the  $\tau$ 's are the lifetimes of the naphthylamine molecules in various vibrational levels  $E_1, E_2, E_3, \dots$ , etc.

The first factor in the complete expression for  $F_2/F_0$  gives the fluorescence change due to the sensitization process and to the redistribution of light absorption in the two-component system, whereas the factor  $V$  gives the enhancement due to vibrational stabilization.

If the total number of quanta absorbed by the benzene were useful in exciting the fluorescer molecules we would have

$$\frac{K_s(F)}{K_s(F) + K_i + K_{fs}} = 1 = f \quad (3)$$

In general this fraction will be  $< 1$  and we can denote it by " $f$ ."

(2) M. Boudart and J. T. Dubois, *J. Chem. Phys.*, **23**, 223 (1955).

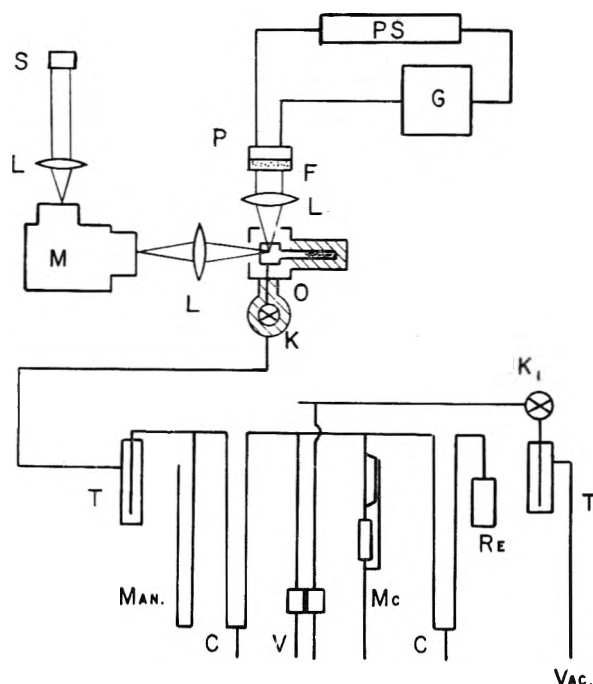


Fig. 1.—S, Hanovia S-100 mercury lamp; L, quartz lenses; M, Gaertner L234-150 quartz monochromator; O, electrically heated oven with quartz windows; separate heating coil for amine supply; K, all-metal Hoke packless valve, type 413;  $K_1$ , stopcock; F, filter; P, RCA 1P21 photomultiplier; PS, power supply Model 710PR, Furst Electronics; G, Speedomax G recorder; T, cold traps; Man., mercury manometer; C, mercury cut-offs; V, special valve; Mc, McLeod; Re, benzene reservoir.

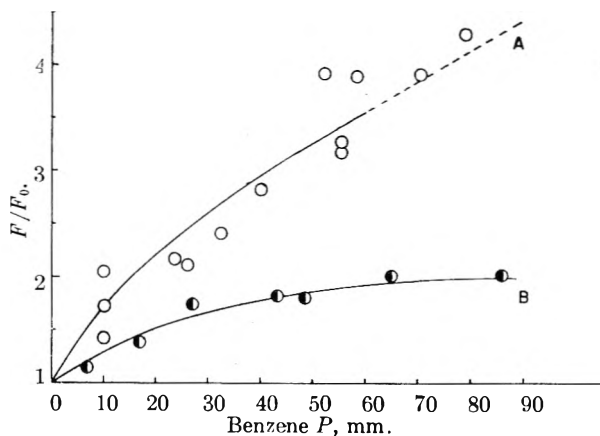


Fig. 2.—O, experimental points at 0.53 mm. pressure of  $\beta$ -naphthylamine; ●, experimental points at 1.25 mm. pressure of  $\beta$ -naphthylamine. Solid curve "A" represents the average of Neporent's results at amine pressure 0.53 mm. Solid curve "A" as well as the dashed portion also represent the calculated results based on the mechanism developed in the Discussion. Solid curve "B" is a calculated curve based on the same mechanism, for the amine pressure of 1.25 mm.

Using for  $V$  the values of pentane at  $\lambda 2537 \text{ \AA}$ . as found by Neporent<sup>1</sup> and shown in Table II, calculating  $I_{as}$  and  $I_{af}$  from known values of the molar extinction coefficients for benzene and  $\beta$ -naphthylamine, and choosing for the sake of argument a value of  $f = 1$ , one obtains curve "A" of Fig. 3 for amine pressure 0.53 mm. If on the other hand for the same system, one assumes that vibrational stabilization plays no role during the process of sensitization, i.e.,  $V = 1$  and the amount

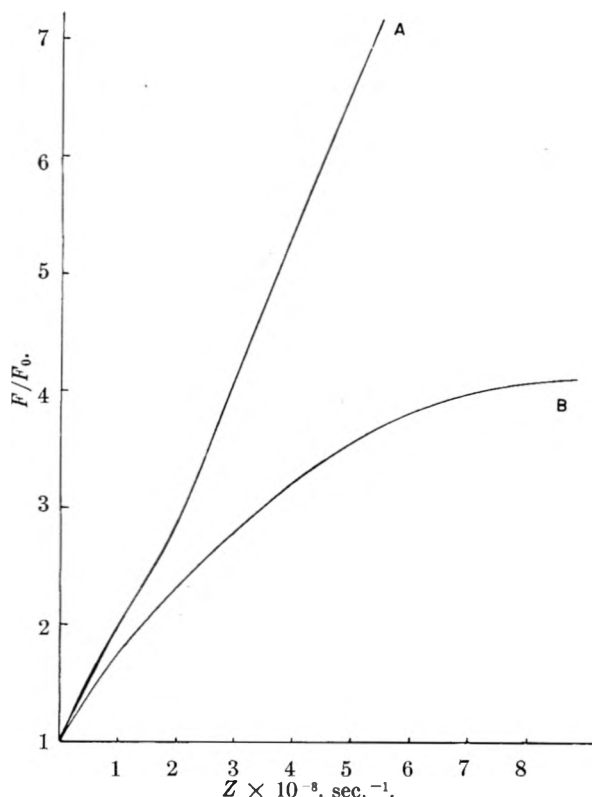


Fig. 3.—A, calculated from equation 1 assuming that all of the energy quanta absorbed by the benzene are transferred to the amine; B, calculated from equation 4 with the same assumptions as for "A."

of fluorescence by direct absorption by the fluorescer is kept small, equation 1 becomes

$$\frac{F_z}{F_0} = \frac{I_{af}}{(I_{af})_0} + \frac{I_{as}}{(I_{af})_0} \times \frac{K_s(F)}{K_s(F) + K_i + K_{ts}} \quad (4)$$

which for  $f = 1$  is represented by curve "B" in Fig. 3.

In calculating the curves shown in the figure, the distribution of light for component "A" in a mixture of "A" and "B" is taken as

$$(\text{fraction})_A = \frac{\epsilon_A C_A}{\epsilon_A C_A + \epsilon_B C_B} \{1 - 10^{-d(\epsilon_A C_A + \epsilon_B C_B)}\} I_0$$

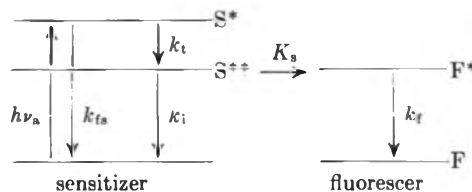
Equation 1 can be rewritten

$$\frac{F_z}{F_0} = \left[ \frac{\epsilon_F C_F}{\epsilon_F C_F + \epsilon_S C_S} \{1 - 10^{-d(\epsilon_F C_F + \epsilon_S C_S)}\} + f \frac{\epsilon_S C_S}{\epsilon_F C_F + \epsilon_S C_S} \{1 - 10^{-d(\epsilon_F C_F + \epsilon_S C_S)}\} \right] V$$

Errors in the chosen values of the molar extinction coefficients will change the value of "f" necessary to match the experimental data but will not change the shape of the  $F_z/F_0$  curve from which the conclusions are drawn. With concentrations in moles/liter the values of  $\epsilon$  at  $\lambda 2537 \text{ \AA}$ . were: benzene (162),  $\beta$ -naphthylamine (2600). The experimental cell was 2 cm. long. For calculations of "Z" the following diameters were used: benzene (5.7  $\text{\AA}$ ),  $\beta$ -naphthylamine (7  $\text{\AA}$ ).

Comparing Fig. 2 and 3 it would seem that only by assuming that vibrational stabilization plays no role in the system considered can one arrive at analytical expressions of the general form obtained by experiment. If this assumption is correct, one must conclude that somehow the amine receives

the energy in the low vibrational levels of its electronically excited state. The postulated mechanism then must be modified to include a step which reduces the size of the quanta absorbed by the sensitizer and at the same time preserves the form of equation 4. This is done easily by considering the scheme



with the result that

$$\frac{F}{F_0} = \frac{I_{af}}{(I_{af})_0} + \frac{I_{as}}{(I_{af})_0} \times \frac{K_s(F)}{K_s(F) + K_i} \times \frac{K_t}{K_t + K_{ts}} \quad (5)$$

$$= \frac{I_{af}}{(I_{af})_0} + \frac{I_{as}}{(I_{af})_0} \times \mathfrak{F} \quad (6)$$

where

$$\begin{aligned} \mathfrak{F} &= \epsilon \eta \\ \epsilon &= \text{the external transfer efficiency} \\ \eta &= \text{the internal transfer efficiency} \end{aligned}$$

The idea that benzene deactivates to a lower electronic level before transferring its energy to the amine is a natural one since the fluorescence efficiency of benzene is low and also because benzene is known to have a low-lying triplet state at  $\lambda 3400 \text{ \AA}$ . (observed in phosphorescence) and that the latter is practically in perfect resonance with the O-O transition in  $\beta$ -naphthylamine (29,200  $\text{cm}^{-1}$ ). From equation 6, the quantity

$$\frac{F}{F_0} (I_{af})_0 - I_{af}/I_{as} = \mathfrak{F}$$

is independent of sensitizer pressure. The results of such a plot are shown in Fig. 4. For amine pressures of 0.53 and 1.25 mm.,  $\mathfrak{F}$  was found to be 0.83 and 0.92, respectively. The large values of  $\mathfrak{F}$  thus calculated indicate that both intra- and intermolecular energy transfer processes are very efficient in this case. Of course we already know that the internal transfer process for benzene is very efficient since the fluorescence efficiency for

that molecule is no more than about 5%. If we denote the fluorescence efficiency by  $\gamma$  then

$$\eta = 1 - \gamma$$

and

$$\epsilon = \frac{\mathfrak{F}}{1 - \gamma} = \frac{K_s(F)}{K_s(F) + K_i} \quad (7)$$

Thus from experimental determinations of  $\mathfrak{F}$  and  $\gamma$  a value could be obtained for the intermolecular transfer efficiency. Furthermore, since from equation 7

$$\frac{1}{\tau_M K_s} = \left( \frac{1 - \epsilon}{\epsilon} \right) (F) \quad (8)$$

values of  $K_s$ , the rate constant for intermolecular transfer of electronic energy can be calculated

if the lifetime  $\tau_m$  of the metastable state of benzene is known. Many of the experimental values needed to carry out these interesting calculations are not known with certainty. The experiments presently reported permitted the elaboration of a plausible scheme for the phenomenon studied and point the way to further research in this area.

A scheme involving self-quenching of the sensitizer could explain the above results without supposing deactivation to and transfer from the low-lying metastable state. However, observations in this laboratory as well as elsewhere<sup>3</sup> indicate that self-quenching in benzene is relatively unimportant.

It is also of interest to note that because  $\beta$ -naphthylamine appears in its lowest vibrational states, in the process under consideration, the system behaves (from the point of view of electronic energy transfer) in the same manner as a liquid or solid system where vibrational energy is dissipated rapidly. In a recent publication on sensitized phosphorescence in organic solutions at low temperatures, Terenin and Ermolaev<sup>4</sup> represent the dependence of naphthalene phosphorescence sensitized by benzaldehyde at fixed concentrations of the phosphorescer by

$$I_c = I_{lim} (1 - e^{-ac})$$

where

- $I_c$  = phosphorescence intensity of naphthalene at concn. "c" of benzaldehyde, which absorbs the exciting radiation  
 $I_{lim}$  = the saturation level of intensity  
 $a$  = constant

This equation is algebraically equivalent to our equation 6, for a system where the fluoescer is completely transparent to the exciting radiation.

(3) P. Pringsheim, "Fluorescence and Phosphorescence," Interscience Publishers, New York, N. Y., 1949, p. 265.

(4) A. Terenin and V. Ermolaev, *Trans. Faraday Soc.*, **52**, 1042 (1956).

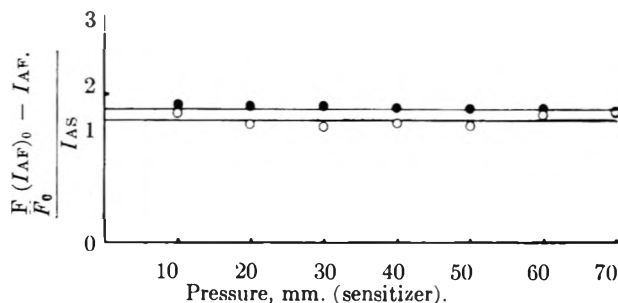


Fig. 4.—Experimental test of equation 6, for two values of  $\beta$ -naphthylamine pressure.

It is of interest to note what other information or applications are latent in this relatively simple type of experiment.

Having an experimental value of  $K_s$ , the rate constant for transfer of electronic energy and assuming no activation energy for the transfer process, one can calculate an effective cross-section. Cross-sections for reactions of electronically excited species are known to differ from those for normal species but *a priori* calculations are not possible using current methods.

Finally, it is an observation in radiation chemistry that small amounts of aromatics stabilize certain compounds which otherwise decompose easily when subjected to the radiation. This stabilization effect is explained by employing energy transfer processes to the aromatic. Since the transfer process from benzene can be very efficient, the reverse process, using benzene as an energy sink, also can take place efficiently under certain conditions.

**Acknowledgment.**—The author wishes to acknowledge helpful conversations with Dr. Michel Boudart and Dr. Brian Stevens.

## THE IGNITION OF EXPLOSIVES BY RADIATION<sup>1</sup>

By J. EGGERT

Federal Institute of Technology, Zürich, Switzerland

Received July 11, 1958

In the known experiments of Norrish<sup>2</sup> and Porter<sup>2</sup> the radiation, which is emitted as very high energy within milliseconds by suitable electric discharges, serves to dissociate gases, such as chlorine, into atoms or radicals. In these cases the absorbed energy is consumed in making possible one or several chemical processes; the system reacts exclusively with the absorbed energy, even if it returns to the original state in some cases by dark reactions afterwards. In this case the absorbed energy is therefore stored as chemical energy; the system operates just as a plant during the photosynthesis. Principally different is the behavior of a mixture of chlorine and hydrogen; for chlorohydrogen can be caused to detonate by sufficiently large quantities of absorbable radiation and is converted to hydrogen chloride even by radiation of lower intensity with a high quantum yield (of the order of  $\phi = 10^6$ ), because in this "endothermic system" chain reactions may occur, as Bodenstein and later Nernst have shown. The impulse for the chain, as previously, is given by the photolytic formation of chlorine atoms. They react according to  $\text{Cl} + \text{H}_2 \rightarrow \text{HCl} + \text{H}$ ,  $\text{H} + \text{Cl}_2 \rightarrow \text{HCl} + \text{Cl}$  with continuous production of HCl molecules and with continuous alternating delivery of H and Cl atoms until either the chain is broken by trapping of the atoms (mutually or by reaction with foreign substances), or until the entire mixture completes the reaction explosively, *i.e.*, thermally.

In Zürich we tried for some time to find the answer to the question whether solid compounds of endothermic character like chlorohydrogen-gas mixture can also be caused to detonate by a

sufficiently large amount of radiation. Principally such systems should be found among the explosives, particularly among those which in other respects, especially mechanically, also possess a high degree of sensitivity. The first representative which we found was nitrogen iodide ( $\text{NH}_3\text{NI}_3$ ) which as brown-black powder can be ignited by the radiation

(1) J. Eggert, *Physik. Bl.*, **10**, 549 (1954).

(2) (a) R. G. W. Norrish, *Z. Elektrochem.*, **56**, 705, 712 (1952);

(b) G. Porter and F. J. Wright, *ibid.*, **56**, 782 (1952).

TABLE I

Detonation temperature in °C. (IV), electrical energy of the discharge in w.s. (V), irradiated energy in w.s./cm.<sup>2</sup> (VI) for electronic flashes of 0.8 ms. duration as minimal values of the radiation to produce detonation for some endothermic compounds (I and II). Compounds in powder form, originally at room temperature.

	I (Compound)	II (Formula)	III (Appearance)	IV (D.T.)	V Dis- charge energy	VI Irr. energy i.e.
1	Nitrogen iodide	N <sub>2</sub> I <sub>2</sub>	Brown-black	50	19	0.16
2	Silver nitride	Ag <sub>3</sub> N	Black	100	24	0.20
3	Cuprous acetylide	Cu <sub>2</sub> C <sub>2</sub>	Brown-black	120	75	0.63
4	Silver acetylide (alk. ppt.)	Ag <sub>2</sub> C <sub>2</sub>	White	165	95	0.79
5	Silver acetylide (neutral ppt.)	Ag <sub>2</sub> C <sub>2</sub> ·AgNO <sub>3</sub>	Yellowish white	225	230	1.9
6	Mercurous acetylide	Hg <sub>2</sub> C <sub>2</sub>	Light gray	280	>350	>2.8
7	Mercuric acetylide	HgC <sub>2</sub>	White	260	180	1.5
8	Silver azide	AgN <sub>3</sub>	White	250	310	2.6
9	Lead azide	Pb(N <sub>3</sub> ) <sub>2</sub>	Yellowish-white	350	240	2.0
10	Mercuric azide	Hg(N <sub>3</sub> ) <sub>2</sub>	White	270	310	2.6
11	Silver fulminate	AgONC	White	170	250	2.1
12	Mercuric fulminate	Hg(ONC) <sub>2</sub>	Light gray	190	200	1.65
13	Diazobenzene nitrate	C <sub>6</sub> H <sub>5</sub> N <sub>2</sub> O <sub>3</sub>	Yellowish	90	110	0.92
14	Diazobenzene perchlorate	C <sub>6</sub> H <sub>5</sub> N <sub>2</sub> ClO <sub>4</sub>	White	155	110	0.92
15	<i>p</i> -Diazodiphenylamine perchlorate	C <sub>12</sub> H <sub>10</sub> N <sub>2</sub> ClO <sub>4</sub>	Yellow	170	95	0.79
16	Ammonium perchromate	(NH <sub>4</sub> ) <sub>2</sub> CrO <sub>8</sub>	Red-brown	90	135	1.10

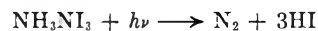
of electronic flashes with remarkable reproducibility with regard to the incident minimal energy. In sunlight, however, the nitrogen iodide undergoes a slow decomposition because the radiation intensity furnished by the sunlight is insufficient to trigger the detonation.

During the course of our investigation we found a series of other compounds having the same property (Table I). The magnitude of the detonation energy (cols. V and VI) indicate that highly colored compounds (col. III) are more "sensitive" than those which are white (colorless) and therefore absorb less of the incident energy. Column IV also indicates that there is a distinct correlation with the detonation temperature,

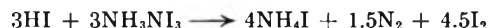
*i.e.*, that temperature at which the explosive detonates in the dark (on rapid heating); high detonation temperatures correspond to high detonation energies; we shall discuss this point later.

Let us consider first the case of nitrogen iodide which my co-worker B. Meerkämper<sup>3</sup> has investigated.

According to older experiments it could be expected that the compound would decompose according to



The hydrogen iodide formed reacts further according to



so that the quantum yield should be at least  $\varphi = 4$ , provided that this value is not still greater because of the energy liberated during the decomposition (60 kcal./mole). Surprisingly it was found that the value  $\varphi = 4$  is far from being reached, even with intense, but for detonation inadequate irradiation, but amounts only to  $\varphi = 0.15$  to maximally  $\varphi = 0.6$  (at 21° and 15 torr.) according to the conditions. The lower values were observed in an ammonia atmosphere, the higher ones in air. In the presence of NH<sub>3</sub> therefore the major part of the primarily formed HI is trapped; it cannot react farther and we observe the low yield  $\varphi = 1/4$ ;  $0.6 = 0.15$ . On the other hand, this figure shows that every 7th quantum only leads to a decomposition of the nitrogen iodide, while the others are converted into heat without taking part photochemically or thermally in the decomposition of the nitrogen iodide. So the absorbed radiation can act either purely photochemically or it can cause the decomposition of the substance by local heating, *i.e.*, thermally. This is supported, *inter alia*, by the fact that the decomposition on irradiation has a temperature coefficient exceeding 1 ( $\tau = 2.3$  for the range from 18.5 to 25°). In order to decide this question, Berchtold<sup>4</sup> carried out the

(3) B. Meerkämper, Thesis No. 2262, ETH Zürich, 1953; *Z. Elektrochem.*, **58**, 387 (1954).

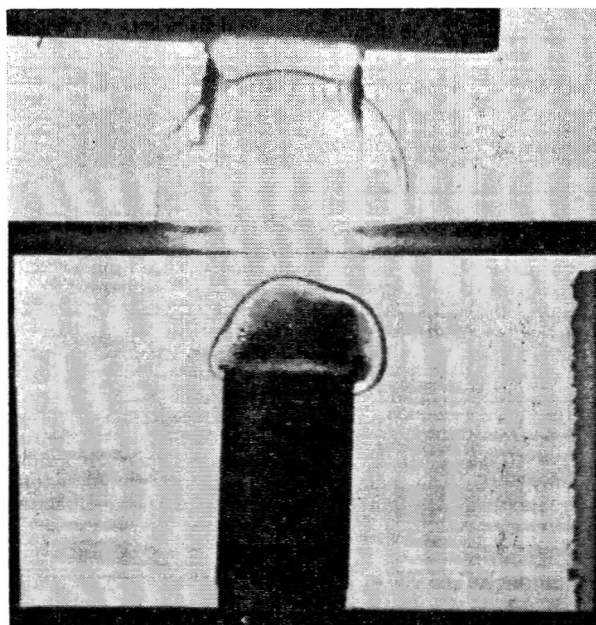


Fig. 1.—Pictorial record of the detonation of nitrogen iodide initiated by an open spark, 27  $\mu$ s. after release of the initiation spark. The separation of the sound wave emanating from the explosion from the smoke is plainly visible. The also visible sound waves from the spark are kept away from the sample by the glass plate.

irradiation of nitrogen iodide with the compound in concentrated aqueous ammonia so that the HI secondary reaction as well as thermal effects were practically excluded. Actually the quantum yield decreased from  $\varphi = 0.15$  to  $0.06$  and the temperature coefficient from  $\tau = 2.3$  to  $1.1$ . This indicates that the "slow" decomposition of the dry nitrogen iodide on irradiation with high intensity light sources is largely photothermal and to a minor part, only about 5–10%, of photochemical nature. Consequently we observed a pronounced ignitability for dry nitrogen iodide, a lower one for water-moistened, and none at all for ammonia-wet compound. The small purely photochemical conversion with "throttled" secondary reaction is insufficient to initiate the detonation.

The detonation of the hydrogen iodide itself also furnished various illuminating observations by means of high speed cinematography. Reference to Fig. 1 anticipates the objection that the initiation may not be caused by radiation but by a mechanical impulse (pressure wave). The deduction from Fig. 1, of course, does not exclude that the substance may be ignited by a pressure wave as was shown by special experiments.

The initiation of the other compounds listed in Table I was purely photothermal. The following experiment proved this. The explosive was first ignited at room temperature ( $20^\circ$ ) by light flash, and the electrical energy of the discharge tube required was entered in a diagram in the manner of Fig. 2. The minimal energy (in w.s.) required for the initiation was determined, after the compound had been raised to a higher temperature as rapidly as possible. Figure 2 shows the curve obtained in this manner for silver acetylide (precipitated from acid solution). We see that the initiation energy decreases with increasing temperature of the compound and converges toward zero at the (dark) ignition temperature of  $225^\circ$ . Consequently the radiation has to supply only the amount of energy which is required to heat the compound surface until it reaches the ignition temperature (col. IV of Table I). Analogous observations were made with nitrogen iodide<sup>3</sup> and lead azide<sup>5</sup> (Figs. 3 and 4).

There are several reasons why, on the other hand, the initiation energies  $J$  for the compounds listed in Table I (all irradiated at room temperature) are in loose relationship only to the corresponding ignition temperatures  $t$  (col. IV), so that there is no simple function  $J = f(t)$  in this case. Firstly, the spectral absorptivities of the compounds differ so that they take up different fractions of the incident energy; secondly, the compounds have different thermal capacities, and finally they differ in heat conductivity. All these properties, however, determine the heating of the surface layer to the ignition temperature, so that we can hardly expect another pattern than the series of dots given in Fig. 5 for the value pairs recorded in Table I for initiation energy (col. V) and initiation temperature (col. IV). The distribution of the dots shows

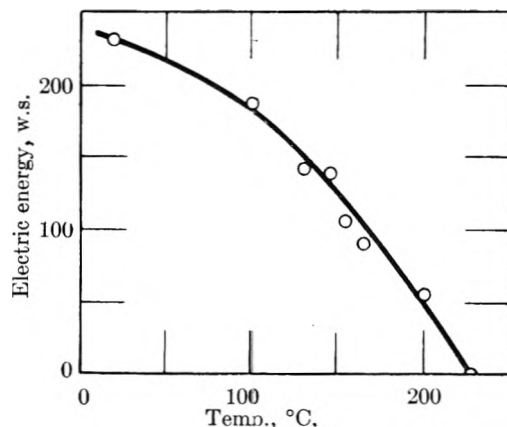


Fig. 2.—The energy of the flash lamp required for the ignition of silver acetylide ( $\text{AgC}_2$ ,  $\text{AgNO}_3$ ) in relation to the initial temperature of the sample.

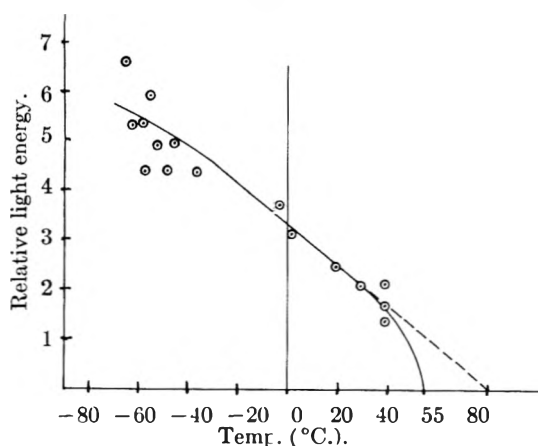


Fig. 3.—The energy of the flash lamp required for the ignition of nitrogen iodide ( $\text{NH}_3\text{NI}_3$ ) in relation to the initial temperature of the sample.

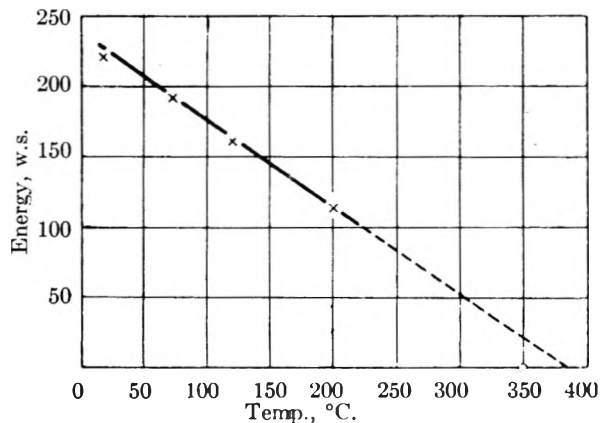


Fig. 4.—The energy of the flash lamp required for the ignition of lead azide,  $\text{Pb}(\text{N}_3)_2$ , in relation to the initial temperature of the sample.

that the effect of the ignition temperature is dominant over the other factors mentioned.

This, however, holds true for a certain duration of the radiation only, which in our case amounted to 0.8 ms., and is valid for a certain layer thickness of the compounds investigated. In order to study these two factors we used silver nitride ( $\text{Ag}_3\text{N}$ ) as test object. Like the other compounds this substance can be prepared as a loose powder, but

(4) J. Berchtold, Thesis No. 2376, ETH Zurich, 1954.

(5) F. Eggert and J. Berchtold, *Naturwiss.*, **40**, 55 (1953).

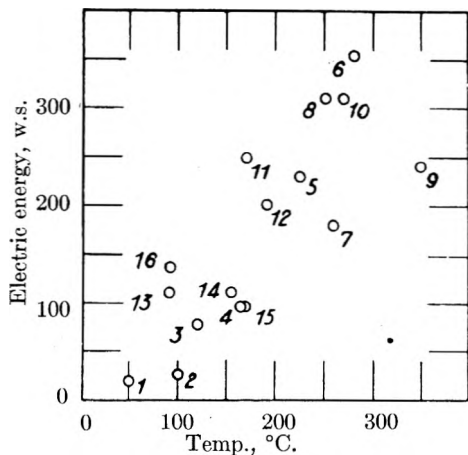


Fig. 5.—Graphic representation of the value pairs: initiation energy I.E. and initiation temperature D.T. from Table I for some endothermic compounds (same numbering).

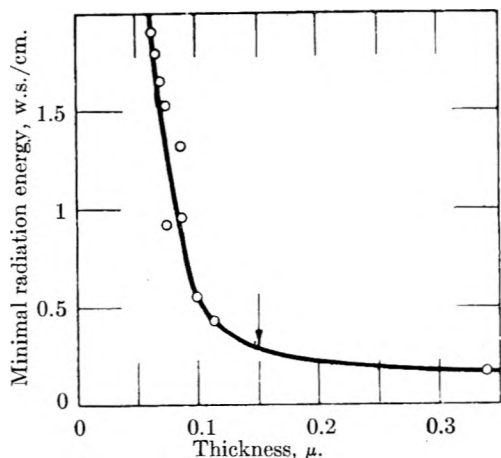


Fig. 6.—The minimum radiation (w.s./cm.<sup>2</sup>) required for the ignition of silver nitride mirrors in relation to the layer thickness of the mirror (μ). The detonation does not spread to the left of the arrow.



Fig. 7.—Flash print of a line original on a silver nitride paper. The black Ag<sub>3</sub>N coating has been destroyed by the detonation in the bright areas so that the paper base is visible through a silver haze; in the dark areas the Ag<sub>3</sub>N coating has gradually changed to silver.

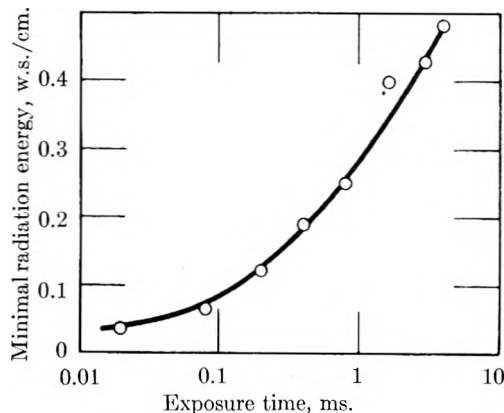


Fig. 8.—Effect of the exposure time (ms.) on the minimal radiation energy (w.s./cm.<sup>2</sup>) required for the ignition of silver nitride.

under suitable experimental conditions it can also be precipitated on smooth surfaces as uniformly dense mirror-like deposits of variable thickness.

We noticed that silver nitride as powder layer and as mirror deposit of about 1 μ thickness (on glass) requires the same irradiation of at least 0.2 w.s./cm.<sup>2</sup> for ignition. If we systematically decrease the thickness, the ignition sensitivity of the mirror decreases at first slowly (as indicated by the curve of Fig. 6), then rapidly, as is evident from the minimal values for the radiation intensity (required to initiate a detonation) which increases steeply toward the lower thicknesses. During the course of these experiments we made the surprising observation that mirrors with a thickness exceeding 0.15 μ (arrow in Fig. 6) detonate, even if only a small fraction of the surface is irradiated; the detonation initiated at the irradiated spot does not spread to non-irradiated areas if the thickness of the layer sinks below 0.15 μ. Apparently the layer in this case loses too much energy to the surroundings (support) to maintain the propagation of the detonation wave.

This effect could be used to prepare copies of line originals by flash illumination on such mechanically quite insensitive layers, as the example of Fig. 7 shows. The silver nitride remaining on the print, which corresponds to the dark areas of the original, after some time spontaneously changes to silver by decomposition, and therefore neither development nor fixation is required for this "dry" printing process which yields positives from positives with a resolution of 10 lines per mm. So far technical reasons make the process unsuitable for practical purposes at this moment.

In a second series of experiments Berchtold investigated the effect of the duration of the flash to the minimal amount of radiation required for the initiation and got the curve of Fig. 8, which was obtained with silver nitride powder. We see that the quantity of radiation directed at the substance can be the smaller the shorter its available time. Whereas, for example, the energy of 0.02 w.s./cm.<sup>2</sup> absorbed in the layer surface after an irradiation time of some milliseconds has time to drain off to colder areas and remain without effect, it accumulates in one hundredth of this time to such an extent



that the ignition temperature is reached and detonation occurs. On the other hand, Meerkämper could prove by high speed cinematographic analysis that the detonation of nitrogen iodide starts long before the light flash ends, and therefore only a fraction of the incident energy is used for the detonation.

A number of phenomena could be reported about the other compounds listed in Table I, for example, that silver azide  $\text{AgN}_3$  (no. 8), which by normal exposure is decomposed with formation of silver and nitrogen, shows the surprisingly low quantum yield of  $\varphi = 0.1$  only, although silver bromide and silver chloride, the compounds used in photography, yield the value  $\varphi = 1^6$  in spite of their

(6) J. Eggert and R. Zemp, *Z. Naturforsch.*, **86**, 389 (1953); also R. Zemp, thesis No. 2150, ETH Zürich, 1953.

similarity to  $\text{Ag}_3\text{N}$ . However, we shall point out in conclusion that the ignitability of thin aluminum foils (of  $0.5 \mu$  thickness) in the presence of oxygen is based on a photothermal process also. It has been shown that the radiation required for the ignition of the aluminum in an  $\text{O}_2$  atmosphere amounts within certain limits to about 2 w.s./cm.<sup>2</sup>. If we assume the average spectral absorption of the used radiation to be 8%, a rise in temperature of about 1200° is indicated by the heat capacity of the system, and this, of course, suffices for the ignition of the aluminum. That in this case a photothermal effect is involved can be concluded also from the fact that the radiation sufficient to cause ignition can be reduced to less than half if the absorption of the aluminum foil is increased by a thin coating of carbon black.

## A METHOD FOR EVALUATING RATE CONSTANTS IN THE JABLONSKI MODEL OF EXCITED SPECIES IN RIGID GLASSES<sup>1</sup>

BY E. H. GILMORE AND E. C. LIM

*Department of Chemistry, Oklahoma State University, Stillwater, Oklahoma*

*Received July 11, 1968*

A method is presented for calculating kinetic rate constants for processes that occur according to the Jablonski model of electronically excited dye molecules in rigid glasses. Non-radiative transitions from excited to ground states are considered in addition to the radiative transitions usually considered. Since the rate constants are found by use of data on fluorescence,  $\alpha$ -phosphorescence and  $\beta$ -phosphorescence, the method is limited in use to temperatures above about 180°K.

### Introduction

The energy level model proposed by Jablonski to explain the qualitative features of observed emissions from excited molecules in rigid media<sup>2</sup> has been used with considerable success in semi-quantitative studies of such systems, and in some instances theoretical justifications for the assumptions regarding the natures of the energy levels have been found.<sup>3-6</sup> Until the appearance of the work by Koizumi and Kato,<sup>7,8</sup> however, no solution to the kinetic problem had been published in which non-radiative transitions were permitted to occur from both excited electronic levels. Their work, which was concerned with identifying the excited level involved in quenching with gaseous agents, led to the most general solution of the kinetic problem presently available.

In the present work, a procedure is presented whereby the individual rate constants for processes occurring in the Jablonski model can be computed with the aid of specific emission data. Use is made of Koizumi and Kato's time-dependent solutions in a slightly modified form, and of steady-state solutions. It is assumed that the only temperature

dependent process is the one by which molecules are thermally activated from the triplet to the singlet level. In some instances such an assumption may not be valid,<sup>9</sup> but it was shown to be satisfactory for at least one system in a semi-quantitative investigation by Lewis, Lipkin and Magel.<sup>10</sup>

**The Use of Emission Data to Solve for Rate Constants.**—The time-dependent solutions given by Koizumi and Kato are written in terms of the symbols appearing in Fig. 1 as

$$N_S = Q[r_1^{-1}(r_1 + R_T)e^{r_1 t} - r_2^{-1}(r_2 + R_T)e^{r_2 t}] (r_2 - r_1)^{-1} \quad (1)$$

and

$$N_T = k_3 Q[r_1^{-1}e^{r_1 t} - r_2^{-1}e^{r_2 t}] (r_2 - r_1)^{-1} \quad (2)$$

in which  $R_S$  is the sum  $k_1 + k_2 + k_3$  and  $R_T$  is the sum  $k_4 + k_5 + k_6$ . The quantities  $r_1$  and  $r_2$  are roots of the auxiliary equations for the second-order differential equation involved in the solution of the rate equations. Steady-state solutions are

$$N_S = R_T Q (R_S R_T - k_3 k_6)^{-1} \quad (3)$$

and

$$N_T = k_3 Q (R_S R_T - k_3 k_6)^{-1} \quad (4)$$

In eq. 1, 2, 3 and 4 all non-radiative processes from a given excited state to the ground level are assigned a single rate constant which is the sum of the rate constants for the several non-radiative processes possible from that state. In this regard the

(1) Supported in part by the Office of Ordnance Research on Contract No. DA-23-072-ORD-581.

(2) A. Jablonski, *Z. Physik*, **94**, 38 (1935).

(3) G. N. Lewis and M. Kasha, *J. Am. Chem. Soc.*, **66**, 2100 (1944).

(4) G. N. Lewis and M. Calvin, *ibid.*, **67**, 1232 (1945).

(5) G. N. Lewis, M. Calvin and M. Kasha, *J. Chem. Phys.*, **17**, 804 (1949).

(6) D. S. McClure, *ibid.*, **17**, 905 (1949).

(7) M. Koizumi and S. Kato, *ibid.*, **21**, 2088 (1953).

(8) M. Koizumi and S. Kato, *J. Inst. Polytechnics (Osaka, Japan)*, **4**, 149 (1953).

(9) E. J. Bowen and D. M. Stebbins, *J. Chem. Soc.*, 360 (1957).

(10) G. N. Lewis, D. Lipkin and E. Magel, *J. Am. Chem. Soc.*, **63**, 3005 (1941).

แผนกฟิสิกส์ มหาวิทยาลัยเชียงใหม่

กระทรวงอุตสาหกรรม

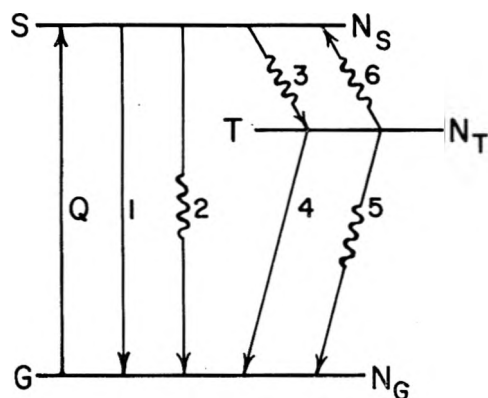


Fig. 1.—Modified Jablonski model for the electronic transitions of dye molecules in rigid glass solution.  $Q$  is the rate at which molecules are excited to the lowest singlet level by absorption processes 1 and 4 are the fluorescence and  $\beta$ -phosphorescence, respectively; and 2 and 5 are radiationless transitions from singlet to ground and triplet to ground respectively; 3 populates  $T$  from  $S$ , and 6 populates  $S$  from  $T$  by a temperature-dependent process. The symbols  $k_1$  and  $k_4$ ,  $k_2$  and  $k_5$ ,  $k_3$  and  $k_6$  represent the specific rate constants, respectively, for these processes.

solutions differ from those of Koizumi and Kato who wrote separate symbols for the quenching constants. All processes are assumed to be first order with respect to the excited species involved. The expanded forms of  $\tau_1$  and  $\tau_2$  given by Koizumi and Kato can be approximated satisfactorily by the expressions

$$\tau_1 = -R_S \quad (5)$$

and

$$\tau_2 = -R_T + k_3 k_6 R_S^{-1} \quad (6)$$

The quantum yield of luminescence from the singlet state  $\Phi_f$  is given by

$$\Phi_f = k_1(\tau_1 + R_T)\tau_1^{-1}(\tau_2 - \tau_1)^{-1} - \frac{k_1(\tau_2 + R_T)\tau_2^{-1}(\tau_2 - \tau_1)^{-1}}{k_1(\tau_2 + R_T)\tau_2^{-1}(\tau_2 - \tau_1)^{-1}} \quad (7)$$

The second term on the right hand side of eq. 7 represents the quantum yield of the long-lived emission designated as  $\alpha$ -phosphorescence by Lewis, Lipkin and Magel.<sup>10</sup> To a high degree of accuracy  $\tau_1 = -\tau_f^{-1}$ , in which  $\tau_f$  is the observed fluorescence mean lifetime, and  $k_1$  is found either by integration of the absorption band or from eq. 7 using measured values of  $\Phi_f$  and of the  $\alpha$ -phosphorescence quantum yield, symbolized here by  $\Phi_{\alpha p}$ , remembering that  $|R_T| \approx |\tau_2| \ll |\tau_1|$ .  $R_T$  can be found by substituting  $k_1$ ,  $\Phi_f$ ,  $\tau_1$  and  $\tau_2$  into the

formal expression for the  $\alpha$ -phosphorescence quantum yield. The quantity  $\tau_2 = -\tau_{\beta p}^{-1}$  to a first approximation in which  $\tau_{\beta p}$  is the  $\beta$ -phosphorescence mean lifetime. The value of the product  $k_3 k_6$  can be found from eq. 6, and one can use the relation for the steady-state quantum yield of  $\beta$ -phosphorescence, given by

$$\Phi_{\beta p} = k_3 k_4 (\tau_1^{-1} - \tau_2^{-1}) (\tau_2 - \tau_1)^{-1}$$

to find a value for the product  $k_3 k_4$ .

If one assumes that the constant  $k_6$  has the form  $p \exp(-\Delta H/RT)$  and that all other rate constants are independent of temperature, then one can arrive at a value of  $k_6$  by differentiating  $\tau_2$  with respect to  $1/T$  and making use of the value of  $\Delta H$  from spectroscopic data. The solution is

$$k_6 = k_3 k_4 R_S^{-1} + (R/\Delta H) \{d\tau_2/d(1/T)\}$$

When the value of  $k_6$  is determined, the values for the other five rate constants are found readily. The method of successive approximations then can be used to improve the accuracy of the values found for the rate constants.

### Discussion

The objective of this work has been to develop a method for computing the various rate constants for the Jablonski model. Such data would provide important information on the processes occurring and even give evidence as to whether the Jablonski model is a generally correct picture. The method described here is such that tests can be made only when fluorescence,  $\alpha$ -phosphorescence and  $\beta$ -phosphorescence are present simultaneously. These luminescences are observable only for dye molecules, in general. Data for making these calculations are presently unavailable.

In this and other treatments of the kinetic problem it is assumed that the energy states are single levels. Since this assumption is not strictly true, especially at higher temperatures, the rate constants obtained will be a composite of the various true values: nevertheless, if for some given system, positive values of reasonable magnitudes are obtained for these rate constants, the Jablonski model will not be ruled out as a possible model for the system.

With values for the various rate constants known, it would be possible to calculate from eq. 3 and 4 the instantaneous numbers of molecules storing photochemical energy in the singlet and in the triplet excited states.

# THE PHOTOLYSIS OF NITROSYL CHLORIDE AND THE STORAGE OF SOLAR ENERGY

By OTTO S. NEUWIRTH

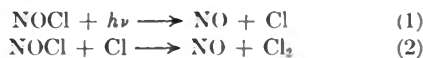
*Contribution from the Department of Chemistry, University of Wisconsin, Madison, Wisconsin*

*Received July 11, 1958*

Nitrosyl chloride, dissolved in carbon tetrachloride, is photochemically decomposed by light below 6400 Å. into nitric oxide and chlorine. The quantum yield is reduced by the reverse reaction and values of 0.75 or less up to approximately 1.0 are obtained. Experiments using sunlight with a flowing system are described. The nitric oxide is insoluble and can be stored and later recombined with chlorine in carbon tetrachloride to give the original nitrosyl chloride and release some of the solar energy consumed in the photolysis.

Photochemical reactions are needed which will absorb energy and store the energy of incident sunlight, the products recombining later under controlled conditions with the release of some of the energy. Suitable reactions of this type are difficult to find. The photolysis of nitrosyl chloride is such a reaction. In the gas phase, nitrosyl chloride absorbs most of the visible sunlight up to 6400 Å. and in the absence of oxygen, gives nitric oxide and chlorine according to a first-order reaction. It was thought that nitrosyl chloride dissolved in carbon tetrachloride would undergo similar photodecomposition and that the chlorine would remain dissolved but that the nitric oxide, which is relatively insoluble in carbon tetrachloride, would escape and thus permit separation and storage. The nitric oxide could then be recombined with the chlorine in carbon tetrachloride to give back the original nitrosyl chloride solution with the evolution of heat.

The reaction has been studied in the gaseous phase by Kiss,<sup>1</sup> Bowen and Sharp<sup>2</sup> and Kistiakowsky.<sup>3</sup> The scheme shown in (1) and (2) has been proposed<sup>3</sup>



where the light absorbing step is followed by the very fast reaction 2. This reaction scheme has been confirmed by some recent investigations,<sup>4</sup> where it was found that chlorine atoms catalyze the reaction by accelerating step 2.

## Experimental Results

The photodecomposition was followed at constant temperature by measuring as a function of time the pressure of nitric oxide produced photochemically and released into the gas space.

The apparatus consisted of a 500-watt tungsten projection lamp, a large glass lens, a shutter and a filter. The circular reaction vessel of Pyrex glass, 1 cm. in thickness, is placed in a Pyrex thermostat, kept at a constant temperature to  $\pm 0.2^\circ$ . From the top of the reaction vessel a connection leads to a mercury manometer. Thorough stirring was carried out during the whole experiment by means of a magnetic stirrer.

The energy of the incoming light was measured with a sensitive bolometer, previously standardized by a carbon filament lamp provided by the U. S. Bureau of Standards. This bolometer was placed in a Wheatstone bridge with a multiflex galvanometer. The energy absorbed by the nitrosyl chloride was obtained from the difference in trans-

mission of pure carbon tetrachloride and the carbon tetrachloride solution of NOCl.

Figure 1 gives the decomposition curves, which show the pressure of nitric oxide released (in mm.) as a function of the time of irradiation. The different curves give the results with different light intensities. As in the gas phase experiments, a steady state is reached when the products, nitric oxide and chlorine, accumulate to such an extent that the reverse reaction is equal to the forward photochemical reaction. The sharp decrease in pressure shown in the curves occurs when the light is turned off. Figure 2 gives the volume of NO liberated in another set of experiments.

The determination of quantum yields for the photodecomposition and separation is only approximate. The light used extended continuously over the whole visible spectrum in order to simulate the conditions of a practical reaction operating with sunlight.

The quantum yield in the gaseous phase is 2. In solution Atwood and Rollefson<sup>5</sup> determined the quantum yield of the photo-oxidation of a similar reaction (nitrosyl chloride + O<sub>2</sub> to give NO<sub>2</sub> + Cl<sub>2</sub>) and found it to be between 0.47 and 0.72.

The back reaction between chlorine and nitric oxide has been investigated by Trautz and co-workers<sup>6</sup>. It is a third-order reaction with an exothermic heat of reaction of 9000 cal. per mole of NOCl formed. The two gases react slowly at room temperature and the reaction is complete over charcoal at slightly increased temperatures.<sup>7</sup> It was found in the present investigation that the reaction is quite rapid in carbon tetrachloride even at room temperature.

In order to store the energy absorbed in the photochemical reaction, the reaction products must be separated and then recombined at a later date. This separation can be performed (a) in the gas phase by removing one of the products by adsorption or absorption, (b) in a solution by dissolving one but not both of the products of photolysis.

The first method is difficult because the products recombine before diffusing to the surface of the adsorbent or absorbent, or at the catalytic surface of an adsorbent.

In the present work the second method was chosen using carbon tetrachloride as the solvent for nitrosyl chloride. Chlorine also is soluble to a large extent, whereas the nitric oxide formed is practically insoluble and escapes into the gas space above the solution. Nitrosyl chloride in carbon tetrachloride shows continuous optical absorption and the shape of the absorption curve is the same as that given in the literature for nitrosyl chloride in the gas phase.<sup>8</sup>

It is likely that the quantum yield is lower in carbon tetrachloride solution than in the gas phase because of the Franck-Rabinowitch cage effect of solvent molecules, which increases the rate of recombination of the nitric oxide and chlorine. The bolometer circuit measures only the amount of incoming and transmitted energy. To obtain the number of quanta absorbed over the whole range it is necessary to calculate a mean value from the energy distribution in the different wave lengths for a 500-watt tungsten projector lamp and the number of quanta per erg for each wave length. A

(1) A. Kiss, *Rec. trav. chim.*, **42**, 665 (1923).

(2) E. J. Bowen and J. F. Sharp, *J. Chem. Soc.*, **127**, 1026 (1925).

(3) G. B. Kistiakowsky, *J. Am. Chem. Soc.*, **52**, 102 (1930).

(4) P. G. Ashmore and J. Channugam, *Trans. Faraday Soc.*, **49**, 254, 265, 270 (1953); W. G. Burns and F. S. Dainton, *ibid.*, **48**, 52 (1952).

(5) K. Atwood and G. K. Rollefson, *J. Chem. Phys.*, **9**, 506 (1941).

(6) M. Trautz, *Z. anorg. Chem.*, **88**, 285 (1914); M. Trautz and C. F. Hinek, *ibid.*, **93**, 177 (1915); M. Trautz and L. Wachenheim, *ibid.*, **97**, 241 (1916); M. Trautz and W. Gerwig, *ibid.*, **146**, 1 (1925).

(7) Chem. Fabrik vorm. E. Schering, German Patent 369,369 (1919).

(8) J. Jander, *J. Chem. Soc.*, 915 (1954); J. A. Leermakers, *J. Am. Chem. Soc.*, **54**, 1841 (1932).

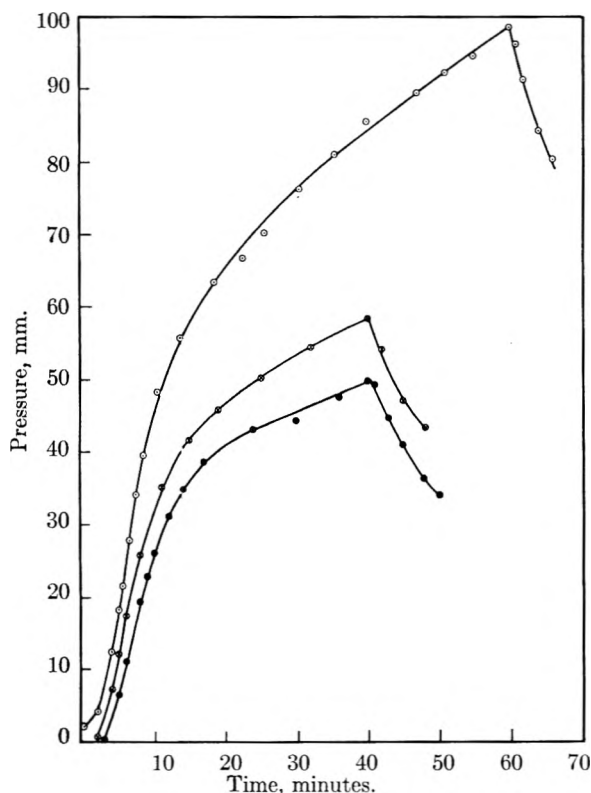


Fig. 1.—Pressure of nitric oxide in a stationary system exposed to light.

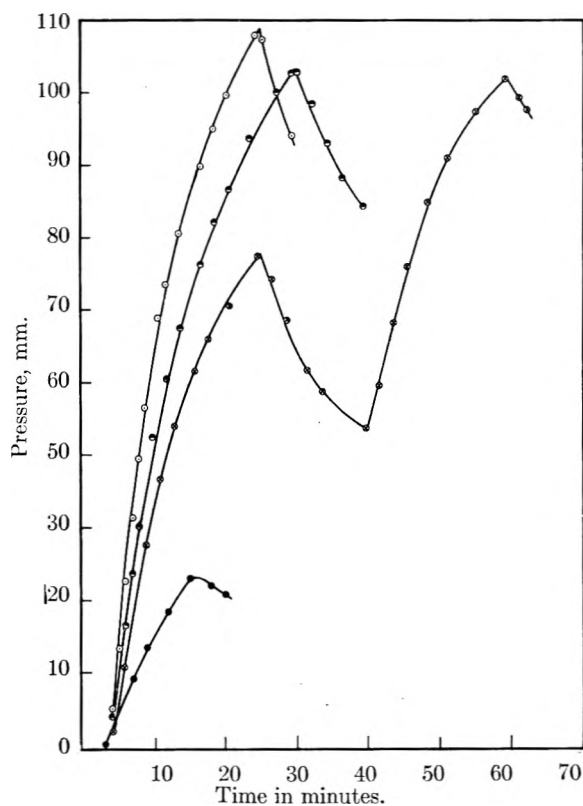


Fig. 3.—Pressure of nitric oxide in a flowing system exposed to light.

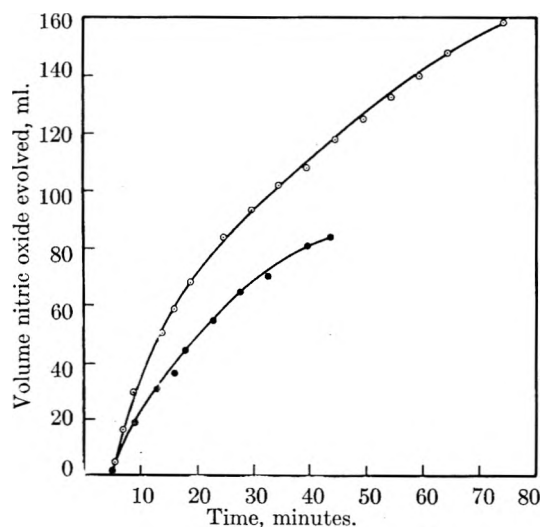


Fig. 2.—Volume of nitric oxide released by exposure to light in a stationary system.

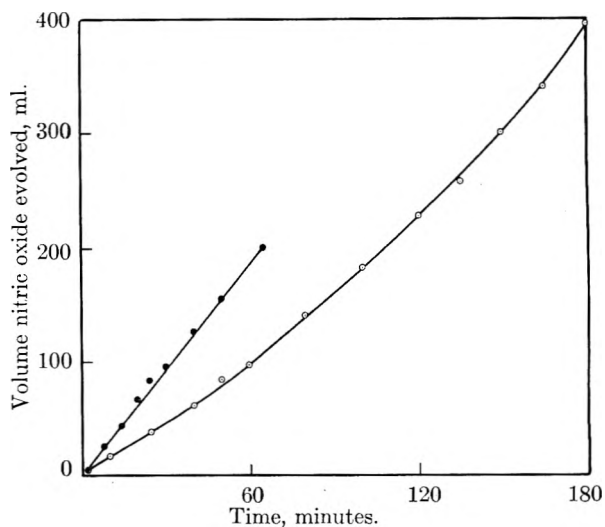


Fig. 4.—Volume of nitric oxide released by exposure to light in a flowing system.

further small correction is needed to allow for the fact that the per cent. of light transmitted and measured by the bolometer is less at the shorter wave lengths where nitrosyl chloride absorbs more strongly.

The calculated quantum yields of decomposition and separation are shown for different concentrations in Table I.

These quantum yields are calculated for the initial reaction corresponding to the first steep part of the decomposition curves shown in Fig. 1. The quantum yields decrease as the reaction proceeds due to the increasing concentration of the reaction products which accelerate the back reaction. After long exposures with the light intensity used in these experiments a steady state is reached, where the quantum yields drop to values from 0.05 to 0.1.

**Flow System.**—The previous experiments were carried out in a stationary system in which the photo products,

TABLE I  
QUANTUM YIELDS FOR THE PHOTOLYSIS OF NOCl IN CCl<sub>4</sub> SOLUTIONS

Concn. NOCl, moles/l.	I	II	III	IV	Av.
0.246	0.68	0.77	0.80	1.0	0.83
.371	0.53	0.67	0.67	0.87	0.74
.511	0.75	0.81	0.91	0.94	0.94
.646	0.95	1.01	1.14		1.08

chlorine and nitric oxide, accumulate. For storage of the converted light energy it is necessary to minimize this back reaction and prevent the decomposition products from recombining. Two different types of back reactions occur:

(1) The recombination in the liquid carbon tetrachloride phase, whereby the products in solution react to form nitrosyl chloride at a rate which depends on their concentration in solution. (2) The back reaction between the chlorine in solution and the nitric oxide in the overlying gas space. The nitric oxide in the gas space reacts at the surface of the carbon tetrachloride solution with the dissolved chlorine. This type of reaction can be seen in the curves of Fig. 1, where after turning off the light the pressure decreases rapidly as the nitric oxide molecules react with the solution. The velocity of this recombination is limited by the diffusion of chlorine molecules to the surface and the decrease in pressure is faster when the solution is stirred.

The best way to reduce the amount of back reaction due to the increasing concentration of the reaction products is to use a dynamic system in which the carbon tetrachloride solution of nitrosyl chloride is removed continuously from the photo reaction vessel. The photochemical reaction then proceeds with a high quantum yield as indicated by the first, steep part of the curves of Fig. 1. The streaming velocity of the solution through the photocell is kept at a rate which does not allow an accumulation of chlorine molecules during the time that the solution is in contact with the nitric oxide gas phase. Another advantage of this dynamic method is that the chlorine does not accumulate and provide an inner optical filter which absorbs some of the light and prevents it from reaching the NOCl.

A few experiments with the dynamic system were made in direct sunlight which was focussed onto a 500-ml. round bottom flask containing the carbon tetrachloride solution of nitrosyl chloride and placed between two 5-liter storage containers. The carbon tetrachloride solution of nitrosyl chloride flowed through the photochemical reaction chamber of 500 ml. at a rate of about 30 ml. per minute.

From the top of the reaction vessel a connection led to a container for storing the nitric oxide gas. Figure 3 gives

the pressures of nitric oxide produced in the photolysis, by focussed sunlight, of the flowing solution of NOCl in carbon tetrachloride. It is evident that the curves retain their steep slope much longer than the curves shown in Fig. 1, obtained with the stationary system, because the reverse reaction, the recombination of nitric oxide and dissolved chlorine, is suppressed.

In Fig. 4 the evolution of nitric oxide produced by the photolysis in focussed sunlight of nitrosyl chloride is shown as measured in the flowing system. The amount of nitric oxide formed photochemically increases continuously with irradiation time, showing that the reverse reaction is small.

### Conclusions

These experiments show that it is possible to bring about an endothermic reaction with sunlight, to separate and store the products and to get back as heat part of the absorbed sunlight, when desired. The photochemical reaction has a reasonably high quantum yield approaching 1, and it absorbs most of the sunlight in the visible range of the spectrum. It is of the general type to be sought after for the utilization of solar energy but the energy storage per gram of material is low and it is hoped that much better photochemical reactions making use of these general principles will be found and tested.

The author is indebted to Professor Farrington Daniels for suggestions and advice throughout the course of this work and to the Rockefeller Foundation for financial support.

---

## KINETIC COMPLICATIONS ASSOCIATED WITH PHOTOCHEMICAL STORAGE OF ENERGY

BY RICHARD M. NOYES<sup>1</sup>

*Contribution from the Chandler Laboratory of Columbia University, New York, N. Y.*

*Received July 11, 1958*

If energy is to be stored in a photochemical process, the initial act of absorption of a photon must be followed rapidly by additional reactions. These can be classified according to whether or not a non-absorbing species must react either with the excited absorber or with a fragment formed from its dissociation. Because of the compressed time scale in which many of these additional reactions must occur, the kinetic treatment requires consideration of the special problems associated with very fast reactions.

### Introduction

The principle of microscopic reversibility requires that if the ground electronic state of a chemical species absorbs radiation efficiently, then the rate constant must be large for re-emission by the excited state first produced. Therefore, if a system is to store photochemical energy, the primary act of absorption must be followed very rapidly by secondary processes that make it improbable the initial excited species will be regenerated.

Three types of secondary processes can be considered. First, some of the energy of the original quantum may be dissipated in thermal motions leaving the absorbing molecule in a metastable triplet state. If selection rules forbid conversion to the ground state with emission of radiation, and if a considerable energy barrier opposes regeneration of the initial excited state, the metastable state may live for some time and thus store a large fraction of the energy of the original quantum.

Second, the energy of the excited absorber may be transferred by electronic excitation or chemical reaction with another molecule that does not absorb or emit radiation. Entropy restrictions then help to prevent regeneration of the excited state formed in the primary absorption.

Third, the absorbing molecule may be dissociated into fragments during or soon after the primary absorption. If these fragments are then separated by diffusion, entropy restrictions can again oppose regeneration of the initial excited state.

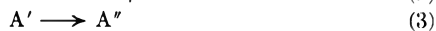
Because the secondary processes must frequently take place in times of the order of  $10^{-9}$  second if re-emission is to be prevented, the kinetics may exhibit features that are not important when molecules are allowed longer times in which to react.

In this paper, we shall classify secondary processes according to whether or not there is dissociation of the original absorber and whether or not a large fraction of the energy of the original

<sup>(1)</sup> Department of Chemistry, University of Oregon, Eugene, Ore.

quantum is transferred to another chemical species. For each classification, we shall consider the problems associated with treating the kinetics of the process, and we shall briefly assess the prospects that this classification might include a satisfactory reaction for energy storage.

**No Dissociation and No Energy Transfer.**—If the initial absorber remains intact, and if no major fraction of the energy of the absorbed quantum is transferred to another specific molecule, the processes can be represented schematically as



This situation does not exhibit any kinetic anomalies. We have no reason to suspect that the age of a particular excited species has any influence on the relative probabilities of reaction by any of the processes from (2) to (5).

Reactions without either energy transfer or dissociation appear to offer rather little promise for storage of energy. Metastable species ( $A''$ ) may be triplet electronic states like those described by others at this Conference, or they may be isomeric molecules as in the photochemical conversion of fumaric to maleic acid. Often these states are unsatisfactory for energy storage because the radiationless transition to the ground state (reaction 5) is too facile. Even when this radiationless transition is unimportant, it is difficult to cause release of the stored energy rapidly enough for the resulting thermal effects to be useful.

**No Dissociation but Energy Transfer.**—If the excited absorber can use a considerable fraction of the absorbed energy for the specific excitation of another species, the process can be represented schematically as



where this step supplants reactions (3–5) above.

This kind of process opens up wider chemical possibilities because it can be used to store energy in species that do not themselves absorb or emit radiation. Also, if reaction 6 is exothermic, the loss of radiation by re-emission is opposed by both energy and entropy barriers. Thus, the reverse of reaction 6 requires a position fluctuation that puts A and B' in juxtaposition at the same time that a thermal fluctuation provides the energy necessary for the excitation to A'.

However, the re-emission of radiation by reaction 2 will occur in about  $10^{-9}$  sec. if A can absorb well in the ground state, and an A' must be able to react this rapidly with B if reaction 6 is to compete effectively. The necessary time scale can be lengthened only if a reaction like (3) can be followed by reaction of A'' with B.

If experimental conditions require that a species undergo a bimolecular reaction within  $10^{-9}$  second after its formation, there must be a high probability for reaction during each encounter with a potential reactant. When an excited A' molecule has just been formed by absorption of a photon, its probability of reaction per unit of time is determined

by the frequency with which an inert molecule with the same diffusive properties would undergo encounters with a random distribution of B molecules; if the excited A' molecule has existed for a sufficient time without reaction, its probability of reaction per unit of time is determined by the rate of steady-state diffusion of B molecules into a sink the size of the A' molecule. Although these two reaction probabilities will not differ significantly for molecules in gas phase, they may differ by at least a factor of two for very reactive species in solution. Since the change of reactivity in solution is rapid for times of the order of  $10^{-9}$  second during which re-emission is most apt to occur, it is not possible to define a rate "constant" for calculating the competition of reactions 2 and 6. More refined kinetic treatments are necessary for estimating the effect of concentration of B on the fraction of absorbed photons that result in storage of energy as B'.

We have already developed the necessary equations to treat this situation for the case that A' and B are electrically neutral so that directions of relative diffusive displacements are randomly distributed in space.<sup>2</sup> The equations were developed for quenching of fluorescence, but they can be applied easily to the energy transfer problem. If  $g$  is the probability reaction 1 is followed by the transfer reaction 6 rather than the re-emission 2 and if transient effects are neglected for times of the order  $10^{-11}$  second, then

$$g = \frac{J[B]}{1 + J[B]} + \frac{1 - \exp\left(-\frac{4K^2[B]^2}{1 + J[B]}\right)}{1 + J[B]} + \frac{2\sqrt{\pi}K[B]\exp\left(-\frac{4K^2[B]^2}{1 + J[B]}\right)}{(1 + J[B])^2} \quad (7)$$

Here,  $J = k_6/k_2$  for A' molecules so old that a limiting concentration gradient has been established, and  $K$  is a measure of the competition between re-emission and establishment of that limiting concentration gradient. The symbols are defined more fully in the previous reference.

Equation 7 predicts that energy transfer will be somewhat more efficient than would be expected from the limiting rate constant for reaction 6 at long times since excitation, but the effects will not be large. Since  $J$  is frequently of the order of 100 l./mole for reactions of this sort, it is usually possible to attain B concentrations sufficient that the energy is trapped efficiently and  $g$  is nearly unity even without including the extra terms.

Although the above discussion has treated reaction 6 as a transfer of electronic excitation energy, the same kinetic considerations would apply to any chemical reaction producing a metastable species. Such a chemical reaction probably offers more promise for energy storage than does transfer of electronic excitation.

As was discussed above for the situation without energy transfer, it is difficult to find excited states that combine long storage lifetime with the possibility of controlled release of energy. If such excited states can be found, it will probably

(2) R. M. Noyes, *J. Am. Chem. Soc.*, **79**, 551 (1957).

be less difficult to obtain photochemical excitation either by direct absorption to a higher energy state of the same species or by transfer of energy from another absorber.

In case the energy transfer in (6) is an actual chemical reaction, there may be more chance that energy can be stored and released as desired, but it may also be that the rate of reaction is slow enough that the considerations of equation 7 become significant.

**Dissociation without Energy Transfer.**—Frequently the absorbing molecule is dissociated either in the primary photochemical act or in a rapid subsequent predissociation. Even if the absorber does not dissociate, it may cause dissociation of another species as in the common use of excited mercury atoms to break bonds in hydrogen or in hydrocarbons.

The quantum yield for dissociation may approach unity in gas phase; it is invariably less than unity in a liquid. The differences are explained by the "cage" theory of liquid dissociations first enunciated by Franck and Rabinowitch.<sup>3</sup> Because of the strong frictional forces in the liquid, the fragments will be reduced to thermal kinetic energies before they have separated by more than a few molecular diameters. Because diffusive displacements in liquids are certainly no larger than a molecular diameter, the two fragments diffusing with a small initial separation are very apt to encounter each other and recombine shortly after they are reduced to thermal energies.

Although the language of the preceding paragraph regarded the surrounding liquid as a continuum, any complete descriptor must recognize the discrete distribution of solvent molecules around a pair of fragments almost in juxtaposition. We have rather arbitrarily distinguished between the "primary" recombination of fragments that never attain a separation of a molecular diameter and the "secondary" recombination of fragments that attain a small initial separation and encounter each other during subsequent diffusion.<sup>4</sup>

Since the fragments from a photochemical dissociation are in much higher potential energy than the original absorber, dissociations offer the possibility of energy storage if the fragments can be prevented from combining. However, the prospects for efficient storage do not look good. The quantum yield for production of fragments will be low because of primary and secondary recombination as discussed above, and fragments that escape their original partners will ordinarily react rapidly with fragments from other dissociations. Although Norman and Porter<sup>5</sup> have shown that radical fragments can be trapped in rigid glasses at low temperatures, these media are not encouraging for practical application. If a high concentration of radicals could be trapped at ambient temperatures in a polymer whose ceiling temperature for polymerization was only a few degrees higher, then the energy of combination of the trapped

radicals could be obtained upon slight warming of the system. Although such a system might function for space heating of buildings, it would not be promising as a power source.

**Dissociation with Energy Transfer.**—If the fragments from a dissociation can undergo secondary chemical reactions, the potential energy represented by the fragments may be stored in a form that is less susceptible to rapid degradation. Chemical reactions of this sort are formally analogous to the energy transfers discussed when no dissociation was involved, but the efficiency with which a reagent can react with fragments is a complex function of concentration because of the extended time scale associated with recombination events. Primary recombination involves times of the order of a molecular vibration and is complete in a few times  $10^{-13}$  second. Probably most secondary recombinations take place between  $10^{-11}$  and  $10^{-8}$  second after the initial dissociation. Fragments that escape recombination with their original partners will live for much longer periods that at low light intensities may be of the order of seconds.

It is not difficult to have a moderately reactive reagent in sufficient concentration to react with all fragments that escape recombination with their original partners. Competition with secondary recombination involves times of the same magnitude as those for competition with re-emission as discussed above; it involves the same kinetic considerations with the additional complication that the probability of secondary recombination is strongly dependent on the time since dissociation. Competition with primary recombination will be impossible unless the competing reagent is also the solvent in which the dissociation occurs.

If energy is to be stored by a reaction with products from a photochemical dissociation, the efficiency will be greater the more the reagent can compete with the secondary recombination of original partners. If two particles are diffusing at random in one dimension the probability that they will occupy the same place at the same time varies inversely as  $t^{1/2}$ , and the probability for particles diffusing in three dimensions varies inversely as  $t^{3/2}$ . If  $h(t) dt$  is the probability that a specific pair of fragments will undergo secondary recombination between  $t$  and  $t + dt$  after dissociation, then  $h(t) = a/t^{3/2}$  for times greater than those needed for a few molecular displacements. Similarly, the probability of secondary recombination at any time after  $t$  is

$$\int_t^{\infty} a dt/t^{3/2} = 2a/t^{1/2}$$

If a reagent B is to compete with secondary recombination by reacting with fragments, the average time necessary for it to do so will be very nearly inversely proportional to the concentration of B. Then the extent to which B can compete with secondary recombination will be proportional to the fraction of secondary recombination that would otherwise take place after time  $t'$  where  $t'$  is the average time needed for B to react with one of the members of the pair of fragments. The answer gives the competition proportional to  $[B]^{1/2}$ .

(3) J. Franck and E. Rabinowitch, *Trans. Faraday Soc.*, **30**, 120 (1934).

(4) R. M. Noyes, *J. Chem. Phys.*, **18**, 999 (1950).

(5) I. Norman and G. Porter, *Proc. Roy. Soc. (London)*, **A230**, 399 (1955).

The above paragraph is a verbalization of a more exact argument presented elsewhere.<sup>6</sup> Although the derivation could be made more precise by using a better model for the time dependence of secondary recombination<sup>7</sup> and by including the time dependence of the reactivity of B, the refinements would not affect the value of the principal term from the integration.

The above argument is also based on the assumption that the fragments from the original dissociation are electrically neutral so that their relative diffusive displacements are not affected by long range intermolecular forces. We hope that these treatments will be extended to ionic reactions in the near future.

If the products of these reactions are sufficiently unreactive, they can be stored as potential sources of energy. Elementary hydrogen is an example of a high energy species that can be stored indefinitely under proper conditions. Although the mechanisms have not been completely elucidated for the photochemical oxidations of solutions of transition metal salts studied by Heidt and co-workers,<sup>8</sup> they apparently involve secondary reactions of high energy species formed either by excitation or dissociation from the original absorber.

### Conclusion

If photochemical energy is to be stored for sub-

(6) R. M. Noyes, *J. Am. Chem. Soc.*, **77**, 2042 (1955).

(7) R. M. Noyes, *ibid.*, **78**, 5426 (1956).

(8) See for example L. J. Heidt and A. F. McMillan, *ibid.*, **76**, 2125 (1954).

sequent release, the primary act of absorption must be followed by secondary processes. If these produce an excited electronic or metastable isomeric form of the original absorber or of some other chemical species, the prospects are not good that the energy can be stored for long periods and released as desired. If the absorption of a quantum causes a dissociation into fragments when the only available subsequent reaction is combination with other fragments, some energy can be stored by physical trapping of these fragments; however, this type of system is not particularly promising either. The best prospect for a storage reaction probably involves a chemical reaction of the excited absorber or of a fragment from it with another chemical species; the product of this reaction must be metastable so that it can be stored until needed and can then liberate considerable energy during regeneration of the starting material.

If such a photochemical storage reaction is to be reasonably efficient, the subsequent secondary reactions must be initiated in a period of  $10^{-8}$  second or less after the original absorption. This period is too short for direct experimental measurement of concentration changes, but theoretical considerations indicate that transient diffusion terms may cause the relative yields of competing reactions to differ from the values predicted by steady state kinetic equations.

**Acknowledgment.**—The development of these ideas was assisted in part by the U. S. Atomic Energy Commission under Contract No. AT(30-1) 1314.

## PHOTODECOMPOSITION OF COMPLEX OXALATES. SOME PRELIMINARY EXPERIMENTS BY FLASH PHOTOLYSIS

By C. A. PARKER AND C. G. HATCHARD

*Admiralty Materials Laboratory, Holton Heath, Poole, Dorset, England*

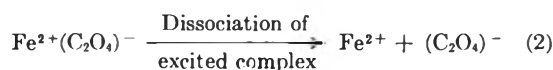
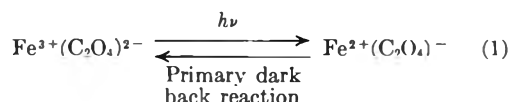
*Received July 11, 1968*

Long-lived intermediates have been observed in solutions of the ferrioxalate, cobaltioxalate and uranyl oxalate ions when they are subjected to flash photolysis. The compound produced in neutral ferrioxalate solutions disappears at a rate which is nearly independent of the concentration of ferrioxalate. Under these conditions, therefore, the rate controlling stage is not the expected bimolecular reaction between radical and ferrioxalate, and the simple reaction scheme originally proposed is not sufficient to explain the results. Some possible additional rate-controlling stages have been considered including dissociation of an excited ferrioxalate ion (or ferrous-radical complex) and dissociation of a complex between ferric iron, oxalate ion and oxalate radical. Oxygen is found to intervene directly in the photochemically initiated reaction chain, not only in neutral solution, but also in acid solution where, with high concentrations of ferrioxalate and continuous irradiation at low intensity, it has little effect. As examples of systems involving efficient electron transfer reactions, both cobaltioxalate and uranyl oxalate as well as ferrioxalate are worth much more detailed investigation.

### Introduction

Earlier experiments with potassium ferrioxalate solutions were concerned with the mechanism of the photodecomposition mainly in so far as it affected the working of the ferrioxalate actinometer.<sup>1,2</sup> For actinometry, solutions in dilute mineral acid are used and under these conditions the main photoactive species present are the mono- and dioxalato compounds.<sup>3</sup> Taking the mono-oxalato

ion as an example, the mechanism was originally represented by the following simple equations involving excitation, dissociation of the excited ion to give the oxalate radical and reaction of this with more ferrioxalate ion<sup>3</sup>

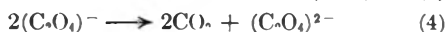
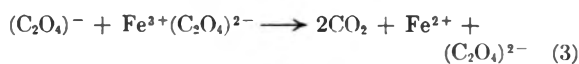


(1) C. A. Parker, *Proc. Roy. Soc. (London)*, **A220**, 104 (1953).

(2) C. G. Hatchard and C. A. Parker, *ibid.*, **A235**, 518 (1956).

(3) C. A. Parker, *Trans. Faraday Soc.*, **60**, 1213 (1954).





Analogous schemes can be written for the di- and trioxalato complexes.

Under normal conditions the radical is apparently consumed almost exclusively by reaction (3) the radical-radical reaction occurring, if at all, only at very high light intensities and low ferrioxalate concentrations.

This type of scheme would explain all the facts then known, but it was not the only scheme which would do so. For example, Livingston<sup>4</sup> had suggested that an excited ferrioxalate ion might be the intermediate species which reacted with the second normal ferrioxalate ion. Some more experiments were made to try to identify the intermediate. Very dilute solutions of ferrioxalate frozen in liquid nitrogen were found to decompose on irradiation with the formation of a brown substance, and examination by paramagnetic resonance<sup>5</sup> showed that free radicals were present which were tentatively assumed to be the oxalate radicals ( $\text{HCO}_2$  or  $\text{HC}_2\text{O}_4$ ) which had been trapped in the glass. The investigation is now being continued in fluid solutions at room temperature and the preliminary results obtained are reported in this paper.

### Experimental Method

The apparatus was of the now-familiar type using photoelectric monitoring at single wave lengths. It was found advantageous to use a mercury lamp, or other intense line source, for the monitoring beam. This allowed narrow monochromator slits to be used, thus reducing the signal from the scattered light received from the continuum of the flash tube. The flash tubes (krypton-filled, internal diameter 0.9 cm., inter-electrode distance 11.0 cm.) were specially made from tungsten-quartz seals obtained from Messrs. Thermal Syndicate. Working with capacities up to 25  $\mu$  F. at 2000-5000 v., flash half-lives between 15 and 50  $\mu$  sec. were obtained. Sixty-ml. quantities of the solutions were placed in the fused silica cylindrical cell (40 mm. diam., 75.5 mm. optical depth) and de-aerated either by boiling under high vacuum or by passage of oxygen-free nitrogen. The percentage transmission of the solutions was measured before flashing on a spectrophotometer at the appropriate wave length and this value was used to adjust the vertical scale of the oscilloscope when the cell had been placed in the monitoring beam. The firing switch opened the camera shutter and simultaneously started the oscilloscope horizontal sweep. The flash-tube was fired automatically, after a short, preset delay. The vertical transmission scale and the time-scale of the oscilloscope were calibrated photographically in separate experiments. Enlarged prints of the photographs of experiments and calibrations were prepared, and the latter were used to construct transparent perspex grids from which the transmission of the test solution at any time after flashing could be read directly by superimposing the grid on the test photograph. In many experiments it was arranged that release of the firing switch initiated a second oscilloscope sweep. This occurred several hundred milliseconds after the first sweep and served to record the final transmission of the solution.

**Results Obtained with Ferrioxalate Solutions.**—It was assumed originally that the reaction in the above scheme which might be slow enough to measure at room temperature was the bimolecular reaction between oxalate radical and excess ferrioxalate ion (reaction 3). It was therefore expected that an instantaneous fall in absorption would occur on

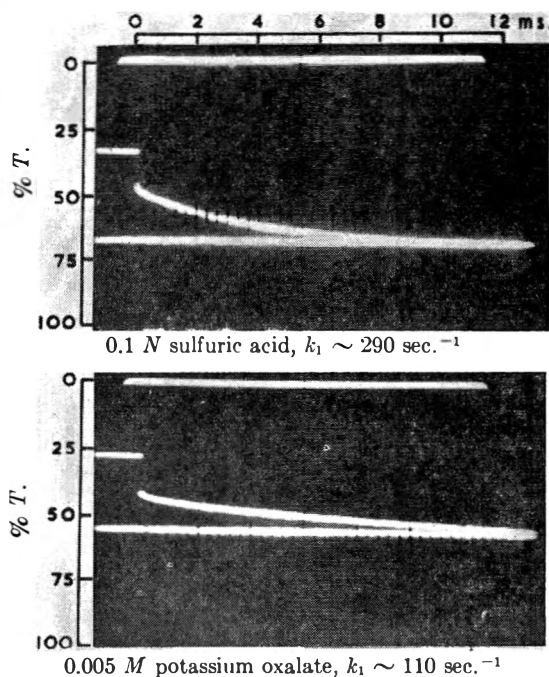


Fig. 1.—Comparison of acid and neutral oxalate solutions (both solutions contained 0.00003 *M* potassium ferrioxalate with the indicated additions—monitoring wave length 313  $\mu$ , energy of flash 127J).

flashing, corresponding to the initial dissociation of one ferrioxalate ion, and that this would be followed by a slow fall in absorption as the radical reacted with more ferrioxalate ion. Preliminary tests at a monitoring wave length of 313  $\mu$ , in both acid and neutral solutions (Fig. 1), did in fact show these features. More detailed experiments were made in neutral solutions containing various concentrations of ferrioxalate in the presence of an excess of oxalate (under these conditions the iron is combined almost entirely as the trioxalato-complex). At wave lengths of 313 and 366  $\mu$  an instantaneous fall in absorption was observed on flashing followed by a slow fall similar to that shown in Fig. 1. At 405 and 436  $\mu$ , however, there was a rise in absorption on flashing, indicating that the intermediate compound absorbs more strongly

TABLE I  
VARIATION OF REACTION VELOCITY WITH  
CONCENTRATION OF FERRIOXALATE  
(Neutral Solution)

Initial compn. of soln. Potassium ferrioxalate $\times 10^4, M$	Potassium oxalate $\times 10^4, M$	Monitoring wave length, $\mu$	Velocity constant calcd. as 1st order sec. <sup>-1</sup>	2nd order 1. mole <sup>-1</sup> sec. <sup>-1</sup> $\times 10^6$
30	5	313	170	17
			140	26
			155	21.5
100	5	366	180	4.1
			210	3.8
			240	7.8
300	10	405	210	5.2
			260	1.4
			220	1.7
600	10	436	240	1.55
			260	0.62
			300	0.71
			280	0.66

(4) R. S. Livingston, *THIS JOURNAL*, **44**, 601 (1940).

(5) D. J. E. Ingram, W. G. Hodgson, C. A. Parker and W. T. Rees, *Nature*, **176**, 1227 (1955).

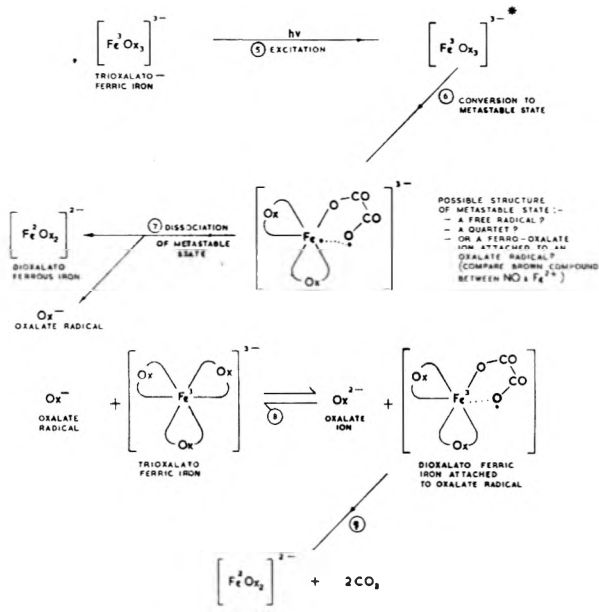


Fig. 2.—Photodecomposition of ferrioxalate, possible stages in the reaction: Alternative to (7) and (8) is the direct reaction of the metastable ion with a second ion of ferrioxalate possibly with the formation of a long-lived intermediate containing two iron atoms.

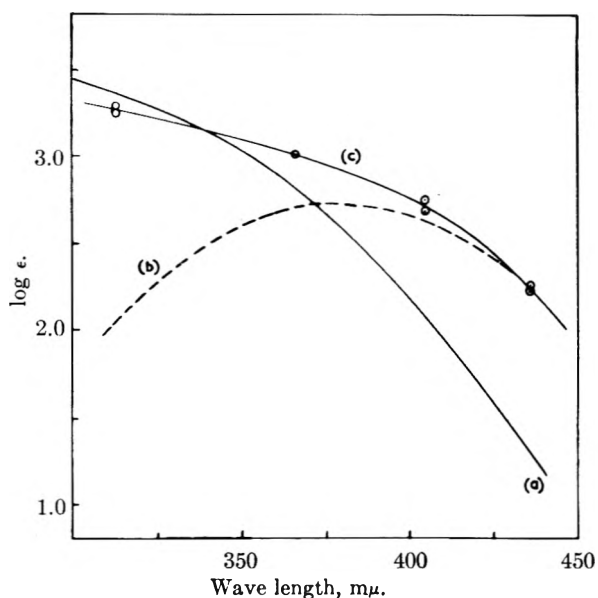


Fig. 3.—Absorption spectra in aqueous solution: (a) potassium ferrioxalate; (b) and (c) intermediate compound calculated in two ways (*i.e.*, assuming that it is formed before or after the reduction of the second molecule of ferrioxalate).

than ferrioxalate. First- and second-order plots were made from each trace (the latter on the assumption that the two reactants were oxalate radical and residual ferrioxalate ion) and reaction velocity constants calculated. The values obtained in different experiments are shown in Table I.

The first-order constants vary by a factor of less than 2 when the initial ferrioxalate concentration varies by a factor of 20. On the other hand the second-order "constants" vary by a factor of about 30. Quite clearly what was observed was not the bimolecular reaction between radical and un-

changed ferrioxalate. The reaction observed was either a first-order reaction with some minor complications or a second-order reaction not involving unchanged ferrioxalate. The original reaction scheme therefore was modified to include some possible first-order stages as shown in Fig. 2. The possible structures of the intermediate compounds are discussed below. The essential additional features in this scheme are either (a) the formation and dissociation of a metastable excited state of the ferrioxalate ion (reactions 6 and 7) or (b) the dissociation of the primary reduction products of the second ferrioxalate ion (reaction 9). Both dissociations would show first-order kinetics and one of them is assumed to be the reaction actually observed. Making one or other of these assumptions, the initial and final optical densities and the intermediate optical density (immediately after the flash), have been used to calculate the absorption spectrum of the intermediate compound formed. This absorption spectrum calculated on each of the two assumptions, is compared in Fig. 3 with that of the ferrioxalate ion itself. Whichever of the two assumptions is made, the compound shows a greater absorption than ferrioxalate in the blue and violet regions, and in this respect is similar to the orange brown substance formed by low temperature irradiation.

**Variation of Light Dosage.**—The effect of size of flash was investigated using 0.0001 *M* ferrioxalate in 0.005 *M* oxalate. The solutions were all monitored at 405  $\mu$  where the intermediate compound absorbs more strongly than the ferrioxalate from which it is formed. Up to the point where the ferrioxalate was completely consumed the initial rise in absorption increased. Beyond this point there was no further increase in the rise in absorption (in fact there was a slight decrease). This suggests that the bimolecular reaction involving the second molecule of ferrioxalate had already taken place at the intermediate stage and that the slow reaction observed was the dissociation of the reduced ferrioxalate ion (reaction 9 in the modified scheme). However, the evidence is not entirely conclusive because other complicating factors appear beyond the point of complete decomposition, *e.g.*, the slight decrease in initial rise of optical density, the increase in the rate of the slow reaction and the decrease in the over-all change in optical density. These changes indicate that some other reaction starts to become significant beyond the point of complete decomposition.

The discontinuity at the point where the flash is great enough to cause complete decomposition is even more marked in more dilute solutions (*e.g.*, 0.0003 *M* potassium ferrioxalate containing no added potassium oxalate and monitored at 313  $\mu$ ). Beyond the flash dosage required to produce complete decomposition (*i.e.*, complete consumption of ferrioxalate at the end of the *slow* reaction), the concentration of absorbing compound present decreases and yet, at the same time, its rate of disappearance increases very considerably. Apparently we have to deal here with a bimolecular reaction involving some other non-absorbing product of the initial dissociation which is present in increasing

concentration as the light available in the flash increases.

**Nature of Possible Intermediate Compounds.**—From the preliminary results obtained it is clear that when an "excess" of light is available in the flash, more than one reaction has to be taken into account. The situation is complicated by the inner filter effect of the intermediate formed in the early part of the flash and by its possible excitation and reaction. More work is therefore required before it can be decided unambiguously whether the slow reaction normally observed takes place before or after the reduction of the second molecule of ferrioxalate. However, the results obtained at lower light doses (Table I) show that the slow stage reaction does not involve the bimolecular reaction of radical with residual ferrioxalate.

If the rate-controlling step takes place before the reduction of the second molecule of ferrioxalate, it must represent the decomposition of some form of excited ferrioxalate ion (reaction 7 in Fig. 2). One might consider that after initial excitation the ferrioxalate ion passes over to a metastable state analogous to the triplet state in aromatic molecules, in which the electrons forming one of the bonds between an oxalate ion and the central atom become unpaired. This structure would effectively be a quartet state, taking the other unpaired electron of the central atom into account. It is considered more likely that the rupture of the oxalate-iron bond would be accompanied by the immediate reduction of the central atom, and the result would then effectively be a ferro-oxalate ion still attached to a free radical. (In this connection, its color brings to mind the color of the compound between ferrous iron and nitric oxide, which is also an odd electron molecule.) The rate-controlling reaction would then be the dissociation of the ferro-oxalate radical complex, this event being followed by the rapid reaction between radical and a second molecule of ferrioxalate.

The reduction of the second molecule of ferrioxalate is represented in Fig. 2 as occurring in two stages, the first of which involves the substitution of an oxalate ion by an oxalate radical. The electron transfer within the resulting complex and the ejection of the residue as  $\text{CO}_2$  might then be the rate-controlling reaction actually observed. Alternatively direct electron transfer from the radical to the trioxalatoferrous ion would produce the unstable trioxalatoferrous ion, and the dissociation from this of one molecule of oxalate might be the observed slow reaction. Other possibilities can also be imagined. For example an alternative to reactions 7 and 8 is the direct reaction of an excited ferrioxalate ion with a normal iron to give a complex containing two iron atoms. Further data are required before a choice can be made between these and other possibilities.

The limiting rate of the bimolecular reaction between radical and ferrioxalate ion calculated from the encounter frequency<sup>7</sup> corresponds to a reaction half-life of about  $6 \mu$  sec. with the most dilute solution of ferrioxalate used. This is just too short to observe with the present flash tube (half-life  $\sim 15 \mu$  sec.).

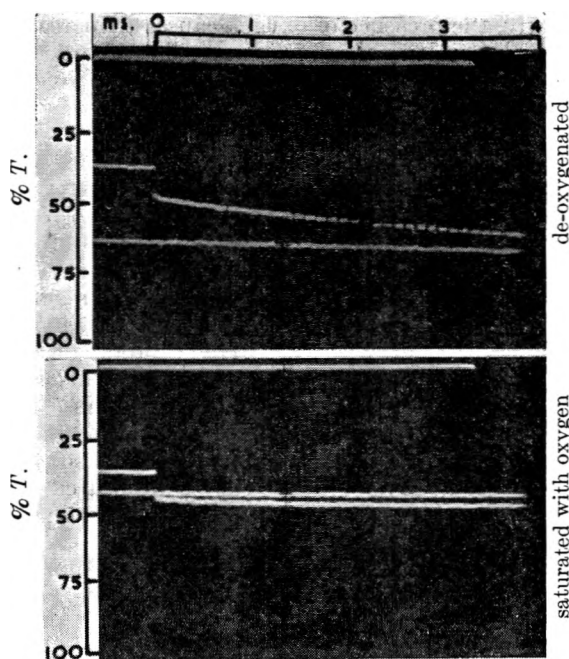
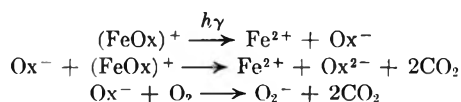


Fig. 4.—Effect of oxygen in acid solution: (0.00003  $M$  potassium ferrioxalate in 0.1  $N$  sulfuric acid—monitoring wave length  $313 \text{ m}\mu$ ; energy of flash 77J).

**Effect of Oxygen.**—In strongly acid solutions of comparatively concentrated potassium ferrioxalate (0.006  $M$ ) and with low light intensities as normally used in chemical actinometry, oxygen has only a very small effect on the quantum yield of ferrous iron.<sup>3</sup> In contrast to this it was found that, with the high light dose from the flash tube, oxygen takes a major part in the reactions (see Fig. 4). Although the initial fall in absorption is  $313 \text{ m}\mu$  is little affected, the subsequent slow fall is suppressed and the absorption then slowly rises again (the second horizontal trace was made after several hundred milliseconds). By repeatedly flashing the solution it was found that ferrioxalate was still present long after it would normally all have been consumed had oxygen not been present. The effect of oxygen can be explained by its competition with unchanged ferrioxalate for the free radical formed in the first stage of the reaction



Further oxidation of ferrous iron would then occur *via*  $\text{HO}_2$  or  $\text{OH}$  radicals (*cf.* Posner<sup>6</sup>) with the reformation of monoxalatoferrous iron. This process would continue until all the oxalate had been consumed.

In neutral solution rather similar results were obtained with monitoring light of wave length  $313 \text{ m}\mu$  although the reoxidation was apparently somewhat more rapid. This was to be expected from the results of previous work at low light intensity<sup>3</sup> where it was shown that oxygen rapidly reoxidizes ferrioxalate in neutral solution. However, the results obtained with monitoring light of wave length  $405 \text{ m}\mu$  do not fit in with this simple theory.

(6) A. M. Posner, *Trans. Faraday Soc.*, **49**, 382 (1953).

Firstly, the presence of oxygen causes an increase in the absorption of the intermediate compound formed by the flash, and secondly the over-all consumption of ferrioxalate (as indicated by the over-all decrease in absorption at  $405\text{ m}\mu$ , measured several hundred milliseconds after the flash) is apparently increased. The oxygen must react rapidly with the primary products of photolysis to produce a compound having a greater absorption at  $405\text{ m}\mu$  than that produced in the absence of oxygen, and after the subsequent slow reaction, products are formed which absorb little at  $405\text{ m}\mu$  but strongly at  $313\text{ m}\mu$ . These products (*i.e.*, those present several hundred milliseconds after the flash) are clearly not ferrioxalate whose concentration at this point must have been reduced considerably in view of the decrease in absorption at  $405\text{ m}\mu$ . The situation is complicated still further by the observation that after standing for several minutes the absorption at  $405\text{ m}\mu$  rose again to a value greater than that corresponding to the initial concentration of ferrioxalate before flashing.

It is clear from these limited experiments that, in dilute neutral solutions at high light intensities, the effect of oxygen is *not* simply to reoxidize the ferrooxalate to ferrioxalate. Different intermediates are formed and an entirely new stable product is finally formed (the solution had a pale red-brown color). The new compound is possibly the ferrate ion ( $\text{FeO}_4^{2-}$ ), which is red in color, or some other complex of tetravalent iron.

**Other Complex Oxalates.**—Some preliminary results were obtained by flashing solutions of cobalti-

oxalate and uranyl oxalate. Cobaltioxalate is particularly interesting in showing three distinct stages, an initial "instantaneous" rise in absorption (at  $313\text{ m}\mu$ ), a rapid (though measurably slow) fall in absorption and finally a slow fall in absorption. It could be suggested that the rapid reaction is the bimolecular one and that the slow reaction represents the dissociation of reduced cobaltioxalate. There are of course other possibilities, and in any event the cobaltioxalate reaction is well worth further study.

Uranyl oxalate also produces long lived intermediates on flashing. In the presence of an excess of oxalic acid the absorption change is reversible, as might be expected from the known results at low light intensities where the over-all reaction corresponds to the decomposition of oxalic acid only, the valency of the uranium remaining unchanged. Without the excess of oxalic acid permanent changes in absorption occur and these depend on whether or not oxygen is present.

Chromioxalate, which is formally analogous to ferrioxalate and cobaltioxalate, does not undergo permanent change under continuous irradiation. It was however subjected to flash photolysis in the hope that reversible absorption changes might be observed. None was detected and it must be concluded that the excited state of this oxalate is shorter than the flash time ( $15\text{ }\mu\text{sec.}$ ).

The authors thank Dr. E. J. Bowen, F.R.S., for much helpful advice and discussion. This paper is published by permission of the Admiralty.

(7) J. Q. Umberger and V. K. La Mer, *J. Am. Chem. Soc.*, **67**, 1099 (1945).

## PHOTOREDUCTION OF METHYLENE BLUE. SOME PRELIMINARY EXPERIMENTS BY FLASH PHOTOLYSIS

BY C. A. PARKER

*Admiralty Materials Laboratory, Holton Heath, Poole, Dorset, England*

*Received July 11, 1968*

Dilute solutions of methylene blue in dilute sulfuric acid are reversibly bleached by flash photolysis, giving rise to two distinct transient species. One species produced by excitation with visible light has a lifetime of the same order as that of the flash ( $15\text{--}20\text{ }\mu\text{sec.}$ ) and is tentatively identified as the lowest triplet state of the dyestuff. The second species is produced by excitation with light of short wave length. Under the conditions investigated it has a lifetime of about  $400\text{ }\mu\text{sec.}$  It is tentatively identified as the semi-quinone free radical produced by electron transfer from a water molecule. On irradiation with red light, in the presence of ferrous sulfate, the "triplet" species is no longer evident. An excited state of the dyestuff (probably the triplet state) reacts to form the semi-quinone free radical which rapidly undergoes dismutation. Approximate rate constants have been determined for the dismutation reaction and for the reaction of ferric iron with the semi-quinone. These reactions are discussed in relation to the slow reoxidation of leuco-methylene blue, and proposals made for further experiments with this and other dyestuffs.

### Introduction

A considerable amount of work has been published on the photo-bleaching of solutions of methylene blue or thionine under continuous irradiation. With many reducing agents the reactions proceed at comparatively high quantum efficiency, and using ferrous sulfate it is well known that the photoreduction is reversible in the dark. The relative rates of the various reactions involved are still not known with certainty, and in particular it has not been established whether appreciable concentrations of the "half-reduced" semi-quinone

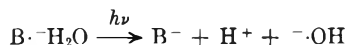
free radical are present in the photostationary state under irradiation at normal light intensities. An investigation of the photoreduction of these dyestuffs therefore was started using the method of flash photolysis, with the object of learning more about the primary photo-processes involved and the primary reduction products formed. Some preliminary experiments have been made with the methylene blue-ferrous sulfate system and the results of these preliminary experiments are described in this paper.

### Experimental

The apparatus and procedure was similar to that used for the investigation of the complex oxalates<sup>1</sup> employing photoelectric monitoring at single wave lengths. Provision was made for the insertion of glass filters between the flash tube and the reaction cell so that bands of wave lengths from the flash tube emission could be selected for excitation. All solutions were de-oxygenated either by boiling under high vacuum or by passing a current of oxygen-free nitrogen.

**Wave Lengths Used For Excitation.**—Dilute solutions of methylene blue in dilute sulfuric acid (0.01 *N*), in the absence of reducing agent, were found to produce long-lived metastable states on flash excitation. If the full light from the flash tube was used, two species were formed which disappeared at markedly different rates. One decayed in a time of the same order as that of the light flash (15-20  $\mu\text{sec.}$ ) while the second had a half-life, under the particular conditions used, of about 400  $\mu\text{sec.}$  If the light of short wave lengths was prevented from entering the solution by using a glass reaction cell, only the short-lived species was formed. The same short-lived species also was produced by ultraviolet light alone, provided that wave lengths shorter than about 250  $m\mu$  were excluded by the use of a Chance OX7 filter.

By analogy with other aromatic systems it is tentatively assumed that the short-lived species is the lowest triplet level of the methylene blue. Since the primary interest at present is in photosensitisation with visible light, the second species produced by short wave length ultraviolet light has not yet been investigated in detail. However, its absorption spectrum (in so far as it is known) is similar to that of the semiquinone of methylene blue produced during photoreduction (see below) and it is tentatively assumed that it is formed by electron transfer brought about by the short wave lengths



The reaction by which it is consumed (half-life approximately 400  $\mu\text{sec.}$  under the conditions of the test) would then correspond to its reoxidation by the hydroxyl radical. The formation of the latter would also account for the fact that a small consumption of methylene blue occurred after each flash when the short wave lengths were included, although no consumption was observed with the longer wave lengths alone.

The further experiments to be described were all performed with an orange filter inserted between the flash tube and the reaction cell, so that only light within the red absorption band of the dye-stuff was used for excitation. Using a solution of  $3 \times 10^{-6}$  *M* methylene blue in 0.095 *N* sulfuric acid it was found that the excited state absorbs less strongly than methylene blue at the longer wave lengths but more strongly at the shorter wave lengths. Owing to its short lifetime it is substantially stationary state concentrations of the excited state which are observed and it is not therefore possible to calculate its exact absorption spectrum from the data at present available. The general

(1) C. A. Parker and C. G. Hatchard, *THIS JOURNAL*, **63**, 22 (1959).

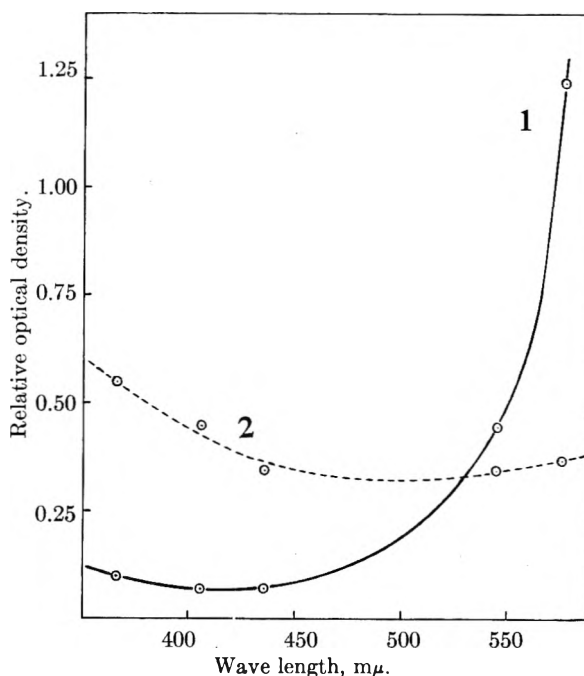
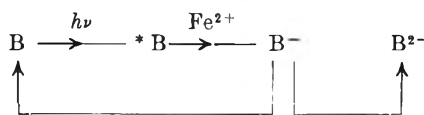


Fig. 1.—Approximate relative absorption spectra (in dilute mineral acid): 1, methylene blue; 2, semiquinone.

shape of its absorption curve is similar to that of the semiquinone which is described in more detail below (see Fig. 1, curve 2).

**Effect of Ferrous Sulfate.**—The previous set of experiments was repeated in the presence of 0.095 *M* ferrous sulfate. Under these conditions the short-lived excited state of methylene blue is no longer observable. The dyestuff reacts to produce a compound of much longer life-time. The absorption changes observed by monitoring at various wave lengths can be interpreted in terms of the reaction scheme



in which an excited state of the methylene blue is reduced by the ferrous sulfate to the semi-quinone which dismutates to give methylene blue and leuco-methylene blue. On this basis the data have been used to calculate the approximate absorption spectrum of the semi-quinone intermediate. This is compared in Fig. 1 with the corresponding part of the absorption spectrum of methylene blue.

The present data are not sufficient to decide whether it is the triplet state of the methylene blue or its first excited singlet state which is actually reduced to the semiquinone. Owing to its longer life-time, the triplet state is, in the absence of other factors, more likely to be reduced. However, Porter<sup>2</sup> has reported that in the case of the quinones the primary act involves the singlet and not the triplet state. In this case the light absorbed from the flash included wave lengths below 250  $m\mu$  where with methylene blue the electron (or hydrogen atom) transfer reaction appears to be of equal importance. The present experiments with long

(2) G. Porter, *ibid.*, **63**, in press.

TABLE I  
RATE OF DISMUTATION REACTION (FROM SOLUTIONS MONITORED AT 405 m $\mu$ )

Methylene blue, $M$	Composition of soln. before flash		Sulfuric acid, $N$	Concn. of semiquinone immediately after flash, $M$	Rate constant for dismutation reaction, $k_d$
	Ferrous sulfate, $M$	Ferric ion, $M$			
$1.24 \times 10^{-4}$	0.08	$1.5 \times 10^{-4}$	0.08	$8.4 \times 10^{-6}$	$0.13 \times 10^{10}$
$1.24 \times 10^{-4}$	0.08	$1.5 \times 10^{-4}$	0.08	7.9	0.14
$1.24 \times 10^{-4}$	0.08	$1.5 \times 10^{-4}$	0.08	4.6	0.16
$2.96 \times 10^{-4}$	0.095	$1.8 \times 10^{-4}$	0.095	2.6	0.16
$1.24 \times 10^{-5}$	0.08	$1.5 \times 10^{-4}$	0.08	2.4	0.17
$1.24 \times 10^{-5}$	0.08	$1.5 \times 10^{-4}$	0.08	1.1	0.14

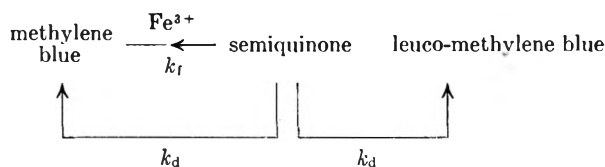
wave lengths show clearly that the triplet state is destroyed by the ferrous sulfate, but whether this reaction is simply deactivation or whether it is responsible for the formation of the semi-quinone has not yet been determined. It is of interest that Oster and Wotherspoon<sup>3</sup> have concluded, from the results of experiments on the photoreduction of methylene blue by EDTA in red light, that the first excited singlet state is not involved. They estimate that the lifetime of the excited state which takes part in the reaction is equal to or greater than 87  $\mu$ sec. This is considerably greater than the lifetime of the excited state of methylene blue observed in the present experiments. However, Oster and Wotherspoon's results were obtained in solutions at pH values in the region 4.8–11.0 which have not yet been investigated by flash photolysis. Some very recent results obtained with thionine<sup>4</sup> have shown that at low ferrous sulfate concentrations the semiquinone of this dyestuff is formed by a route other than the direct reaction of the singlet state.

On the assumption that the intermediate compound observed in the presence of ferrous sulfate is in fact the semiquinone, some data obtained by using varying flash intensities have been used to determine the approximate rate constant for its dismutation. The results (Table I) indicate a value of  $0.1\text{--}0.2 \times 10^{10}$  l. mole<sup>-1</sup> sec.<sup>-1</sup> which is of the same order as the maximum possible rate calculated from the encounter frequency<sup>5</sup> ( $0.6 \times 10^{10}$  l. mole<sup>-1</sup> sec.<sup>-1</sup>) and shows that the dismutation reaction takes place with very high efficiency.

**Effect of Added Ferric Iron.**—The ferric iron produced during the reduction of methylene blue by ferrous sulfate slowly reoxidizes the leuco-methylene blue in the dark. The ferric iron should also be capable of oxidizing the semiquinone radical but the degree to which this reaction occurs will of course depend on its rate as compared with that of the dismutation reaction and it will be accelerated by the addition of extra ferric iron to the solution. The solutions used to obtain the results shown in Table I above did in fact contain additional small quantities of ferric iron which were present in the ferrous sulfate used. The effect of ferric iron was neglected in calculating the rate of the dismutation reaction and it was therefore necessary to

confirm that the direct oxidation by ferric iron was in fact slow under these conditions.

A series of experiments were carried out in which increasing quantities of ferric sulfate were added to the solution before flashing and the over-all changes in optical density which occurred (a) during the flash and (b) during the subsequent simultaneous reactions of the semiquinone were measured. Thus if the two simultaneous reactions of the semiquinone are represented as



and if  $A_1$ ,  $A_2$  and  $A_3$  represent, respectively, the optical densities of the solution before the flash, immediately after the flash and after all the semiquinone has reacted (but before the leuco-methylene blue has reacted appreciably), then

$$\frac{A_1 - A_3}{A_1 - A_2} \left(1 - \frac{E_S}{E_B}\right) = \frac{1}{2} \left[1 - \frac{k_f C_f}{k_d C_S} \log_e \left(1 + \frac{k_d C_S}{k_f C_f}\right)\right]$$

in which  $E_S$  and  $E_B$  are, respectively, the extinction coefficients of the semiquinone and methylene blue and  $C_f$  and  $C_S$  are, respectively, the concentrations of ferric iron and semiquinone immediately after the flash.

The results obtained with various added concentrations of ferric iron are shown in Table II. The value of  $(1 - E_S/E_B)$  was calculated from the results obtained on the first solution, to which a small quantity of phosphate had been added and in which therefore the "free ferric iron" concentration was assumed to be considerably reduced (that it was in fact very low was confirmed by the very slow rate of reoxidation of leuco-methylene blue in this solution). The remaining values of  $(A_1 - A_3)/(A_1 - A_2)$  and the corresponding calculated values of  $k_f C_f/k_d C_S$  indicate that the ferric iron oxidation of the semiquinone is not significant below ferric iron concentrations in the region of  $5 \times 10^{-4}$   $M$ . Taking into account the comparatively large experimental errors involved in measuring the traces, the constancy of the values for  $k_f/k_d$  lends support to the assumptions made.

From these results it is possible to write down the more complete reaction scheme for the photoreduction of methylene blue by ferrous sulfate in approximately 0.09  $N$  sulfuric acid as

(3) G. Oster and N. Wotherspoon, *J. Am. Chem. Soc.*, **79**, 4836 (1957).

(4) C. A. Parker, *Nature*, **182**, 245 (1958).

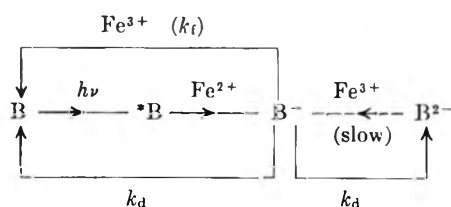
(5) J. Q. Umberger and V. K. La Mer, *J. Am. Chem. Soc.*, **67**, 1099 (1945).

TABLE II

## EFFECT OF FERRIC IRON ON THE DEGREE OF DISMUTATION

Initial concn. of methylene blue =  $3.13 \times 10^{-6} M$ ;  $[FeSO_4] = 0.093 M$ ;  $[H_2SO_4] = 0.093 N$ ;  $(1 - E_S/E_B)$  calculated from the first experiment = 0.70;  $(E_B - E_S) = 0.73 \times 10^6$  l. per mole for 7.55 cm.

$\frac{[Fe(SO_4)_{3/2}]}{= C_t, M}$	$(A_1 - A_2)$	$C_s \times 10^6$	$\frac{A_1 - A_2}{A_1 - A_2}$	$\frac{k_t C_t}{k_d C_s}$	$\frac{k_t}{k_d} \times 10^4$
$1.70 \times 10^{-4}$ (containing $M NaH_2PO_4$ )	0.204		0.716	Very small	...
$1.78 \times 10^{-4}$	.203	2.8	.704	0.003	...
6.10	.200	2.7	.652	.024	1.1
11.9	.195	2.7	.580	.069	1.6
31.3	.191	2.6	.433	.24	2.0
101	.191	2.6	.298	.59	1.5
294	.168	2.3	.119	2.4	1.9
907	.126	1.7	.006	Large	...



$$\frac{d[L]}{dt} = K[L]$$

in which

$$k_d = 1.5 \times 10^9 \text{ l. mole}^{-1} \text{ sec.}^{-1}$$

$$k_t = 2.4 \times 10^6 \text{ l. mole}^{-1} \text{ sec.}^{-1}$$

both of these reactions being very much faster than the reoxidation of leuco-methylene blue in the dark (under the conditions investigated). Since the experiments were all carried out in the presence of a high and substantially constant concentration of sulfate ion the value of  $k_t$  does not of course represent the true rate constant for uncomplexed  $Fe^{3+}$ .

### Discussion

One additional reaction needs to be considered, that is, the reverse of the dismutation reaction, which if very rapid, would lead to an appreciable equilibrium concentration of the semiquinone in partly reduced methylene blue solutions in the dark. From electrometric data Michaelis and co-workers<sup>6</sup> have concluded that in partly reduced solutions of methylene blue in dilute acid a few per cent. of the total dyestuff can be present as the semiquinone. On this basis the complications introduced by the reverse of the dismutation reaction can be safely neglected for the purpose of calculating the approximate values of  $E_S/E_B$  and  $k_t$  in Table II.

If the equilibrium concentration of the semiquinone in partly reduced solutions is appreciable, the reoxidation of leuco-methylene blue in the dark may proceed by two reactions, *i.e.*, the direct reaction with ferric iron, and by the reaction of ferric iron with the equilibrium concentration of semiquinone. Thus

$$\frac{d[L]}{dt} = k_p[Fe][L] + \frac{1}{2}k_t[Fe][S]$$

where  $[S]$  is the equilibrium concentration of semiquinone. Observations of the rate of re-formation of methylene blue after the completion of the dismutation reaction provide a very approximate value for the constant  $K$  in

For solutions containing between  $3 \times 10^{-4}$  and  $3 \times 10^{-3} M$  ferric iron (where about  $1/4$ – $1/3$  of the dyestuff was in the reduced form after dismutation)  $K$  was apparently of the order 0.03–0.1  $\text{sec.}^{-1}$  (although it did not appear to be directly proportional to the ferric iron concentration). Assuming a value of 0.03 for  $K$  at  $(Fe^{3+}) = 3 \times 10^{-4} M$ , it is calculated that the maximum possible equilibrium concentration of semiquinone is less than 0.1% of the total dyestuff present. This is so much less than the value quoted by Michaelis and co-workers that some complicating factors in the reoxidation of leuco-methylene blue are indicated and this reaction calls for a careful investigation.

The thionine-ferrous iron system was investigated by Rabinowitch<sup>7</sup> under photostationary conditions and to explain the results a reaction scheme similar to that described above for methylene blue was set up. He deduced values for  $k_d$  and for  $k_s$  or  $k_p$  (velocity of oxidation of semiquinone or the leuco compound by ferric iron). The values compared with those obtained in the present work, are

	Methylene blue (present work)	Thionine (Rabinowitch)
Dismutation	$1.5 \times 10^9$	$0.5-2.5 \times 10^6$
Reverse of dismutation	$\leq 10^4$	$2.5 \times 10^4$
Oxidation of semiquinone	$1.8 \times 10^6$	$2.5 \times 10^3$
Oxidation of leuco compd. (apparent)	30-100	

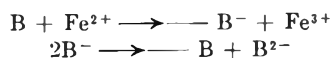
Clearly a reinvestigation of the thionine system using the method of flash photolysis would be most desirable.

It is of interest to compare the oxidation of ferrous iron by methylene blue with the reduction of ferric iron by oxalate. Both reactions require the over-all transfer of two electrons, and both therefore involve the formation of an intermediate "half reduced" free radical state. With the former reaction, this intermediate state is the semiquinone which disappears primarily by dismutation except in the presence of high concentrations of product ( $Fe^{3+}$ ). With the latter reaction, the intermediate is the oxalate radical ion (or some complex of it) and this only disappears by dismutation at low concentrations of reactant ( $Fe^{3+}$ ). At high con-

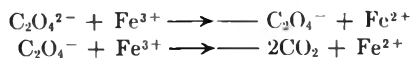
(6) L. Michaelis, M. P. Schubert and S. Granick, *J. Am. Chem. Soc.*, **62**, 204 (1940).

(7) E. Rabinowitch, *J. Chem. Phys.*, **8**, 551 (1940).

centrations of reactant it reacts further with the reactant, an apparently negligible amount then undergoing dismutation, thus



compared with



### Conclusions

The results obtained in the present experiments are only of a preliminary nature, they cover only a very limited range of conditions and require more precise investigation. They do however show that the high rate of the dismutation reaction of the semiquinone intermediate can be the dominating factor governing the course of the photoreduction

of this type of dyestuff. Further work is now required to determine: (a) whether this holds also for other ionic forms of the intermediate (*i.e.*, when photoreduction is carried out in solutions of widely different *pH* value), (b) whether it is true also for other dyestuffs such as thionine, (c) to what degree other oxidizing or reducing agents can compete with the dismutation reaction by reacting with the semiquinone and (d) to determine the effect of polymeric substances upon the dismutation reaction (*i.e.*, in systems previously investigated by Wotherspoon and Oster<sup>8</sup> by methods involving continuous irradiation at normal light intensities).

The author thanks Dr. E. J. Bowen, F. R. S., for much helpful advice and discussion. This paper is published by permission of the Admiralty.

(8) N. Wotherspoon and G. Oster, *J. Am. Chem. Soc.*, **79**, 3992 (1957).

## EVIDENCE OF PHOTOREDUCTION OF CHLOROPHYLL *IN VIVO*†

BY J. W. COLEMAN AND E. RABINOWITCH

*Photosynthesis Laboratory, Department of Botany, University of Illinois, Urbana, Ill.*

*Received July 11, 1958*

It has been suggested repeatedly that chlorophyll plays in photosynthesis the role of a "photo-enzyme"—more specifically, a "photo-oxido-reductase"—mediating, in the light-excited state, the transfer of hydrogen atoms (or electrons) from a reductant with a low reduction potential to an oxidant with a low oxidation potential, thus storing a part of its excitation energy as chemical energy of the products.

From this point of view, it would be very important to find evidence of reversible formation of reduced (or oxidized) chlorophyll during photosynthesis. Observations of changes in the absorption spectrum of photosynthesizing organisms in light provide one possible approach to this problem.

Sensitive measurements of the "difference spectrum" (difference between the absorption spectra of dark and illuminated cells), by a method similar to that first used by Rabinowitch<sup>1</sup> for the study of photodissociation of halogen molecules, were first made by Duysens<sup>2-6</sup> later by Witt,<sup>7-10</sup>

Lundegårdh,<sup>11</sup> Strehler *et al.*,<sup>12</sup> Chance<sup>13</sup> and Kok.<sup>14-16</sup> With the exception of Kok, these authors covered only the spectral region <660 *mμ*, and did not find in it any changes attributable to reversible transformations of chlorophyll, but only such associated with the reversible oxidation of cytochromes (perhaps, also with reversible reduction of pyridine nucleotides), and with the transformations of "unknown pigments." In the case of the green alga, *Chlorella*, the most prominent change was of the last-named type, involving the weakening, in light, of a band at 480 *mμ* and growth of a band at 515-520 *mμ* (Duysens, Witt, and others).

The appearance of a band at 520 *mμ* was suggestive of certain known transformations of chlorophyll—particularly, of its conversion into a "pink" reduced product, observed in solution by Krasnovsky,<sup>17</sup> Evstigneev, *et al.*,<sup>18</sup> and Bannister.<sup>19</sup> The name "eosinophyll" is suggested for this compound.

However, this interpretation was not considered by Duysens, or Witt, and this for two reasons: (a) their failure to observe a correlated decrease in absorption in the red (or blue-violet) band of

(†) Work supported by a grant from the Office of Naval Research.  
(1) E. Rabinowitch and H. L. Lehman, *Trans. Faraday Soc.*, **167**, 689 (1935).

(2) L. N. M. Duysens, Thesis, Univ. of Utrecht, 1952.

(3) L. N. M. Duysens, *Nature*, **173**, 692 (1954).

(4) L. N. M. Duysens, *Science*, **120**, 353 (1954).

(5) L. N. M. Duysens, *ibid.*, **121**, 210 (1955).

(6) L. N. M. Duysens, W. J. Huiskamp, J. J. Vos and J. M. van der Hart, *Biochim et Biophys. Acta*, **19**, 188 (1956); see also "Research in Photosynthesis," Interscience Pub., New York, N. Y., 1957, pp. 164-175.

(7) H. T. Witt, *Naturwiss.*, **42**, 72 (1955); *Z. physik. Chem.*, **4**, 120 (1955).

(8) H. T. Witt, *Z. Elektrochem.*, **59**, 10, 981 (1955).

(9) H. T. Witt, *ibid.*, **60**, 1148 (1956).

(10) H. T. Witt, "Research in Photosynthesis," Ed. by Hans Graffron, *et al.*, Interscience Publishers, New York, N. Y., 1957, pp. 75-84.

(10a) H. T. Witt and R. Moraw, *Z. physik. Chem.*, **12**, 343 (1957); **13**, 113 (1957).

(10b) H. T. Witt, R. Moraw and A. Miller, *ibid.*, **13**, 113 (1957).

(11) H. Lundegårdh, *Physiol. Plantarum*, **7**, 575 (1954).

(12) B. L. Strehler and V. M. Lynch, *Arch. Biochem. et Biophys.*, **70**, 527 (1957); "Research in Photosynthesis," Interscience Publishers, New York, N. Y., 1957, pp. 85-99.

(13) B. Chance and L. Smith, *Nature*, **175**, 803 (1955); "Research in Photosynthesis," Interscience Publishers, New York, N. Y., 1957, pp. 179-197.

(14) B. Kok, *Biochim. et Biophys. Acta*, **22**, 401 (1956).

(15) B. Kok, *Nature*, **179**, 583 (1957).

(16) B. Kok, *Acta Botanica Neerlandica*, **6**, 316 (1957).

(17) A. A. Krasnovsky, *Compt. rend. (Doklady) Acad. Sci. U.S.S.R.*, **60**, 421 (1948); **61**, 91 (1948).

(18) V. B. Evstigneev and V. A. Gavrilova, *ibid.*, **91**, 899 (1953).

(19) T. T. Bannister, Thesis, Univ. of Illinois, 1958; presented at the Endicott House Conference on Photochemistry of Condensed Systems, Sept. 1957, in press.



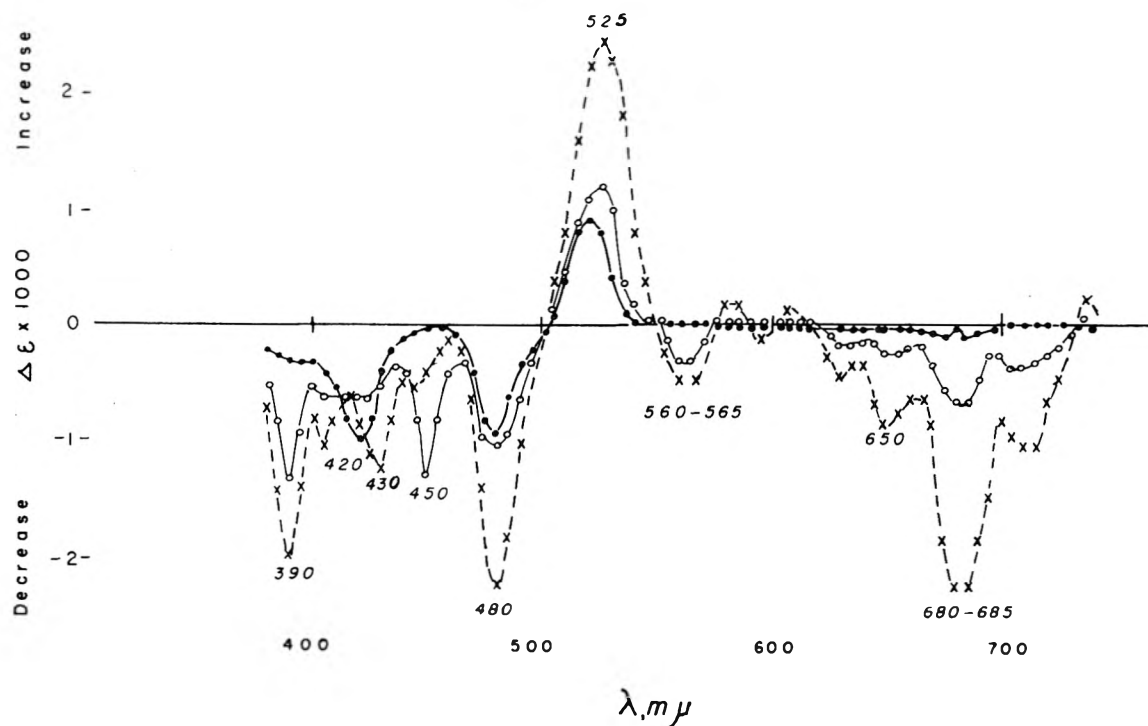


Fig. 1.—Difference spectra of *Chlorella pyrenoidosa* ("thin" suspension in carbonate buffer, no. 9) in white light ( $\lambda_{\max} = 555$   $m\mu$ ) of different intensities: dots, incident light intensity,  $3.4 \times 10^{14} h\nu/(\text{sec.} \times \text{cm.}^2)$ ; circles, incident light intensity,  $12.0 \times 10^{14} h\nu/(\text{sec.} \times \text{cm.}^2)$ ; crosses: incident light intensity,  $31.4 \times 10^{14} h\nu/(\text{sec.} \times \text{cm.}^2)$ .

chlorophyll, and (b) the apparent correlation of the absorption increase at 520  $m\mu$  with the absorption decrease at 480  $m\mu$ —a region where chlorophyll *a* does not absorb. (The location of the blue absorption peak of chlorophyll *b* *in vivo* is not well known, but it may lie near 475  $m\mu$ ; however, that of the reduced form of chlorophyll *b* is located, according to Evstigneev, at 560, and not at 520  $m\mu$ .)

Coleman and Holt have first measured in our laboratory the difference spectrum of illuminated *Chlorella* cells up to 720  $m\mu$ , and found a "negative" band (a decrease in absorption in light), at 680  $m\mu$ —*i.e.*, in the position of the main absorption band of chlorophyll *a* *in vivo*.<sup>20</sup> The relation of this "negative" band to the "positive" band at 520  $m\mu$  remained, however, uncertain, because of the use of different sources of actinic light for measurement in the two spectral regions.

Following are some results of the continuation of this study by Coleman. The instrumentation was essentially the same as in 20; improvements (including the provision of a device to measure the difference spectrum of scattering) will be described elsewhere.

Figure 1 gives a selection of the results. It represents difference spectra of *Chlorella* cells suspended in bicarbonate buffer no. 9, for three intensities of white light [ $3.4$ ,  $12$  and  $31 \times 10^{14}$  incident quanta per sec. per  $\text{cm.}^2$ ]. The curves correspond to completely reversible and practically steady changes, observed after 1–3 minutes of illumination. With longer illuminations, slower, and not immediately reversible, changes in absorption began

to occur. One of the important points, which will have to be elucidated by further studies, is to what extent the observed difference spectra can be considered as characteristic of the *steady state* of photosynthesis, and to what extent they may be affected by induction phenomena.

One would not expect changes characteristic of the transient induction phase to remain constant during the period from 1 to 3 minutes after the beginning of illumination; also, one would expect such changes to be strongly affected by the duration of the preceding dark period, temperature and other factors, which Coleman found to have little influence on the changes represented in Fig. 1. Nevertheless, a closer study is needed to separate clearly steady-state effects from transient phenomena. In particular, the sometimes complicated relations observed by Coleman between the amplitude of a difference band and the intensity of illumination may be due, at least in part, to the superposition of transient changes upon the steady state effect.

Figure 1 reveals a complicated picture of a difference spectrum containing about a dozen "negative" and two (or three) "positive" bands; each of these may represent a potentially valuable piece of information concerning reversible changes in the photocatalytic apparatus of the cell.

The ordinates in Fig. 1, marked  $1000 \times \epsilon$ , are fractional changes in absorption,  $\Delta I/I$  (expressed in tenths of a per cent.). For a change  $dc$  in the concentration of an absorber with molar absorption coefficient  $\epsilon$ , in a vessel 1 cm. deep, we can write

$$\epsilon = \frac{d \log (I_0/I)}{dc} = -\frac{I_0}{I} \frac{dI}{I_0 dc} = -\frac{dI}{I dc}$$

Since we deal with small changes ( $\Delta I/I < 0.3\%$ ),  $\Delta I/\Delta c = dI/dc$ , and consequently

$$-\frac{\Delta I}{I} = \epsilon \Delta c \quad (1)$$

(20) T. W. Coleman, A. S. Holt, and E. Rabinowitch, "Research in Photosynthesis," Interscience Publishers, New York, 1957, pp. 68–74.

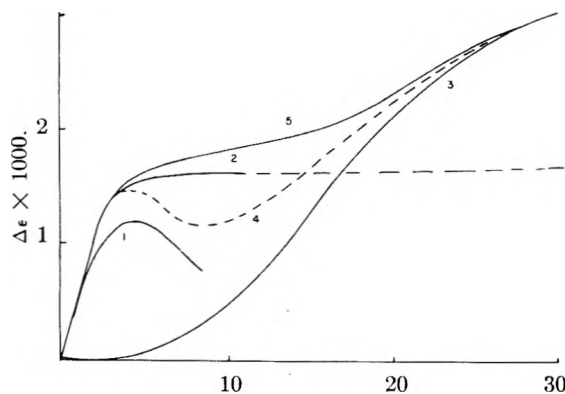


Fig. 2.—Dependence of the intensity of difference spectrum bands on light intensity: 1, effect saturated in low light, then declining (420  $m\mu$ ); 2, effect saturated in low light, then constant (hypothetical); 3, effect disappearing in low light, approaching saturation in high light (680  $m\mu$ ); 4, superposition of (1) and (3) (480  $m\mu$ ); 5, superposition of (2) and (3) (520  $m\mu$ ).

In other words, the curves in Fig. 1 are proportional to the molar extinction curves of appearing (or disappearing) molecular species. However, this is only true if their bands *do not overlap*. If a disappearing molecular species is replaced, molecule-for-molecule, by another one, with an overlapping band, then

$$-\frac{\Delta I}{I} = (\epsilon_1 - \epsilon_2)\Delta c \quad (2)$$

The case of a certain molecular species merely changing its *state*, causing a *shift* of its absorption band (or a change in its *shape*) is a special case of (2). Overlapping of an appearing band with a disappearing band can lead to a difference spectrum with several (positive and negative) peaks. (For example, replacement of a sharp band by a broader band in the same position obviously will result in a difference spectrum with two positive peaks on two sides and a negative peak in the middle.) It is thus not permissible to consider each peak in the difference spectrum as evidence of a molecular species with an absorption band in this position.

In our difference spectrum in Fig. 1, the peak at 520–530  $m\mu$  almost certainly corresponds to a new species with a band in this position (although its shape on the short wave side may be affected by overlapping with the negative band at 480  $m\mu$ ). The same is likely to be true of the strongest “negative” bands—at 420 and 480  $m\mu$  in weaker light, and at 390, 480 and 680  $m\mu$  in strong light.

The negative peaks at 420 and 560–565  $m\mu$  are the ones attributed by Duysens, Lundegårdh, and Chance to the reversible oxidation of a cytochrome (perhaps, cytochrome f) in light. They are relatively prominent in weak light, but soon become light-saturated. In fact, the main cytochrome difference band at 420  $m\mu$  has the highest observed intensity in the weakest light used,  $3.4 \times 10^{14} h\nu/(\text{sec. cm.}^2)$ , and then declines (Fig. 2). It may be that the cytochrome changes are largely induction phenomena, which are more rapidly completed in stronger light.

In weak actinic light, the most prominent bands are those observed by Duysens, *et al.*—the negative bands at 420  $m\mu$  (cytochrome f?), and at 480  $m\mu$ ,

and the positive band at 520  $m\mu$ ; we recall that the latter two bands were attributed by Duysens to the transformation of an “unknown pigment.” In stronger light, new negative bands appear at 390 and 450  $m\mu$ ; the former continues to grow with increasing light intensity, while the latter becomes saturated and disappears almost completely at the higher intensities.

However, what interests us most is the appearance, in strong light, of a system of negative bands in the red region. These bands, absent in weaker light (in agreement with Duysens’ observations!) become, in the strongest light used ( $31 \times 10^{14} h\nu/(\text{sec.} \times \text{cm.}^2)$ ), of equal prominence with the negative band at 480  $m\mu$  and the positive band at 520  $m\mu$  (the peak of the latter is shifted in strong light, toward 530  $m\mu$ ).

In Fig. 3, the difference spectrum of *Chlorella*, in the strongest light used by Coleman, is shown again and compared with the difference spectrum of chlorophyll *a* and its “pink” reduction product “eosinophyll” [cf. Krasnovsky *et al.* and Evstigneev and Gavrilova,<sup>18</sup>], as determined by Bannister<sup>19</sup> in our laboratory, using ether as solvent and phenylhydrazine as reductant. The scale on the right applies to Coleman’s dashed curve; that on the left, to Bannister’s solid curve. The latter was shifted on the frequency scale so as to make the two red peaks coincide, as is customary in the comparison of spectra *in vivo* and *in vitro*. The ordinates are marked  $\Delta\epsilon$  on both sides, although those on the left represent absolute changes in optical density, and those on the right, relative changes in transmission (as explained above, for small changes the latter, too, are proportional to changes in concentration of the absorbing species).

The coincidence of the peaks at 430, 525 and 680  $m\mu$  in the two curves in Fig. 2 makes it permissible to assume, as a working hypothesis, that the difference spectrum of *Chlorella* in “strong” light does contain, as one of its main components, the spectral change caused by the reduction of chlorophyll *a* to a compound of the type of Krasnovsky’s “eosinophyll”. (The negative peak at 650  $m\mu$  and the positive peak at 575  $m\mu$  may be due to a similar transformation of chlorophyll *b*!).

Other component processes obviously must be postulated, among them the one that predominates in weaker light: the conversion of a compound absorbing at 480  $m\mu$  into one absorbing at 520  $m\mu$ . Figure 2 shows that the intensity dependence of the 480 and the 520  $m\mu$  peaks make them appear as superpositions of two changes—one saturated in relatively weak light, the other only in much stronger light, similarly to the 680  $m\mu$  peak.

As to the nature of the compound, responsible for the 480→520 shift, the temptation is great to implicate a *carotenoid*. The shifting of the absorption band from 480 to 520  $m\mu$  could be caused, for example, by the addition of one double bond to the conjugated system—*i.e.*, by a reversible oxidation. Another possibility is to relate the 480→515  $m\mu$  band shift to the strong displacement the carotenoid bands show upon transition from molecular dispersion to the colloidal form (the long wave

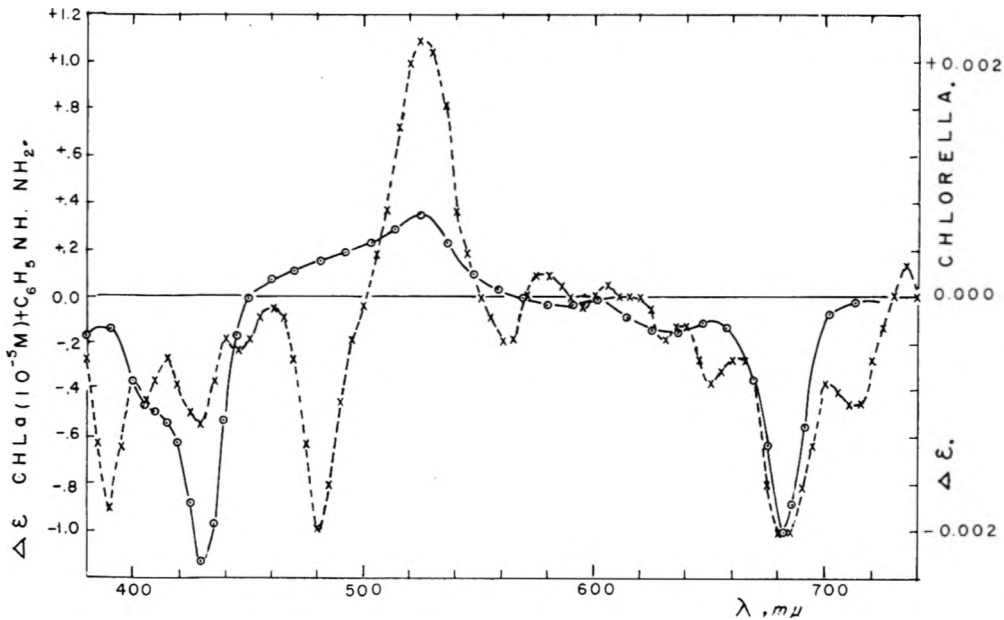


Fig. 3.—Comparison of difference spectra of *Chlorella* [at  $31.4 \times 10^{14} \text{ } h\nu/(\text{sec. cm.}^2)$ ] (scale at right—relative change in transmission) with that of chlorophyll *a* solution in ether in the presence of phenylhydrazine (scale at left—absolute change in optical density). Adjusted so that the two red peaks coincide.

band of colloidal carotene  $\beta$  in water lies at 510–535  $m\mu$ ). Equally strong shifts are caused by association of carotenoids with highly polarizable molecules (e.g., the absorption band at carotene  $\beta$  in  $\text{CS}_2$  lies at 521  $m\mu$ ). One difficulty of the hypothesis is that the principal carotenoids of green cells have, *in vitro*, absorption spectra with 2 or 3 peaks (e.g., carotene  $\beta$  in ether, at 478 and 449  $m\mu$ ). The difference spectrum of *Chlorella* <480  $m\mu$  is quite complex; it does show a band at 450  $m\mu$ , but this band is absent in low light, when the 480  $m\mu$  peak already is prominent.

If one postulates, as a working hypothesis, that the negative difference bands around 680  $m\mu$ , as well as a large part of the positive difference band at 530  $m\mu$ , are caused by a reversible reduction of chlorophyll *in vivo* to an analog of Krasnovsky's "pink" intermediate, then two observations appear significant. (a) Saturation of these changes occurs in (white) light of about  $5 \times 10^{15} \text{ } h\nu/(\text{cm.}^2 \text{ sec.})$ , corresponding to about  $5 \times 10^3$  lux. This is approximately the order of magnitude of light intensity needed to saturate photosynthesis in *Chlorella*. (A variety of values have been given in the literature for the latter intensity—ranging from 2 to  $20 \times 10^3$  lux). (b) The roughly extrapolated maximum of the difference effect at 680  $m\mu$  is about 0.3% (maximum actually observed effect, 0.23%). Calculation shows that this corresponds to the disappearance of one chlorophyll molecule out of about 300–400. The similarity of this number with the number of molecules in the "photosynthetic unit," as suggested, e.g., by measurements of Thomas and co-workers<sup>21</sup> on the effect of particle size on the activity of chloroplasts, is suggestive: photosynthesis appears saturated when one chlorophyll molecule in each "unit" is in the decolorized state.

(21) J. B. Thomas, D. H. Blaauw and L. N. M. Duysens, *Biochem. Biophys. Acta*, **10**, 230 (1953).

The sigmoid shape of the 680  $m\mu$  curve in Fig. 2 suggests that in the light-limited state of photosynthesis, chlorophyll is not markedly bleached. One can suggest that in this state chlorophyll is photo-reduced only to the unstable intermediate (semiquinone?)—whose existence is clearly indicated by the kinetics of the Krasnovsky reaction (cf., e.g., Bannister<sup>19</sup>)—which is practically instantaneously re-oxidized to chlorophyll. Only when light saturation of photosynthesis sets in, does the intermediate accumulate in amounts which permit some of it to dismutate, forming the more stable, pink "eosinophyll."

ADDENDUM: Since the presentation of this paper at the Endicott House Symposium in September, 1957, a detailed paper by Kok<sup>16</sup> appeared, describing difference spectra between 310 and 820  $m\mu$  observed in different strains of *Chlorella*, *Scenedesmus*, *Nitzschia*, *Nostoc*, and in chloroplast suspensions. (Kok's technique was based on the use of flashing actinic light, with absorption measurements made between flashes). While Kok's pictures of the difference spectra show striking general similarity to our Fig. 1, individual spectra display a considerable variety, particularly in the long wave region. In general, the same three negative bands—650, 680 and 705  $m\mu$  (cf. Fig. 1)—appear in this region. However, only in a few of Kok's pictures is the 680  $m\mu$  band predominant; more often it is the 705  $m\mu$  band, which Kok first<sup>14</sup> considered particularly significant, because it could be associated with a type of chlorophyll molecules able to serve as ultimate "energy sinks" in the resonance energy transfer chain. Later, Kok<sup>16</sup> became concerned with the possibility that the several band peaks in the red region can be caused by band shifts or changes in shape, rather than by the disappearance (or appearance) of separate bands. Obviously, more

extensive, systematic studies will be needed to secure the interpretation of even the main positive and negative difference bands; but we feel that

in difference spectra of the shape of those in Fig. 1, the prominent negative peak at  $680\text{ m}\mu$  definitely indicates reversible bleaching of chlorophyll.

## STUDIES OF THE PHOTOINITIATED ADDITION OF MERCAPTANS TO OLEFINS. IV. GENERAL COMMENTS ON THE KINETICS OF MERCAPTAN ADDITION REACTIONS TO OLEFINS INCLUDING *CIS-TRANS* FORMS

BY C. SIVERTZ

*The University of Western Ontario, London, Canada*

Received July 11, 1958

Some aspects of previous work are drawn together to illustrate some common problems in free radical kinetics with particular reference to termination. It is shown how useful information can be elicited by the study (a) of the attack of a common radical on various substrates and (b) of different radicals on a common substrate. Reference is made to a mechanism for "buried" radicals. Finally, a preliminary report is made of a new technique which employs *cis* and *trans* forms to help penetrate the micro kinetics of a radical attack on  $\pi$  bonds.

### Introduction

Since the advent of a quantitative approach to free radical chemistry in terms of the measurement of absolute rate constants, much effort and ingenuity has been spent on the "isolation" of a given radical so that its termination fate and action on functional groups may be unambiguously interpreted. This neat arrangement cannot easily be achieved nor is it always desirable, so that one is usually involved with two primary radicals at least. These in turn may attack several functional groups yielding other radicals in side reactions which can soon produce intractable equations.

In the work to be described, the object has been primarily to learn about radicals, not to elucidate a particular mechanism, no matter how complex.

The reactions chosen involve the free radical addition of mercaptans to various olefins, for example,  $\text{CH}_3\text{SH} + \text{CH}_2=\text{CH}_2 \rightarrow \text{CH}_3\text{SCH}_2\text{CH}_3$ . Several reasons influenced this choice after some necessary preliminary facts were known. First the propagation steps, attack and transfer, are ordinarily very fast for mercaptan addition so that a long kinetic chain producing a single main product is ensured. A long chain permits neglect of termination reaction products compared to the main chain products. Secondly, we hoped to make studies of the same basic process in both liquid and gas phase. Even  $\text{CH}_3\dot{\text{S}}$  radicals terminate without the ministrations of a third body in the gaseous phase thus avoiding a termination complication in that phase. For example, this is not true for the gaseous addition of  $\text{HBr}$  to olefins.<sup>1</sup> Finally one can be assured that the field of bio-kinetics will welcome any and all knowledge about the chemistry of mercaptans.

If one is to draw conclusions from rate measurements concerning the specific activity of radicals and relate the structures involved, it is essential that *absolute* constants be measured since the overall rates of such reactions always involve at least a termination constant in addition to propagation. Consequently in the work described a dilatometer-

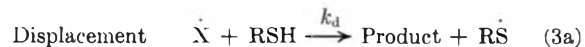
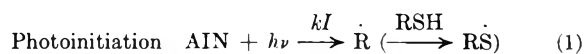
sector technique was employed, descriptions of which may be found elsewhere.<sup>2</sup>

### Basic Equations

A set of basic equations for a given reaction cannot be given *a priori*. Even the termination of methyl radicals in the gas phase required hundreds of man hours of research time before it was possible to assert that the mechanism is  $\text{CH}_3 + \text{CH}_3 \rightarrow \text{C}_2\text{H}_6^*$ . Some are not yet convinced.

Preliminary work involving product analysis, but not termination products, with the system under discussion, suggested the following were the main reactions. We will not complicate the preliminary kinetics with another reaction reversing (2) which was discovered in gas phase work.

In the liquid phase, reactions were initiated by the photolysis of azoisobutyronitrile (AIN), and of mercaptan in the gas phase. The rate of initiation  $kI$  was determined as in ref. 3 and by NO in the gas phase.<sup>4</sup>



### Steady States

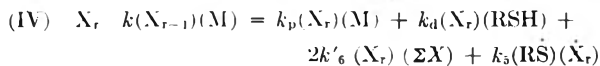
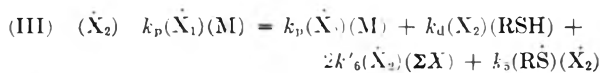
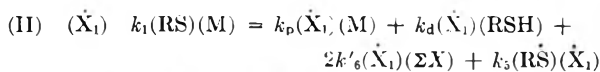
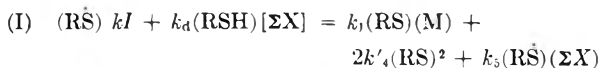
We will write the steady states for the general case of a monomer such as styrene, capable of propagation and hence the production of a family of  $\dot{\text{X}}$  radicals whose total concentration will be designated  $\Sigma \dot{\text{X}} = \dot{\text{X}}_1 + \dot{\text{X}}_2 + \dots + \dot{\text{X}}_\infty$

(2) J. P. Flory, "Principles of Polymer Chemistry," Cornell Univ. Press, Ithaca, N. Y., 1953, p. 148.

(3) R. Back and C. Sivertz, *Can. J. Chem.*, **32**, 1061 (1954).

(4) W. Andrews, Thesis, University of Western Ontario, London, Canada.

(1) K. Graham, Thesis, University of Western Ontario, London, Canada.



This statement assumes as usual that  $k_p$  and  $k_6$  are independent of radical size. In summing II to  $\infty$  we have a useful relation

$$k_1(\dot{R}S)(M) = k_d(\text{RSH})(\Sigma X) + \text{Partial terminations} \quad (7)$$

which permits us to express  $(\dot{R}S)$  in terms of  $(\Sigma X)$  provided the terminations ( $kI$ ) are relatively negligible.

### The Termination Problem

Summing the steady-state equations

$$kI = 2k'_4(\text{RS})^2 + 2k_5(\text{RS})(\Sigma X) + 2k'_6(\Sigma X)^2 \quad (8)$$

This can be expressed more usefully by defining  $2k'_4 = k_4$ ,  $2k'_6 = k_6$ ,  $k_5 = \phi \sqrt{k_4 k_6}$ , ( $\phi \geq 0$ ) and  $u^2 = k_4/k_6$ . Also through (7)  $(\dot{R}S) = [k_d(\text{RSH})/k_1(M)]/(\Sigma X)$ . We will henceforth write  $\Sigma X = \dot{X}$ , and we then have

$$\frac{kI}{k_6} = u^2 \left[ \frac{k_d(\text{RSH})}{k_1(M)} \right]^2 + 2u\phi \left[ \frac{k_d(\text{RSH})}{k_1(M)} \right] + 1 \left( \dot{X} \right)^2 \quad (9)$$

Any theoretical anticipation of  $\phi$  values will involve the same fundamental principles of quantum chemistry and kinetic theory as the much treated problem of "crossed" interaction of molecules through van der Waals forces where, for example, we find the geometric mean, corresponding to  $\phi = 1$ , applies to all London-force molecules. Where considerable difference in polarity or resonance stabilization exists this would not be true.  $\phi$  values as high as 150 have been observed,<sup>5</sup> but most reported values are much less.<sup>6</sup> There should also exist differences in  $\phi$  between gas and liquid phase, and steric effects could play a big role.

These considerations suggest two ways of dealing with (9).

(1) **Measure  $\phi$  and  $\mu$ .**—Isolate the  $\dot{X}$  radical by arranging  $(M) \gg \gg (\text{RSH})$ . Then  $(\dot{X}) = (kI/k_6)^{1/2}$  and the half-life sector measurements evaluate  $k_6$ ; similarly with  $\dot{R}S$  and  $k_4$ . The magnitude of  $\phi$  may then be evaluated from observations of rates where both radicals are present. This procedure was first applied by Melville, Robb and Tutton.<sup>7</sup> It can be followed readily in copolymer studies. In systems such as ours the success in isolating a radical depends on the ratio  $uk_d/k_1$ . If one has some approximate knowledge of this ratio, the isolation can perhaps be achieved at least for one of the pair.

(5) C. Walling, "Free Radicals in Solution," John Wiley and Sons, Inc., New York, N. Y., 1957, p. 323.

(6) L. Fateman, *Quart. Rev.*, **8**, 147 (1954).

(7) H. W. Melville, J. C. Robb and R. C. Tutton, *Disc. Faraday Soc.*, **10**, 5595 (1951).

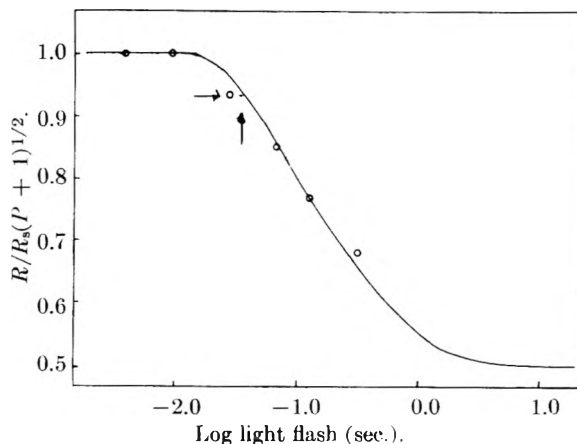


Fig. 1.—Cyclohexene *n*-BuSH reaction; half-life determination.

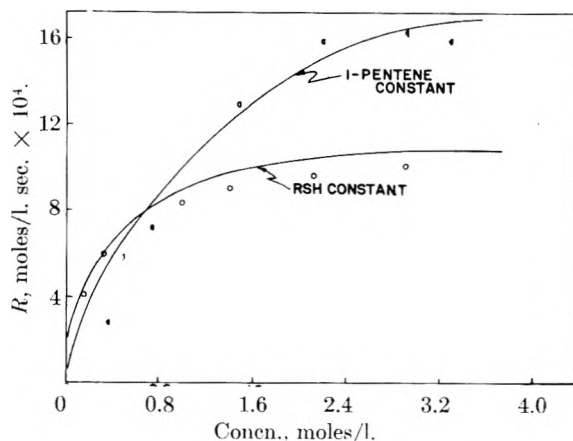


Fig. 2.—1-Pentene-*n*-butyl mercaptan; rates vs. concentration.

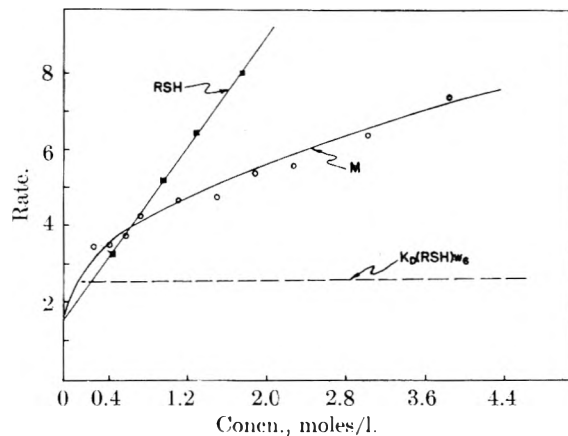


Fig. 3.

(2) **Assume the Geometric Mean  $\phi = 1$**  (which one may regard as the "ideal" law of termination).—A good approximate value of  $u$  may be employed based on a half-life for a large excess of  $M$  which gives  $k_6$  approximately and we may employ an estimated value of  $5 \times 10^{11}$  for normal thiyl radicals.<sup>8</sup> This permits us to explore the important concentration effects implicit in (9). We will see that certain important and firm conclusions can be drawn. Meanwhile, work is proceeding on a new

(8) M. Onyszczuk and C. Sivertz, *Can. J. Chem.*, **32**, 1034 (1954).

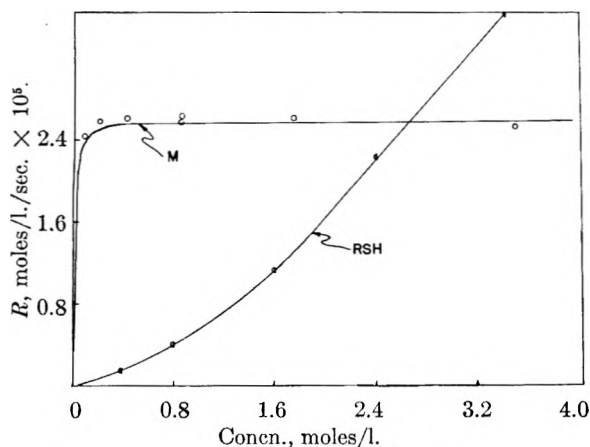


Fig. 4.—Cyclohexene *n*-butyl mercaptan; rates vs. concentration.

method for  $k_4$  referred to below. With this procedure we have from (9)

$$\dot{X} = \frac{\omega_6}{1 + \frac{\mu k_d(\text{RSH})}{k_1(\text{M})}} \quad (10)$$

where

$$\omega_6 = \sqrt{kI/k_6}$$

**Rates in the Liquid Phase.**—Benzene was employed as solvent. From (10) the rate

$$R = -\frac{\partial(\text{RSH})}{\partial t} = \frac{[k_d(\text{RSH}) + k_p(\text{M})](kI/k_6)^{1/2}}{1 + \frac{\mu k_d(\text{RSH})}{k_1(\text{M})}} \quad (11)$$

Figure 1 shows a typical determination of the half-life  $\lambda$  for radicals in the system cyclohexene *n*-butylmercaptan with a considerable excess of the olefin. From the relation  $k_6 = 1/kI\lambda^2$  we find  $k_6 = 1.3 \times 10^9$  l./moles sec.

Somewhat arbitrarily we can define addition reactions which can be interpreted by equation 11 as normal. Certain reactions described below require additional basic reactions and hence may be called abnormal. All velocity constants are expressed as liters/moles sec.

**Normal Reactions.** (a) **Figure 2. *n*-Butyl Mercaptan and 1-Pentene.**<sup>8</sup>—In this case

$k_p = 0$  and  $uk_d/k_1 = 0.5$  for a best fit to both curves  
 $k_6 = 5 \times 10^{10}$  and  $k_4$  estimated to be  $5 \times 10^{11}$  and hence  
 $u = 3$   
 $k_d = 1.4 \times 10^6$  and  $k_1 = 7 \times 10^8$

Since the term in the denominator of (10) ( $uk_d/k_1 = 0.5$ ) is of the order of unity, consequently, on increasing monomer with RSH constant, we pass from regions where the rate is monomer dependent to a plateau where monomer has no further significant influence and similarly with the variation of RSH with monomer fixed. This interpretation is one way of concluding that one is indeed dealing with consecutive reactions 2 and 3a involving independent or "free" radicals.

(b) **Figure 3. *n*-Butyl Mercaptan and Styrene.**<sup>9</sup>—In this case we find  $k_6 = 5 \times 10^8$ ,  $k_d = 1.24 \times 10^3$ . By analysis of the competition for butyl mercaptan radicals (between small amounts of

styrene with 1-pentene, when the former is added to the 1-pentene butyl mercaptan reaction) we conclude that  $k_1$  styrene is about  $180 \times k_1$  for 1-pentene or *ca.*  $1.2 \times 10^9$  l./moles sec.<sup>9</sup> Even when we estimate  $u$  to be about 30 this gives for  $uk_d/k_1 = 3 \times 10^{-5}$ . Consequently the rate can be expressed as

$$R = (k_d(\text{RSH}) + k_p(\text{M}))\omega_6 \quad (12)$$

From the gentle rise of rate with M at constant RSH, we calculate  $k_p = 230$  when  $(\text{RSH})/(\text{M}) = 1$ . This propagation will be due chiefly to  $\dot{X}_1$  at these concentrations. It is much larger than for the macro styryl radical, *viz.*, *ca.* 30 at 25°. Note that the termination constant  $k_6 = 5 \times 10^8$  is also several hundred times greater than for the macro styryl radical which is about  $2 \times 10^6$  at 25°. This is to be expected from previous work<sup>10</sup> here. Likewise, when RSH is varied we obtain a linear dependence over a wide range with an intercept which yields a value of  $k_p = 94$  much nearer the macro styryl value.

**Abnormal Reactions.** (c) **Figure 4. *n*-Butyl Mercaptan and Cyclohexene.**<sup>9</sup>—In this case  $k_p = 0$  and inspection shows at once that as in the case of styrene  $uk_d/k_1$  must be quite small. From  $k_6$  for cyclohexene we estimate  $u = 20$  in spite of which again  $uk_d \ll k_1$ . The sharp plateau in Fig. 4 with M varied, hence requires that the displacement reaction is possibly several hundred times less than the attack. Moreover, the variation in rate with RSH shows an opposite behavior from 1-pentene; accelerating at first with approximately the second power of the mercaptan. This has a reasonable explanation when we make these assumptions: (a) the radical attacks the double bond in such a manner as to introduce steric hindrance to the displacement reaction. The first work of Goering, *et al.*, on the addition of HBr to bromocyclohexene, supports this view<sup>11</sup>; (b) the low value of  $k_d$  for the mercaptan transfer of hydrogen makes the ordinary  $\alpha$ -hydrogen abstraction of relative importance; and (c) finally it follows from considerations discussed below for thiophenol, that a reverse step to basic equation 2 must also become important. (See equation 14 below.)

These and other details will be discussed in a paper devoted to the cyclohexene reaction.<sup>9</sup> Meanwhile, it will suffice to say that when assumptions (b) and (c) are included in the basic equations, we have for the rate

$$R = \frac{k_d(\text{RSH})\omega_6}{1 + \frac{\mu k_d(\text{RSH})}{k_1(\text{M})} + \frac{uk_{-1}}{k_1(\text{M})} + \frac{\sigma k_H(\text{M})}{k_d(\text{RSH})}$$

in which  $\sigma = \sqrt{k_7/k_6}$ ,  $k_7$  is the termination constant for the allylic radicals resulting from  $\alpha$ -dehydrogenation of cyclohexene, *viz.*, C1=CCCCC1.

$k_H$  is the velocity constant for such dehydrogenation and  $k'_d$  is the rather low mercaptan hydrogen transfer constant for the allylic radical. Now provided the last two terms of the denominator dominate, the results

(10) J. Longfield, R. Jones and C. Sivertz, *Can. J. Res.*, **B28**, 373 (1950).

(11) H. L. Goering, P. I. Abell and B. F. Aycok, *J. Am. Chem. Soc.*, **74**, 3588 (1952).

(9) A. Harrison, Thesis, to be published, University of Western Ontario, London, Canada.

shown in Fig. 4 follow. Pursuit of the implications of this in other related systems promises to throw special light on the micro process of double bond kinetics.

(d) **Figure 5. Thiophenol-1-Pentene.**<sup>12</sup>—In this case the rate is first order in both monomer and mercaptan. This mechanism in turn did not become clear until the gas phase kinetics, discussed below, showed the existence of the reverse

step in (2)  $\dot{X}_1 \xrightarrow{k_{-1}} \dot{R}S + M$ . The thiyl radical  $C_6H_5S$  now is resonance stabilized and hence again results in a weak composite radical  $\dot{X}$ . Indeed the reaction  $C_6H_5S + M \rightarrow \dot{X}$  should be endothermic when the composite radical represents a structure for the electron localized on the number two carbon. When this is incorporated in the steady-state equations, without propagation, we find in place of (7)

$$k_1^T(RS)(M_p) + k_1^e(RS)(M_e) = k(RSH)(\dot{X}) + k_{-1}^e(\dot{X}) + k_{T-1}^T(X) + \text{Terminations} \quad (13)$$

in which is shown the two alternative paths from the intermediate state, one leading to *cis* and the other to *trans*, when isomeric forms are relevant. We now have in place of (11)

$$\text{Rate} = \frac{k_d(RSH)\omega_6}{1 + \frac{u[k_d(RSH) + k_{-1}^e + k_{T-1}^T]}{k_1^T(M_T) + k_1^e(M)_e}} \quad (14)$$

and for the attack of thiophenyl radicals on 1-octene we conclude that  $uk_{-1}/k_1(M) > uk_d(RSH)/k_1(M) > 1$  and the rate is first order in both M and RSH as found

$$R = k_d(k_1/k_{-1})(M)(RSH)\omega_6/u \quad (15)$$

In other studies of *cis-trans* inversion in the liquid state (paper in preparation),<sup>13</sup> it has been shown that when *cis*-2-butene is employed instead of 1-octene, a *trans* form is soon formed. This was also found for the case of butyl mercaptanyl radical, but for this strong thiyl radical, the relative rates involved are such that  $k_d(RSH) > k_{-1}$ , and hence we do not observe the effects of the term  $k_{-1}(X)$  in the primary kinetics.<sup>12</sup> Nevertheless it is a very active process and the determination of  $k_1$  without considering  $k_{-1}$  will be too low (see below) as pointed out by Walling<sup>5</sup> in reference to our work and observed independently in this Laboratory.<sup>12,14</sup>

In the 1-pentene-thiophenol reaction half-lives have not been measured, and from (15) and Fig. 5 one can at present do no more than extract a value for  $k_d k_1/k_{-1}$ .

A study also has been made of the addition of thiophenol to *styrene*<sup>12</sup> in which the system returns to a "normal" behavior similar to butyl mercaptan-styrene. This is to be expected since now in spite of the "weak" thiyl radical,  $k_1 > k_d$  due to resonance stabilization in the composite radical,  $C_6H_5S-CH_2-\dot{C}H-C_6H_5$ .

(12) R. Pallen and C. Sivertz, *Can. J. Chem.*, **35**, 723 (1957).

(13) R. Townshend, Thesis, to be published, University of Western Ontario, London, Canada.

(14) C. Sivertz, W. Andrews, W. Elsdon and K. Graham, *J. Polymer Sci.*, **19**, 587 (1956).

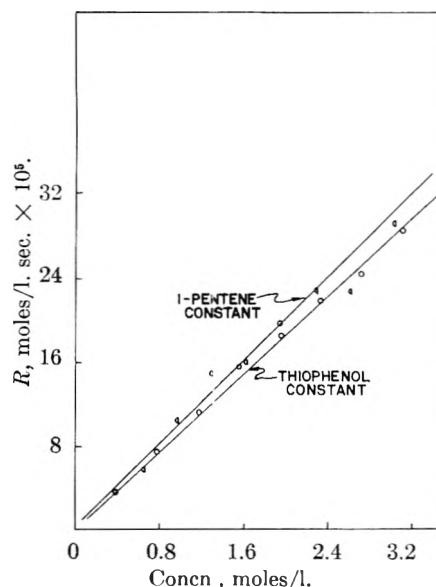


Fig. 5.—1-Pentene-thiophenol; rates vs. concentration.

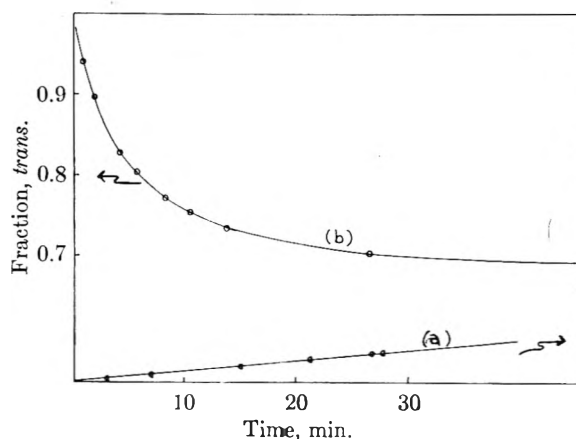


Fig. 6.—(a) Addition of  $CH_3SH$  to *cis*- and *trans*-2-butene; (b) simultaneous conversion of *cis* to *trans*.

### Gas Phase

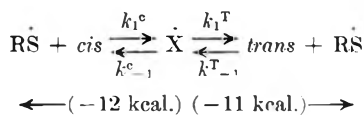
Preliminary studies, some previously reported<sup>14</sup> of the gas phase addition of methyl mercaptan to a series of olefins, have indicated that the kinetics responds to one additional basic equation which, as in the case of thiophenol, requires us to postulate an active dissociation of the composite radical  $\dot{X}$  whose steady state now requires equation 14 instead of (7), and the rate for a 1-olefin is found to be represented by equation 15 and for *cis*-2-butene by (14). The experimental evidence for this is as given: (a) a rate first order in both mercaptan and olefin<sup>15</sup> similar to Fig. 5; (b) an over-all negative activation energy<sup>14</sup>; (c) the appearance of *trans*-2-butene from *cis* as the addition reaction proceeds<sup>13,15,16</sup> (see Fig. 6); (d) preliminary measurements of the half-life with a semi-square wave character indicated a very high value for the termination constant *ca.*  $10^{12}$  l./moles sec.<sup>4</sup> If this is confirmed, it suggests  $CH_3S$  termi-

(15) P. Pallen, Thesis, to be published, University of Western Ontario, London, Canada.

(16) R. Townshend, R. Pallen and C. Sivertz, "The Mechanisms of Radical Induced *cis-trans* Inversion," paper presented at N. Y. meeting A.C.S., Sept. 13, 1957.

nation predominates as a consequence of a strong dissociation of the composite radical  $\dot{X}$ .

It should be noted that equation 15 has the form of a third-order process when one recalls that  $\omega_6/u = \omega_4$  represents the concentration of the thiy radical. There seems, however, little doubt that it concerns, so far as the half-life of the  $\dot{X}$  radical is concerned, a rather sticky collision, defined by  $k_{-1}$ . It should be recalled<sup>14</sup> from data on the over-all negative activation energy, that the exothermic enthalpy change for the process  $\text{CH}_3\dot{\text{S}} + \text{C}_2\text{H}_4 \xrightarrow{k_1} \text{X}$  is ca. 12 kcal. or roughly about half the  $\Delta H$  for the complete addition. On the other hand, for 2-butene,  $\text{cis} \rightarrow \text{trans}$   $\Delta H \div 1000$  cal. ( $T = 25^\circ$ ). We therefore have the following energetics in mind for the  $\text{cis-trans}$  radical induced inversion



The equilibrium constant for  $\text{cis} \rightarrow \text{trans}$  then is  $K = k_1^c k_{-1}^T / k_1^T k_{-1}^c$  which can be expressed  $K = \lambda k_1^c / k_1^T$ .

**Determination of the True Magnitude of the Attack Constant  $k_1$ .**—As pointed out above, observations of the inversion of  $\text{cis}$  to  $\text{trans}$  for the addition of butyl mercaptan to  $\text{cis-2-butene}$  in the liquid phase<sup>13</sup> prove that the attack constants deduced above for, e.g., 1-pentene are low. We now attempt to measure the "true" value for  $k_1$ .

We assume as implied in equation 13 that one form only of the composite radical ( $\dot{X}$ ) is involved in both the dissociation reaction  $k_{-1}(\dot{X})$  and the displacement reaction  $k_d(\text{RSH})(\dot{X})$ , and also that an attack on  $\text{cis}$  or  $\text{trans}$  results in the same intermediate. While these assumptions may not be correct, it follows from the energetics of  $\text{cis}$ ,  $\text{trans}$  that any values thus derived cannot be much in error.

Figure 6 represents the experimental results from preliminary observations made by Pallen<sup>15</sup> of the simultaneous rate of addition and formation of  $\text{trans}$  from  $\text{cis-2-butene}$  ( $T = 25^\circ$ ) the latter determined by stopping the reaction and making gas chromatographic analysis. Details of this in gas and liquid phase will be published. In 20 minutes while the  $\text{cis-trans}$  inversion has nearly reached equilibrium, the addition reaction has consumed only about 3% of the mercaptan. If one measures the ratio of these rates at zero time expressed in proper units one evaluates  $k_{-1}^T(\dot{X}) / k_d(\text{RSH})\dot{X}$ ; similarly by starting with the  $\text{trans}$  form  $k_{-1}^c \dot{X} / k_d(\text{RSH})(\dot{X})$  and hence the value for  $\lambda$  could be determined. An integrated expression

for the entire conversion of  $\text{cis}$  to  $\text{trans}$  may then be set up based on (13). This involves some quite complex kinetics to be discussed later. Meanwhile, two simplifying assumptions appear justified by the analysis, namely, that the principal termination is due to the  $\text{CH}_3\dot{\text{S}}$  radical ( $\omega_4$ ), and  $\lambda = 1$ . While the latter is obviously not true, from the magnitude of the equilibrium constant for  $\text{cis-trans}$  at  $25^\circ$  ( $K = 0.76$ ) and the energetics of the reaction,  $\lambda$  could not be far from unity.

The net rate of disappearance of  $\text{cis}$  may then be written

$$\frac{-d(\text{Mc})}{dt} = k_1^c (\text{Mc})(\text{RS}) - k_{-1}^c(\dot{X}) \quad (16)$$

and if we define  $(\text{Mc}) = (\text{Mc}^\circ \alpha)$ , substitution for ( $\dot{X}$ ) made from (13),  $(\text{RS}) = \omega_4$  and  $\lambda = 1$  we have

$$-\log [1 - (K + 1)\alpha] = \frac{k_1^T(K + 1)\omega_4}{2 \times 2.303} \times t \quad (17)$$

$K = \text{equilibrium constant for } \text{cis} \rightleftharpoons \text{trans}$   $\alpha = \text{conversion}$

The rate of initiation  $kI$  was determined by NO inhibition and  $k_4$  by the sector technique.<sup>4</sup> The plot of data from Fig. 6 in the form of 17 yielded a straight line from whose slope a value of  $6 \times 10^7$  l./moles sec. for  $k_1^T$  was calculated.<sup>15</sup> This is about 8 to 9 times faster than that reported above for butyl mercaptan and 1-pentene.

It is intended to carry through a program designed to observe such  $\text{cis-trans}$  kinetics in both liquid and gas phase, induced by an array of radicals and also with the same radicals in media of varying properties as to, for example, dielectric and viscosity.

Special interest attaches to the use of  $\text{cis}$  and  $\text{trans}$  dideuterated ethylene as a basic structure in preliminary work now underway by Dr. D. Graham in this Laboratory. Here, complications due to monomer dehydrogenations should be eliminated at normal temperatures. After such studies it will be instructive to observe a series of substituted  $\text{cis-trans}$  structures attacked by a single or selected radical from which conclusions may be drawn with regard to steric and inductive effects.

Finally, when  $\text{cis-trans}$  rates are sectored in these systems under conditions where little addition occurs, one should be in a position to derive the termination constants for relatively isolated radicals derived from, for example, the photolysis of R-S-S-R.

**Acknowledgment** is made of student workers contributions besides those mentioned in reference works, namely, A. Harrison, R. Dyble, R. Townshend, Y. Ebisuzaki and J. McIntyre. Also we are pleased to acknowledge some financial support from the National Research Council of Canada, and scholarships held by A. Harrison, R. Townshend and Y. Ebisuzaki granted by the Ontario Research Foundation.



# FLUORESCENCE INDUCTION PHENOMENA IN GRANULAR AND LAMELLATE CHLOROPLASTS

By J. B. THOMAS AND J. F. W. NUBOER

*Biophysical Research Group, Physical Institute of the State University, Utrecht (The Netherlands)*

Received July 11, 1958

Fluorescence induction phenomena were studied in seven species with granular chloroplasts and seven species with lamellate ones. The duration of the induction period was found to be shorter in the latter objects than in the former ones. In the discussion it was suggested that the stroma substance probably contains part of the photosynthetic enzymes and cofactors.

## Introduction

When studying the conversion of solar energy in nature, it is of interest to examine the commonly occurring, light converting, apparatus, the chloroplast, and to try to get some more insight into the relation between its structure and function.

Generally, two types of chloroplasts can be distinguished.<sup>1-3</sup> In one of them the pigment-carrying lamellae constitute sub-units, the grana, which are embedded in a colorless stroma. As a rule, these "granular" chloroplasts occur in higher plants.

Chloroplasts of the second type, the lamellate chloroplasts, most probably contain pigment-carrying lamellae extended throughout the whole body. In a number of species the lamellae are evidently bundled up into portions of 4-8. In between these lamellar bundles, stroma occurs in relatively thin layers.<sup>4</sup>

The latter plastids, which are found in some algal species, are also called grana-free chloroplasts. Recently, however, Butterfasz<sup>5</sup> demonstrated the occurrence of thin grana, of a thickness less than  $0.15\mu$ , in the lamellate chloroplasts of *Spirogyra majuscula*. It remains to be studied whether—and, if so, to what extent—the plastids of this species are exceptionally built. Future study may show whether it is advisable to discard the term "grana-free" chloroplast. In any case, the mentioned structural differences between the presently studied "granular" and "lamellate" chloroplasts are pronounced to such a degree that it seems justified to retain the latter denominations. It is interesting that Chardard and Rouiller<sup>6</sup> observed intermediate forms in three species of *Desmidiaceae*.

Since photosynthesis seems to consist of a typically structure-bound chain of processes, cf. Arnon, *et al.*,<sup>7,8</sup> and Thomas, *et al.*,<sup>9</sup> a comparative study of photosynthetic phenomena in both types of chloroplasts might enable a better understanding of the relation between these processes and structure. If differences are observed, two possibilities

are to be envisioned. First, photosynthesis may proceed along different chemical pathways in both mentioned types, or, second, photosynthesis may proceed in the same way, but differences may be due to structural variations. The latter situation may occur if, *e.g.*, difference of structure means different distances between reactants and enzymic centers. A study on temperature dependence may enable discriminating between both possibilities. However, in both cases a difference between the photosynthetic activities of granular and lamellate chloroplasts may preferentially show up in the induction period.

Because of the time needed for a gas to diffuse from the interior of the cell into the medium in which it is measured, determinations of gas exchange always are considerably retarded. According to Wassink and Spruit,<sup>10,11</sup> this retardation

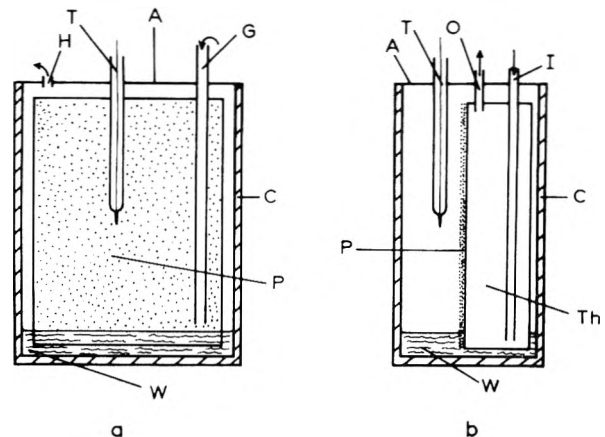


Fig. 1.—Container of the object. For explanation see text.

is about 20 seconds in experiments with *Chlorella* cells. Measurement of fluorescence, however, enables instantaneous registration of fluctuations in the photosynthetic mechanism. For this reason, fluorescence induction phenomena were studied as an attempt to decide whether differences occur in the initial photosynthetic activities of lamellate and granular chloroplasts. The results of this study are reported below.

**Material.**—Seven species of each type of chloroplasts were studied. The selection of these species was based on the fact that clear-cut evidence concerning their structure was examined electron microscopically. The following species were used for granular chloroplasts: *Agapanthus*

(10) E. C. Wassink and C. J. P. Spruit, *Compt. rend. 8<sup>e</sup> Congr. Int. Bot. Paris* (1954).

(11) C. J. P. Spruit and E. C. Wassink, *Biochim. Biophys. Acta*, **15**, 357 (1954).

- (1) H. Leyon, *Svensk Kem. Tidskr.*, **68**, 70 (1956).
- (2) J. B. Thomas, *Progr. Biophys. Biophys. Chem.*, **5**, 109 (1955).
- (3) D. Von Wettstein, *Exptl. Cell Res.*, **12**, 427 (1957).
- (4) P. F. Elbers, K. Minnaert and J. B. Thomas, *Acta Bot. Neerl.*, **6**, 345 (1957).
- (5) Th. Butterfasz, *Protoplasma*, **48**, 368 (1957).
- (6) R. Chardard and C. Rouiller, *Rev. Cytol. Biol. Végétales*, **18**, 153 (1957).
- (7) D. I. Arnon, M. B. Allen and F. R. Whatley, *Biochim. Biophys. Acta*, **20**, 449 (1956).
- (8) F. R. Whatley, M. B. Allen, L. L. Rosenberg, J. B. Capindale and D. I. Arnon, *ibid.*, **20**, 462 (1956).
- (9) J. B. Thomas, A. J. M. Haans, A. A. J. Van der Leun and J. Koning, *ibid.*, **25**, 53 (1957).

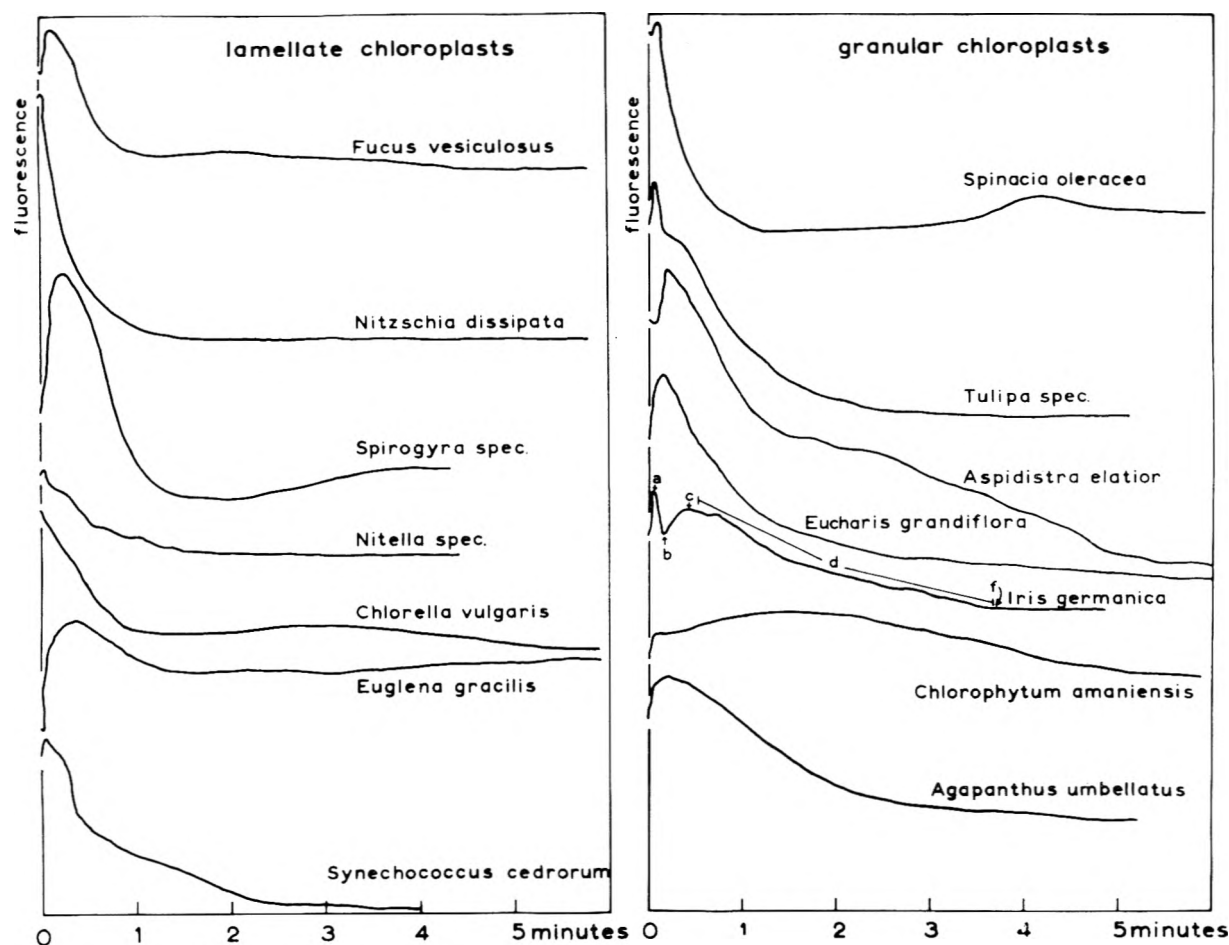


Fig. 2.—Examples of fluorescence induction phenomena at 19° in the objects studied.

*umbellatus*,<sup>12</sup> *Aspidistra elatior*,<sup>13</sup> *Chlorophytum amaniense*, *Eucharis grandifolia*<sup>15</sup> (ultraviolet microscope), *Iris germanica*<sup>16</sup> (light microscope), *Spinacia oleracea*<sup>16</sup> and *Tulipa*<sup>4</sup> spec., and, for lamellate chloroplasts: *Chlorella vulgaris*<sup>4</sup> spec., *Euglena*<sup>18</sup> spec., *Fucus vesiculosus*,<sup>19</sup> *Nitella*<sup>20</sup> spec., *Nitzschia dissipata*,<sup>4</sup> *Spirogyra*<sup>21</sup> spec. and *Synechococcus cedrorum*.<sup>4</sup> Most probably, the latter species contains "chromatoplasm" instead of lamellate chloroplasts. Because of a relatively close resemblance in structure, this organism was included in the present study. The higher plants as well as *Nitella* were obtained from the Utrecht Botanic gardens. The sea-weed *Fucus* was kindly furnished by the Biological Marine Station at Den Helder. *Spirogyra* was collected at its habitat, while the remaining organisms were taken from cultures grown in this institute.

**Methods.**—The objects to be studied were mounted in a container as shown in Fig. 1. In a glass cuvette C, as used for absorption measurements, a small brass thermostat Th was mounted. Temperature-controlled water was flown through the inlet and outlet tubes I and O. Black velvet paper P was fixed to the front side of the thermostat by means of adhesive tape. The temperature-sensitive end of a thermistor T was adjusted near to the object to be

studied. The temperature was read from a mirror galvanometer. The gas mixture was introduced *via* the gas inlet G, while a perforation H of the adhesive tape S, covering the top of the cuvette, served as a gas outlet. During the experiment a slow gas flow was maintained. Additional perforations of the adhesive tape cover enabled introduction of the mentioned tubings. The bottom of the cuvette was covered with a thin layer of water W.

The object was mounted on the black velvet paper. Pieces of leaves or thalli were fixed by means of adhesive tape strips. Care was taken that these strips did not cover the irradiated region. Unicellular algae and isolated chloroplasts were collected from liquid cultures by centrifugation. The sedimental paste was brought onto the velvet paper with a slice. The diatoms were taken from agar cultures. A thin slice of agar, covered with these algae, was adjusted on the velvet paper by gentle pressing.

The gas mixture consisted of air with 3% carbon dioxide saturated with water.

After adjustment, the specimen was allowed to equilibrate in the dark for at least 15 minutes. Then, light was admitted and the amplifier was properly adjusted with regard to the fluorescence intensity. Next, the light was turned off again and the object was kept in the dark for 10 minutes. Each light period during the experiments was preceded by a 10 minutes dark period as well.

Each experiment was done in triplicate at two temperatures and three light intensities.

Except for the following details, the apparatus used for fluorescence measurements equalled the earlier described<sup>22</sup> one. The incident light beam passed a GAB calflex 87 filter and a 1 cm. 6% CuSO<sub>4</sub> solution, while a Schott RG5 2 mm. glass filter was placed in the fluorescence light beam. The signal was fed into a quick, 0.5 second, Honeywell-Brown recorder.

- (12) G. Grave, *Protoplasma*, **44**, 273 (1955).  
 (13) H. Leyon, *Exptl. Cell Res.*, **7**, 265 (1954).  
 (14) S. Strugger, *Eur.*, **69**, 177 (1956).  
 (15) A. Frey-Wyssling, F. Ruch and X. Berger, *Protoplasma*, **45**, 97 (1955).  
 (16) H. Leyon, *Svensk Kem. Tidskr.*, **68**, 70 (1956).  
 (17) P. A. Albertsson and H. Leyon, *Exptl. Cell Res.*, **7**, 288 (1954).  
 (18) J. J. Wolken and G. E. Palade, *Nature*, **170**, 114 (1952).  
 (19) H. Leyon and D. Von Wettstein, *Z. Naturforsch.*, **9B**, 471 (1954).  
 (20) F. V. Mercer, A. J. Hodge, A. B. Hope and J. D. McLean, *Australian J. Biol. Sci.*, **8**, 1 (1955).  
 (21) E. Steinmann *Exptl. Cell Res.*, **3**, 367 (1952).

- (22) J. B. Thomas, J. C. Goedheer and J. G. Komen, *Biochim. Biophys. Acta*, **22**, 342 (1956).

TABLE I  
FLUORESCENCE INDUCTION PHENOMENA IN GRANULAR AND LAMELLATE CHLOROPLASTS

Type of chloroplasts	Temp., °C.	Intensity of actinic light, ergs cm. <sup>-2</sup> sec. <sup>-1</sup> × 10 <sup>5</sup>	Interval between start of illumination and occurrence of—				Duration of L.A.S., sec. (d)	Time of reaching steady-state conditions, sec. (f)	Steady state level in % of initial level
			1st max. (a) sec.	1st min. (b) sec.	2nd max. (c) sec.	3rd max. (e) sec.			
Granular	18.5	0.13	4.7 ± 0.7 (100%)	17 ± 2 (81%)	46 ± 5 (95%)	[270] (5%)	119 ± 27 (91%)	244 ± 29 (100%)	101 ± 6 (100%)
		1.32	4.1 ± 1.2 (100%)	11 ± 2 (76%)	36 ± 12 (86%)	[266] (19%)	233 ± 23 (95%)	318 ± 12 (100%)	63 ± 9 (100%)
		4.95 <sup>b</sup>	3.8 ± 0.9 (100%)	[8] (57%)	51 ± 28 (86%)	[220] (5%)	261 ± 32 (100%)	363 ± 48 (100%)	62 ± 10 (100%)
	25.5	0.13	4.5 ± 1.3 (100%)	19 ± 7 (57%)	32 ± 7 (62%)	152 ± 27 (38%)	66 ± 9 (95%)	178 ± 20 (100%)	101 ± 6 (100%)
		1.32	4.7 ± 0.8 (100%)	10 ± 2 (81%)	22 ± 5 (81%)	171 ± 21 (57%)	98 ± 15 (100%)	260 ± 27 (100%)	62 ± 6 (100%)
		4.95 <sup>b</sup>	3.3 ± 0.9 (100%)	[6] (48%)	26 ± 14 (67%)	145 ± 13 (43%)	116 ± 20 (100%)	284 ± 21 (100%)	53 ± 9 (100%)
Lamellate	18.5	0.13 <sup>a</sup>	2.6 ± 0.8 (100%)	[7] (24%)	[16] (24%)	[80] (5%)	58 ± 15 (71%)	127 ± 30 (100%)	107 ± 4 (100%)
		1.32	2.0 ± 0.8 (100%)	5 ± 2 (52%)	19 ± 4 (67%)	[92] (19%)	86 ± 24 (100%)	228 ± 26 (100%)	78 ± 9 (100%)
		4.95 <sup>b</sup>	1.3 ± 0.6 (100%)	5 ± 1 (52%)	14 ± 3 (71%)	[75] (10%)	112 ± 28 (100%)	229 ± 20 (100%)	72 ± 11 (100%)
	25.5	0.13 <sup>a</sup>	2.9 ± 0.5 (100%)	[8] (14%)	[16] (19%)	[50] (10%)	45 ± 10 (43%)	108 ± 28 (100%)	118 ± 9 (100%)
		1.32	1.4 ± 0.6 (100%)	[3] (33%)	6 ± 2 (52%)	[96] (29%)	73 ± 16 (100%)	184 ± 18 (100%)	78 ± 10 (100%)
		4.95 <sup>b</sup>	0.5 ± 0.3 (100%)	4 ± 1 (48%)	5 ± 1 (62%)	[90] (14%)	85 ± 17 (95%)	188 ± 26 (100%)	69 ± 10 (100%)

<sup>a</sup> In some experiments, 0.20. <sup>b</sup> In some experiments, 4.49.

### Results

Figure 2 shows examples of fluorescence induction phenomena at 19° and a light intensity of  $1.32 \times 10^5$  ergs cm.<sup>-2</sup> sec.<sup>-1</sup> in the studied granular and lamellate chloroplasts, respectively. It is obvious that the initial fluorescence changes differ for different species. Though to a minor degree, this is also true of various samples of a single species. The ordinate scales are arbitrary and differ for different experiments. The recordings were chosen as the most characteristic ones for each kind of chloroplasts. The time needed for reaching steady-state conditions was measured. Moreover the fluorescence time course was determined by measuring the time at which maxima and minima occurred. This procedure was based on the assumption that Van der Veen's<sup>23</sup> analysis of the fluorescence induction period represents the most complete picture of the phenomena in question. Working with leaves of higher plants this author distinguished in succession: a first maximum (a), a first minimum (b), a second maximum (c), an "adaptation slope" (d) and steady-state fluorescence (f), while in some cases "secondary peaks" (e) were observed. Except for the latter peaks, such a "complete" induction period is shown in Fig. 2 with *Iris germanica*.

It is evident from Fig. 2 that, in many cases, the induction period was but "incomplete." Sometimes it proved difficult to decide which part was absent. However, comparison with experiments

from the same series enabled a reasonable conclusion.

The time lapse between start of illumination and occurrence of the mentioned maxima a, c and e, the minimum b and the moment at which steady-state conditions were established, f, as well as the duration of the "light adaptation slope (L. A.S.)," d, were measured. The results are summarized in Table I. The values were obtained by computing the mean one for a set of three experiments with each object. Thus, seven figures resulted. The means of these figures, with mean error, are shown in the table. For cases in which a maximum or minimum occurred only a few times or if their occurrence was restricted to a few species no mean errors were computed while the mean values were placed in brackets. The percentages given indicate the frequency of occurrence of the phenomenon in question. All of these figures are in parentheses.

From the latter figures it can be seen that quite a number of fluorescence time courses are "incomplete." The features which all induction periods have in common are: a first maximum which may be of very short duration, and the attainment of steady-state conditions. Though both features suggest the same conclusion, because of the lower per cent. error, the values regarding the latter phenomenon are the most convincing ones for showing that, in general, steady-state conditions are attained earlier in plants with lamellate chloroplasts than in plants containing granular ones.

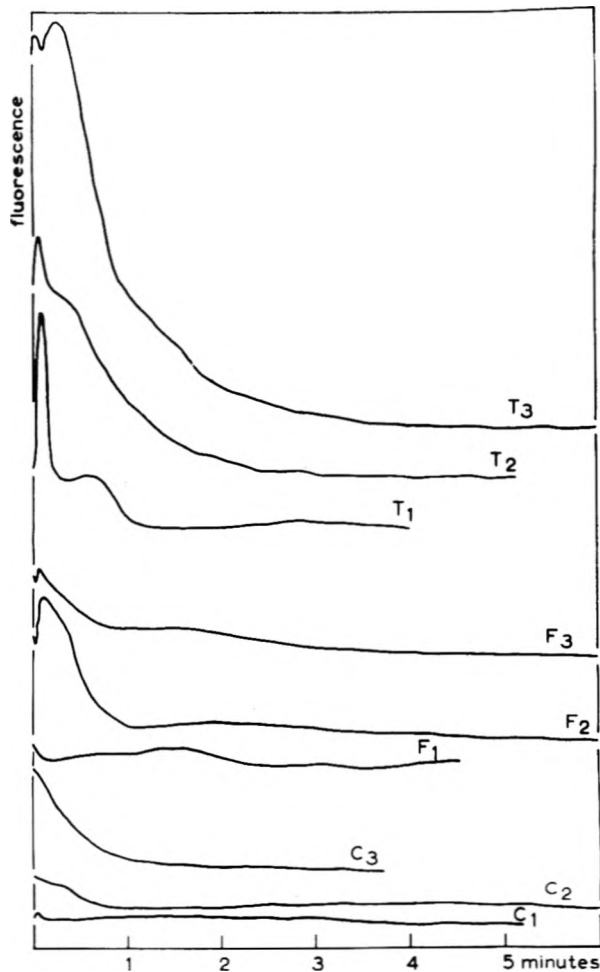


Fig. 3.—Comparison of fluorescence induction phenomena at  $19^{\circ}$  in a leaf piece of the tulip (T), a piece of *Fucus* thallus (F), and *Chlorella* paste (C) at light intensities of  $0.13 \times 10^5$  (1),  $1.32 \times 10^5$  (2), and  $4.95 \times 10^5$  (3) ergs  $\text{cm.}^{-2} \text{sec.}^{-1}$ .

This holds for the lowest light intensity used, at which no photosynthesis saturation occurs, as well as for both higher intensities at which this process is saturated.

If the light intensity is increased until photosynthesis saturation is reached, the establishment of steady-state conditions is retarded. It is evident from column f that increasing the light intensity still further has little or no effect. The time at which steady-state conditions are attained seems to be mainly determined by the duration of the light adaptation slope (d).

Raising the temperature, however, causes earlier attainment of steady-state conditions. The temperature dependency of this phenomenon at three light intensities is shown in Table II. Assuming that this dependency is a linear one in the range under consideration, the given ratios:  $f$  at  $(n + 10)^{\circ} / f$  at  $n^{\circ}$  ( $f$  defined in Table I),  $Q_{10}^f$ , were computed from the observed ones:  $f$  at  $16^{\circ} / f$  at  $19^{\circ}$  ( $Q_{10}^f$ ).

Because of the low  $Q_{10}^f$  values, Table II suggests that the moment at which steady-state conditions are established is mainly determined by processes which are but slightly temperature-dependent.

TABLE II  
TEMPERATURE DEPENDENCY OF THE ATTAINMENT OF STEADY-STATE CONDITIONS ( $Q_{10}^f$ ) AT DIFFERENT LIGHT INTENSITIES

Intensity of actinic light, ergs $\text{cm.}^{-2} \text{sec.}^{-1} \times 10^5$	$Q_{10}^f$ in plants with chloroplasts of type	
	Granular	Lamellate
0.13 <sup>a</sup>	1.5	1.3
1.32	1.3	1.3
4.95 <sup>b</sup>	1.4	1.3

<sup>a, b</sup> Cf. Table I.

They are independent of light intensity. The  $Q_{10}^f$  values are in the range of the  $Q_{10}^f$  for diffusion phenomena.

The following, additional, conclusions can be drawn from Table I.

At the lowest intensity of the actinic light, the fluorescence intensity at steady-state conditions about equals that at the start of irradiation. At actinic light intensities higher than the photosynthesis saturating one, the intensity of steady-state fluorescence is 20–40% lower than that of the primary light emission. In accordance with Van der Veen's<sup>23</sup> observations the intensity of steady-state fluorescence is not markedly influenced by changing the temperature. At both lower light intensities the first minimum (b) occurs more frequently in plants with granular chloroplasts than in plants with lamellate ones. At the highest intensity used, this difference is absent. In general, the same can be said of the second maximum (c).

The third maximum (e) occurs less often. It is mainly encountered in plants with granular chloroplasts at the highest temperature used.

## Discussion

It has been mentioned by many authors, *cf.*<sup>11,23</sup> that the pretreatment and the condition of the object largely influences fluorescence induction phenomena. Since, presently, both origin and medium conditions of the studied species are mutually different, it was impossible to establish a comparable pretreatment of the objects in question. As mentioned earlier, care was taken to keep constant only the conditions during the preceding dark periods. But, if there is some fundamental correlation between chloroplast structure and fluorescence induction phenomena, this correlation can be envisioned to show up nevertheless.

However, both sets of studied plants did not differ only in chloroplast structure; one of them consisted of land plants while the other one was constituted by aquatic plants. This coincidence is due to the fact that the choice of objects was limited by the condition that the structure of the chloroplasts to be studied should be satisfactorily known. Because of other diffusion conditions, *cf.* Rabinowitch,<sup>24</sup> prevailing in land plants rather than in aquatic ones, *e.g.*, by the presence of stomata and relatively long intercellular gas spaces in the former plants, establishment of equilibrium conditions of oxygen and carbon dioxide at the cell boundary might require a longer time to run to completion. Now it has been stated by others,

(24) E. I. Rabinowitch, "Photosynthesis and Related Processes," Vol. II, part 2 Interscience Publ., New York, N. Y., 1956.

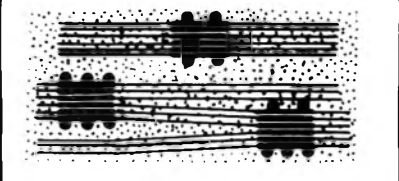
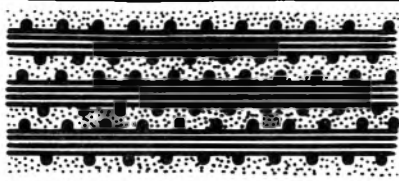
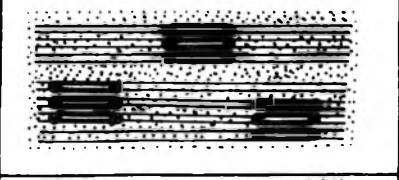
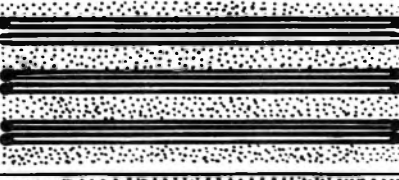
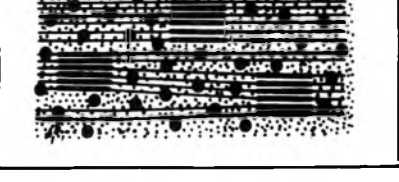
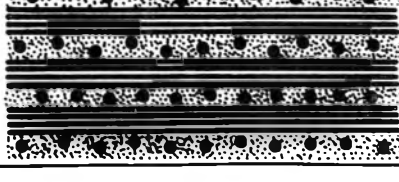
possibility	granular chloroplast	lamellate chloroplast
1		
2		
3		

Fig. 4.—Schematic representation of possible distributions of "reaction centers" in granular and lamellate chloroplasts. For explanation see text.

*cf.*,<sup>11,23</sup> that changes in concentration of these gas components affect fluorescence. Consequently, the period required to attain steady-state conditions might also be longer in the studied plants with granular chloroplasts than in those with lamellate ones because of the fact that these plants belong to the land type and the aquatic type, respectively. Kautsky and Hirsch<sup>25</sup> stated that in many "lower" plants such as algae, ferns and higher aquatic plants the duration of light adaptation,  $d$  from the present Table I, is shorter than that commonly occurring in land plants. Unfortunately, no details concerning the chloroplasts of these "lower" plants are known. In any case, however, these experiments demonstrate that the presence (ferns and floating aquatic plants) or absence (submersed aquatic plants) of stomata is not appreciably correlated with the length of the fluorescence induction period. Nor does it seem that the packing of cells is of major importance in this respect. The present experiments suggest the same conclusion for the following reason. *Fucus vesiculosus* is a plant with both lamellate chloroplasts and a complicated thallus with a relatively thick cuticle. If the time needed for diffusion of the gases in question between the surface of the thallus and the chloroplast-containing cells would act as a factor influencing induction phenomena, the duration of the fluorescence induction period in *Fucus* may equal that of land plants rather than that of aquatic ones. Figure 3 shows the fluorescence time course in a tulip leaf piece, *Chlorella* "paste," and a piece of *Fucus* thallus. The duration of the *Fucus* induction period agrees better with that of *Chlorella* than with that of the tulip. Thus, it may be concluded that diffusion condi-

tions outside of the cell did not affect the studied phenomena to an appreciable extent.

Assuming the correctness of this conclusion and considering that the conditions inside the cells are not likely to differ considerably in both groups of plants, it seems probable that the observed differences in time required for the attainment of steady-state fluorescence are to be associated with the structural differences between granular and lamellate chloroplasts.

Such a phenomenon suggests the following discussion. Most likely,<sup>26</sup> the distribution of chlorophyll molecules over the pigment carrying lamellae is about the same for granular and lamellate chloroplasts. Since even small lamellar fragments, freed from stroma substance, are capable of performing the Hill reaction, *cf.*,<sup>27</sup> the pigment molecules necessarily are associated with enzymic centers situated in the lamellae. Because of the fact that, moreover, about the same quantum yield of the Hill reaction in suspensions of both types of chloroplasts, *cf.*,<sup>28</sup> is found, it can be concluded that, most probably, the "spacing" of the enzymic centers in which the first photoproducts are formed is the same for the pigment carrying lamellae from both granular and lamellate chloroplasts. For this reason, it seems less likely that the observed differences are due to differences in such combinations of pigment molecules and enzymes involved in the very first dark reaction. The photoproducts are to be stabilized and introduced into the chain of dark processes. To this purpose they should react with certain substances. Thus, the photo-

(26) J. B. Thomas, K. Minnaert and P. F. Elbers, *Acta Bot. Neerl.*, **5**, 315 (1956).

(27) J. B. Thomas, O. H. Blaauw and L. N. M. Duysens, *ibid.*, **10**, 230 (1953).

(28) Ref. 24, 1951, Vol. II, part 1.

(25) H. Kautsky and A. Hirsch, *Biochem. Z.*, **274**, 423 (1934).

products are to be transported from their site of origin to the cofactors and enzymes involved, and in this way some time will be needed for the establishment of a concentration equilibrium at the beginning of a light period. The same holds for intermediary products. In general, the ultimate concentration of each product is a function of the velocities of reaction and back reaction and the mentioned transportation time. If such a product either functions as an acceptor for the excitation energy of the chlorophyll or influences the concentration of some other acceptor for this energy, the fluorescence intensity changes with variations of the product concentration. Because of the observed temperature dependence the present study indicates that the duration of the fluorescence induction period is mainly determined by this transportation (diffusion) time rather than by reaction velocities. This implies the suggestion that the observed differences between the induction periods of granular and lamellate chloroplasts are to be ascribed to differences of distances between the enzymic centers at which the first products are formed and enzymes and cofactors involved in subsequent dark reactions.

Since a grana suspension is no longer capable of photosynthesis, it is unlikely that all photosynthetic enzymes and cofactors are located in the lamellae. In a preceding paper<sup>9</sup> it has been argued that intactness of stroma is a prerequisite for the complete functioning of the photosynthetic apparatus. The earlier experiments did not allow a conclusion with regard to the question whether photosynthetic enzymes and cofactors are either located in the stroma or fixed to the surface of the pigmented lamellae. In the latter case the stroma might merely act as a protective colloid. The present experiments, however, suggest the following conclusion concerning this matter.

The possibilities to be envisioned are shown in Fig. 4. The enzymes and cofactors, briefly called "reaction centers," other than the Hill reaction enzymes are represented by black spots. The dotted area indicates stroma while the lamellae are shown by thick lines as far as they are considered to be pigmented and by thin ones in pigment-free regions. In the first case, the reaction centers are supposed to be located at the surface of grana and lamellar strands. Since, as a rule, grana are built up of more layers than the lamellar strands of lamellate chloroplasts the distance between cen-

trally located enzymic centers and the "reaction centers" in question in grana will surpass that in "strands" and thus account for a longer induction period. If this were true, the length of the induction period will also depend on the number of lamellae in a granum. However, as it is shown in Table III, such a correlation does not occur. Consequently, the first possibility seems less probable.

TABLE III

LACK OF RELATION BETWEEN NUMBER OF LAMELLAE CONSTITUTING A GRANUM AND LENGTH OF THE FLUORESCENCE INDUCTION PERIOD

Species	Mean no. of lamellae per granum	Length of induction period at 19° in sec. at light intensities in ergs cm. <sup>-2</sup> sec. <sup>-1</sup> of		
		0.13 × 10 <sup>5</sup>	1.32 × 10 <sup>5</sup>	4.95 × 10 <sup>5</sup>
<i>Tulipa spec.</i>	6	138	300	307
<i>Spinacia oleracea</i>	9	270 <sup>a</sup>	370	237
<i>Hibiscus rosa sinensis</i>	15	200	333	367
<i>Aspidistra elatior</i>	26	220	303	287

<sup>a</sup> Mean of two experiments. Other values, means of three experiments.

The second possibility regards the case in which the "reaction centers" are located at the ends of the pigmented lamellae. Since, in this case, the diffusion path from the middle region in the strands to their ends considerably would surpass that in grana, the induction period would last longer in lamellate chloroplast than in granular ones. However, as the reverse is observed, this possibility can be ruled out.

The third possibility represents the situation in which the "reaction centers" are located in the stroma. As granular chloroplasts contain more stroma substance in relation to the amount of pigment carrying lamellae than lamellate chloroplasts do, "reaction centers" may occur at larger distances from grana in the former chloroplasts than from lamellar strands in the latter ones. It is evident from the figure that, in this case, the thickness of the grana is of minor importance. Thus, this scheme enables an explanation of the observed differences in length of the fluorescence induction periods of granular and lamellate chloroplasts in terms of diffusion phenomena.

Consequently, the present experiments suggest that, probably, part of the photosynthetic enzymes and cofactors is located in the stroma substance.

# PHOTOCHEMICAL PROCESSES IN THIN SINGLE CRYSTALS OF SILVER BROMIDE: THE DISTRIBUTION AND BEHAVIOR OF LATENT-IMAGE AND OF PHOTOLYTIC SILVER IN PURE CRYSTALS AND IN CRYSTALS CONTAINING FOREIGN CATIONS

BY W. WEST AND V. I. SAUNDERS

*Communication No. 1943 from the Kodak Research Laboratories, Eastman Kodak Co., Rochester, N. Y.*

*Received July 11, 1958*

The distribution-in-depth of latent-image centers and of visible print-out centers has been investigated in purified thin crystals of silver bromide made from the melt and in crystals containing small additions of cadmium ion, lead ion and cuprous ion. With respect to latent-image centers, three sensitometrically distinct regions are found in pure crystals—the non-sensitive surface, a subsurface region of low sensitivity, and the deeper interior, of relatively high sensitivity. Internal latent-image is found at depths much greater than those to which light can penetrate with appreciable intensity. Latent image is formed throughout the whole thickness of pure crystals exposed to penetrating light, except for the subsurface layers of low sensitivity, but no print-out silver is formed in the central regions. The distribution of print-out silver in pure crystals appears to be governed by the ease of diffusion of positive holes to the surface from regions at different depths within the crystal. This distribution can be modified by the introduction of traps for positive holes. The silver-ion vacancies introduced by divalent cadmium or lead ions do not act as deep traps for positive holes; on the contrary, by inhibiting diffusion, they increase the attack of positive holes on photolytic centers over that in pure crystals. The image formed in crystals containing cadmium or lead ions contains a non-silver "complementary photolytic image," consisting of oriented pits at the surface, apparently formed by the escape of bromine at localized sites. Cuprous ion acts as a deep trap for positive holes by electron exchange, increasing the yield of print-out silver on exposure to visible light by about an order of magnitude over that for pure crystals, without any increase in the bromine evolution. Penetrating light causes the appearance of print-out centers throughout the whole illuminated volume of cuprous-containing crystals. At elevated temperatures, the trapping of positive holes by cuprous ions is reversible, and the processes of image formation at room temperature, followed by thermal fading at higher temperature, can be repeated at will.

Single crystals of silver halide, some 10 to 100  $\mu$  thick and a few millimeters in the other linear dimensions, cut from sheets prepared from the melt, constitute a photographic system in a sense intermediate between massive crystals prepared by the Bridgman or Kyropoulos techniques and the grains of a normal photographic emulsion, and Mitchell and co-workers<sup>1-5</sup> have amply shown the utility of such crystals in performing model experiments on fundamental questions of photographic sensitivity. The crystals are large enough to be handled easily, they can be subjected to controlled treatments before and after exposure, and images can be developed by the normal processes of photographic development; hence they form to some degree a readily manipulable model for the emulsion grain. Nevertheless, apart from their large linear dimensions and particularly their relatively great thickness, which permits exploration of the photographic behavior of silver halide crystals at much greater depths from the surface than are available in normal emulsions, the mode of formation of these crystals is very different from that of emulsion grains. The large crystals have their own characteristic photographic and photochemical behavior, conditioned partly by the intrinsic properties of silver bromide, partly by the dimensions of the crystals and partly by the nature of the impurities and crystal defects, which probably are determined to a large degree by the specific mode of formation of the crystal. Not all aspects of the photographic behavior of the large crystals can be expected to apply to emulsion grains, and judgment

must be exercised as to the validity of the large crystal model for the study of any given photographic phenomenon. The present communication is concerned with aspects of the photochemical behavior of the large crystals in themselves, in the endeavor to secure background for the further application of the system to problems of photographic sensitivity.

**I. Preparation of the Crystals and General Procedure.**—Pure crystals have been studied as well as crystals containing small amounts of divalent cations and cuprous ions. The starting material was the purest available silver bromide precipitate made from silver nitrate and hydrobromic acid, for which we are indebted to F. Urbach and co-workers, of these Laboratories.<sup>6</sup> The crystalline sheets were prepared following the procedures of Mitchell and co-workers.<sup>2,4</sup> The essential steps in this preparation are: the removal of a small quantity of solid siliceous material from the bromide precipitate by filtering the melt through Pyrex-glass capillary tubes; a further purification by melting the bromide under vacuum, which removes some volatile materials; the formation of a film of silver halide by melting a pellet of the purified halide between Vycor plates; solidification by slowly drawing the plates through a horizontal temperature gradient; and separation of the crystalline film from the plates by immersion in water. The resulting crystalline sheets, about 2 inches in diameter and usually between 50 and 100  $\mu$  thick (determined by Pyrex glass or platinum spacers), consisted of a few single crystals, from which small pieces of single crystal could be cut. With the object of minimizing silver or silver oxide production in the making of the sheets, a halogen atmosphere was maintained during all heating operations except when it was desired to incorporate cuprous ion. In this latter case, the sheets were prepared under an atmosphere of nitrogen. Usually, the crystals were not annealed after separation from the plates.

Bromide films were examined at the wave lengths 365, 405 and 436  $m\mu$ , isolated from the radiation of an AH-4 mercury lamp by filters. (For 365  $m\mu$ , Corning Filter No. 3860 + aqueous copper sulfate 0.75 *M*, 3.2 cm. thick; for 405  $m\mu$ , Corning Filters No. 3060 + 5970 + aqueous copper sulfate as before; for 436  $m\mu$ , one thickness of Kodak Wratten Filter No. 2A + two thicknesses of Kodak Wratten Filter No. 47 + aqueous copper sulfate as before.)

- (1) J. W. Mitchell, *J. Phot. Sci.*, [2] **1**, 110 (1953).
- (2) J. M. Hedges and J. W. Mitchell, *Phil. Mag.*, [7] **44**, 357 (1953).
- (3) T. Evans, J. M. Hedges and J. W. Mitchell, *J. Phot. Sci.*, [2] **3**, 73 (1955).
- (4) P. V. McD. Clark and J. W. Mitchell, *ibid.*, [2] **4**, 1 (1956).
- (5) J. W. Mitchell, *ibid.*, [2] **5**, 49 (1957).

- (6) N. R. Nail, F. Moser, P. E. Goddard and F. Urbach, *Rev. Sci. Instr.*, **28**, 275 (1957).

Light of wave lengths 365 and 405  $m\mu$  is completely absorbed within a few microns of the surface of incidence, while 90% absorption of light of wave length 436  $m\mu$  takes place in penetrating about 50  $\mu$ . In addition, experiments were performed using exposures to light which penetrated the crystal with only about 50% absorption by a layer 100  $\mu$  thick. A tungsten source, filtered by means of a Kodak Wratten Filter No. 4, sometimes combined with the copper sulfate filter and sometimes without this filter, as described later, was used for this purpose. The effective wave lengths in these exposures to penetrating light comprised a band between 470 and 480  $m\mu$ .

Crystals carefully prepared by these procedures show little or no surface sensitivity; no reduced silver image appears on the surface after exposure and development.<sup>2,3</sup> Latent image is produced in the interior, however, which can be developed after the application of suitable etching procedures.<sup>2,3</sup> The observations to be described in this communication are concerned with the formation of this internal latent-image and of the visible print-out or photolytic image formed by long exposures. As was first shown by Hedges, Evans and Mitchell, latent-image centers and photolytic centers are produced mostly at sites in the dislocation networks which constitute the polyhedral substructure of the crystal.<sup>2,3,7</sup>

A method of "graded etching" which reveals the distribution of internal latent-image throughout the depth of the exposed crystal has been described.<sup>8</sup> After exposure, the crystal, with one side protected by mounting on glass, is gradually immersed in an etching bath of 4.2 *M* potassium bromide solution containing 0.1 *M* potassium ferricyanide, so that, at the end of the operation, the crystal is wedge-shaped. The etched surface then cuts through the original distribution of latent image and, on development, the distribution in depth of the centers is revealed. The function of the ferricyanide is to oxidize the latent-image centers as soon as they are uncovered by the etchant. Without the oxidizing agent, these centers accumulate because of a tendency to adhere to the newly formed etched surface, and, on development, the distribution of developed centers does not match that of the original latent-image centers. When the etch bath contains ferricyanide, the surface formed is completely free from latent image, but an additional shallow etch of a fraction of a micron by means of potassium bromide solution alone forms a new surface containing latent-image centers in the amounts corresponding to the true distribution in depth.

The general procedure was to expose through a narrow slit a piece of single crystal mounted on glass, carry out a graded etch as just described, apply a thin layer of gelatin by momentary immersion of the crystal in 2% aqueous gelatin, followed by draining and drying, then to develop by immersing about 30 seconds in a *p*-methylaminophenol-ascorbic acid developer.<sup>9</sup> A slit-like image appeared along the inclined surface formed by the etching operation, the distribution of density along the length of which reflected the distribution in depth of latent-image centers from the original surface of incidence. The depths were determined by microscopic observations of the thicknesses of the original and etched crystal. The distribution in depth of photolytic silver was determined by direct microscopic observation of the discrete particles of silver in the unetched crystal. In the subsequent discussion, the term "latent-image sensitivity" will be used to denote the sensitivity associated with the production of developable silver from microscopically invisible latent-image centers, while "photolytic sensitivity" will denote the sensitivity associated with the production of directly visible deposits of silver.

It is not the object of this communication to discuss, other than incidentally, the details of the formation of latent-image centers or of photolytic centers. Surveys of these topics have been made recently by Mitchell, and mechanisms have been proposed.<sup>5,10,11</sup>

In the following discussions, it is assumed that the ab-

sorption of light by silver halide crystals causes the appearance of electrons in the conduction band and of positive holes in the valence band. In chemically pure and highly perfect crystals, most of the electrons and positive holes recombine, and photographic sensitivity depends on the prevention of this process. This may be accomplished by the introduction of suitable traps which will capture the electrons and positive holes separately, and, according to Mitchell,<sup>5,11</sup> it is of special importance that the trapped electron be at a site which will repel a positive hole. The holes may eventually escape as free halogen, or they may be deeply trapped chemically. The trapped electrons combine with silver ions, forming silver atoms and aggregates of silver atoms. The latent image is assumed to be a stable aggregate containing a small number of silver atoms, which, on the addition of developer, catalyzes the reduction of the silver halide so as to yield a visible image of reduced silver. Prolonged exposure results in the formation of deposits of colloidal silver which are visible without development, the so-called "print-out" or "photolytic" silver. Latent-image centers and photolytic centers are formed at the same type of site in sheet crystals, namely, at dislocations,<sup>3</sup> and it seems probable that under certain circumstances the latent-image center may, on prolonged exposure, grow into a particle of photolytic silver.

One of the results of the observations to be reported here is that the conditions for the growth of latent-image centers to photolytic centers are severely limited and much of the following discussion is concerned with the origin of the peculiarities which are found in the distribution of latent image and of photolytic centers in pure and impure sheet crystals of silver bromide.

**II. Surface, Subsurface and Internal Latent-image Sensitivity.**<sup>11a</sup>—Three distinct regions, exhibiting characteristic latent-image sensitivity, can be recognized in the sheet crystals: the insensitive surface layer already alluded to, a subsurface region extending a few tenths of a micron from the surface and the deep interior. Latent image is found at depths slightly below the surface and extending to depths within the crystal considerably below those to which light can penetrate.<sup>4,8,12</sup> For example, radiation of wave length 365  $m\mu$  is attenuated to 1% of the incident value after penetrating about 8  $\mu$  into the crystal, but latent image can be found at depths up to 50  $\mu$  from the surface in unannealed crystals and to 90  $\mu$  in lightly annealed crystals. The immediate subsurface region differs sharply in sensitometric behavior from regions deeper in the interior of the crystal: (a) the general sensitivity in the subsurface layer is lower than in the deeper layers; (b) the subsurface layer shows a greater reciprocity failure at low intensities than the interior; and (c) the image produced in the subsurface region by illumination through a narrow slit shows no broadening outside the geometrical image of the slit, while in the interior, the image spreads laterally in a manner suggesting that it is formed in this region by the diffusion of electrons from the light-absorption zone near the surface. When the surface is chemically sensitized, e.g., by means of sodium aurothio-sulfate with ammonium chloroiridite,<sup>1,3</sup> the developed image in the surface does not spread beyond the illuminated area.<sup>1,3</sup>

The differences in the sensitivity and in the reciprocity behavior of the subsurface and of the deeper regions within the crystal are illustrated by the data in Table I. A sheet crystal was exposed to 436  $m\mu$  radiation through a slit 100  $\mu$  wide so as to receive the same energy (intensity  $\times$  exposure time) at three different intensity levels. After graded etching and development, the densities of the images were measured at various levels from the original surface by means of a recording microdensitometer, which scanned the slit-like image from side to side. As already mentioned, the internal image occupies a width greater than the geometrical image of the slit; hence as a measure of the total photographic effects at various levels, the densities were integrated over the width of the image. These quantities are listed in the table as relative integrated densities. Data are reported for exposures in air and under a layer of 50% aqueous sodium ni-

(7) J. M. Hedges and J. W. Mitchell, *Phil. Mag.*, [7] **44**, 223 (1953).

(8) W. West and V. I. Saunders, "Proc. Internat. Congress for Scientific Phot.," Cologne, 1956, in press.

(9) T. H. James, W. Vanselow and R. F. Quirk, *PSA J. (Phot. Sci. and Tech.)*, **19B**, 170 (1953).

(10) J. W. Mitchell, *Phot. Korr.*, **93**, I, Sonderheft (1957).

(11) J. W. Mitchell and N. F. Mott, *Phil. Mag.*, [8] **2**, 1149 (1957).

(11a) Examination of surface and of subsurface regions formed by etching well into the interior of the original crystal shows that the properties described in the following section pertain to surface and subsurface regions *per se* and are not restricted to the original surface prepared in contact with the hot Vycor plates.

(12) W. West and V. I. Saunders, *Phys. Rev.*, [2] **98**, 1557 (1955).



trite solution, 40  $\mu$  thick, in contact with the surface of incidence.

TABLE I

INTEGRATED DENSITIES OF DEVELOPED SUBSURFACE AND DEEPER INTERNAL LATENT-IMAGES IN PURE SILVER BROMIDE

Exposure in	Position of image	Relative integrated densities		
		Intensity, quanta $\text{cm.}^{-2} \text{sec.}^{-1}$ $1.6 \times 10^{12}$	$1.6 \times 10^{14}$	$1.6 \times 10^{15}$
Time, sec.		10	1	0.1
Air	Subsurface	0	3	15
Air	6 $\mu$ below	20	20	20
Air	10 $\mu$ below	23	24	18
Air	15 $\mu$ below	22	26	12
Air	30 $\mu$ below	10	1	0
Nitrite	Subsurface	10	17	36
Nitrite	6 $\mu$ below	22	20	19
Nitrite	10 $\mu$ below	22	20	11
Nitrite	15 $\mu$ below	20	16	0
Nitrite	30 $\mu$ below	7	0	0

The images produced in the subsurface region at low intensity are much feebler than the images produced by the same exposures some distance within the crystal and also than the subsurface images produced by the same exposure (intensity  $\times$  time) at the higher intensities; *i.e.*, the subsurface image shows a marked reciprocity failure at low intensities, greater than that of the internal image. The deeper internal images, in fact, show distinct high-intensity reciprocity failure.

The distinction between the subsurface layer and the interior of the crystal is especially marked for exposures to weakly absorbed penetrating radiation of wave length 470–480  $m\mu$ . The incident intensity of this radiation was comparable to that of the blue and ultraviolet mercury lines used for exposures at shorter wave lengths, but the low absorption coefficient of the light at the longer wave lengths causes the volume concentration of the absorbed quanta to be only about  $1/50$  of that of the radiation of wave length 365  $m\mu$ . Under these conditions, very little subsurface image was formed by exposures which produced strong latent image in the interior. The relatively insensitive subsurface layer was found under both the surfaces of incidence and of exit of the light, showing that the behavior of this region is definitely associated with some condition prevailing near the surface. Surface states are well known in germanium, and it has been recognized that the surfaces of semi-conductors in general may be regions of intense trapping and recombination of charge carriers.

The sensitivity of the subsurface layer was found to be considerably increased when the sheet was exposed to light of wave length 436  $m\mu$  through a thin layer of concentrated aqueous sodium nitrite solution (Table I). Since the best-known photographic action of nitrite is halogen acceptance, this observation suggests that the low sensitivity of the subsurface layer is connected with inefficiency of removal of photobromine from the surface in the normal mode of exposure in an atmosphere of air. Various lines of evidence indicate that bromine may dissolve in silver bromide at room temperature as positive holes.<sup>8,13–15</sup> If, as a result of exposure, an adsorbed layer of bromine accumulates on the surface of a silver bromide crystal, the concentration of positive holes in the subsurface region will be greater than when the bromine is immediately removed, and since positive holes at sufficiently high concentrations can attack trapped electrons and silver atoms, the prevention of this attack by a layer of nitrite will increase the subsurface sensitivity. It is to be noted that exposure under nitrite induced no more than a trace of latent-image sensitivity at the extreme surface, an effect paralleling the inefficiency of halogen acceptors such as semicarbazides or phenol observed by Sutherns and

Loening<sup>16</sup> in sensitizing sols of silver bromide. The inefficiency of nitrite as a surface sensitizer, contrasted with its sensitizing effect on the subsurface region with which it has no immediate contact, is at first sight surprising, but is consistent with the distinction which Mitchell has made between a surface sensitizer, functioning by capturing positive holes which approach the surface,<sup>5</sup> and a halogen acceptor like nitrite ion which is unable to transfer an electron to a positive hole in silver bromide, although able to do so to free bromine in aqueous medium.

The deep internal latent-image has already been described in some detail.<sup>8</sup> In addition to its appearance at depths greater than those to which light can penetrate with significant intensity, important characteristics of this image are: (a) it persists without much decrease in maximum depth when the exposure is carried out at  $-50^\circ$ , followed by etching and development at room temperature; and (b) when formed at intermediate depths by prolonged exposure at  $-50^\circ$ , followed by normal etching and development, it is strongly solarized, while no solarization of the internal image in pure crystals is observed when exposures are made at room temperature. The existence of the deep internal latent-image can scarcely leave any doubt that electrons or silver atoms diffuse into the interior, possibly along dislocations, from the absorption layer near the surface wherein the primary photoelectrons and positive holes are produced. If the bromination hypothesis of solarization is adopted,<sup>17</sup> bromine also in some form must diffuse into the interior and attack latent image at low temperature.

It does not seem possible at present to say decisively whether the deep internal image in these crystals is produced by diffusion of electrons or of silver atoms from the absorption zone. The deep image might conceivably be formed by a redistribution of latent image near the surface on absorption of radiation, but since it is found to be produced with no less efficiency by short exposures (0.01 sec.) than by longer exposures at the same intensity, this mechanism appears to be excluded. The relatively high rate at which the equilibrium distribution of the deep latent image is attained is consistent with its formation by diffusion of primary electrons. The operations of etching and development impose a time interval of a few minutes from the end of the exposure before the distribution can be ascertained, but it is certainly set up within that interval, since no increase in the maximum depth of the internal latent-image is observed if the interval between exposure and development is increased. It is true that surface films of silver deposited on silver bromide by evaporation in vacuum have been shown by Evans, Hedges and Mitchell<sup>3</sup> to lose silver by migration along the surface and into the interior, probably by an electron-silver-ion process, but this migration seems to be a slower process than that involved in the formation of the deep internal latent-image. On the whole, the known facts regarding the formation of the deep internal latent-image seem most consistent with its formation by the migration of primary electrons from the absorption layer. Similarly, although the observed solarization of the deep internal image at low temperatures might be caused by the diffusion of atomic or molecular bromine along internal surfaces, the conclusive evidence for the motion of positive holes in sheet crystals at room temperature afforded by the increase in the electrical conductivity of the crystals when placed in bromine vapor<sup>14,15</sup> makes it highly probable that the solarization is caused by the migration of positive holes into the interior from the absorption zone of the crystal.

**III. Distribution of Internal Latent-Image and Photolytic Silver throughout the Depth of Sheet Crystals.**—It has been shown by Hedges and Mitchell<sup>2</sup> that the photolytic silver formed by prolonged exposure of unsensitized sheet crystals is situated below the surface. Our measurements show that the photolytic centers produced by ultraviolet radiation are confined to a shallow layer just below the surface, few particles being more than about 2  $\mu$  from the surface (Fig. 2a).

(13) G. W. W. Stevens, "Fundamental Mechanisms of Photographic Sensitivity," J. W. Mitchell (editor), Butterworths Sci. Publications Ltd., London, 1951, p. 227.

(14) G. W. Luckey and W. West, *J. Chem. Phys.*, **24**, 879 (1956).

(15) L. M. Shamovskii, A. A. Durina and M. L. Gosteva, *J. Exptl. Theoret. Phys. USSR*, **30**, 640 (1956).

(16) E. A. Sutherns and E. E. Loening, *J. Phot. Sci.*, [2] **4**, 154 (1956).

(17) C. E. K. Mees, "The Theory of the Photographic Process," revised ed., The Macmillan Co., New York, N. Y., 1954, p. 257.

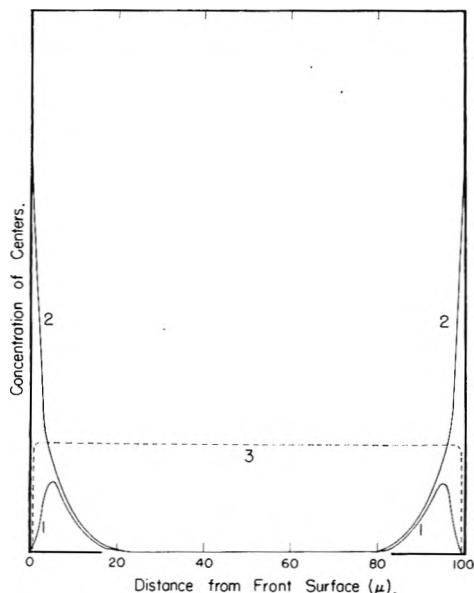


Fig. 1.—Distribution of photolytic and of latent-image centers throughout the depth of a crystal of pure silver bromide,  $100\ \mu$  thick, exposed to penetrating visible light (diagrammatic): 1, photolytic silver in crystal exposed in air; 2, photolytic silver in crystal exposed under sodium nitrite; 3, latent image in crystal exposed in air.

Especially interesting is the relative distribution of latent-image centers and of photolytic centers produced by penetrating light of long wave lengths, shown in Fig. 1. Pure sheet crystals of silver bromide exposed to light of wave length about  $470\text{--}480\ m\mu$ , which penetrates a  $100\text{-}\mu$  crystal with only about a 30% loss of the incident intensity at the rear surface, show developable latent image throughout the thickness of the crystal in amounts roughly proportional to the intensity prevailing at the various depths within the crystal, with the exception of insensitive subsurface layers extending within the crystal to about a micron from the surfaces of incidence and exit. The internal latent-image spreads about  $50\ m\mu$  laterally from the illuminated volume, the result of lateral diffusion analogous to the diffusion which causes the formation of deep internal latent-image in crystals exposed to radiation of short wave lengths. No lateral spread is observed in the very feeble images formed by penetrating radiation in the insensitive subsurface layers.

In contrast, photolytic silver particles formed by exposure to penetrating radiation are concentrated in two zones extending a number of microns within the crystal from the two surfaces, the central regions being devoid of visible particles,<sup>18</sup> (Figs. 1

(18) In estimating the concentration of photolytic silver as a function of depth within the crystal exposed to penetrating radiation, it is advantageous to choose conditions under which the photolytic silver appears as microscopically resolvable discrete particles. This condition can be secured by exposing to the penetrating light, of wave length about  $470\text{--}480\ m\mu$ , without removing red light. If red light is removed from the radiation of the incandescent tungsten source by interposing the copper sulfate filter, the visible image of photolytic silver formed by radiation of wave lengths longer than  $470\ m\mu$  often appears as a microscopically unresolvable brownish haze. If red light is present along with the actinic light, individual particles in any plane within the crystal can be discerned and brought into sharp focus against the hazy background which results from the out-of-focus particles at other depths. Heating the crystal containing unresolvable

and 3a). This difference in the nature of the distribution of latent-image and photolytic centers is not connected with any difference in the time of exposure required to form the respective images, for the difference is observed when the photolytic image and the latent image are produced by one and the same exposure of a given crystal. It appears, therefore, that latent-image centers persist in the interior during the whole of the duration of the exposure, but that they cannot grow to photolytic centers in the deeper parts of the interior, while they can, in regions nearer the surface.

The details of the distribution of photolytic silver formed by penetrating light depend upon the nature of the crystal and on the conditions of exposure. Unannealed crystals exposed in air show no photolytic silver at the surface and the maximum density of the photolytic centers occurs about  $5\text{--}7\ \mu$  from the surface, and about twice as far from the surface in crystals annealed for four hours of heating in nitrogen at  $200^\circ$ . If the exposure is made under the halogen acceptor, sodium nitrite, the total amount of photolytic action is increased, and dense deposits of photolytic particles appear at and immediately below the surface, sinking to very low concentrations of particles toward the center of the crystal.

These observations seem to be connected with observations by Luckey on the bromine evolution from sheet and slab crystals of silver bromide photolyzed *in vacuo*.<sup>19,20</sup> From the variation of the quantum yield of the bromine evolution from such material with wave length, crystal thickness, temperature and light intensity, it appears that most of the absorption effective in producing gaseous bromine in photolytic exposures occurs within a thin surface layer about  $\frac{1}{3}\ \mu$  thick. Between this level and the surface, positive holes can diffuse to the surface and there escape into vacuum sufficiently rapidly to ensure a relatively low rate of recombination with trapped electrons and hence allow the build-up of silver particles. If light is absorbed below this layer, the positive holes formed cannot diffuse rapidly to the surface; a relatively high concentration of holes builds up, and much recombination prevents the formation of silver particles.

This general view seems consistent with the distribution of photolytic silver observed in sheet crystals as a result of exposures to penetrating light. Positive holes produced by absorption in the interior of the sheet accumulate with increasing time of exposure, and, by attack of electrons trapped in latent-image centers, prevent these centers from growing to microscopically visible particles. Nearer the surface, the positive holes are removed by diffusion, and latent-image centers can grow to photolytic centers. When the crystals are exposed to

particles causes a similar, but less efficient, growth of photolytic particles, and, still less efficiently, merely holding the crystals at room temperature for some days also causes growth. The distribution-in-depth of the unresolved particles is difficult to determine by microscopic observation, but our general observations convince us that the distribution is not essentially changed when the particles grow under the influence of red light.

(19) (a) G. W. Luckey, *THIS JOURNAL*, **57**, 791 (1953); (b) *J. Chem. Phys.*, **23**, 882 (1955).

(20) C. A. Duboc, *Phys. Rev.*, [2] **98**, 1557 (1955).

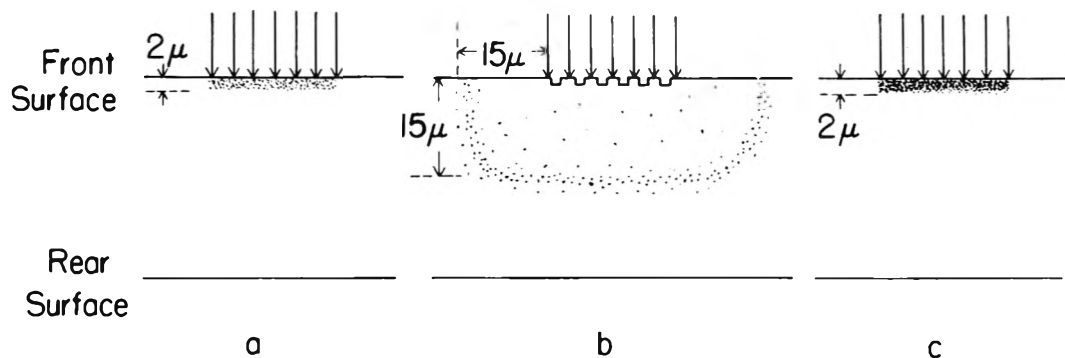


Fig. 2.—Depth-distribution of photolytic silver in silver bromide crystals exposed to ultraviolet radiation: a, pure silver bromide; b, silver bromide containing cadmium ion; note the complementary photolytic image on the surface of incidence; c, silver bromide containing cuprous ion.

penetrating radiation under nitrite solution, the zone within which most of the photolytic silver is deposited is not more than a micron in thickness from the surface, comparable with the thickness of the zone in which, according to Luckey's and Duboc's analyses,<sup>19,20</sup> diffusion to the surface keeps the concentration of positive holes below the value at which they are most likely to combine with electrons. These calculations depend on the assumption of very rapid liberation of holes at the surface into vacuum, as bromine molecules, so that the concentration of holes at the surface is kept very low, a condition which is approximately fulfilled in exposures under nitrite solution. As already mentioned, the position of the maximum concentration of photolytic particles formed during exposures in air is some 5–7  $\mu$  from the surface, suggesting that, in such exposures, the escape of adsorbed bromine from the surface is sufficiently slow to allow an appreciable build-up of positive holes in the region immediately below the surface, with a consequent inhibition of the growth of photolytic centers in this region.

It is clear, however, that these recombination processes in the interior of the crystal, effective though they may be in preventing the growth of the microscopically invisible latent-image centers to visible photolytic centers, do not prevent the formation of the latent-image particles themselves, nor are these particles in pure bromide crystals attacked by the accumulating positive holes which prevent their growth to the larger particles; the absence of photolytic silver in the deep interior of pure bromide crystals is not accompanied, at room temperature, by solarization of the latent image. The situation is, therefore, that, at a given concentration of positive holes in the interior of an illuminated sheet crystal, particles of latent-image size are stable, and photolytic particles are unstable. A diminished chemical or electrochemical activity of the photolytic-image particles with respect to attack by positive holes seems to be indicated. Mitchell<sup>5,11</sup> has suggested recently that an important factor in stabilizing latent-image centers against attack by positive holes is their acquiring a positive charge by adsorbing silver ions, the positive hole being repelled electrostatically. Such an explanation is tentatively consistent with our observations of the stability of latent-image centers in the interior of thin crystals, if the further as-

sumption is made that, in the growth of the latent-image centers toward photolytic centers, the rate of growth of the positive potential conferred by the adsorption of silver ions is not great enough to overcome the chemical affinity of a positive hole for the valence electron of a silver atom in the photolytic center. Moreover, the solarizability of internal latent-image at low temperatures already referred to suggests that even latent-image centers may be attacked by positive holes under these conditions, a circumstance which, on the hypothesis of charge-stabilization of latent-image centers, would indicate diminished adsorption of silver ions by the latent-image centers at low temperature.

**IV. Effect of Cadmium Ion on the Distribution of Latent and of Photolytic Image in Silver Bromide.**—If the absence of photolytic silver in the interior of crystals of silver bromide is associated with the accumulation in these regions of positive holes, it should be possible to modify the distribution of photolytic centers by the introduction of internal hole-traps. The effect of cadmium ion, introduced into the crystals by co-fusion, was first studied. As is well known, the substitution of divalent cadmium ions for silver ions in the silver bromide lattice introduces an equivalent concentration of silver-ion vacancies, accompanied by a decrease in the concentration of interstitial silver ions, signalled by a fall in electrical conductivity on the addition of very small amounts of cadmium ion, followed by large increases in conductivity on further additions of the divalent ion.<sup>21,22</sup> The cation vacancies, which are centers of negative charge, might trap positive holes to some degree, although available information suggested that any such trapping in silver bromide must be considerably less efficient than the corresponding process in the alkali halides, in which positive holes trapped at cationic vacancies form *V*-centers, characterized by well-defined ultraviolet absorption bands.<sup>23</sup>

Sheet crystals of silver bromide containing 1 mole % of cadmium bromide were found to be optically inhomogeneous at room temperature; those containing 0.01 mole % of cadmium bromide were optically homogeneous, while those containing 0.03 and 0.1 mole % scattered more than pure crystals, much of the additional scattering being

(21) E. Koch and C. Wagner, *Z. physik. Chem.*, **B38**, 295 (1937).

(22) J. Teltow, *Ann. Physik*, [6] **5**, 62 (1949).

(23) E. Mollwo, *ibid.*, [5] **29**, 394 (1937).

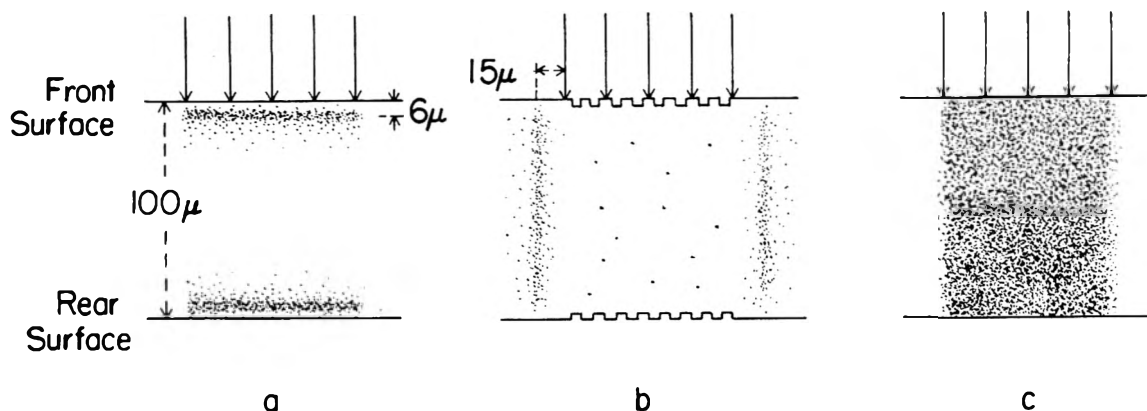


Fig. 3.—Depth-distribution of photolytic silver in silver bromide crystals exposed to penetrating visible light: a, pure silver bromide; b, silver bromide containing cadmium ion; note the complementary photolytic images on the surfaces of incidence and exit. c, silver bromide containing cuprous ion.

confined to the surface layers. The electrical conductivity of the crystals at room temperature increased regularly between cadmium bromide contents, 0.001 to 0.1 mole %, consistent with increasing concentrations of mobile cationic vacancies.

The effects of cadmium ion on the photolytic sensitivity of sheet crystals of silver bromide can be summarized as follows. (a) Cadmium ion greatly diminishes the total production of photolytic silver, as already found by Burgers and Kooy,<sup>24</sup> especially for excitation by light of long wave length.

(b) The distribution pattern of the photolytic centers formed in cadmium-containing crystals is characteristically different from that in pure crystals. If cadmium-containing crystals are exposed through a slit to light which is strongly absorbed within the crystal, most of the photolytic silver is formed in a shell-like structure outside the illuminated volume as shown diagrammatically in Fig. 2b. The lateral and downward displacements from the illuminated volume of the layers of photolytic silver formed in cadmium-containing crystals depend somewhat on the conditions of illumination, but when produced by non-penetrating light, the maxima in the concentration of photolytic product occur in regions beyond the range to which actinic light can penetrate with appreciable intensity by direct propagation or by scattering. Strong "wings" in the pattern of photolytic silver are characteristic of silver bromide crystals containing divalent cadmium or lead ions, and seem therefore associated with the presence of divalent ions as such. For exposures through a slit to penetrating light of long wave lengths, the total production of photolytic silver is very small, and practically all the product is formed in two lateral wings which penetrate from front to rear of the crystal (Fig. 3b). The illuminated volume itself contains only a few large photolytic centers, scattered through greater depths than for the same illumination of pure bromide.

(c) The surface of exposed cadmium-containing crystals displays a non-silver photolytic image, confined within the geometrical image of the slit,

and constituted of regularly oriented pits of square cross-section with sides parallel to  $\langle 100 \rangle$  crystallographic directions. The pits may grow with increasing duration of exposure to a size of several microns square, although as they become larger they become less regular. These surface bodies survive treatment with nitric acid following a shallow etch, which completely removes photolytic silver, and also remain after heating the crystal to about  $300^\circ$ , which also causes the disappearance of photolytic silver centers. Sometimes localized patterns and concentrations of pits seem to be associated with corresponding patterns of photolytic silver centers in the subsurface layer. This surface image of pits will be referred to as the complementary photolytic image. When a photolyzed cadmium-containing crystal of silver bromide is observed by transmitted light, much of the loss in density which discriminates between exposed and unexposed areas is caused by loss of light by scatter by the pits of the complementary image. If the crystal is exposed to penetrating light, complementary images appear at both the surfaces of incidence and of exit (Fig. 3b).

It seems likely that the surface pits represent localized escape of bromine from sites at which positive holes have been trapped at silver-ion vacancies. Positive holes and silver-ion vacancies participate in the formation of this image in much the same way as the complementary particles, electrons and interstitial or mobile silver ions, participate in the formation of the normal photolytic silver image, and the term "complementary photolytic image" seems appropriate for this image-wise formation of pits in the surface of crystals containing divalent ions.

The general characteristics of the photolytic image and of the complementary photolytic image in cadmium-containing crystals also appear in crystals of silver bromide containing divalent lead ion, and these characteristics therefore seem associated with the presence in the crystal of divalent ions as such and probably especially of the associated cationic vacancies.

Observations on the formation of internal latent-image in crystals containing cadmium ion appear to throw some light on the shell-like distribution of print-out silver outside the illuminated volume in

(24) W. G. Burgers and J. N. Kooy, *Rec. trav. chim. Pays Bas*, **67**, 16 (1948).

these crystals. The crucial facts on the internal latent-image in cadmiated crystals are that, for short exposures at room temperature, either to penetrating light or to strongly absorbed light, the amount and distribution of the latent image in the subsurface regions and deep in the interior of the crystal are similar to those for pure crystals subjected to the corresponding exposures, but that strong solarization of the deep internal latent-image is caused at room temperature by long exposures to penetrating light, but not to strongly absorbed light. The solarization of internal latent-image by penetrating light occurs at exposure levels below those required to produce visible silver (which, as just discussed, is concentrated in wings outside the illuminated volume). The significant point appears to be that solarization of the deep internal latent-image at room temperature in cadmiated crystals occurs only if light can penetrate to the regions in which this latent image is formed. Unsolarized internal latent-image can exist in these same regions, if formed as a result of exposure to ultraviolet light, even when the number of absorbed quanta of the ultraviolet light exceeds that for strongly solarizing exposures at long wave lengths.

The observed facts of low over-all photolytic sensitivity, the peculiar distribution of photolytic silver and the solarizability of the deep internal latent-image in sheet crystals containing cadmium ion can be accounted for if it is supposed that the silver-ion vacancies which are introduced into the lattice by the presence of cadmium ion form traps for positive holes adequately deep to retard diffusion of the holes from their place of origin at the site of an absorbed photon, but not deep enough to prevent attack of photolytic centers and even, when prolonged exposure to penetrating radiation produces enough holes, attack of already formed latent image. Some of the electrons produced in the illuminated volume diffuse out and are ultimately trapped to form silver atoms which aggregate to latent-image centers and to specks of photolytic silver. The silver centers will grow most rapidly where the concentration of the diffusing electrons is high, not far from the absorption layer in which they are produced. When the silver aggregates have become relatively large, they will probably act as efficient electron traps, so that, in the photolytic stage, most of the electrons will be trapped before they have diffused very far, resulting in the formation of a shell of photolytic silver closer to the illuminated volume than the maximum distance to which, in an earlier stage of the exposure, electrons can diffuse and form latent-image centers.

The positive holes accumulate, lightly trapped to silver-ion vacancies, in the illuminated volume. The positive space charge set up within the illuminated volume can be relieved by a motion of silver ions into the non-illuminated volume, where they may assist in the formation of silver atoms. The process of selective trapping of the positive holes within the illuminated volume and of diffusion of electrons out, may perhaps occur to some extent in pure silver bromide, but to a much smaller degree than in crystals containing divalent

ions; the two factors which make the separation of the positive holes and electrons by this process so marked in the impure crystals are the numerous shallow hole-traps provided by the silver-ion vacancies, and the high ionic mobility which tends to reduce space charge.

At low concentrations, the captured positive holes have little effect on the internal latent-image sensitivity of crystals containing divalent cations, possibly because of the repulsive effect of silver ions adsorbed to the latent-image centers already alluded to.<sup>5,11</sup> As the holes accumulate, however, they begin to act as recombination centers for electrons, and additional latent image ceases to form. The probability of attack of latent image by free positive holes is not very great at room temperature, as is shown by the non-solarizability of the deep internal latent-image in pure crystals, formed, as discussed in Section II, in a region to which both electrons and positive holes probably diffuse from the absorption zone. Nevertheless, high concentrations of positive holes can attack latent image, as is shown by the bleaching of the deep internal latent-image in those crystals by bromine and other oxidants applied to the surface,<sup>8</sup> and the solarization of the internal latent-image formed in crystals containing divalent cations on exposure to penetrating light shows that, before the photolytic stage of the exposure begins, the concentration of free positive holes becomes great enough for attack to take place on the latent-image centers. At the photolytic stage of the exposure, very few latent-image centers remain within the illuminated zone, and growth of latent-image centers to particles of photolytic silver can take place practically only in regions outside the illuminated volume, to which electrons, but not positive holes, can diffuse. In ultraviolet exposures, on the other hand, the production of positive holes is confined to the thin absorption layer near the surface, and since, in the presence of high concentrations of cationic vacancies, they cannot migrate far from this layer, they cannot attack the latent image formed by diffusion of the electrons to greater depths, and no solarization of the deep internal latent-image.

**V. Effects of Cuprous Ion on the Photolytic Sensitivity of Sheet Crystals.**—Earlier work in these Laboratories on the behavior of silver chloride containing cuprous ion shows that this ion may act as an effective trap for positive holes,<sup>25,26</sup> probably by electron exchange between the cuprous ion and the hole. The effect of cuprous ion in sheet bromide crystals has, therefore, been studied in comparison with the effects of cadmium and lead ions. The valence condition of copper ion added to silver halides by co-fusion has been investigated by Urbach and co-workers,<sup>25,26</sup> who found that cuprous or cupric ion incorporated by fusion into silver halides in the absence of a halogen atmosphere entirely assumes the cuprous state on cooling to room temperature. The radius of the cuprous ion, 0.96 Å., is somewhat smaller than that of the

(25) N. R. Nail, F. Moser, F. E. Goddard and F. Urbach, *Phys. Rev.*, [2] **98**, 1557 (1955).

(26) F. Moser, N. R. Nail and F. Urbach, *Phys. Chem. Solids*, **3**, 153 (1957).

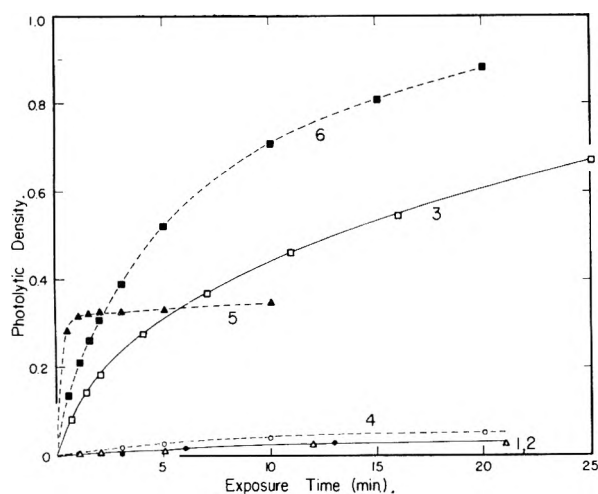


Fig. 4.—Rate of photolysis of cuprous-containing silver chloride and silver bromide: 1, 2, 3, silver bromide containing 0.00, 0.01 and 0.1 mole % cuprous ion; 4, 5, 6, silver chloride containing 0.00, 0.01 and 0.1 mole % cuprous ion, respectively.

silver ion, 1.13 Å. At room temperature, the cuprous ions in silver bromide appear to occupy silver-ion lattice sites substitutionally, as is indicated by the negligible difference in the electrical conductivity of pure crystals and of those containing cuprous ions under these conditions, although Teltow<sup>27</sup> from measurements of conductivity at temperatures above 200° concludes that cuprous ions at elevated temperatures occupy interstitial sites in the silver bromide lattice. Crystals containing 0.01 mole % cuprous ion appeared optically homogeneous in the interior, but the surfaces displayed microscopically small dot-like markings absent in sheets of pure silver bromide; larger amounts of cuprous ion increased the concentration of surface marks, and some discrete scattering particles were microscopically visible in the interior of the sheets.

In large crystals of silver chloride,<sup>25,26</sup> quantities of cuprous ion less than one part per million cause a marked increase in the amount of photolytic product throughout the volume of a crystal exposed to penetrating light, but in the bromide little effect of cuprous ion was observed until the concentration of the foreign ion was increased to more than 0.01 mole % (34 parts cuprous bromide per million). The rate of photolysis of silver bromide increased regularly with cuprous-ion concentration in the range 0.01 to 1 mole %, the highest used in the experiments. Accelerated photolysis of silver bromide containing cuprous ion has been observed by Clark and Mitchell.<sup>4</sup> The relatively high concentrations of cuprous ion necessary to alter the rate of photolysis of silver bromide in contrast to the minute quantities effective in the chloride suggests that inhomogeneities may be concerned in the effect in bromide. The effects of cuprous ion on the photolysis of thin crystals of silver bromide and chloride on exposure to penetrating radiation are compared in Fig. 4, which shows the densities of the photolytic images in the two halides, measured by means of a photoelectric densitometer, as a

function of the time of exposure. The saturation plateau in the density of the photolytic product, found by Urbach and co-workers to be characteristic of the photolysis of thick crystals of silver chloride exposed to penetrating light<sup>25,26</sup> and reproduced also in thin crystals of silver chloride, is not found for the bromide. The effective wave lengths in the exposure of the bromide were between about 470 and 480 m $\mu$ , and for the chloride 436 m $\mu$ , for which the absorption coefficient is approximately the same as for the bromide at 470 m $\mu$ .

At room temperature, the absorption of thin sheet crystals of bromide showing enhanced photolysis as a result of the addition of cuprous ion was found to be substantially the same for the actinic radiation used as for the pure bromide; hence the increased photolysis is not a consequence of increased absorption of radiation. At elevated temperatures, additional absorption, reversible on cooling, at wave lengths longer than the absorption edge in pure bromide sheets was observed in sheets containing cuprous ion, but no photolytic experiments at those temperatures were carried out.

With respect to the distribution of photolytic silver throughout the depth of the copper-containing silver bromide, the most instructive result is that exposure to penetrating light produces photolytic silver in enhanced yield over that for the pure bromide throughout the thickness of the crystal, except for layers of low photolytic sensitivity immediately under the surface. Side wings, although not absent, are much less prominent than in crystals containing cadmium ion. This distribution is very different from that in a pure crystal, in which photolytic silver is not formed in the interior by penetrating light. Figure 3c shows diagrammatically the distribution of photolytic silver formed by penetrating light in copper-containing crystals of silver bromide.

The observations fulfill the expectation that sufficiently deep traps for positive holes throughout the crystal will permit photolytic silver to be formed by penetrating light in the interior of the crystal, and are consistent with the hypothesis that the absence of photolytic silver in the interior of pure or cadmium crystals is caused by attack of photolytic centers by positive holes which accumulate there on exposure to penetrating light.

**Relative Silver and Bromine Quantum Yields in Copper-containing Silver Bromide.**—If the function of cuprous ion in silver bromide is to trap positive holes tightly with the formation of cupric ion and lattice bromide ion, it follows that the bromine yield in the photolysis of crystals containing cuprous ion, in spite of the enhanced silver production, should not be greatly increased over that of similarly exposed pure crystals. This expectation has been found to be true, and the experimental evidence for the supposition that cuprous ion acts as a positive hole-trap is therefore very strong.

For excitation by wave length 436 m $\mu$ , the silver yield in the impure crystals, as measured by the optical density of the photolytic image, was found in a number of experiments, to be about eight

(27) J. Teltow, *Z. Physik. Chem.*, **195**, 197 (1950).

TABLE II

RELATIVE SILVER AND BROMINE PRODUCTION ON PHOTOLYSIS OF PURE AND CUPROUS-CONTAINING SILVER BROMIDE								
Wave length, $m\mu$	Intensity, quanta $cm.^{-2} sec.^{-1}$	Duration, min.	Br evolved. $10^{-8}$ equiv. Pure AgBr	AgBr, $Cu^+$	Density of silver image Pure AgBr	AgBr, $Cu^+$	Ratio of yield Silver Bromine	
436	$1.7 \times 10^{16}$	7	2.04	1.77	0.07	0.58	8.3	0.87

times that in pure crystals, although for illumination by wave length  $365 m\mu$ , the ratio was only 1.5. The bromine evolution was measured by absorption of the photolytic bromine by fluorescein paper, followed by extraction and photometric measurement of the brominated dye. A piece of sheet crystal some 5 by 10 mm. in dimensions was placed in a thin glass cell provided with entrance and exit tubes for the passage of a stream of nitrogen. Photolytic bromine was carried by the gas stream to a piece of moistened filter paper, impregnated with fluorescein, clamped between the members of a small ball-and-socket joint.<sup>28</sup> After exposure of the crystal for 5–10 minutes to suitably filtered radiation from a 100-watt quartz-mercury arc, the paper was removed, extracted with a small volume of boiling 0.02 *M* sodium bicarbonate solution, and the brominated dye measured by means of the Beckman DU spectrophotometer in a narrow 5-cm. cell.

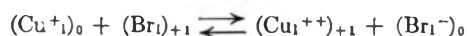
An empirical calibration curve was made by similarly collecting the bromine resulting from the oxidation of known small amounts of potassium bromide by ceric ion in dilute sulfuric acid, in an apparatus similar to that used in the photolysis. In the calculation of the analytical results, it is assumed that the brominated product has the molar extinction coefficient of eosin; actually, the product may be partly dibromofluorescein, but calculation shows that no great error is thereby incurred. The bromine content of the dye product is not involved in the calculation. Table II gives representative data for the relative bromine and silver yields of the pure and the copper-containing crystals produced by exposure to light of wave length  $436 m\mu$ .

Averaged over five runs of about seven minutes' duration, the bromine evolution from the crystals containing cuprous ion amounted to 80% of that from the pure material, while the silver density at the wave length of maximum absorption was about eight times greater for the impure than for the pure material. The difference in the ratio of silver production to that of bromine evolution in the impure and pure crystals is a measure of the trapped holes in the impure crystal.

**Reversible Thermal Fading of the Photolytic Image in AgBr + Cu<sup>+</sup>.**—Comparison of the photolytic effects of cuprous ion and cadmium ion indicates that the cuprous ion forms a much deeper positive hole-trap than the silver-ion vacancy, but even this trapping is not permanent. An appreciable fading of the photolytic image formed in silver bromide containing cuprous ion occurs at room temperature, and at 170° the fading is nearly complete within a few seconds. The amount of fading at room temperature or at 170° is considerably less for the photolytic image produced by light of wave length  $365 m\mu$  than by blue light. On being

cooled to room temperature, a crystal in which a photolytic image has been subjected to thermal fading regains its original high sensitivity, and the process of image formation at room temperature, followed by thermal bleaching at elevated temperature, can be repeated many times. No appreciable fading occurs in the course of several days in a photolytic image formed at room temperature when the sample is maintained at  $-70^\circ$ .

The reaction between  $Cu^+$  in the lattice and the positive hole is therefore reversible, according to the equation



where the suffix l indicates that the species occupies a lattice site, the symbol  $(Br)_{+1}$  is the untrapped positive hole, and the suffixes outside the brackets indicate the effective charge of the lattice site. The right-hand side of the equation represents a cupric ion occupying a lattice cation site, constituting the trapped hole, adjacent to a bromide ion in an anion site. The thermal bleaching of the photolytic image in these crystals is not accompanied by detectable bromine evolution; the mobile untrapped holes attack the photolytic silver, forming silver bromide.

**Photochemical Storage of Energy.**—The photochemistry of silver bromide crystals containing cuprous ion illustrates a possible type of controlled storage of energy in crystalline solids. The primary endoenergetic photochemical separation of electrons and positive holes is brought about by energy absorbed from light, while the subsequent trapping and recombination processes are exothermal. In pure crystals or in normal photographic material, the exothermal reactions take place within a very short interval of time after the absorption, and the energy derived from the light is stored for a very short time. In crystals containing cuprous ions, however, the positive holes at room temperature, and especially at lower temperatures, are trapped for prolonged periods. The trapping of the holes is accompanied by a large increase in the yield of photolytic silver, but the energy of activation for untrapping is sufficiently low to allow exothermal recombination of the positive holes with photolytic silver at moderately elevated temperatures. Silver ions and cuprous ions are regenerated, and, on cooling to room temperature, the system is restored to its original light-sensitive condition. The endoenergetic photoprocess and the exothermal recombination can be repeated at will. The heat available per gram of crystal in this recombination is small compared with the heat of combustion of one gram of carbon, even when the photochemical process proceeds with high efficiency, but the silver bromide-cuprous ion system seems of some interest as a model of one type of photochemical storage of energy in solids.

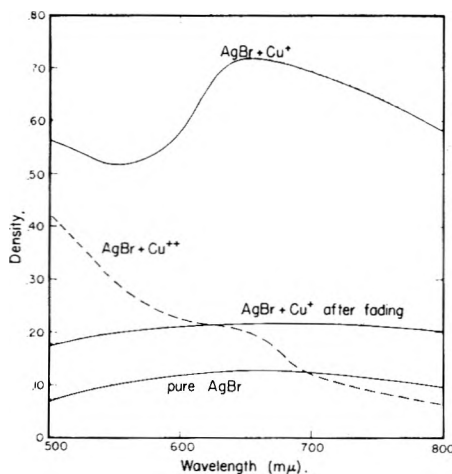


Fig. 5.—Absorption spectra of photolytic products in pure and cuprous-containing silver bromide, and (dotted curve) the spectrum of unphotolyzed, cuprous-containing silver bromide after exposure to bromine.

**Spectroscopic Evidence for the Presence of  $\text{Cu}^{++}$  in Photolytic Images in  $\text{AgBr} + \text{Cu}^+$ .**—As is shown by the topmost curve in Fig. 5, the absorption of the photolytic product formed by exposure to blue light of sheet crystals of silver bromide containing cuprous ion increases in intensity toward shorter wave lengths, until it becomes lost in the absorption of the silver bromide. This branch of rising absorption is absent from the spectrum of the photolytic product resulting by blue radiation in pure silver bromide sheets, and is much feebler in the spectrum of the product formed in copper-containing sheets exposed to light of wave length  $365 \text{ m}\mu$ .

Urbach and co-workers have shown that exposure to chlorine of silver chloride containing cuprous ion causes an absorption band to be developed, which they attribute to absorption by cupric ion formed in the lattice by oxidation of the cuprous ion.<sup>26</sup> A similar coloration of thin crystals of silver bromide by bromine is observed. The dotted curve of Fig. 5 represents the absorption spectrum of a silver bromide sheet originally containing cuprous ion at 0.1 mole % which has been colored by exposure to bromine. The absorption increases with decreasing wave length from a low value in the red. At constant bromine pressure, the rate of growth of this absorption at  $540 \text{ m}\mu$  follows the first-order equation  $da/dt = k(a_s - a)$ , where  $a$  is the density at time  $t$  and  $a_s$  is the limiting saturation value of the density,  $\log(a_s - a)$ , decreasing linearly with time.

The saturation value of the absorption increases with the original cuprous-ion content of the crystal. The equation indicates that every cuprous ion produces a color center by reaction with bromine, and that, if the bromine concentration is maintained constant, the rate of formation of the color centers at any instant is proportional to the concentration of residual cuprous ions. It is therefore very likely that the absorbing centers induced by bromine in silver bromide containing cuprous ion are cupric ions formed by reaction of the cuprous ions with positive holes.

The color induced by bromine in these crystals fades very slowly at room temperature (about 6% per day for an initial optical density of about 0.7) and rapidly at about  $200^\circ$ . The fluorescein test shows the liberation of bromine during fading at elevated temperatures. Free positive holes are produced in the crystal containing the oxidized copper ion by the reverse reaction in equation 1, and are liberated as bromine, in contrast to the situation in which the holes are untrapped thermally in these crystals in the presence of photolytic silver. Silver bromide is then produced, and no bromine is formed.

The branch at short wave lengths of the absorption spectrum of the photolytic product in silver bromide containing cuprous ion runs parallel with the spectrum produced by the action of bromine on these crystals, and it seems very probable that this branch is indeed the absorption spectrum of the cupric ion produced in the photolysis. It is significant that, for excitation by  $365\text{-m}\mu$  radiation compared with  $436\text{-m}\mu$  radiation, (a) the increase in photolytic yield caused by cuprous ion is lower, (b) the rate and amount of fading, both at room temperature and at elevated temperature, are lower and (c) the contribution of cupric ion to the spectrum of the photolytic product is smaller; thus, the yield of photolytic silver is highest and the rate of fading is highest when the spectral evidence indicates greatest production of cupric ion in the photolytic product.

The explanation of the difference in the effect of cuprous ions at different wave lengths probably lies in the relation between the volume concentration of absorbed photons and cuprous ions when the exciting wave lengths are in the ultraviolet and the blue regions, respectively. The ultraviolet radiation is absorbed in a thin layer near the surface, while blue light penetrates farther. The number of cuprous ions per  $\text{cm}^2$  of material  $1 \mu$  thick at a cuprous ion concentration of 0.1 mole % is some  $1.4 \times 10^{15}$  and the incident intensity of ultraviolet radiation and of blue light in the experiments was about  $10^{15}$  quanta  $\text{cm}^{-2} \text{sec}^{-1}$ . Radiation of wave length  $365 \text{ m}\mu$  is absorbed to the extent of 40% of the incident intensity in penetrating  $1 \mu$ , but a thickness of  $11 \mu$  is required to absorb 40% of the incident radiation of wave length  $436 \text{ m}\mu$ . It is probable, therefore, that cuprous ions in the absorption layer for ultraviolet illumination soon become saturated with trapped positive holes; hence in prolonged exposure, most of the photolytic action would be produced without benefit of these ions and a large fraction of the positive holes would escape as bromine to the atmosphere. The thicker actinic layer associated with excitation by blue light contains a greater number of cuprous ions per absorbed photon, and saturation of the hole traps will not occur at the very start of the exposure; the resulting image will contain relatively more cupric ions, but at the same time will be more unstable than the image obtained from ultraviolet exposure.

We wish to acknowledge the assistance of J. H. Altman of these Laboratories in making the microdensitometer measurements reported in Table I.



## IONIC MIGRATION IN ION-EXCHANGE MEMBRANES

BY W. T. GRUBB

*General Electric Research Laboratory, Schenectady, New York**Received April 16, 1958*

The resistivities of some ion-exchange membranes have been measured at a frequency of 1000 cycles per second using a Shedlovsky conductivity bridge. The resistivities of three commercial types of membranes have been compared at 25°. In addition, one type of sulfonated phenol-formaldehyde ion-exchange membrane has been further investigated under a variety of conditions. The effects of the size of the mobile ion, the temperature and the level of water activity in this membrane upon its resistivity, have been measured. It has been observed that the resistivity of the membrane is a linear function of the Stokes law radius of the mobile ion for a series of alkali metal ions. For membranes saturated with water the temperature coefficient of the specific conductance indicates an activation energy for ionic migration of about 3 kcal. per mole. When the activity of water in phenolic membranes in the hydrogen ion form is varied, it has been observed that the logarithm of the specific conductivity is a linear function of the activity of water. These results were obtained by equilibrating these membranes in solutions in water in ethylene glycol of varying composition. The implications of these results with regard to the mechanism of ionic migration in ion-exchange polymers are discussed.

## Introduction

The electrolytic properties of ion-exchange membranes have been studied to a relatively slight extent compared to other properties of these materials. This is true despite the convenience of making such measurements and the close relation of ionic conductivity to the self-diffusion constant for the ion in question.<sup>1</sup> Although the relatively new class of materials comprising the ion-exchange membranes have found only a few applications notably in the purification of saline waters by electro dialysis,<sup>2</sup> other uses would seem to be inevitable for the very special properties of these polymeric solid electrolytes. An excellent review of general properties of ion-exchange membranes recently has been published.<sup>3</sup> Their application as solid state battery electrolytes<sup>4</sup> has been reported.

It is the purpose of this paper to describe a method of obtaining the volume resistivity of ion-exchange membranes under well defined conditions and to report the results of a study of the effect of some variables upon the volume resistivity.

Many determinations of electrolytic properties of ion-exchange membranes have been carried out by the method of compartmented cells in which the conductivity of the membrane is determined by difference between the cell containing a membrane separator and the cell containing only the aqueous electrolyte.<sup>5-7</sup> If the conductivity of the membrane containing no leachable electrolyte (*i.e.*, in equilibrium with pure water) is desired, this may be found by extrapolation of the results of compartment cell measurements at increasingly lower concentrations of electrolyte.

Ion-exchange membranes can also be measured by a *direct method* consisting of clamping a sheet of the membrane directly in contact with inert metal electrodes and employing a conductivity bridge

in the usual way. In this manner, Spiegler and Coryell<sup>1</sup> have investigated a phenol sulfonate formaldehyde membrane in its sodium, zinc and calcium forms near room temperature. They have also measured self diffusion rates of the cations using radioactive ions and have found that the Einstein<sup>8</sup> relation is approximately correct in describing the relation between electrolytic conductivity and self diffusion.

Since the *direct method* for conductivity measurements on ion-exchange membranes gives results of greatest interest in considering their solid state properties, it has been refined and extended to the measurement of membranes under a variety of conditions. The characteristics of three types of cation-exchange membranes have been determined for the acid form and one type of membrane has been investigated under a variety of conditions to determine the effects upon its electrolytic conductivity of varying the ionic form, the temperature and the solvation of the membrane. In the latter instance water-ethylene glycol solutions of various compositions have been employed.

## Experimental

The conductivity cell used to clamp the membrane in place between electrodes was constructed of Teflon. With a membrane in place, the electrolyte conductance was obtained directly at the terminals of the cell. However, since the contact resistance of the electrode-membrane interface might not be negligible, the cell was designed to eliminate this error by providing a number of fixed positions of the electrodes on the membrane such that a series of measurements at different cell constants was made. The plot of resistance *versus* cell constant (in the form of cell length divided by the product of membrane width by membrane thickness) was linear, and from its slope was obtained the volume resistivity of the membrane. The physical dimensions of the membranes were obtained by measurements with a micrometer caliper. The length in each measurement was determined by measuring the distance between the leading edges of the cell electrodes using a travelling microscope. Any errors in this arbitrary choice of reference points also cancel out when the method of variable cell constants is employed. The method of variable cell constants has been employed by Hills, *et al.*,<sup>9</sup> in the measurement of resistivities of some polyelectrolyte gels and found to be satisfactory.

The electrical measuring equipment consisted of a Shedlovsky conductivity bridge. A Wagner earthing circuit was employed to balance out unsymmetrical capacity paths to

(1) K. S. Spiegler and C. D. Coryell, *THIS JOURNAL*, **57**, 687 (1953).  
 (2) C. B. Ellis, "Fresh Water from the Ocean," The Ronald Press, New York, N. Y., 1954.

(3) K. S. Spiegler, Chapter 6 of "Ion Exchange Technology," ed. by F. C. Nachod and J. Schubert, Academic Press, New York, N. Y., 1956.

(4) W. T. Grubb, *J. Electrochem. Soc.*, in press.

(5) *Ann. Rev. Phys. Chem.*, **3**, 126 (1952).

(6) G. Manecke and E. Otto-Laupenmühlen, *Z. physik. Chem. N. F.*, **2**, 336 (1954).

(7) A. G. Winger, G. W. Bodamer and R. Kunin, *J. Electrochem. Soc.*, **100**, 178 (1953).

(8) W. E. Garner, "Chemistry of the Solid State," Butterworth's Scientific Publications, London, 1955, p. 27.

(9) G. J. Hills, J. A. Kitchene and P. J. Ovenden, *Trans. Faraday Soc.*, **51**, 719 (1955).

ground. The detector was a pair of sensitive headphones behind a 2-stage amplifier. In many of the ion-exchange membrane samples, the capacity compensation component is large, and to obtain a completely silent minimum, the capacitor of the bridge included a General Radio Co. Decade capacitor, which permitted capacity readings up to 1.2 microfarads.

The conductivity cell was kept at constant temperature in a heavy copper box immersed in a water thermostat. This box served the purposes of providing shielding, distributing any thermal gradients and confining the cell and membrane sample in a known atmosphere. Used in this manner, the copper box is an air thermostat, and if electrically grounded, the usual objection<sup>10</sup> to the use of water thermostats in conductivity measurements is avoided. The atmosphere inside the copper box usually was kept at 100% relative humidity by the presence of a small beaker of water with a wick immersed in it.

Measurements in the present report have been confined to membranes in their leached states. Three commercial ion-exchange membranes of different type and manufacture have been employed. The procedures of Juda, *et al.*,<sup>11</sup> were employed to ensure complete conversion into one ionic state and removal of counter electrolyte.

The effect of the electrode surface upon the measurements was investigated. The resistance is a linear function of the variable cell constant for the same membrane whether bright platinum electrodes or platinized platinum electrodes are employed. Platinizing has mainly the effect of reducing the apparent contact resistance and does not markedly influence the slope. This means that the condition of the electrodes is not too critical in determining resistivities. Platinized platinum electrodes have been employed in all the experiments described.

Cation membranes from three commercial suppliers have been compared in their hydrogen ion forms. These membranes are known under these trade names: "Amberplex C-1" manufactured by the Rohm & Haas Co., Philadelphia, Pa., "Zerolit 315" manufactured by the Permutit Co. Ltd., London, England, and "Nepton CR-51" manufactured by Ionics, Inc., Cambridge, Mass. Their resistivities at 25.00  $\pm$  0.03° and 1000 cycles/sec. are, respectively, 38.2, 16.7 and 9.6 ohm cm. Unless otherwise indicated all resistivity data in this paper refer to 25° and 1000 cycles/sec.

Various samples of membranes from a given manufacturer vary in resistivity from one sample to the next somewhat more than experimental errors could explain. Nine separate pieces of Nepton CR-51 were measured and the results are shown in Table I.

TABLE I

Sample no.	1	2	3	4	5	6	7	8	9	Av.
Resistivity	9.59	10.0	9.54	9.37	9.66	9.50	9.73	9.42	9.78	9.62
(ohm cm.)										

The conductivities of ion-exchange membranes are affected not only by the membrane type but also by the ionic form of the membrane, the temperature and the solvating liquid. The effects of these other factors have been determined for "Nepton CR-51," a condensation product of phenol-sulfonic acid and formaldehyde<sup>12</sup> (hereafter called the phenolic membrane). Selected pieces with conductivity close to the average value of 104 milliohm cm. (see above) have been employed, and conclusions of the present work are based only upon the relative values of conductivity as a function of varying conditions, thus avoiding the variability indicated in Table I above.

The phenolic ion-exchange membrane is characterized by its capacity in terms of amount of exchangeable ions per unit volume and its relative degree of cross-linking as indicated by the amount of swelling in water. These properties have been determined for a membrane of typical conductivity value and compared with previous values in the literature.<sup>11</sup>

Measured dimensions of leached H<sup>+</sup> and Na<sup>+</sup> membranes indicate approximately 1% linear shrinkage in the conver-

(10) G. Jones and R. C. Josephs, *J. Am. Chem. Soc.*, **50**, 1065 (1928).

(11) W. Juda, N. W. Rosenberg, J. A. Marinsky and A. A. Kasper, *ibid.*, **74**, 3736 (1952).

(12) W. Juda *et al.*, U. S. Patent 2,636,851.

TABLE II

	Present work (H <sup>+</sup> form)	Lit. <sup>11</sup> (Na <sup>+</sup> form)
Water content, %	54 $\pm$ 1 <sup>a</sup>	55.3 $\pm$ 1 <sup>a</sup>
Wet density	1.2 $\pm$ 0.1 <sup>a</sup>	1.33 $\pm$ 0.01 <sup>a</sup>
Capacity	1.2 $\pm$ 0.1 meq./ml. <sup>a</sup>	1.26 $\pm$ 0.02 meq./ml. <sup>a</sup>
	1.01 meq./g.	0.94 meq./g. <sup>a</sup>
	2.2 meq./dry g.	2.1 meq./dry g.

<sup>a</sup> Based on leached aqueous sample wiped dry.

sion from H<sup>+</sup> to Na<sup>+</sup> for Nepton CR-51. The data of Table I indicate that the present samples of Nepton CR-51 are very similar to materials of the same manufacturer that have been characterized previously.<sup>11</sup>

## Results and Discussion

**Electrical Conductivity as a Function of Ionic Type.**—A single strip of the phenolic ion-exchange membrane was measured in a series of ionic states through the cycle H<sup>+</sup>, Na<sup>+</sup>, Li<sup>+</sup>, K<sup>+</sup>, H<sup>+</sup>. The results are presented in Table III.

TABLE III

RESISTIVITY OF PHENOLIC ION-EXCHANGE MEMBRANE IN UNIVALENT IONIC FORMS AT 25°

Ionic form	Specific resistance, ohm cm.	Specific conductance, millimho cm. <sup>-1</sup>
H <sup>+</sup>	9.6	104
K <sup>+</sup>	50.3	19.9
Na <sup>+</sup>	71	14.1
Li <sup>+</sup>	93.3	10.7
H <sup>+</sup>	9.7	103

The final measurement of the H<sup>+</sup> membrane shows a variation of about 1% from its initial value. The relative values of ionic conductance have therefore about this limit of accuracy. The conductivity values in the present work are somewhat higher than those previously reported by Rosenberg,<sup>13</sup> who has not published this work in detail. It is probable that only the relative values of conductivity have real significance at the present time since the absolute values depend upon frequency, variations of the membrane, contact resistances and also upon the method of measurement. It was pointed out<sup>14</sup> that absolute resistivities are very sensitive to details of preparation of the membrane.

The resistivities are found to be linear with the hydrated ionic radii ( $R_i$ ) as calculated by Remy.<sup>15</sup>

The values of  $R_i$  were computed by Remy from Stokes law and the mobilities of the ions (at infinite dilution). This particularly simple relation of  $\rho$  to  $R_i$  does not extend to ions of different valence or heavy metal ions. This is illustrated by measurements on zinc and copper presented in Table IV which includes a measurement upon the H<sup>+</sup> state of the same membrane sample (differing from that of Table III).

**Effect of Temperature upon Conductance of Phenolic Membranes.**—The conductivity of aqueous solutions of electrolytes at varying temperatures frequently obeys Walden's rule in that

(13) *Ann. Rev. Phys. Chem.*, **4**, 389 (1953) (reference to a Gordon Conference Presentation on Ion Exchange, July, 1951).

(14) K. Sollner, *Ann. N. Y. Acad. Sci.*, **57**, 192 (1953).

(15) H. Remy, *Z. physik. Chem.*, **89**, 467 (1915).

TABLE IV

RESISTIVITY OF PHENOLIC ION-EXCHANGE MEMBRANE IN DIVALENT IONIC FORMS AT 25°

Ionic form	Specific resistance, ohm cm.	Specific conductance, millimho cm. <sup>-1</sup>
Zn <sup>++</sup>	210	4.8
Cu <sup>++</sup>	176	5.7
H <sup>+</sup>	9.1	110

the increased conductance with rising temperature is proportional to the decrease in viscosity of the solvent. At 25° for example the viscosity of water decreases 2.2% per degree.<sup>16</sup> Since no measurable viscosity exists in a polyelectrolyte gel swelled with water, interest attaches to the measurement of ionic conductivity as a function of temperature. A single strip of the phenolic ion exchange membrane was measured at a series of temperatures between 0 and 41°.

TABLE V

RESISTIVITY OF PHENOLIC ION-EXCHANGE MEMBRANES IN THE H<sup>+</sup> FORM AT VARIOUS TEMPERATURES

Temp. (t), °C.	10 <sup>3</sup> /T	Specific resistance, ohm cm.	Specific conductance, millimho cm.
25.00	3.356	9.7	103
0.1	3.661	16.2	61.7
12.6	3.502	12.3	81.4
20.0	3.413	10.4	96.1
40.6	3.190	7.4	126.7

These data fall approximately upon a straight line when plotted as  $\log \kappa$  vs  $10^3/T$ . A least squares calculation (minimizing the squares of the  $\log \kappa$  residuals) shows the equation of the line to be

$$\log \kappa = 9.79 - 1.54 \times 10^3/T \quad (1)$$

or

$$\ln \kappa = 22.6 - 3.54 \times 10^3/T \quad (2)$$

where

$$T = \text{temperature in degrees Kelvin}$$

$$\kappa = \text{conductance in millimho cm.}^{-1}$$

This equation yields a temperature coefficient of 2% per degree centigrade near 25°.

Equation 2 may also be interpreted in terms of an enthalpy of activation for ionic migration. The calculated value of  $\Delta H^\ddagger$  for ionic migration is 3.0 kcal./mole. This conductivity-temperature relation confirms the generally accepted view of nearly complete ionization of the sulfonated polymeric ion exchangers, otherwise, a temperature dependent ionization constant would lead to a higher apparent value of  $\Delta H^\ddagger$  for ionic migration. The identity of the  $\Delta\kappa/\Delta t$  coefficient of the membrane with that of aqueous solutions also indicates that in H<sup>+</sup> migration the polymer network is not activated when the ion migrates.

**Effect of Solvation upon the Electrical Conductivity of Phenolic Ion-exchange Membranes.**—The mechanism of ionic conduction of the H<sup>+</sup> form of phenolic ion-exchange membranes is further elucidated by their conductive properties in equilibrium partially non-aqueous solutions. The system eth-

ylene glycol-water was selected somewhat arbitrarily for this part of the investigation. Leached H<sup>+</sup> membranes were equilibrated for at least 150 hours in the selected solution of H<sub>2</sub>O in ethylene glycol. While the membranes swell approximately 100% in water alone, the swelling in ethylene glycol is about 14% greater than this, and intermediate swellings are observed for the solutions. Because the swelling is so nearly constant the effect of the polymer network itself upon conductance is expected to remain roughly constant over the range of solvate composition.

Actual analysis for H<sub>2</sub>O in the polymer phase was not obtained in this work. However, the activity of H<sub>2</sub>O was calculated from the water analysis (Karl Fischer titration) in the solution, published vapor pressure data,<sup>17</sup> and density data of Curme and Johnston<sup>18</sup> for the water-ethylene glycol system. The H<sub>2</sub>O activity in the solution phase is, of course, equal to that in the membrane.

The following table presents the conductivity of the H<sup>+</sup> membranes as a function of the solvate composition expressed in various ways.

TABLE VI

RESISTIVITY OF H<sup>+</sup> PHENOLIC ION-EXCHANGE MEMBRANES AS A FUNCTION OF SOLVATION AT 25° USING THE SOLVATE SYSTEM H<sub>2</sub>O-ETHYLENE GLYCOL

Concn. H <sub>2</sub> O, <sup>a</sup> mg./ml.	Composition of solvating soln.			Resistivity of membrane, ohm cm.	Conductivity of membrane, millimho cm. <sup>-1</sup>
	% H <sub>2</sub> O by wt.	Mole fraction H <sub>2</sub> O	Activity H <sub>2</sub> O (a <sub>H<sub>2</sub>O</sub> )		
98	8.9	0.252	0.20 <sub>6</sub>	335	2.98
200	19.2	.434	.37 <sub>2</sub>	150	6.7
310	28.5	.579	.51 <sub>6</sub>	89.2	11.2
395	36.6	.665	.59 <sub>4</sub>	58.5	17.1
997	100	1.000	1.00	9.6	104

<sup>a</sup> From Karl Fischer titration.

The conductivity  $\kappa$  of the membranes is a strong function of the activity of water in the solvate solution and therefore also in the membrane. The logarithm of  $\kappa$  is very nearly linear with  $a_{H_2O}$ . This is true over the range of water activity from 0.2 to 1.0. The best linear relation has been calculated by the method of least squares (minimum of squares of  $\log \kappa$  residuals). This line is expressed by the equations

$$\log \kappa = 0.0899 + 1.920a_{H_2O} \quad (3)$$

$$\ln \kappa = 0.207 + 4.42a_{H_2O} \quad (4)$$

The actual reason for this linearity of  $\log \kappa$  with  $a_{H_2O}$  is not obvious. It means that the free energy of activation of ionic migration decreases linearly with rising water activity. Further work at varying temperatures is needed to establish whether this is the effect of solvation upon  $\Delta H^\ddagger$  or  $\Delta S^\ddagger$  or both. However, if it is assumed that  $\Delta S^\ddagger$  is constant, then it might be postulated that  $\Delta H^\ddagger$  would be inversely proportional to the dielectric constant of the solvate since the migration of ions from the vicinity of one site to another in the polymer network requires separation of charges in a di-

(17) H. M. Trimble and W. Potts, *Ind. Eng. Chem.*, **27**, 66 (1935).

(18) G. O. Curme, Jr., and F. Johnston, "Glycols," Reinhold Publ. Corp., New York, N. Y., 1952.

(16) "Handbook," 30th Edition, Chemical Rubber Co., Cleveland, Ohio, 1948, p. 1729.

electric medium and the well known rule of electrostatic forces would apply.

Equation 4 yields at  $a_{H_2O} = 0$  (pure glycol) the value  $\ln \kappa = 0.207$  and  $\Delta H^\ddagger = 5.4$  kcal./mole. This predicts the dielectric constant of ethylene glycol at 25° to be 43 using the above assumption while the measured value is 37.7. Such agreement as this is satisfactory in view of the crudeness of the assumptions. Further investigation to determine the actual polymer phase composition (in terms of water content) and measurements of  $\kappa$  at varying temperatures to separate out entropy effects are needed to determine whether  $\Delta H^\ddagger$  actually inversely proportional to dielectric constant.

If the linearity of  $\log \kappa$  with  $a_{H_2O}$  observed is general to other solvating solutions, *e.g.*, water

plus alcohols, this simple rule will permit data on the diffusion of ions in ion-exchange polymers in partially non-aqueous media to be extended with a minimum of experimental effort.

The present approach to the conductivity of a partially hydrated ion-exchange polymer may differ only formally from that of ion pair formation employed by Gregor<sup>19</sup> and that of hydration shells employed by Glueckauf.<sup>20</sup>

**Acknowledgment.**—The author thanks Dr. G. L. Gaines of this Laboratory for several helpful discussions in connection with this work.

(19) H. P. Gregor, D. Nobel and M. H. Gottlieb, *THIS JOURNAL*, **59**, 10 (1955).

(20) E. Glueckauf and G. P. Kitt, *Proc. Roy. Soc. (London)*, **A228**, 322 (1955).

## VISCOSITIES OF LIQUID MIXTURES

BY T. M. REED III AND T. E. TAYLOR

*Department of Chemical Engineering, University of Florida, Gainesville, Florida*

*Received April 24, 1958*

The viscosities of ten binary liquid systems have been determined as a function of composition and of temperature in the range 25 to 45°. The thermodynamics of these systems range from the ideal solution to partially miscible liquids. The free energy of mixing alone is insufficient thermodynamic information in attempting to correlate the thermodynamic behavior with the viscosity behavior of solutions. The volume change on mixing and the entropy of mixing each are related to separate viscosity effects. Based upon the absolute reaction rate theory of Eyring these systems have been divided into three classes which differ in the dependence of the temperature coefficient of viscosity on temperature. It is found that as the temperature is decreased to approach the two liquid phase region of a mixture, the viscosity as a function of composition displays an abnormally high value. This effect is found at 22° above the critical unmixing temperature for the system composed of isoöctane and perfluoroheptane. This analysis shows that the enthalpy of activation for all solutions may be considered as essentially independent of temperature even though the temperature coefficient of viscosity varies with temperature.

Viscosities of liquid mixtures have been discussed by various authors.<sup>1-3</sup> A familiar approach is the hypothesis that there is a direct correlation between the viscosity and the thermodynamic behavior of the solution.<sup>3</sup> In this work it has been found that no simple relationship, such as that proposed by Grunberg<sup>3</sup> and others,<sup>4</sup> exists. It has been found to be insufficient to limit the thermodynamic considerations to the free energy of mixing (activity coefficients). The entropy of mixing is related to viscosity effects.

The ten binary systems studied in this work are listed in Table I in the order of increasing positive deviation from ideal behavior (positive free energies of mixing). The values  $B$  in this table are those which appear in Hildebrand's theory<sup>5</sup> ( $B$  equals zero for an ideal solution and increases with larger deviations from the thermodynamic ideal solution behavior). Solutions of hydrocarbons with fluorocarbons require special treatment.<sup>6,7</sup> It has been shown<sup>7</sup> that the  $B$ -values

listed in Table II describe fairly accurately the activity coefficients in systems 1, 2, 3, 4.

### Experimental

Densities were measured in calibrated pycnometers.<sup>8</sup> Precisions of  $\pm 0.00005$  and  $\pm 0.0002$  g. per milliliter were obtained for the ten- and one-milliliter pycnometers, respectively.

**Viscosity.**—Cannon-Fenske<sup>9</sup> viscometers were calibrated with a National Bureau of Standards oil and with pure toluene (properties identical to those in the literature<sup>10</sup>), at each temperature. Ubbelohde suspended level viscometers<sup>9</sup> calibrated by the Cannon Instrument Company were used for about 60% of the measurements and reproduced the data obtained with the other viscometers.

Temperatures were read from thermometers or thermocouples calibrated with a National Bureau of Standards calibrated thermocouple having an accuracy of  $\pm 0.01^\circ$ .

Vapor pressures were determined by boiling the liquid in a Cottrell apparatus under air pressure.

Gas-liquid chromatography was used for determinations of purity. The stationary media were those reported by Reed.<sup>11</sup>

**Materials.** Perfluoroheptane ( $C_7F_{16}$ ).—A fluorocarbon material (Minnesota Mining and Manufacturing Co. material FM 3130) was distilled in a 60-plate column.<sup>12</sup> The

(1) D. B. Macleod, *Trans. Faraday Soc.*, **20**, 348 (1924).

(2) F. W. Lima, *J. Chem. Phys.*, **19**, 137 (1951).

(3) L. Grunberg, *Trans. Faraday Soc.*, **50**, 1293 (1954).

(4) S. Glasstone, K. J. Laidler and H. Eyring, "The Theory of Rate Processes," 1st ed., McGraw-Hill Book Co., Inc., New York, N. Y., 1941, p. 516.

(5) J. H. Hildebrand and R. L. Scott, "Solubility of Nonelectrolytes," 3rd ed., Reinhold Publ. Corp., New York, N. Y., 1950. The activity coefficient of compound  $a = B_a \cdot \phi_b^2 / T$ .

(6) T. M. Reed, III, *THIS JOURNAL*, **59**, 425 (1955).

(7) L. C. Yen and T. M. Reed, III, *Ind. Eng. Chem.*, in press (1958).

(8) M. R. Lipkin, *et al.*, *Ind. Eng. Chem., Anal. Ed.*, **16**, 55 (1944).

(9) ASTM Designation: D445-53T.

(10) Project 44 of the American Petroleum Institute at the Carnegie Institute of Technology.

(11) T. M. Reed, III, *Anal. Chem.*, **30**, 221 (1958).

(12) The distillation columns used in this work were packed with  $1/16$ -inch single-turn helices. It has been shown<sup>13</sup> that such columns have about one-half as many theoretical plates when distilling fluorocarbons as when distilling hydrocarbons. The values quoted in this report for the number of theoretical plates apply when the columns are

TABLE I

## PHYSICAL PROPERTIES OF COMPOUNDS

Compound	Formula	B. p., °C.	Refrac. index, 25°	density, 25°	$\frac{d\rho}{dt}$ g./ml. X °C. X 10 <sup>3</sup>	Vapor pressure constants <sup>b</sup>			Heat of vaporization, 25° cal./mole, at	Viscosity 25° μ, cs.	η, cp.	$\frac{\partial \ln \mu}{\partial (1/T)}$ , at 25° °K.	$\frac{\Delta E_v}{R \ln \mu / \partial (1/T)}$ at 25° cal./cc.
						A	B	C					
<i>n</i> -Hexane	<i>n</i> -C <sub>6</sub> H <sub>14</sub>	68.74	1.3723	0.6550	0.91	...	...	7540 <sup>a</sup>	0.4468	0.2938	755	4.63	7.27
2,2,4-Trimethyl- pentane	<i>i</i> -C <sub>8</sub> H <sub>18</sub>	99.24	1.3890	0.6879	0.83	...	...	8396 <sup>a</sup>	0.6869	0.4725	910	4.31	6.85
1,2-Dichloro- hexafluoro- cyclopentene	C <sub>5</sub> Cl <sub>2</sub> F <sub>6</sub>	90.81	1.3657	1.6433	2.18	6.78904	1163.9	8730	0.5528	0.9084	1070	3.83	7.39
2,2,3-Trichloro- heptafluoro- butane	C <sub>4</sub> Cl <sub>3</sub> F <sub>7</sub>	97.51	1.3505	1.7386	2.20	6.81718	1240.14	8510	1.1271	1.9596	1640	2.43	6.92
Perfluoroheptane	C <sub>7</sub> F <sub>16</sub>	82.26	1.2599	1.7275	2.78	6.07134	771.4	8215	0.5184	0.8955	1290	2.97	5.83
Perfluorocyclic oxide	C <sub>8</sub> F <sub>16</sub> O	103.05	1.2772	1.7640	2.58	6.98072	1284.6	9440	0.7916	1.3964	1520	2.93	6.13

<sup>a</sup> Ref. 10. <sup>b</sup>  $\log P(\text{mm.}) = A - B/(C + t)$ ,  $t$  in °C.

TABLE II

System	a	b	V <sub>a</sub> /V <sub>b</sub>	[ $\delta_a - \delta_b$ ],	
				(cal./ cc.) <sup>1/2</sup>	B <sub>a</sub> , °K.
1. C <sub>7</sub> F <sub>16</sub> :	C <sub>8</sub> F <sub>16</sub> O	0.960	0.30	1.0 <sup>a</sup>	
2. C <sub>6</sub> Cl <sub>2</sub> F <sub>6</sub> :	C <sub>4</sub> Cl <sub>3</sub> F <sub>7</sub>	.904	.47	16.6 <sup>a</sup>	
3. C <sub>6</sub> Cl <sub>3</sub> F <sub>7</sub> :	C <sub>8</sub> F <sub>16</sub> O	.702	.79	52.0 <sup>a</sup>	
4. C <sub>6</sub> Cl <sub>2</sub> F <sub>6</sub> :	C <sub>8</sub> F <sub>16</sub> O	.634	1.26	119 <sup>a</sup>	
5. C <sub>6</sub> Cl <sub>2</sub> F <sub>6</sub> :	C <sub>7</sub> F <sub>16</sub>	.666	1.56	182 <sup>a</sup>	
6. <i>n</i> -C <sub>6</sub> H <sub>14</sub> :	C <sub>6</sub> Cl <sub>2</sub> F <sub>6</sub>	.882	0.12	213 <sup>b</sup>	
7. C <sub>6</sub> Cl <sub>3</sub> F <sub>7</sub> :	<i>i</i> -C <sub>8</sub> H <sub>18</sub>	.898	.54	250 <sup>b</sup>	
8. <i>i</i> -C <sub>8</sub> H <sub>18</sub> :	C <sub>8</sub> F <sub>16</sub> O	.706	.72	254 <sup>b</sup>	
9. <i>n</i> -C <sub>6</sub> H <sub>14</sub> :	C <sub>8</sub> F <sub>16</sub> O	.559	1.14	262 <sup>b</sup>	
10. <i>i</i> -C <sub>8</sub> H <sub>18</sub> :	C <sub>7</sub> F <sub>16</sub>	.740	1.02	286 <sup>b</sup>	

<sup>a</sup>  $B_a = (V_a/R) (\delta_a - \delta_b)^2$ . <sup>b</sup>  $B_a = (V_a/R) [(\delta_a - \delta_b)^2 + 0.06 \delta_a \delta_b]$ .

constant boiling center position, containing an impurity of 1-2%, was azeotroped with *n*-heptane. The first material overhead was a perfluoroheptane-*n*-heptane azeotrope. The azeotrope mixture was separated at Dry Ice temperature and the final traces of *n*-heptane then removed from the fluorocarbon layer as the azeotrope. The residue was taken as pure C<sub>7</sub>F<sub>16</sub>.

Under high sensitivity on the vapor chromatograph this C<sub>7</sub>F<sub>16</sub> material showed a small shoulder on the back of the main peak. Since these two materials appear so close together, they appear to be two different C<sub>7</sub>F<sub>16</sub> isomers. This is further borne out by the nuclear magnetic resonance spectrum run on the C<sub>7</sub>F<sub>16</sub> sample which showed the presence of (CF<sub>3</sub>)<sub>2</sub>C< structure in an amount no greater than 10% as a C<sub>7</sub>F<sub>16</sub> isomer.<sup>14</sup> The only other peaks in the n.m.r. spectrum were those for *n*-C<sub>7</sub>F<sub>16</sub>.

**Perfluorocyclic Oxide (C<sub>8</sub>F<sub>16</sub>O).**—A constant boiling fraction of Minnesota Mining and Manufacturing Co. Fluorochemical 101 refluxing at 101° in a 60-plate column contained one major component (>95%) and three minor components. This material was refluxed for a total of 140 hours over two 80-gram charges of KOH, then washed, dried and simple distilled. Vapor chromatography still indicated three minor components. These impurities were removed as lower boiling azeotropes with *n*-heptane. The residue was cooled to Dry Ice temperature and the layers separated. The final traces of *n*-heptane were removed as the azeotrope leaving a residue containing less than 1% impurity. This residue was taken as the C<sub>8</sub>F<sub>16</sub>O for the viscosity studies. C<sub>8</sub>F<sub>16</sub>O is a cyclic perfluoro oxide of unknown structure. It is believed that the oxygen atom is in the ring, however.<sup>15</sup>

**1,2-Dichlorohexafluorocyclopentene (C<sub>5</sub>Cl<sub>2</sub>F<sub>6</sub>) and 2,2,3-Trichloroheptafluorobutane (C<sub>4</sub>Cl<sub>3</sub>F<sub>7</sub>).**—These materials were constant boiling fractions from the distillations, in a 60-plate column, of two crude materials obtained from the Hooker Electrochemical Company. Vapor chromatography indicated less than 0.5% impurities in both materials.

***n*-Hexane (*n*-C<sub>6</sub>H<sub>14</sub>).**—Commercial grade hexane was washed with H<sub>2</sub>SO<sub>4</sub>, passed through silica gel and distilled in a 60-plate column. The fractions containing predominantly *n*-hexane were again washed with H<sub>2</sub>SO<sub>4</sub> and azeotroped with excess ethanol in the 60-plate column. The azeotrope was washed with water, dried, and the remaining ethanol removed as the azeotrope in a 30-plate column. The *n*-hexane used in these studies was a constant boiling fraction from this distillation in which no impurities were indicated by vapor chromatography.

**Isooctane (2,2,4-Trimethylpentane, *i*-C<sub>8</sub>H<sub>18</sub>).**—The isooctane used in these studies was Phillips 99 mole % minimum grade. Vapor chromatograms of this material showed no impurities.

## Results

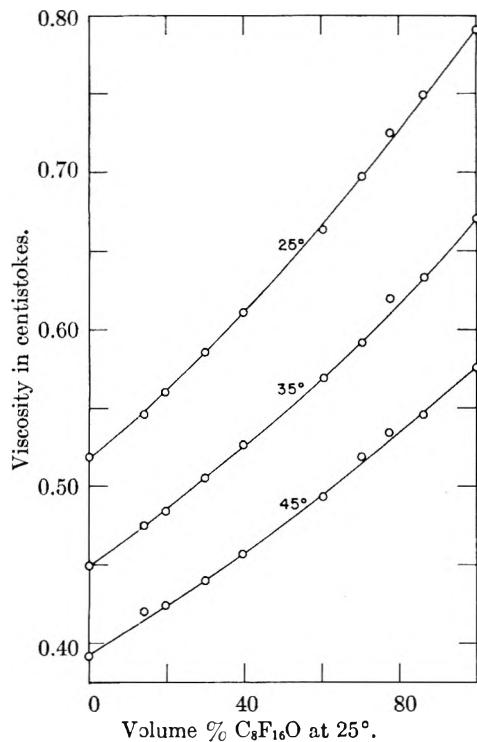
The experimental viscosities are given in Figs. 1

distilling hydrocarbons. When fractionating fluorocarbons, the number of theoretical plates actually operating should be one-half the value quoted.

(13) L. C. Yen, M. S. Thesis, University of Florida, 1957.

(14) Max Rogers, Department of Chemistry, Michigan State University, private communication.

(15) Minnesota Mining and Manufacturing Company.

Fig. 1.— $C_7F_{16}$ — $C_8F_{16}O$ .

through 10. This series of mixtures allows a systematic study of solutions varying from the ideal to those with large positive deviations in the activity coefficients. From Table III, it can be seen that the per cent. volume change on mixing increases steadily from a very small negative value through larger positive volume changes.

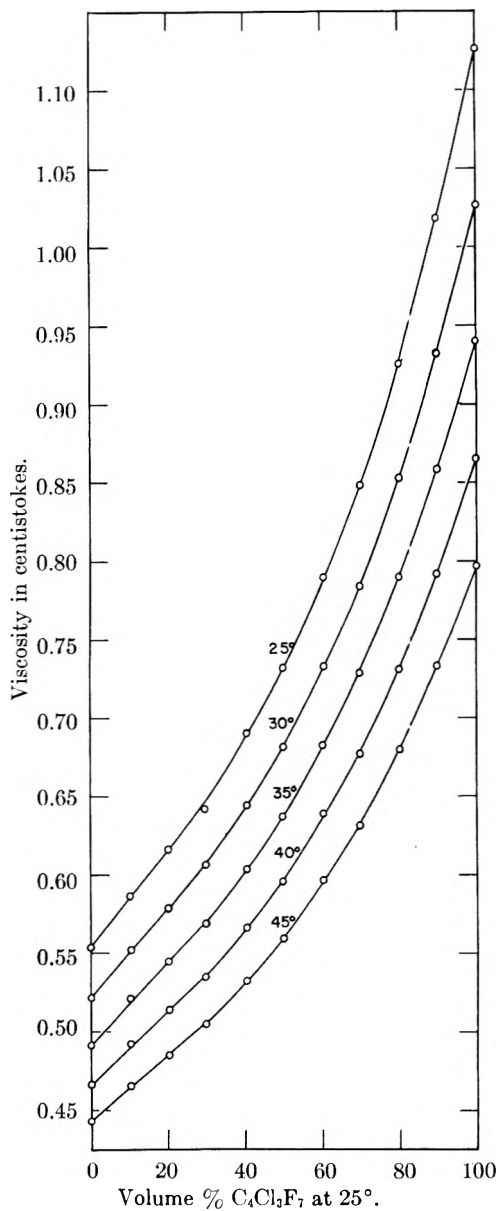
Vapor-liquid equilibrium data for systems<sup>7</sup> 1 and 2 show that these components form solutions very close to ideal while system 3 is sufficiently non-ideal to form an azeotrope<sup>7</sup> at atmospheric pressure. Vapor-liquid equilibrium data are not available for system 5, but for system 4 positive deviations from Raoult's law are known.<sup>7</sup> Systems 6 and 7 are shown to be less ideal than those of the chlorofluorocarbons with fluorocarbons by the  $B$ -values of Table II. (It is known that  $C_4Cl_3F_7$  forms a minimum boiling azeotrope with  $n$ -heptane at atmospheric pressure.<sup>7</sup>) No thermodynamic data are available for system 8, but like all fluorocarbon-hydrocarbon solutions this one undoubtedly has large activity coefficients. No thermodynamic data are available for system 9. The critical unmixing temperature was determined in this work as  $26^\circ$  at 27 mole %  $C_8F_{16}O$ .

For system 10, both vapor-liquid<sup>16</sup> and liquid-liquid<sup>17</sup> data are available. The critical unmixing temperature for this system has been observed variously at  $23.7^\circ$  in reference 17 (for  $n$ - $C_7F_{16}$ ) and at  $23.65^\circ$  in this work for the  $C_7F_{16}$  material used. The dashed line on Fig. 10 is a portion of the approximate locus of the viscosities corresponding to the consolute curve.  $\mu_c$  is the viscosity at the critical temperature of  $23.65^\circ$ .

The isotherms of viscosity versus composition

(16) C. Mueller and J. Lewis, *J. Chem. Phys.*, **26**, 286 (1957).

(17) J. H. Hildebrand, B. B. Fisher and H. A. Benesi, *J. Am. Chem. Soc.*, **72**, 4348 (1950).

Fig. 2.— $C_4Cl_2F_8$ — $C_4Cl_3F_7$ .

are similar to those of system 9 near the unmixing curve. The viscosities of that system and those of systems 8 and 10 reveal that changes in the structure of the solution which ultimately produce separation into two equilibrium phases begin at temperatures at least  $10^\circ$  above the temperature at which two liquid phases are observed.

- $B_a$  theoretical constant detg. activity coefficient in soln.
- $\Delta E^v$  molal energy of vaporization
- $\Delta G^*$  molal free energy of activation for viscous flow
- $\Delta H^*$  molal enthalpy of activation for viscous flow
- $N$  Avogadro's number
- $R$  ideal gas law constant
- $T$  absolute temperature
- $V$  molal volume
- $a$  distance through which shearing force acts
- $f$  defined by equation 7
- $g(x)$  residual free energy of activation
- $h(x)$  residual enthalpy of activation.
- $h$  Planck's constant
- $s(x)$  residual entropy of activation
- $x$  mole fraction in liquid
- $\delta$  solubility parameter,  $(\Delta E^v/V)^{1/2}$

- $\phi$  volume fraction
- $\lambda$  distance between adjacent moving layers of molecules
- $\eta$  absolute viscosity
- $\mu$  kinematic viscosity
- $\rho$  liquid density
- Subscripts
- a pure compound
- b pure compound
- o value when effects of variation  $\lambda/a$  are removed
- s property of solution
- v property associated with vol. change on mixing
- Superscript:
- i ideal solution

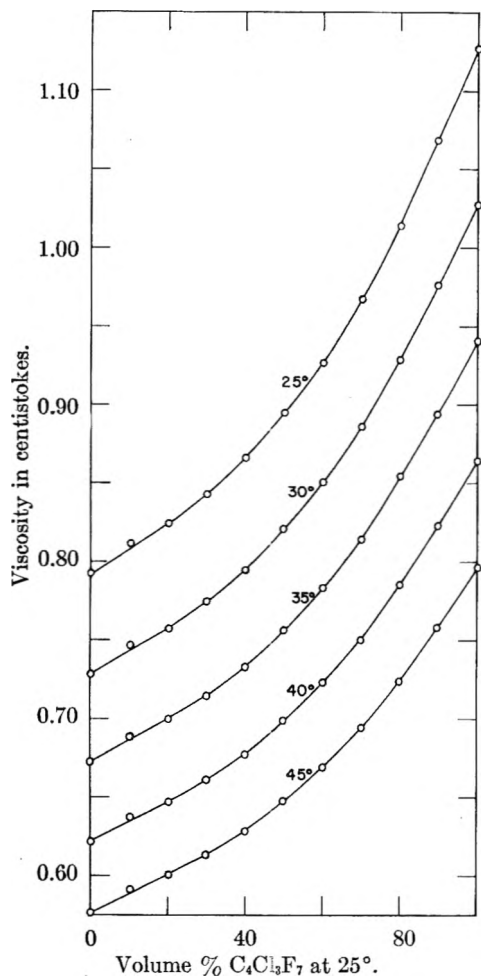


Fig. 3.— $C_4Cl_3F_7-C_8F_{16}O$ .

**Discussion**

Eyring's rate process theory gives the absolute viscosity as

$$\eta = \left(\frac{\lambda}{a}\right)^2 \frac{hN}{V} e^{\Delta G^*/RT}$$

For ideal solutions in the thermodynamic sense it has been suggested<sup>4,13</sup> that the viscosity be given by

$$\ln \eta_s = x_a \ln \eta_a + x_b \ln \eta_b \quad (2)$$

Since the volume of a solution varies with composition, a more reasonable relationship for ideal solutions might better be

$$\ln \eta_s V_s = x_a \ln \eta_a V_a + x_b \ln \eta_b V_b \quad (3)$$

$\Delta G_s^{*i}$  is given by

(18) L. Grunberg and A. H. Nissan, *Nature*, **164**, 799 (1949).

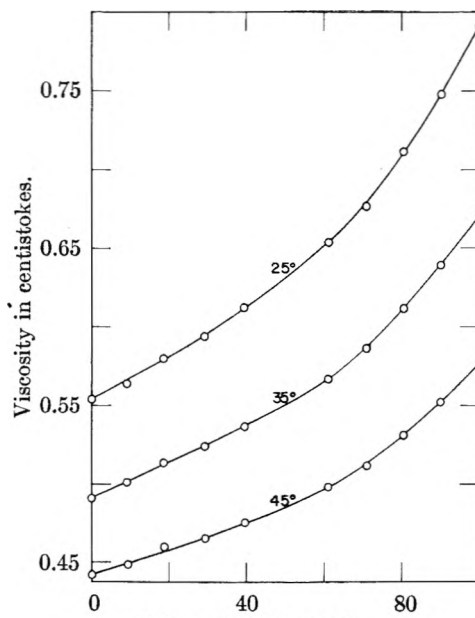


Fig. 4.— $C_6Cl_2F_6-C_8F_{16}O$ .

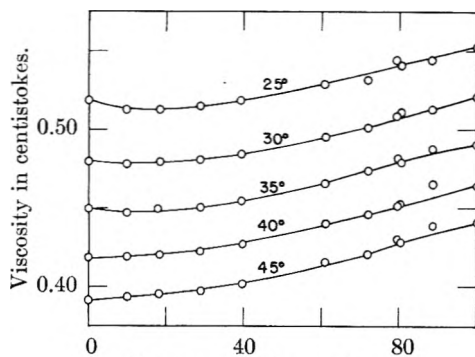


Fig. 5.— $C_5Cl_2F_6-C_7F_{16}$ .

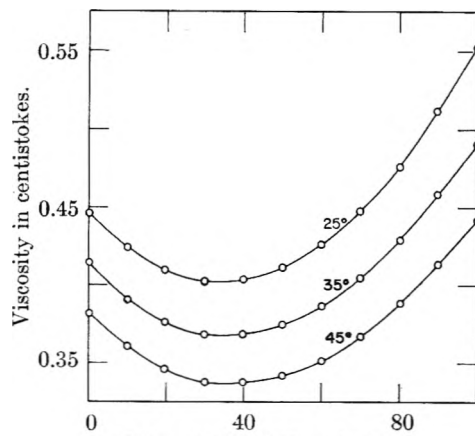


Fig. 6.— $n-C_6H_{14}-C_5Cl_2F_6$ .

$$\Delta G_s^{*i} = x_a \Delta G_a^* + x_b \Delta G_b^* \quad (4)$$

For non-ideal solutions the free energy of activation differs from  $\Delta G_s^{*i}$  by a term  $g(x)$  which is a function of concentration

$$\Delta G_s^* = \Delta G_s^{*i} + g(x) \quad (5)$$





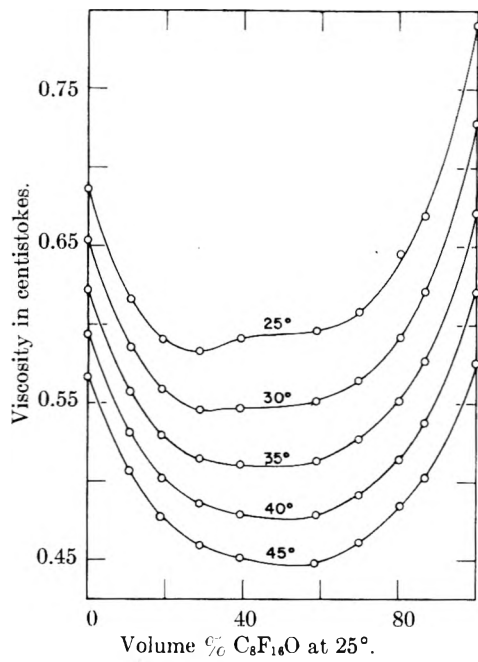


Fig. 8.— $i\text{-C}_8\text{H}_{18}\text{-C}_8\text{F}_{16}\text{O}$ .

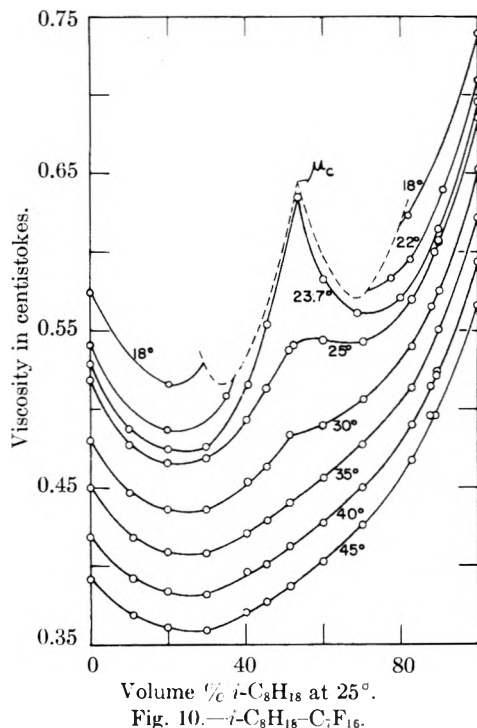


Fig. 10.— $i\text{-C}_8\text{H}_{18}\text{-C}_7\text{F}_{16}$ .

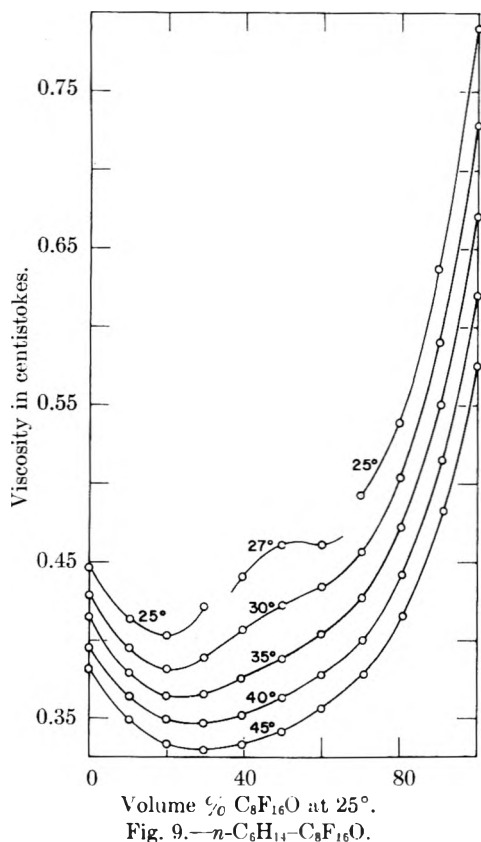


Fig. 9.— $n\text{-C}_8\text{H}_{14}\text{-C}_8\text{F}_{16}\text{O}$ .

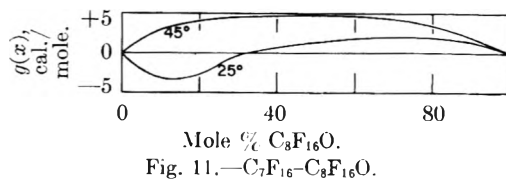


Fig. 11.— $\text{C}_7\text{F}_{16}\text{-C}_8\text{F}_{16}\text{O}$ .

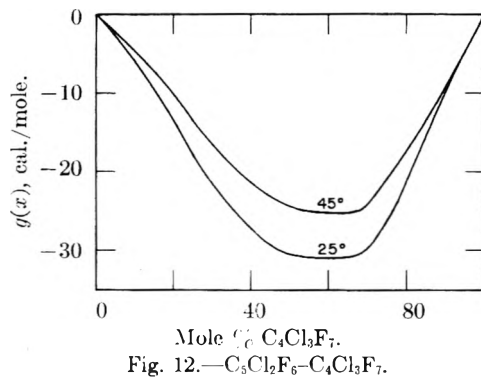


Fig. 12.— $\text{C}_5\text{Cl}_2\text{F}_6\text{-C}_4\text{Cl}_3\text{F}_7$ .

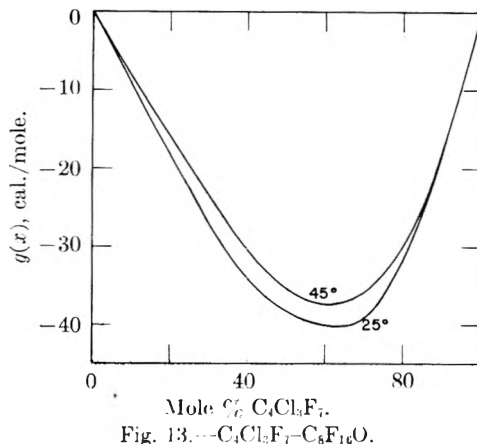
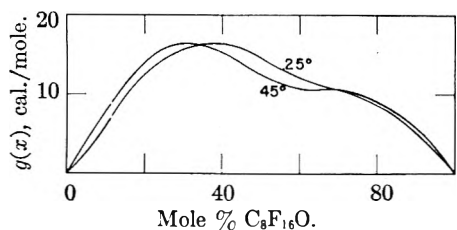
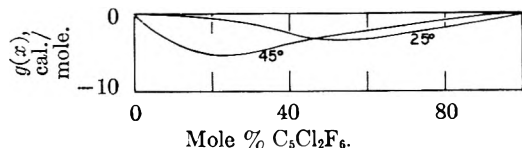
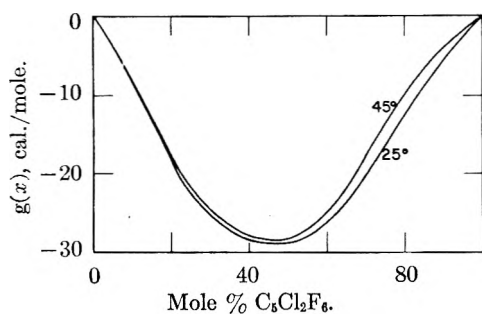
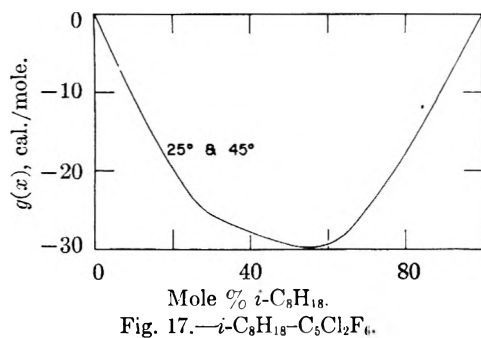
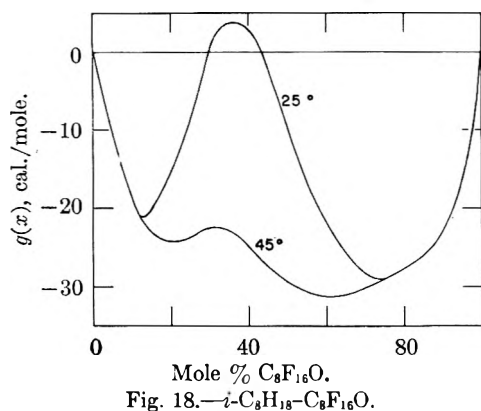


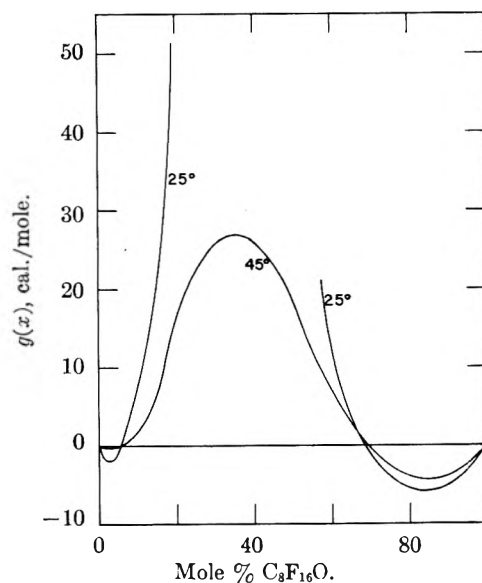
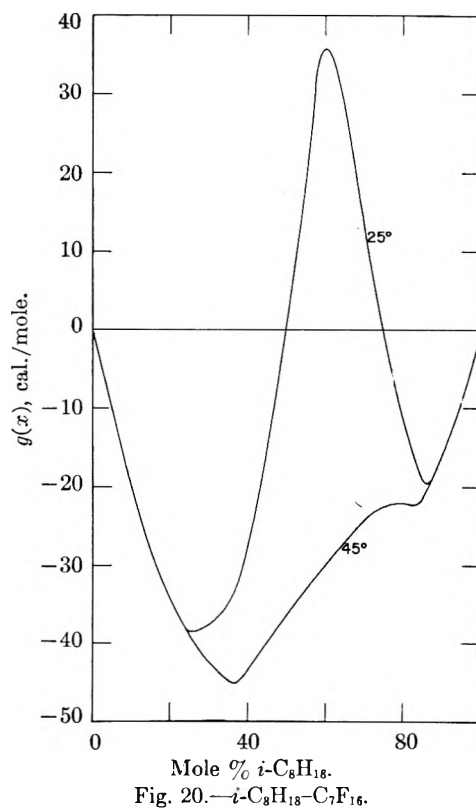
Fig. 13.— $\text{C}_4\text{Cl}_2\text{F}_7\text{-C}_8\text{F}_{16}\text{O}$ .

System 4 (Fig. 14) is particularly interesting in that it displays large positive values for  $g(x)$  when all the other systems from 2 through 7 have negative values for  $g(x)$ . Every one of these six systems shows expansion on mixing.

It is immediately apparent that there is no simple correlation between non-ideal behavior in the thermodynamic sense and non-ideal behavior in the viscosities of solutions. At least two general

Fig. 14.— $C_6Cl_2F_6-C_3F_{16}O$ .Fig. 15.— $C_6Cl_2F_6-C_7F_{16}$ .Fig. 16.— $n-C_6H_{14}-C_6Cl_2F_6$ .Fig. 17.— $i-C_8H_{18}-C_6Cl_2F_6$ .Fig. 18.— $i-C_8H_{18}-C_8F_{16}O$ .

effects may be singled out from these studies. The more obvious one is illustrated by systems 6 and 7 (Figs. 16 and 17) where expansions on mixing are accompanied by decreases in the free energy of activation for viscous flow. In Fig. 21A we have plotted  $g(x)/RT$  versus the total volume change on mixing for these systems at 25 and at 45°. The lowering in the viscosities of these solutions may

Fig. 19.— $n-C_6H_{14}-C_8F_{16}O$ .Fig. 20.— $i-C_8H_{18}-C_7F_{16}$ .

be attributed directly and entirely to the expansion on mixing.

The existence of a second effect in the viscosities is obvious from the plots of  $g(x)$  for systems 8, 9 and 10 (Figs. 18–20.) In dilute solutions the expansion produces negative values for  $g(x)$ . At intermediate compositions this expansion effect is superimposed on another one which produces an apparent rise in the free energy of activation calculated by eq. 5. This effect is noticeable at 45°, some 21° above the maximum unmixing temperature for system 10. At 25° this second effect produces viscosities for these solutions which are

greater than those expected on the basis of the ideal solution eq. 3. The volume changes on mixing for these solutions show no inflections corresponding to the curves for  $g(x)$ . The predominance of this second effect in mixtures of system 4, where  $g(x)$  is always positive, is overwhelmingly large compared to the volume expansion effect. The fact that  $g(x)$  in system 5 has such small negative values out of proportion to the expansion no doubt arises from the interplay of both effects in this solution. Systems 4 and 5 are similar to systems 1, 2, 3, 6 and 7 in that the thermodynamic free energies of mixing are not sufficiently large to produce partial miscibility. Inasmuch as they show a dominating value for the second effect, these solutions are similar to those solutions (8, 9 and 10) which have large thermodynamic free energies of mixing. The conclusion to be drawn from these similarities and differences is that the second effect is associated with the thermodynamic entropy of mixing for the solutions. We will show that the positive part of  $g(x)$  may be accounted for by allowing  $\lambda/a$  to be a variable in eq. 1.

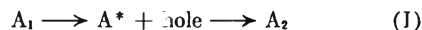
**The Factor  $\lambda/a$  as a Variable.**—A theoretical expression for the enthalpy of activation,  $\Delta H^*$ , is obtained from eq. 1 as

$$\Delta H^* = R \frac{\partial \ln \eta V}{\partial (1/T)} - 2R \frac{\partial \ln (\lambda/a)}{\partial (1/T)} \quad (6)$$

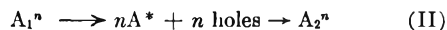
It is found for mixtures which obey the ideal law of eq. 4 that  $\partial \ln \eta V / \partial (1/T)$  at each composition is constant. Furthermore, it is found for non-ideal mixtures, in which  $g(x)$  shows no inflection point, that  $\partial \ln \eta V / \partial (1/T)$  is independent of temperature. In systems 8, 9 and 10, however, where  $g(x)$  shows maxima and minima with respect to change in composition,  $\partial \ln \eta V / \partial (1/T)$  varies with temperature in a manner illustrated by Fig. 22 for some data of system 10. The maximum unmixing temperature of 23.65° for this system occurs at 61.4 mole % isoöctane (54 volume % at 25°). At 27°  $R \partial \ln \eta V / \partial (1/T)$  is 4000 cal./mole and rises to 87,000 cal./mole at 23.7°.

As an hypothesis we assume the schemes.

I. In pure liquids or in solutions where  $g(x)$  is zero or negative



II. In liquids where  $g(x)$  has a positive part



In I,  $A_1$  represents a molecule in position 1, and  $A_2$  is the molecule displaced to position 2. In II,  $A_1^n$  represents  $n$  molecules in some association.  $A_2^n$  represents the molecules displaced to new positions and included in a new group.

The enthalpy of activation  $\Delta H^*$  per mole in a given liquid for process I and for process II are identical since the holes required possess the same properties in both processes. Thus,  $\Delta H^*$  per mole will be a function only of composition in either process I or II. In the temperature region where the viscosity or  $g(x)$  versus composition show the maxima, the excessively high temperature coefficient of viscosity above those values expected in the absence of the grouping effect must be exactly

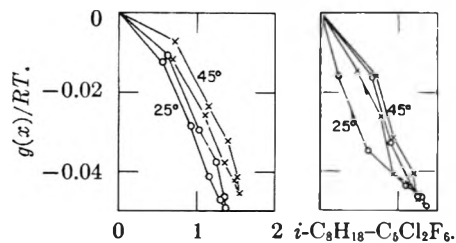


Fig. 21A.— $C_6Cl_2F_6$ - $n$ - $C_8H_{14}$ .

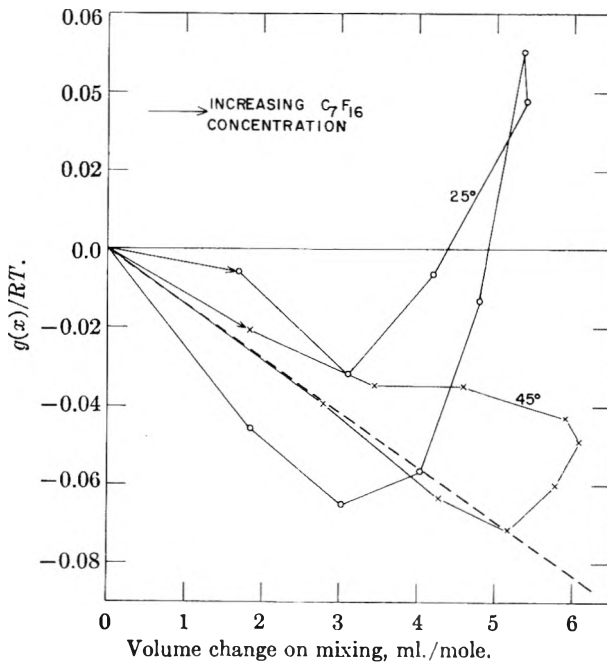


Fig. 21B.— $i$ - $C_8H_{18}$ - $C_7F_{16}$ .

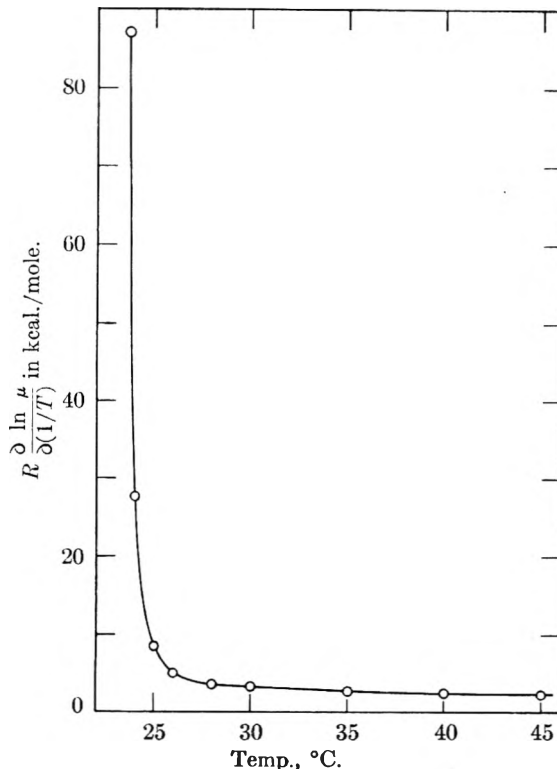


Fig. 22.— $i$ - $C_8H_{18}$ - $C_7F_{16}$  at 61.4 mole %  $i$ - $C_8H_{18}$ .

compensated by the term  $-2R \partial \ln (\lambda/a)/\partial (1/T)$  in eq. 6. We are thus attributing a positive portion of the total  $g(x)$  to a change in cluster size with temperature. The shearing force acts on an area  $(\lambda)^2$  which is larger when clusters are present than when they are absent. An alternate interpretation is to allow the heat capacity in the activated state to be much less than that in the normal state when clustering is involved. This leads to negative values for  $C_p^*$  for these data.

**Classification of Solutions.**—A more explicit form of eq. 5 may now be written, which includes values of  $\lambda/a$  different from unity.  $g_v(x)$  is that part

$$\ln \eta_s V_s / h N = \Delta G_s^* / RT + \ln (\lambda/a)_s^2 = x_a [\Delta G_a^* / RT + \ln (\lambda/a)_a^2] + x_b [\Delta G_b^* / RT + \ln (\lambda/a)_b^2] + g_v(x) / RT + \ln f \quad (5a)$$

of  $g(x)$  which arises from the change in volume on mixing, and

$$\ln f = \ln (\lambda/a)_s^2 - x_a \ln (\lambda/a)_a^2 - x_b \ln (\lambda/a)_b^2 \quad (7)$$

so that

$$g(x) = g_v(x) + RT \ln f \quad (8)$$

Equations 5a, 6, 7 and 8 are the basis for classifying the viscosity behavior of solutions:

1. For ideal solutions  $\ln f = 0$  and  $g_v(x) = 0$  to give eq. 3. System 1 is the closest to this case.

2. When  $g(x)$  is not zero but  $[\partial \ln \eta V / \partial (1/T)]_x$  is independent of temperature,  $[\partial \ln (\lambda/a)_s / \partial (1/T)]_x = 0$  (eq. 6).<sup>19</sup> Systems 2 through 7 fall in this class. Subclasses are those for which  $g(x)$  is positive (or small negative values), *i.e.*,  $f > 1$  when  $\Delta V$  is positive (systems 4 and 5); and those for which  $g(x)$  is negative, *e.g.*, either  $g_v(x)$  is negative (positive  $\Delta V$ ) or  $f < 1$  or both (systems 2, 3, 6 and 7, and also systems 8 and 10 at temperatures considerably above the unmixing temperature). Figure 17 shows further that  $g(x)$  for system 7 is independent of temperature. This means that

$$\left( \frac{\partial g(x)}{\partial T} \right)_x = 0 \quad (9)$$

From eq. 8 and 9

$$\left( \frac{\partial g_v(x)}{\partial T} \right)_x = -R \ln f = -s_v(x) \quad (10)$$

Substituting in eq. 8

$$g(x) = g_v(x) + T s_v(x) = h_v(x) \quad (11)$$

Thus, even though  $\ln f$  is not necessarily zero,  $g(x)$  in system 7 depends only upon the volume change effect.

3. A third type of mixture is the one in which  $g(x)$  is not zero and  $[\partial \ln \eta V / \partial (1/T)]_x$  is a function of temperature. Systems 8, 9 and 10 in the neighborhood of the two-liquid phase region fall in this class.

**Treatment of Class 3 Solutions.**— $\Delta H^*$  may be evaluated at sufficiently high temperatures where  $[\partial \ln \eta V / \partial (1/T)]_x$  is a constant value independent of temperature. Alternately,  $\Delta H^*$  may be evaluated from that of the pure compounds by assuming it linear in mole fraction. This latter method was used in these calculations as being sufficiently accurate, since  $h(x)$  was found not to be

(19) See, however, the discussion under treatments of class 2 and class 3 solutions regarding  $\partial \ln (\lambda/a) / \partial (1/T)$ .

greater than a few per cent. of the total ideal  $\Delta H^*$  when  $\partial \ln \eta V / \partial (1/T)$  was independent of the temperature. Then  $\partial \ln f / \partial (1/T) = 2 \partial \ln (\lambda/a)_s / \partial (1/T)$ <sup>20</sup> may be evaluated from eq. 6

$$R \partial \ln f / \partial (1/T) = R \partial \ln \eta_s V_s / \partial (1/T) - \Delta H^* \quad (6a)$$

Between two temperatures  $T_1$  and  $T_2$  this becomes

$$\ln f_2 / f_1 = \ln \mu_2 / \mu_1 - (\Delta H^* / R) [(1/T_2) - (1/T_1)] \quad (12)$$

where  $\mu$  is the kinematic viscosity  $\eta / \rho$ . This eq. gives the ratio of shape factors at two temperatures. It is shown in Fig. 21A that  $g_v(x) / RT$  at two temperatures, 25 and 45°, are essentially equal if the volume change on mixing is not very different at the two temperatures. Setting

$$g_v(x)_1 / RT_1 = g_v(x)_2 / RT_2$$

and combining eq. 8 and 12 gives

$$g(x)_1 / RT_1 = g(x)_2 / RT_2 - \ln \mu_2 / \mu_1 + (\Delta H^* / R) [(1/T_2) - (1/T_1)] \quad (13)$$

Referring now to Fig. 24 for system 10 and taking  $T_1 = 45^\circ$  and  $T_2$  equal to the various temperatures between 45° and the critical unmixing temperature, we have computed  $g(x) / RT$  at 45° from  $g(x) / RT$  at lower temperatures by means of eq. 13. It is obvious that the theory accounts for the difference in  $g(x) / RT$  between the lower temperatures and 45° since the calculated points shown in the figure coincide almost exactly with the experimental curve at 45°. The dashed curve on Fig. 24 is  $g_v(x) / RT$  at 45° estimated from the volume changes on mixing by means of the dashed line on Fig. 21b. We have also made the same computation for the 25°-curve of system 8 (Fig. 23).

The small magnitude of the variation in  $(\lambda/a)_s$  is illustrated by Table IV. An increase of about 6% is sufficient to account for the greatest increase in viscosity at 25° above the value expected from the volume change effect.

TABLE IV

Mole fraction	$2 \ln [f_{25}/f_{45}]$	$f_{25}/f_{45}$
System 8— $C_8F_{16}O$ with $i-C_3H_8$		
$C_8F_{16}O$		
25	+0.0252	1.013
36	+ .0444	1.022
50	+ .0306	1.015
64	+ .0057	1.003
75	- .0051	0.99
System 10— $i-C_3H_8$ with $C_7F_{16}$		
$i-C_3H_8$		
45	+0.0416	1.021
53.1	.0790	1.040
61	.1066	1.055
70	.0660	1.034
80	.0137	1.007

A value for the viscosity at the critical unmixing point ( $T = 23.65^\circ$ ,  $x = 0.614$  isoöctane) for system 10 has been estimated by extrapolating the values shown in Table V of  $\ln f_T / f_{45}^\circ$  at this composition. The viscosity at the critical point is 0.645 centistoke.  $\lambda/a$  at 23.65° and 0.614 mole fraction isoöctane is 15% larger than its value at 45°.

(20)  $\partial \ln (\lambda/a) / \partial (1/T)$  for the pure compounds is taken as zero since  $\partial \ln \eta V / \partial (1/T)$  for the pure compounds is independent of temperature. See treatment of class 2 solutions.

From the dashed curve on Fig. 24 a value for  $f/f_0$  at  $45^\circ$  may be estimated as 1.04 at 0.614 mole fraction isoöctane, so that  $f/f_0$  at the critical unmixing point is approximately 1.19.

TABLE V

SYSTEM 10 AT THE CRITICAL COMPOSITION, 61.4 MOLE %

$T, ^\circ\text{C.}$	ISOÖCTANE	
	$2 \ln [f_T/f_0]$	$f_T/f_0$
23.65	(+0.2814)	1.15
23.7	.2459	1.130
24	.1777	1.093
25	.1066	1.055
30	.0461	1.023
45	0	1.00

Vapor-liquid equilibria of  $n\text{-C}_7\text{F}_{16}$  with isoöctane have been reported<sup>16</sup> at the three temperatures 30, 50 and  $70^\circ$ . The total excess free energy and entropy of mixing at these temperatures are positive. At the lower temperatures the excess entropy as a function of composition resembles the negative of the curve for  $g(x)$  at  $45^\circ$  on Fig. 20. The increase in  $\lambda/a$  with decrease in temperature is accompanied by an increase in order among the molecules in the solution. This conclusion is also obvious from the behavior of the heat capacity of this solution in the neighborhood of the critical unmixing temperature.<sup>21</sup>

Data<sup>22</sup> for methanol-toluene solutions fall in this class and fit eq. 13. The maximum value for  $f_{25}/f_{50}$  for this system is 1.03 and occurs at approximately 75 mole % methanol.

**Treatment of Class 2 Solutions.**—System 4 has small positive volume changes accompanying mixing. Nevertheless  $g(x)$  for this system is positive at all compositions (Fig. 14). The positive portion of  $g(x)$  is far greater than the negative value of  $g_v(x)$  in this system. If it be true in this case, as was suggested above for system 10, that large values of  $\lambda/a$  (and consequently large values of  $f$  by eq. 7) mean abnormally low entropies of mixing, it should be expected that system 4 would exhibit negative excess entropies of mixing. The thermodynamics of mixtures of  $\text{C}_8\text{F}_{16}\text{O}$  with  $\text{C}_6\text{Cl}_2\text{F}_6$  should be interesting in this respect.

We have postulated throughout that the enthalpy of activation is the same for a given mixture whether the process be I or II. By eq. 6 this hypothesis leads to

$$\left[\frac{\partial \ln (\lambda/a)_s}{\partial (1/T)}\right]_x = C_x \quad (14)$$

as a characteristic of class 2 solutions.  $C_x$  is a constant independent of temperature but a function of composition. In the treatment of classes 2 and 3 we have taken  $C_x$  arbitrarily as zero, whenever  $\partial \ln \eta V / \partial (1/T)$  is independent of  $T$ . If  $C_x$  is not zero, then the base  $\Delta H^*$  appearing in eq. 12 is

(21) G. Jura, D. Fraga, G. Mika and J. H. Hildebrand, *Proc. Natl. Acad. Sci.*, **39**, 19 (1953).

(22) L. W. Hammond, K. S. Howard and R. A. McAllister, *This Journal*, **62**, 637 (1958).

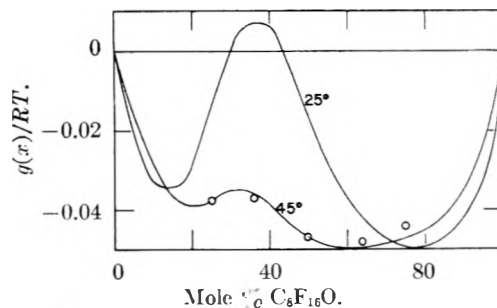


Fig. 23.— $i\text{-C}_8\text{H}_{18}\text{-C}_8\text{F}_{16}\text{O}$ : points calculated by eq. 13 at  $45^\circ$  from values at  $25^\circ$ .

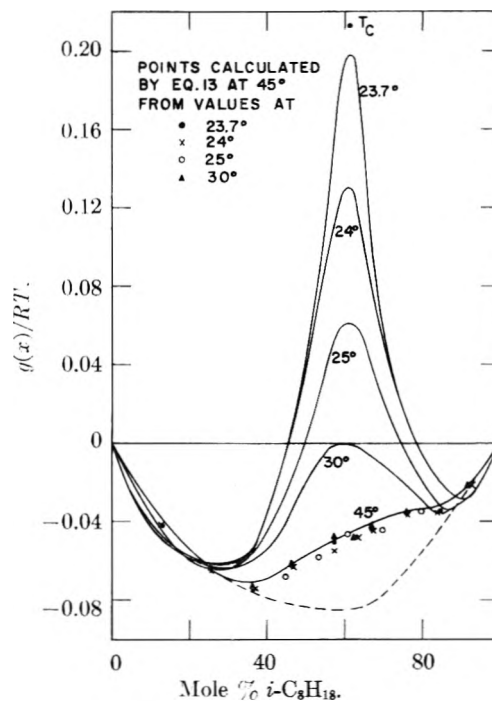


Fig. 24.— $i\text{-C}_8\text{H}_{18}\text{-C}_7\text{F}_{16}$ .

actually  $\Delta H^* + 2RC_x$ . The treatment of class 3 on this basis would not be altered.

**Single Components.**—It has been noted<sup>23</sup> that the ratio of the energy of vaporization to  $R \partial \ln \eta / \partial (1/T)$  for fluorocarbons is about 2.5 whereas this ratio for hydrocarbons is about 4. If the enthalpy of activation defined by eq. 5a together with eq. 14 is used to compute  $\Delta E^v / \Delta H^*$  for hydrocarbons and fluorocarbons, a value around 4.5 is obtained for both types of substances when  $C_x$  is arbitrarily assigned zero for hydrocarbons and  $(1/4)[\partial \ln \eta V / \partial (1/T)]$  for fluorocarbons and chlorofluorocarbons. The difference in the temperature coefficient of viscosity for these types of compounds may thus be accounted for by a dependence of the factor  $\lambda/a$  on temperature which is different for hydrocarbons compared to fluorocarbons.

**Acknowledgment.**—This work was made possible by a grant from the National Science Foundation.

(23) T. J. Brice and R. I. Coon, *J. Am. Chem. Soc.*, **75**, 2921 (1953)

# DETERMINATION OF THE SOLUBILITY OF OXYGEN BEARING IMPURITIES IN SODIUM, POTASSIUM AND THEIR ALLOYS<sup>1</sup>

BY D. D. WILLIAMS, J. A. GRAND AND R. R. MILLER

*Inorganic and Nuclear Chemistry, U. S. Naval Research Lab., Washington, D. C.*

*Received June 16, 1958*

Current interest in liquid metals, particularly sodium, as heat transfer media has emphasized the need for basic information on impurity solubility. Such data are important in the interpretation of corrosion and physical property experiments. The compounds resulting from partial oxidation of potassium and sodium metal have been isolated and identified as the respective monoxides. The equilibrium oxide in a sodium-potassium (NaK)-oxygen system is sodium monoxide. The various solubilities have been determined: sodium monoxide in sodium, potassium and NaK alloys; potassium monoxide in potassium; sodium hydroxide in sodium; mixed sodium hydroxide-sodium monoxide in sodium; and sodium carbonate in sodium. Positive errors in oxide content may result from failure to account for each species of impurity if separation and analysis of a sample depends solely upon total alkalinity calculation.

## Introduction

The current interest in heat transfer media for high temperature exchangers has emphasized a need for basic information on a variety of low melting materials. Considerable interest has centered on sodium, potassium and their alloys usually referred to as NaK. One important area related to corrosion and system plugging is the solubility of oxygen bearing compounds in these metals.

The initial phases of these studies were experiments designed to establish the identity of the equilibrium oxide in a system containing excess alkali metal. This information was important, inasmuch as the calculation in the method of sample analysis used<sup>2,3</sup> was based on an assumption of the presence of monoxide only.

**Experimental Equilibrium Studies.**—The equilibrium studies were made by treating an excess of metal with dry oxygen, removing the excess metal and chemically analyzing the residual oxides. Two apparatuses were used. They differed in that one allowed for filtration, following oxidation and prior to excess metal removal, thus establishing the identity of soluble oxide as opposed to contained oxide.

The apparatus for contained oxide consisted of two 50-ml. Pyrex flasks joined by 10 mm. tubing and equipped with connections to a dry oxygen source and a vacuum-inert gas manifold. After the apparatus was purged, 5 to 15 g. of metal or alloy was placed in one flask by a vacuum pipetting technique, dry oxygen was passed in slowly, and the assembly agitated. Excess metal was then vacuum distilled into the second flask, and the flasks separated by flame sealing. The first flask containing the oxide residue, was weighed, opened by cracking, and the residue dissolved in distilled water. After drying, the flask was reweighed, the difference from the original weight being equal to the oxide residue weight. In a like manner, the metal in the second flask was weighed, treated with methyl alcohol and analyzed by the procedure developed by Walters and Miller.<sup>4</sup>

The water solution of the oxide residue was titrated for total alkalinity and analyzed for sodium and potassium content by the mixed chloride, perchlorate method.<sup>5</sup> The quantities of sodium and/or potassium thus obtained were calculated to corresponding weights of the various possible oxides ( $\text{Na}_2\text{O}$ ,  $\text{Na}_2\text{O}_2$ ,  $\text{K}_2\text{O}$ ,  $\text{K}_2\text{O}_2$  and  $\text{KO}_2$ ). The oxide or combination of oxides whose weight or weights most nearly agreed with the original residue weight was assumed to be the equilibrium oxide at test conditions. The total alkalinity titrations provided an excellent check on the gravimetric results.

A similar apparatus was used to identify the oxide or oxides in NaK alloys and potassium. The metal was distilled from one flask to a second flask and the pure material thus obtained was oxidized as before. This mixture was then heated to an arbitrarily chosen temperature of 250° and filtered into a third flask. The excess metal was again distilled into a fourth flask, and the various flasks separated by flame sealing. The residues and metal analyses were performed as described previously.

The data from these equilibrium oxide experiments are presented in Table I.

It is shown in Table I that calculation of the residue fractions as sodium and/or potassium monoxide closely approximates the original residue weights. While most of the data would indicate equilibrium at distillation temperature (250–350°), runs 7 and 8 were made at room temperature with excess metal removed by amalgamation. The residue analysis again indicates the lower oxide. Hence, it is reasonably assumed that, in an incompletely oxidized system, the monoxides are produced, and they are stable and somewhat soluble.

A very significant result of these experiments is shown by the data from runs 1, 3, 5 and 7, wherein oxidation was halted before all of the sodium metal in the NaK was consumed. The residues from these runs contained no potassium oxide. It must follow therefore that sodium is preferentially removed as oxide from alloys containing even as much as 99.8% potassium (run 3). It is not inferred that sodium alone is initially oxidized, but rather that the equilibrium oxide in any NaK alloy is sodium monoxide.

The preferential removal of sodium from NaK alloys was studied further by a method involving stepwise oxidation with interposing alloy analyses by melting point determination.<sup>4</sup> With subsequently determined solubility data, it became apparent that the error in analysis by the freezing point method without correction for freezing point lowering due to dissolved impurities, was less than the precision of the temperature determination.

The apparatus consisted of an equilibrium chamber equipped with a thermometer, oxygen reservoir of known volume and appropriate outlets for connection to a vacuum-inert gas manifold.

After purging the apparatus by evacuating and flushing with inert gas, a weighed quantity of NaK was introduced into the equilibrium chamber through the thermometer joint. The thermometer was then inserted and the alloy composition determined by the freezing point method. The chamber and reservoir were re-evacuated and the reservoir filled with dry oxygen to a pressure of one atmosphere. The NaK was heated to 70° and the oxygen bled in slowly. The apparatus was agitated vigorously, at temperature, for 15 minutes. The freezing point of the remaining alloy was again determined, followed by another oxygen addition. This cycle was repeated until the freezing point analysis indicated that only potassium metal remained. A second run was made exactly as above with the exception that oxidation occurred at 225° instead of 70°.

Each oxygen increment was equal to 43.9 cc. (STP). This was equivalent to 0.18 g. of sodium or 0.306 g. of potassium when reacting to form the monoxide. From these equivalents and from the weight of alloy originally added, the weight per cent. of potassium remaining in the

(1) These data are presented in part in NRL Reports 3856 (1951), 3895 (1951) and Memo Report 424 (1955).

(2) L. P. Pepkowitz and W. C. Judd, *Anal. Chem.*, **22**, 1283 (1950).

(3) D. D. Williams and R. R. Miller, *ibid.*, **23**, 1865 (1951).

(4) S. L. Walters and R. R. Miller, *ibid.*, **18**, 658 (1946).

(5) W. F. Hillebrand and G. E. F. Lundell, "Applied Inorganic Analysis," John Wiley and Sons, Inc., New York, N. Y., 1929.

TABLE I

Run	Metal compn., wt. %		wt. <sup>a</sup> (g.)	Residue analysis				
	Before oxidn.	After oxidn.		Gravimetric		Total	Volumetric	
				Na as Na <sub>2</sub> O (g.)	K as K <sub>2</sub> O (g.)		Na <sub>2</sub> O, wt. %	K <sub>2</sub> O, wt. %
1	92.6% K	94.9% K	0.1562	0.1552	0.0000	0.1552	99.9	0.1
2	95.0% K	100.0% K	.2605	.2387	.0226	.2613	91.1	8.9
3 <sup>b</sup>	96.0% K	99.8% K	.0055	.0056	.0000	.0056	99.9	0.1
4 <sup>b</sup>	96.0% K	100.0% K	.3255	.0015	.3230	.3245	1.0	99.0
5 <sup>b</sup>	95.0% K	99.5% K	.0035	.0035	.0000	.0035	100.0	0.0
6 <sup>b</sup>	93.0% K	100.0% K	.0559	.0010	.0543	.0553	1.5	98.5
7	50.0% K	61.4% K	.1139	.1140	.0000	.1140		
8	100.0% K	100.0% K	.0582	.0000	.0581	.0581	0.0	100.0
9	100.0% Na	100.0% Na	.1469	.1475	.0000	.1475	100.0	0.0
10	100.0% Na	100.0% Na	.0941	.0938	.0000	.0938	100.0	0.0

<sup>a</sup> Corrected for SiO<sub>2</sub> from distillation and washing operations. <sup>b</sup> These analyses for that portion of the oxides soluble in excess metal at 250°.

alloy following any oxygen addition could be calculated, assuming only sodium monoxide was formed.

The data from the two runs are presented in Table II.

TABLE II  
EQUILIBRIUM IN THE NaK OXYGEN SYSTEM

Run	O <sub>2</sub> shot	O <sub>2</sub> added (cc., STP)	F.p., (°C.) <sup>a</sup>	Wt. % K in alloy (from f.p.)	Wt. % K in alloy (calcd.) <sup>b</sup>
	0	0	30.9	91.5	91.5
1	1	43.9	38.1	93.4	93.4
70°, 15 min. agitation	2	87.8	45.0	95.2	95.3
	3	131.7	53.0	97.2	97.3
	4	175.6	61.4	99.4	99.3
	5	219.5	63.7	100.0	100.0
	0	0	35.5	92.7	92.7
2	1	43.9	40.6	94.0	94.0
225°, 15 min. agitation	2	87.8	46.5	95.6	95.6
	3	131.7	52.7	97.2	97.3
	4	175.6	60.5	99.2	99.1
	5	219.5	63.7	100.0	100.0
	6	263.4	63.7	100.0	100.0

<sup>a</sup> Stem corrected. <sup>b</sup> Calcd. as if only sodium removed by oxidation.

It should be evident that if the oxidation of the NaK removed potassium only, the freezing point would have been lowered. Similarly, the removal of both sodium and potassium would have resulted in either a constant (stoichiometric oxidation) or an erratic and unpredictable (random oxidation) freezing point. As shown in Table II, however, calculation as if sodium only were removed results in excellent agreement between observed and calculated values. Since this preferential sodium removal occurs at potassium contents up to 99+%, it seems reasonable to assume that it would occur as readily with sodium-rich alloys.

It should be noted here that the presence of moisture would result in the formation of hydroxides of the alkali metals. Such a reaction would establish a different equilibrium which, from the data of Rinck,<sup>6</sup> should result in the simultaneous removal of sodium and potassium as hydroxides.

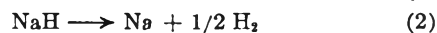
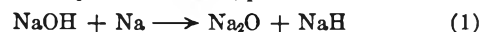
**Solubility of Sodium Monoxide in Sodium, Potassium and NaK, and of Potassium Monoxide in Potassium.**—Having established the identity of the oxide species to be found under a given set of conditions, the solubility of that oxide in its respective medium could now be determined without having to rely upon assumed compounds and/or valences. Thus, the preceding equilibrium studies demonstrate that only monoxides of sodium and potassium need be considered when studying oxide solubilities in the pure metals. Furthermore, they show that only sodium monoxide need be studied in the case of NaK alloys. This latter fact indicates that sodium monoxide in potassium metal also should be studied.

The apparatus for determining the solubility of sodium

monoxide in sodium and NaK and of potassium monoxide in potassium is shown in Fig. 1. It consists of an oxidation and saturation chamber (A), oxygen reservoir (B), filter (D), sample bulb (C), thermocouple well, and appropriate connectors to a vacuum-inert gas manifold. For temperatures above 400°, a stainless steel apparatus of similar constituent parts was used.

After purging the apparatus, approximately 2 g. of metal was pipetted into chamber (A) through joint (E), nitrogen flow being maintained throughout this operation. Chamber (B) was then fitted and the apparatus re-evacuated. Reservoir (B) was filled to atmospheric pressure with dry oxygen which was then allowed to flow slowly into chamber (A). Sufficient oxygen was admitted to ensure a quantity of monoxide in excess of saturation, the filtration data in Table I having afforded an order of magnitude for this calculation. The apparatus then was rotated in such a manner as to bring the metal and oxide onto filter (D); the temperature was raised to the desired saturation level and held for 5 to 15 minutes. (For the small quantity of metal involved and the low solubility, saturation was nearly instantaneous, soaking times of from 1 minute to 1 hour giving identical results.) At the end of the soaking period, a slight nitrogen pressure was admitted, forcing the now saturated metal into bulb (C). This bulb was removed by flame sealing at point (X), and analyzed for oxygen content by the amalgamation procedure proposed by Pepkowitz and Judd,<sup>2</sup> but using the modified apparatus developed by the authors.<sup>3</sup>

For the study of the solubility of sodium monoxide in potassium metal, sodium monoxide of high purity was prepared by the high vacuum, 400°, reaction of sodium hydroxide with sodium metal in a stainless steel vessel, followed by the distillation of excess sodium metal. The reaction, under dynamic vacuum, proceeds as



The removal from the vessel and all subsequent handling of the Na<sub>2</sub>O was performed in a dry room. The material analyzed 98.2% Na<sub>2</sub>O and 1.7% Na<sub>2</sub>CO<sub>3</sub>.

The solubility apparatus for sodium monoxide in potassium was similar to that used for sodium, except that provision was made for distilling potassium metal onto the filter, upon which had been placed the sodium monoxide. The remainder of the operation was identical with that previously described for the sodium oxide in sodium and NaK study.

The data from these solubility runs are shown in Fig. 2. The equation for the curve shown is

$$\log (\text{wt. \% sodium monoxide oxygen} \times 10^3) = -0.0535 + 0.00351t$$

where  $t$  is C°.

This equation will determine a curve for sodium monoxide oxygen content of sodium, potassium and NaK from their melting points to 555, 310 and 360°, respectively.

The NaK alloys used for the data in Fig. 2 ranged from 27 to 86 wt. % potassium with no deviation due to varying potassium content. This lack of deviation is in agreement with the sodium monoxide in pure metal data.

The data for the solubility of potassium monoxide in

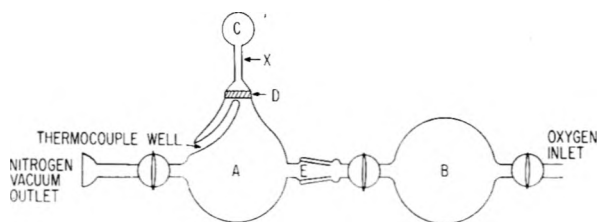
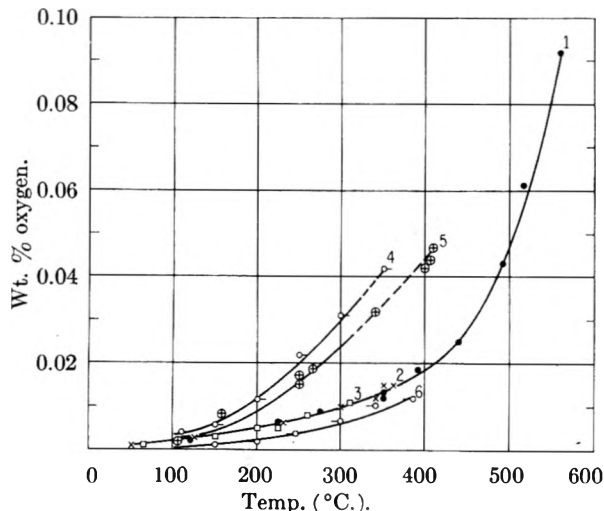
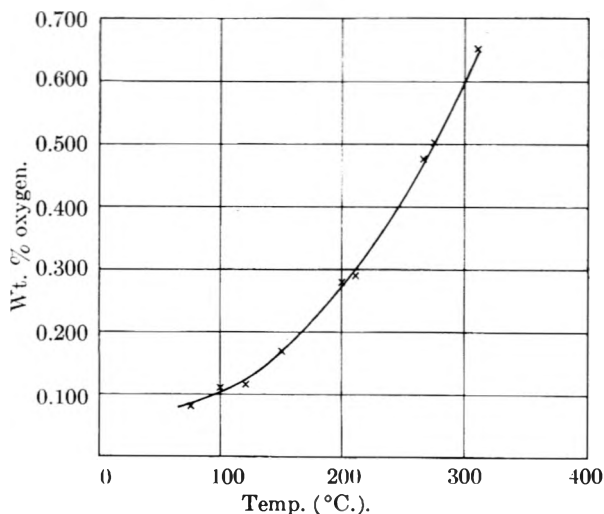


Fig. 1.—Oxide solubility apparatus (with oxygen reservoir).

Fig. 2.—Solubilities in Na, NaK and K: 1, Na<sub>2</sub>O oxygen in Na; 2 X, Na<sub>2</sub>O oxygen in NaK; 3 □, Na<sub>2</sub>O oxygen in K; 4 ◊, NaOH oxygen in Na; 5 ⊕, NaOH-Na<sub>2</sub>O oxygen in Na (calcd. as Na<sub>2</sub>O); 6 ⊙, Na<sub>2</sub>CO<sub>3</sub> oxygen in Na.Fig. 3.—K<sub>2</sub>O solubility in K.

potassium is shown in Fig. 3. The equation for the curve shown is

$$\text{wt. \% potassium monoxide oxygen} = 0.0865 - 0.000609t + 0.00000771t^2$$

where  $t = ^\circ\text{C.}$  for the range 75–305°.

The relatively high solubility of potassium monoxide in potassium afforded an excellent opportunity to test the efficiency of vacuum distillation as a means of separating metal and oxide. Potassium metal, saturated with oxide at its melting point, was pipetted into a nickel still containing an amount of K<sub>2</sub>O equivalent to 5 wt. % oxygen, and distilled under vacuum. The distillate was caught in three thin-walled glass ampules, which were sealed off and analyzed for oxygen content. Less than 0.001 wt. % oxygen was found in each of the three samples. Subsequent sodium runs gave similar data. Thus, it is evident that

vacuum distillation will effect essentially complete separation of sodium and potassium from their oxides.

**The Solubility of Sodium Hydroxide in Sodium.**—The possibility of atmospheric contamination in alkali metal systems poses the question of hydroxide as well as oxide solubility in the metals. This problem was studied by two methods: the solubility of pure sodium hydroxide and the solubility of mixed hydroxide-oxide. The latter study was made to determine whether there was interdependence of the solutes upon saturation.

The apparatus and method of operation used for these experiments were the same as previously described for sodium monoxide in potassium. Sodium was distilled onto pure sodium hydroxide, in the first case, and onto a mixture of sodium monoxide-hydroxide in the second. After saturation and filtration at temperature, the filtrate was analyzed for oxygen content by the amalgamation procedure.

In the case of pure hydroxide solubility, the alkalinity resulting from the residue hydrolysis during the analysis procedure was calculated on the basis of hydroxide oxygen content (equivalent wt. = 16) as opposed to monoxide oxygen content (equivalent wt. = 8). In the runs involving mixed oxide-hydroxide, the data were arbitrarily calculated as if present only as the monoxide.

The data from the hydroxide and mixed oxide runs are shown in Fig. 2. The equation for hydroxide oxygen content of sodium is

$$\text{wt. \% hydroxide oxygen} = 3.71 \times 10^{-7} t^2 - 7.14 \times 10^{-6} t - 5.7 \times 10^{-4}$$

where  $t$  is  $^\circ\text{C.}$  for the range 100–350°.

The equation for mixed oxide-hydroxide oxygen content of sodium is

$$\text{wt. \% O}_2 = 2.03 \times 10^{-7} t^2 + 3.82 \times 10^{-5} t - 3.09 \times 10^{-3}$$

where  $t$  is  $^\circ\text{C.}$  for the range 100 to 410° and where the oxygen is present as both hydroxide and monoxide, but is calculated as if present as monoxide only.

An apparent anomaly in the hydroxide and hydroxide-oxide data in Fig. 2 results from the reporting of solubilities above the melting point of sodium hydroxide (320°). At this temperature, as has been stated and demonstrated,<sup>2,7</sup> hydroxide and sodium react to form monoxide, and/or hydride and hydrogen depending upon pressure conditions. If the technique of operation in solubility experiments is such that hydroxide saturation occurs under dynamic vacuum, and, if sufficient time is allowed for complete hydrogen removal, the hydroxide curve will break sharply downward at 320° to the monoxide curve. If, however, saturation occurs in a closed system of small volume, albeit evacuated, the hydride formed by the Na-NaOH reaction will not completely dissociate; and some will be soluble in the filtered melt, giving high apparent oxide values.<sup>8</sup> The latter system, static vacuum, was used for the data herein reported, thus giving the data shown by the dotted extensions of curves 4 and 5 in Fig. 2. These points are included to demonstrate an error of data interpretation if the contaminant species is not definitely known.

If the hydroxide oxygen in sodium be recalculated as monoxide oxygen and added to the monoxide oxygen in sodium, one finds nearly perfect agreement with the mixed hydroxide-oxide curve. This demonstrates additive solubilities and lack of solute interdependence.

It should be pointed out that the hydroxide-oxide samples also contained sodium carbonate. However, as the next section of this article demonstrates, this contributes a minor error when calculated as monoxide oxygen.

A. D. Bogard, formerly of this Laboratory, concurrently determined the solubility of mixed hydroxide-oxide in sodium by a radioactive technique, using Na<sup>24</sup> as a tracer.<sup>9</sup> His results are in excellent agreement with the chemical data herein reported.

**The Solubility of Sodium Carbonate in Sodium.**—Although available corrosion data indicate that sodium carbonate contributes little or nothing to total corrosion, its solubility was determined as a means of comparing apparent and true oxygen contents of sodium. That is, if a

(7) D. D. Williams, NRL Memo Report 33, June, 1951.

(8) D. D. Williams, J. A. Grand and R. R. Miller, THIS JOURNAL, 61, 379 (1957).

(9) A. D. Bogard and D. D. Williams, NRL Report 3865, 1951.



sample were saturated with oxide, hydroxide and carbonate, but calculated as if present as monoxide only (apparent oxygen content), it would be important to determine the magnitude of the difference between this value and that calculated from individual solubilities (true oxygen content).

The apparatus and method of operation were the same as for sodium monoxide in potassium and for sodium hydroxide in sodium. Thus, sodium metal was distilled onto dry, C.P. sodium carbonate, saturated and filtered at temperature, and analyzed by amalgamation. The residue from the amalgamation separation was titrated, using a double indicator end-point (phenolphthalein and methyl orange) to ensure that the measured alkalinity was present as carbonate only.

The data are shown in Fig. 2. The plot shows the solubility as oxygen content calculated from the sodium carbonate data (equivalent wt.  $O_2 = 24$ ).

**Summary.**—Coördinating the data in this paper, one finds relatively low solubilities of the various impurities in the alkali metals studied. Their sig-

nificance, at least with respect to oxide, has been demonstrated adequately by corrosion data.<sup>10</sup>

In the interest of accurate sample analysis, the effects of the various solubilities should not be ignored. The magnitude of these effects will depend almost entirely upon the history of individual samples. For example, sodium hydroxide can be eliminated from a sodium system by heating to 350–400°; but, if this is not done under high vacuum, one of the reaction products is sodium hydride which is soluble and stable at these and even higher temperatures.<sup>7</sup> Therefore, while hydroxide has been eliminated, an even more soluble component<sup>8</sup> has been introduced, and the deviation from true oxygen content is still present.

(10) "Liquid Metals Handbook," 2nd Ed., Navexos P-733 (Rev.), June, 1952.

## THE OXIDATION OF METHYL RADICALS AT ROOM TEMPERATURE<sup>1</sup>

By PHILIP L. HANST AND JACK G. CALVERT

Contribution from the McPherson Chemical Laboratory, The Ohio State University, Columbus 10, Ohio

Received June 1, 1958

Methyl radicals were produced by photolysis of azomethane. Infrared analysis showed that in the presence of oxygen these radicals reacted to produce as major products, methanol and formic acid and as lesser products, formaldehyde, carbon monoxide and possibly dimethyl peroxide. Methyl hydroperoxide and peroxyformic acid were not detected. Experiments with additives and studies of the properties of possible intermediates also yielded data which were useful in determining the free radical reactions taking place. The important reactions appear to be:  $CH_3 + O_2 \rightarrow CH_3OO$ ,  $CH_3OO + O_2 \rightarrow CH_3O + O_3$ , and  $CH_3O + CH_3O \rightarrow CH_3OH + H_2CO$ ; the formaldehyde is further oxidized to formic acid. The results also indicate that the reactions  $2CH_3OO \rightarrow 2CH_3O + O_2$  and  $CH_3OO + RH \rightarrow CH_3OOH + R$  are probably not important in this system.

### I. Introduction

Although it has long been recognized that most gas phase reactions and many condensed phase reactions proceed *via* mechanisms involving free radicals, knowledge of these mechanisms is still in an incomplete state. Recent attempts to explain the formation of ozone in polluted city air have shown that photochemical oxidations in particular need further study.

Reported herein are the results of an investigation on this subject involving the photo-oxidation of azomethane in an oxygen-rich system. The reaction mechanism deduced is of a type not usually postulated, especially in that it involves ozone formation.

### II. Experimental Technique

(a) **Apparatus.**—Free radicals were generated photolytically in a 5-liter Pyrex flask. The light source was a 550-watt medium pressure Hanovia mercury arc. Its cooling jacket was built of Pyrex glass in the form of a Dewar flask with water flowing between the walls. The two layers of Pyrex glass absorbed practically all of the light of wave length shorter than 3130 Å., thus minimizing photolysis of reaction products and ensuring that no ozone was generated by direct photolysis of oxygen. The cooling jacket and arc were located in the center of the photolysis flask which was wrapped in aluminum foil and immersed in water. This arrangement got a maximum of near ultraviolet light into the reactants. All photolyses reported in this paper were done at room temperature. The absorbed light intensity was such

that the azomethane was 50% decomposed in the apparatus in about 10 minutes. Pressures of reactants in the range of a few millimeters of mercury were measured on a manometer containing silicone vacuum pump oil. Higher pressures were measured on a mercury manometer. A reaction was started when the lighted arc was lowered into its place at the center of the 5-liter chamber and was ended when the arc was raised.

Analyses were made by means of infrared absorption spectroscopy using ten centimeter and one meter gas absorption cells on Perkin-Elmer Model 21 double beam spectrophotometer. The photolysis products were either expanded into the absorption cell and then pressurized with extra oxygen until the total pressure in the cell was one atmosphere, or they were forced into the cell by air or oxygen in such a way that the total pressure of products in the cell reached one atmosphere. Measurements of concentrations of products were made by comparisons to reference spectra run on pure compounds under conditions of resolution, pressure broadening, per cent. absorption, etc., as near as possible to those existing during the analysis. No major infrared bands remained unidentified.

(b) **Materials.**—Azomethane ( $CH_3-N=N-CH_3$ ) was prepared by the reduction of dimethylhydrazine with mercuric oxide according to the method of Renaud and Leitch.<sup>2</sup> An aqueous solution of dimethylhydrazine was prepared by the reaction of dimethylhydrazine dihydrochloride with an equivalent amount of sodium hydroxide in dilute solution; this was dropped slowly with stirring at room temperature into a suspension of excess mercuric oxide in water. The azomethane gas which issued from the mixture was collected in a trap immersed in Dry Ice and then dried by distillation to the storage vessel at reduced pressure.

Methyl hydroperoxide and dimethyl peroxide were prepared by slowly dropping 40% aqueous potassium hydroxide into a stirred ice-cold mixture of dimethyl sulfate and 30% hydrogen peroxide. The dimethyl peroxide issued from the

(1) Presented in part before the Division of Physical Chemistry, 133rd Meeting of the American Chemical Society, San Francisco, April, 1958.

(2) R. Renaud and L. C. Leitch, *Can. J. Chem.*, **32**, 545 (1954).

TABLE I

PRODUCTS OF THE PHOTOLYSIS OF AZOMETHANE IN ONE ATMOSPHERE OF OXYGEN-PHOTOLYZED 10 MIN. WITH MERCURY ARC THROUGH PYREX

	Pressure (mm.)			
Initial azomethane	31.6	15.8	7.9	5.3
CH <sub>3</sub> OH	8.30	5.00	2.80	1.95
HCOOH	7.26	5.28	2.97	1.91
CO	1.40	0.7	0.5	0.3
CH <sub>3</sub> OOCH <sub>3</sub>	small, if any	small, if any	small, if any	small, if any
HCHO	present, but less than 1.0	present, but less than 0.5	present, but less than 0.3	present, but less than 0.2
CH <sub>3</sub> OOH	less than 1.0, if any	less than 0.5, if any	less than 0.3, if any	less than 0.15, if any
CO <sub>2</sub>	less than 0.1, if any	less than 0.05, if any	less than 0.01, if any	less than 0.01, if any
Peroxyformic acid	less than 0.5, if any	less than 0.3, if any	less than 0.15, if any	less than 0.1, if any
Unreacted azomethane	12.0	6.1	3.9	2.5
Total azomethane accounted for	21.0	11.9	7.2	4.7

mixture during reaction and was captured in a liquid nitrogen trap. The methyl hydroperoxide was extracted from the aqueous solution with ether and distilled.

Monomeric formaldehyde vapor was obtained by heating paraformaldehyde under vacuum. All other compounds were obtained from commercial sources.

### III. Experimental Results

(a) **The Final Products of the Oxidation of Methyl Radicals.**—Methyl radicals were obtained by photolysis of azomethane. It has been demonstrated that the only primary process is  $\text{CH}_3\text{N}=\text{NCH}_3 + h\nu \rightarrow 2\text{CH}_3 + \text{N}_2$ , with a quantum efficiency near unity.<sup>3,4</sup> The products of some of the photolyses in oxygen are listed in Table I. It is to be noted that the major part of the azomethane is accounted for in the observed products, and that the fraction not accounted for becomes smaller as the azomethane concentration is reduced. Nitrous oxide is not a product under any of the conditions used in this work. Spectrum 1 is the infrared absorption spectrum of the products of the run which had an initial azomethane partial pressure of 5.3 mm. It can be seen that methanol and formic acid predominate as products. The lack of formation of methyl hydroperoxide is particularly significant, as will be discussed. Spectra 3 and 4 of methyl hydroperoxide and dimethyl peroxide are shown for comparison. Spectrum 2 shows the results of the photolysis of 8 mm. of azomethane in one atmosphere of oxygen with 5.6 mm. of formaldehyde added. The purpose of the added formaldehyde was to provide additional easily abstracted hydrogens so that methyl hydroperoxide might have a better chance to form. The resulting spectrum shows a complete lack of the characteristic methyl hydroperoxide bands at about 12.2  $\mu$ . It can be seen that at the same time the methanol and formic acid yields were large. An estimate of the limit of detectability of methyl hydroperoxide leads to the conclusion that the methanol yield exceeded the methyl hydroperoxide yield (if any) by at least a factor of 50.

(b) **Tests for the Presence of Ozone during the**

(3) M. H. Jones and E. W. R. Steacie, *J. Chem. Phys.*, **21**, 1018 (1953).

(4) G. R. Hoey and K. O. Kutschke, *Can. J. Chem.*, **33**, 496 (1955).

**Oxidation of Methyl Radicals.**—Table II shows the results of a test for the presence of ozone during the reaction by means of the additive tetramethylethylene. The acetone is formed in the fast ozone-tetramethylethylene reaction, as is discussed in section (f) below. Spectrum 5 is the infrared spectrum of the products obtained in this experiment. Acetone formation suggests the presence

TABLE II

THE EFFECT OF ADDED TETRAMETHYLETHYLENE ON THE PRODUCTS OF PHOTOLYSIS OF AZOMETHANE (2.4 MM.) IN OXYGEN (748 MM.)

Exposure time, 10 minutes.

Compound formed	Methyl alcohol	Formic acid	Carbon monoxide	Formaldehyde	Acetone
Amount formed (mm. Hg) without added tetramethylethylene	1.0	0.8	0.1	small	none
Amount formed (mm. Hg) in the presence of 13.5 mm. Hg of tetramethylethylene	1.0	0.35	none	0.8	0.7

of ozone as an intermediate, and the suppression of formic acid formation with the resulting accumulation of formaldehyde indicates an important role for ozone in the formaldehyde oxidation. The use of isobutylene as an additive produced only traces of acetone, and did not change significantly the ratios of products formed. From a rough estimate of the rate of acetone formation and with the use of an approximate rate constant for the isobutylene-ozone reaction,<sup>5</sup> it is estimated that the average steady state ozone concentration in a typical experiment was on the order of  $10^{-5}$  mm. of mercury. This is far below the limits of detection with the spectroscopic equipment used in this study.

(c) **The Photooxidation of Formaldehyde Vapor.**—It was shown that formaldehyde vapor (monomer) is converted to formic acid under the conditions of the experiments. Five minutes photolysis of 2.7 mm. of formaldehyde in one atmosphere of

(5) R. D. Cadle and P. L. Magill, "Air Pollution Handbook," Section 3. McGraw-Hill Book Co., New York, N. Y., 1956, pp. 3-21.

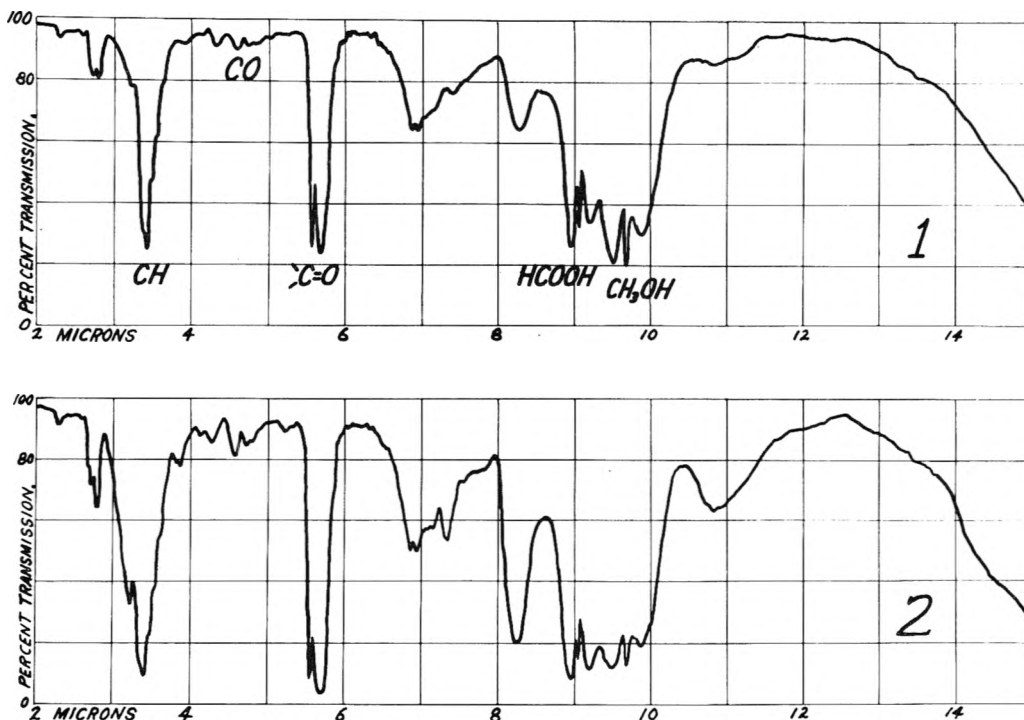


Fig. 1.—Products of azomethane (5.3 mm.) photolyzed 10 min. in one atm. of oxygen (60 cm. of products plus 14 cm. of added oxygen in a one meter cell).

Fig. 2.—Products of azomethane (8 mm.) plus formaldehyde (5.6 mm.) photolyzed 10 min. in one atm. of oxygen (58 cm. of products plus 16 cm. Hg added oxygen in a one meter cell).

oxygen produced 0.9 mm. of formic acid and 0.1 mm. of carbon monoxide with 1.4 mm. of formaldehyde remaining. Spectrum 6 shows these results.

(d) **Some Properties of Dimethyl Peroxide.**—Dimethyl peroxide vapor was not decomposed by photolysis in oxygen under the conditions of these experiments. It was also thermally stable in oxygen at room temperature; however, it was decomposed when moderately heated; its half-life is approximately 20 minutes at 147°. This thermal decomposition was studied in detail and will be reported in a separate paper. The infrared spectrum of dimethyl peroxide (spectrum 4) has its strongest characteristic band in the same region as the strongest characteristic band of methanol. This interference can be removed to a certain extent by placing methanol in the reference cell; however, overcompensation of the methanol can also obliterate the other bands. Therefore it is difficult to prove the presence or absence of a small amount of dimethyl peroxide in the present work. It is apparent that it is not a major product.

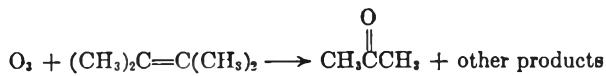
(e) **Some Properties of Methyl Hydroperoxide.**—Methyl hydroperoxide vapor was not decomposed when photolyzed in the apparatus in the presence of one atmosphere of oxygen. It is considerably more stable thermally than dimethyl peroxide, since several hours at 200° did not decompose a sample of it appreciably. Its infrared spectrum (spectrum 3) has characteristic bands in spectral regions where there is no interference from the observed products. This is especially true of the band at about 12.2  $\mu$ . Methyl hydroperoxide can definitely be ruled out as major reaction product.

It should be mentioned that the collection of in-

frared spectra of organic peroxides presented by Minkoff<sup>6</sup> appears to contain errors and is not very much help in the interpretation of gas-phase spectra. This already has been pointed out in an article by Stephens, *et al.*, with regard to the aliphatic peroxy acids,<sup>7</sup> and it again appears to be the case with regard to the methyl hydroperoxide. The most prominent band in Minkoff's methyl hydroperoxide spectrum occurs at about 8.9  $\mu$  and is very likely due to ether impurity. It was found in the present work that it is extremely difficult to remove completely the ether by distillation. The ether contaminant was blanked out of spectrum 3 by pure ether in the reference cell.

(f) **The Behavior of Ozone in the System.**—It was shown that ozone did not react thermally with azomethane under the conditions of these experiments. The ozone did disappear fast, however, when the ozone-oxygen-azomethane mixture was photolyzed. In a typical experiment several mm. of ozone were mixed with several mm. of azomethane in one atmosphere of oxygen and the infrared spectrum was recorded at intervals of 5 or 10 minutes. In the absence of irradiation there was no reaction, but when the arc was turned on the ozone disappeared within a few minutes.

Ozone was shown to react extremely fast with tetramethylethylene to produce acetone with 1 to 1 stoichiometry according to the equation



One mole of ozone reacts with one mole of tetra-

(6) G. J. Minkoff, *Proc. Roy. Soc. (London)*, **A224**, 176 (1954).

(7) E. R. Stephens, P. L. Hanst and R. C. Doerr, *Anal. Chem.*, **29**, 776 (1957).

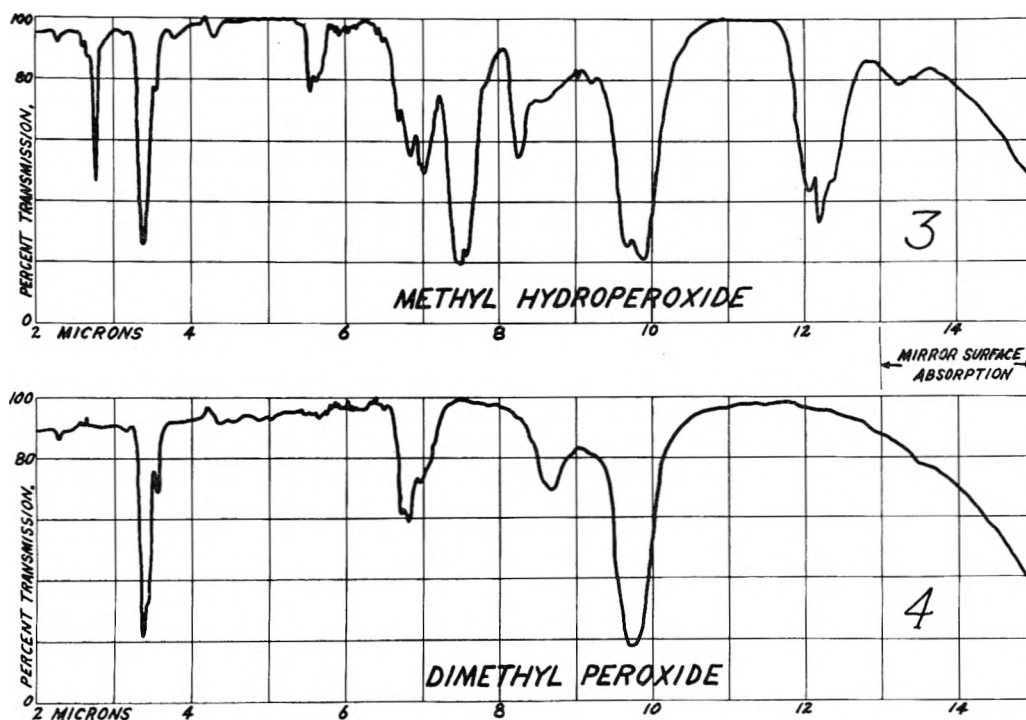


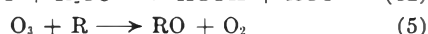
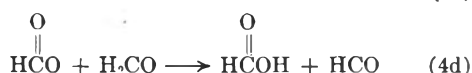
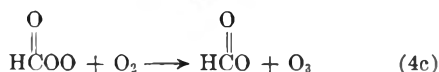
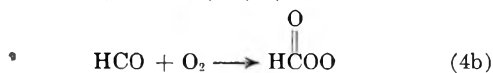
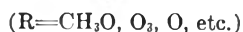
Fig. 3.—Methyl hydroperoxide reference spectrum (6 mm.  $\text{CH}_3\text{OOH}$  in one atm. of oxygen in a one meter cell).

Fig. 4.—Dimethyl peroxide reference spectrum (2.5 mm.  $\text{CH}_3\text{OOCH}_3$  in a one meter cell).

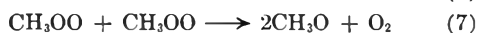
methylethylene to produce one mole of acetone. Ozonides do not form in the gas phase at room temperature.<sup>8,9</sup> The spectra showed that acetone was the only carbonyl compound formed in significant amounts. Thus the acetone carbonyl band at  $5.8 \mu$  as well as the characteristic acetone band at  $8.2 \mu$  can be used as a measure of the amount of ozone reacted.

#### IV. Conclusions and Discussion

(a) **The Oxidation of Methyl Radicals.**—Reactions 1, 2, 3, 4a, 4b, 4c, 4d and 5 comprise the mechanism of oxidation of methyl radicals indicated by our results.



Reactions 6 and 7 do not appear to take place under the conditions of our experiments.



It will be convenient to consider the evidence concerning the various reactions in the order (1), (3), (6), (7), (2), (4a, b, c, d) and (5).

**Reaction (1):**  $\text{CH}_3 + \text{O}_2 (+\text{M}) \rightarrow \text{CH}_3\text{O}_2 (+\text{M})$ .—A number of investigators have presented evidence that reaction 1 is the initial reaction of methyl radicals in the presence of oxygen.<sup>4,10</sup> There appears to be no good reason to suspect anything else.

**Reaction (3):**  $\text{CH}_3\text{O} + \text{CH}_3\text{O} \rightarrow \text{CH}_3\text{OH} + \text{H}_2\text{CO}$ .—The formation of methanol seems to require the presence of methoxy radicals which abstract hydrogen from some other molecule or radical. Raley, *et al.*, invoke reaction (3) to explain this methanol formation.<sup>11</sup> Hoey and Kutschke also present evidence for reaction 3.<sup>4</sup> The near equivalence of the yields of methanol and formic acid in the present work makes reaction 3 seem probable, since the formic acid undoubtedly results from the oxidation of formaldehyde as shown in equations (4a, b, c, d) and discussed below.

**Reaction (6):**  $\text{CH}_3\text{OO} + \text{RH} \rightarrow \text{CH}_3\text{OOH} + \text{R}$  (where RH may be  $\text{CH}_3\text{O}$ ).—If  $\text{CH}_3\text{OO}$  were present in the system with a lifetime comparable to the lifetime of  $\text{CH}_3\text{O}$ , it seems likely that it would react in accordance with reaction 6, which is analogous to reaction 3. Walsh<sup>12</sup> and many other investigators have presented evidence for reactions like (6). Hanst, *et al.*, have shown that peroxy acids are produced in the oxidation of higher aldehydes at room temperature, but are not produced in the oxidation of formaldehyde.<sup>13</sup> Thus there

(8) R. Criegee, A. Kerckow and H. Zinke, *Ber.*, **88**, 1878 (1955).

(9) W. E. Scott, E. R. Stephens, P. L. Hanst and R. C. Doerr, a paper presented at the 22nd Midyear Meeting of the American Petroleum Institute's Division of Refining, Philadelphia, Pa., May 14, 1957.

(10) D. E. Hoare and A. D. Walsh, *Trans. Faraday Soc.*, **53**, 1102 (1957).

(11) J. H. Raley, L. M. Porter, F. F. Rust and W. E. Vaughan, *J. Am. Chem. Soc.*, **73**, 15 (1951).

(12) A. D. Walsh, *Trans. Faraday Soc.*, **42**, 269 (1946).

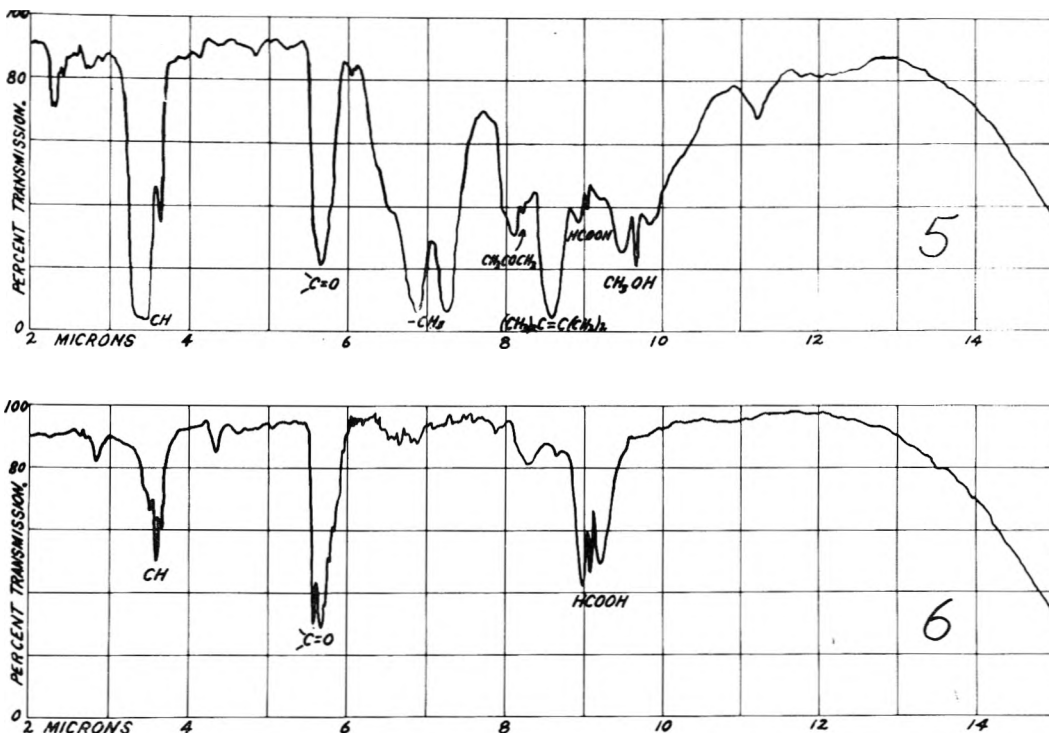
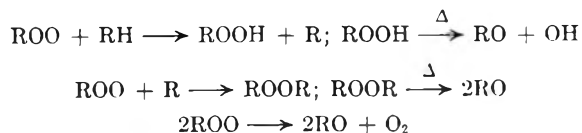


Fig. 5.—Products of azomethane (2.4 mm.) plus tetramethylethylene (13.5 mm.) photolyzed 10 min. in one atm. of oxygen (one atm. in a one meter cell).

Fig. 6.—Products of formaldehyde (2.7 mm.) photolyzed 5 min. in one atm. of oxygen (one atm. in a one meter cell).

is ample reason to believe that reaction 6 ought to take place. However, the fact that no methyl hydroperoxide is observed as product in our system indicates that it is unimportant here. It must be concluded, therefore, that  $\text{CH}_3\text{OO}$  has a considerably shorter lifetime in the system than  $\text{CH}_3\text{O}$ . There must be a reaction which consumes  $\text{CH}_3\text{OO}$  very fast and yields  $\text{CH}_3\text{O}$ .<sup>14</sup>

**Reaction (7):**  $2\text{CH}_3\text{OO} \rightarrow 2\text{CH}_3\text{O} + \text{O}_2$ .—Bell, *et al.*, have presented three alternative schemes of converting alkyl peroxy radicals,  $\text{ROO}$ , to alkoxy radicals,  $\text{RO}$ .<sup>15</sup> They are



None of these reactions appears to have taken place to any great extent in the system we have studied. The first two of them involving thermal decomposition of intermediate peroxides must be rejected because we have demonstrated that the peroxides are stable under the conditions of our experiments. The third, which is our reaction 7, does not seem likely to us for two reasons. First, it appears that if  $\text{CH}_3\text{OO}$  had a long enough life-

time in the system to undergo radical-radical reactions as in (7), it ought to also abstract hydrogen in a reaction analogous to the hydrogen abstraction by methoxy radicals, reaction 3. The fact is that it does not. Second, and even more important, is that the demonstration that substantial quantities of ozone are formed during the photooxidation requires the importance of reaction 2. The possible reaction  $\text{CH}_3 + \text{CH}_3\text{OO} \rightarrow \text{CH}_3\text{O} + \text{CH}_3\text{O}$  must also be ruled out because the complete lack of methane and ethane formation shows that  $\text{CH}_3$  has an extremely short lifetime; that is, it undergoes reaction (1) to the exclusion of all others in this system.

**Reaction (2):**  $\text{CH}_3\text{OO} + \text{O}_2 \rightarrow \text{CH}_3\text{O} + \text{O}_3$ .—The evidence in support of reaction 2 is, in our opinion, the most important result of this work. It is a reaction not often postulated in oxidation mechanisms, although it has been considered as a possible reaction in "smog" by many different investigators. Probably the main reason for the apparent disregard of reaction 2 in oxidation studies is the transient nature of the ozone which is formed. It is difficult to identify the ozone in a system containing free radicals and other active molecular species because it is quickly consumed in reactions of the type of reaction 5.

An approximate calculation of the enthalpy change of reaction 2, gives +6.3 kcal./mole,<sup>16</sup> which, if correct, is consistent with the importance

(13) P. L. Hanst, E. R. Stephens and W. E. Scott, *Proc. Am. Petrol. Inst.*, [III] **35**, 175 (1955).

(14) The unimportance of the alternative mechanism of methanol and formaldehyde formation through the direct interaction of peroxy radicals,  $2\text{CH}_3\text{O}_2 \rightarrow \text{CH}_2\text{O} + \text{CH}_3\text{OH} + \text{O}_2$  (see G. A. Russell, *J. Am. Chem. Soc.*, **79**, 387 (1957)) seems likely in view of the evidence herein presented for the formation of the intermediate ozone and the occurrence of reaction (2).

(15) E. R. Bell, J. H. Raley, F. F. Rust, F. H. Seibold and W. E. Vaughan, *Disc. Faraday Soc.*, **10**, 242 (1951).

(16) The standard enthalpy of formation of ozone is taken as +34 kcal./mole ("Selected Values of Chemical Thermodynamic Properties," Circular of the National Bureau of Standards, 500); it is assumed that the O-O bond dissociation energy in  $\text{CH}_3\text{OO}$  is the same as in diethyl peroxide, namely, 31.5 kcal./mole (R. E. Rebert and K. J. Laidler *J. Chem. Phys.*, **20**, 574 (1952)).

of this reaction. In this calculation it is assumed that the possible stabilization of the  $\text{CH}_3\text{O}_2$  by a three electron bond in the radical is unimportant, presumably as a consequence of the dissimilarity in the two oxygen atoms. If this assumption is incorrect, then reaction 1 will be more exothermic and reaction 2 more endothermic, such that the relation  $\Delta H_2 \cong 1.5 - \Delta H_1$  is satisfied.<sup>17</sup> If this is the case then the demonstrated rapidity of reaction 2 must be explained in terms of a reaction between newly-formed, vibrationally excited  $\text{CH}_3\text{O}_2$  radicals and oxygen. This mechanism is consistent with the Hoare and Walsh three body mechanism for reaction 1.<sup>10</sup>

This idea of a "hot" peroxy radical could explain the observation of Hanst, *et al.*,<sup>13</sup> that in the room temperature oxidation of a series of aldehydes in air, the amount of peroxy acid increased as the hydrocarbon chain was lengthened. The explanation would be as follows. In the case of formaldehyde (where no peroxy acid was formed), the radi-

$$\begin{array}{c} \text{O} \\ || \\ \text{HCOO} \end{array}$$
 cals  $\text{HCOO}$  reacted quickly to produce ozone as in our reaction 2. In the case of the higher aldehydes, the excess energy was absorbed in molecular vibrations in the hydrocarbon chain so that the probability of reaction 2 was reduced, and it was superseded by peroxy acid production analogous to our reaction 6.

Haagen-Smit, *et al.*, brought consideration of reaction 2 to the fore several years ago in their investigations on "smog."<sup>18</sup> By a sensitive analytical technique which made use of the fact that extremely low concentrations of ozone will crack stretched rubber, they showed that the photolysis of hydrocarbon- $\text{NO}_2$ -air mixtures, organic nitrites in air without  $\text{NO}_2$ , diacetyl in air without  $\text{NO}_2$ , and pyruvic acid in air without  $\text{NO}_2$  all produced ozone. Stephens, *et al.*, have demonstrated spectroscopically the formation of ozone in these photooxidations.<sup>9,19,20</sup> Taylor and Blacet have suggested two alternative reactions to explain ozone formation in diacetyl photolysis.<sup>21</sup>

Thus previous results have indicated that an ozone forming step is likely in methyl radical oxidation. Whether it was a major reaction or only a side reaction remained unresolved. Consideration of the products of our azomethane photooxidation apparently requires that it be a major reaction. This follows from our previous discussion. Since the evidence for reaction 1 which produces  $\text{CH}_3\text{OO}$  is very strong, and since the evidence for reaction 3 which consumes  $\text{CH}_3\text{O}$  is also very strong, there must be a reaction converting  $\text{CH}_3\text{OO}$  to  $\text{CH}_3\text{O}$ . Our rejection of reaction 7 and the Russell mech-

anism<sup>14</sup> of product formation left reaction 2 as the only obvious possibility.

The general evidence for (2) was good, but since the reaction is rather unconventional and rarely considered in oxidation mechanisms, an experimental detection of the intermediate ozone in our system was imperative. Since the steady state concentration of ozone was below the detection limit of our spectroscopic equipment, an indirect method of identification had to be used. Therefore the experiment with added tetramethylethylene was conducted. The results of this test discussed previously and shown in Table II and Spectrum 5 confirmed our expectations. That is, acetone formation indicated that ozone was reacting with tetramethylethylene. It seems unlikely to us that the interaction of peroxy methyl radicals with tetramethylethylene would lead to a significant amount of acetone, although this possibility cannot be excluded unambiguously. Since the methanol yield is not lowered by tetramethylethylene addition, presumably the interaction of the  $\text{CH}_3\text{O}_2$  with the olefin would be one of O-atom transfer to the double bond. Cvetanovic<sup>22</sup> reports that the reaction of oxygen atoms (generated by the Hg-photo-sensitized decomposition of  $\text{N}_2\text{O}$ ) with tetramethylethylene yields about equal quantities of the epoxide of tetramethylethylene and pinacolone; acetone is not reported as a product.<sup>23</sup> Thus we interpret the data as indicating that the tetramethylethylene reacted with an amount of ozone equivalent to 70% of the methanol yield. While the methanol yield was not reduced by the olefin, the formic acid yield was decreased as formaldehyde became a major product. A rough estimate showed the average steady-state ozone concentration in a typical experiment to be on the order of  $10^{-5}$  mm. Long-path infrared techniques are being applied to the analysis for the intermediate ozone in continuing experiments in this Laboratory. Preliminary results with a 40-meter path length cell substantiate ozone formation in this system.

**Reactions (4a, b, c, d).**—Reactions (4a, b, c, d) constitute a path from the intermediate formaldehyde to the final product formic acid. The four together constitute a chain reaction. This is a secondary series of reactions in the photooxidation of azomethane, and the demonstration that under the experimental conditions employed formaldehyde is converted to formic acid would be sufficient for our main purpose without the steps in the conversion being listed. However, since we interpret the results embodied in equations 1, 2 and 3 as having a somewhat general significance, we have applied them in reactions (4a, b, c, d). Many of the arguments used to establish reactions 1, 2 and 3 can also be used in favor of reactions 4b, 4c and 4d. For example, the fact that formic acid but no peroxyformic acid is produced indicates that the

(17) Calculated assuming  $\Delta H^\circ(\text{CH}_3\text{O}) = -0.5$  kcal./mole (P. Gray, *Trans. Faraday Soc.*, **51**, 1367 (1955));  $\Delta H^\circ(\text{CH}_3) = 32.0$  kcal./mole (W. M. D. Bryant, *J. Polymer Sci.*, **6**, 359 (1951)).

(18) A. J. Haagen-Smith, C. E. Bradley and M. M. Fox, *Ind. Eng. Chem.*, **45**, 2086 (1953).

(19) E. R. Stephens, P. L. Hanst, R. C. Doerr and W. E. Scott, *ibid.*, **48**, 1498 (1956).

(20) E. R. Stephens, W. E. Scott, P. L. Hanst and R. C. Doerr, *Proc. Am. Petrol. Inst.*, Sec. III, **36**, 288 (1956).

(21) R. P. Taylor and F. E. Blacet, *Ind. Eng. Chem.*, **48**, 1505 (1956).

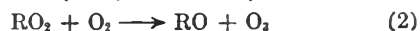
(22) R. J. Cvetanovic, *Can. J. Chem.*, **36**, 623 (1958).

(23) When molecular oxygen is added to olefin- $\text{N}_2\text{O}$  systems and Hg-photosensitization is effected, then ketones and aldehydes become major products; e.g., isobutene gives acetone. Of course in this case the reaction  $\text{O} + \text{O}_2 + \text{M} \rightarrow \text{O}_3 + \text{M}$  may compete with the O-atom addition to the double bond, and the ozone so formed may react with the olefin in the usual fashion to give the carbonyl compounds.

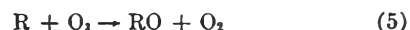
radical  $\overset{\text{O}}{\parallel}\text{HCOO}$  is quickly converted to  $\overset{\text{O}}{\parallel}\text{HCO}$ , just as the non-formation of methyl hydroperoxide indicated a quick conversion of  $\text{CH}_3\text{OO}$  to  $\text{CH}_3\text{O}$ . The actual system is undoubtedly more complicated than shown; for example, no reactions producing CO are shown, and no chain terminating reactions are shown. Nevertheless we believe that the main reactions are the ones indicated. The initiating reaction 4a is purposely stated vaguely. Ozone apparently is involved in some fashion since the presence of tetramethylethylene suppressed reactions (4a, b, c, d). Reaction 4b is the analog of (1); (4c) is the analog of (2) and (4d) is the chain continuing step.

**Reaction (5):**  $\text{R} + \text{O}_3 \rightarrow \text{RO} + \text{O}_2$ .—Reactions such as (5) which consume ozone are obviously required by the fact that the ozone is only an intermediate and not a stable final product and by the fact that ozone mixed with azomethane disappears when irradiated. One specific reaction which may use up some of the ozone is (4a), since the removal of ozone by tetramethylethylene inhibited the series (4a, b, c, d). It was shown in this work by the photolysis of known azomethane-oxygen-ozone mixtures that even at small concentrations of ozone, reaction 5 can compete successfully with

reactions 1 and 4b. The reason for the great difference in the rates probably lies in the fact that (5), by virtue of being two-body, will be many times faster than three-body reactions like (1) and (4b); (5) competing with (1) and (4b) would not only consume ozone but would at the same time reduce the over-all ozone yield. The system may adjust itself to a competition between the pair of reactions



and the reaction



Such a competition would be in accord with the fact that when the reactant concentration is reduced to very low values such as exist in polluted air, the ozone concentration attains values comparable to or larger than the hydrocarbon concentration. Under those conditions the ozone concentration is very low compared to the oxygen concentration (even though high compared to the hydrocarbon concentration) and reaction 5 is much slowed down while reactions 1 and 2 are not.

**Acknowledgment.**—The authors gratefully acknowledge the support of this work by the Public Health Service, National Institutes of Health, Bethesda, Maryland.

## ANION-EXCHANGE STUDIES. XXV. THE RARE EARTHS IN NITRATE SOLUTIONS<sup>1</sup>

BY Y. MARCUS<sup>2</sup> AND FREDERICK NELSON

*Contribution from the Oak Ridge National Laboratory, Chemistry Division, Oak Ridge, Tennessee*

*Received July 17, 1958*

Adsorbabilities of several rare earths—La, Ce, Pr, Nd, Pm, Sm, Eu, Tb and Yb—in slightly acidified lithium nitrate solutions have been investigated with a strong base anion-exchange resin. Adsorbabilities increase with increasing lithium nitrate concentration, and the lighter rare earths are more strongly adsorbed than the heavier. Sufficient differences in adsorbabilities were found to permit separation of the lighter rare earths with relatively short columns.

Most ion-exchange separations of rare earth elements have been based on the use of cation exchangers with eluents containing organic complexing agents. Some separations involving anion exchange and organic eluents have been reported,<sup>3</sup> and more recently attention has turned toward possible utilization of anion exchangers with inorganic eluents. While the rare earths are not appreciably adsorbed from the common mineral acids HCl, HNO<sub>3</sub> and H<sub>2</sub>SO<sub>4</sub>, adsorption from slightly acidified nitrate solutions has been reported.<sup>4</sup> Thus a typical rare earth, Eu(III), is adsorbed sufficiently from concentrated ammonium nitrate solutions to permit its separation from non-adsorbable elements. With

other nitrates, *e.g.*, LiNO<sub>3</sub>, considerable enhancement of adsorbability occurs.<sup>5</sup>

Surlis and Choppin<sup>6</sup> have shown that lanthanides and actinides may be separated with strongly basic anion exchangers in thiocyanate solutions. Adsorption of a rare earth-like element, Y(III), from dilute ammonium sulfate and sodium carbonate solutions has been reported<sup>7</sup> as well as adsorption of a number of rare earths from sulfite solutions.<sup>8</sup>

On the basis of these observations it appeared of interest to investigate further the possibilities of utilizing anion exchangers for rare earth separations. Adsorption from sulfite solutions was confirmed and distribution coefficients were found to increase with sulfite concentration and pH. The rare earths were also found to adsorb from dilute nitrite, thio-sulfate and sulfate solutions with adsorbability decreasing with increasing electrolyte concentration.

(1) This document is based on work performed for the U. S. Atomic Energy Commission at the Oak Ridge National Laboratory, operated by Union Carbide Corporation.

(2) Visiting Scientist, 1958, on leave from the Israel Atomic Energy Commission, Post Office Box 7056, Hakiryah, Tel Aviv, Israel.

(3) E. H. Huffman and R. L. Oswald, *J. Am. Chem. Soc.*, **72**, 3323 (1950).

(4) K. A. Kraus and F. Nelson, "Symposium on Ion Exchange and Chromatography in Analytical Chemistry," Am. Soc. for Testing Materials, Special Publication No. 195 (June, 1956).

(5) J. Dannon, private communication.

(6) J. P. Surlis, Jr., and G. R. Choppin, *J. Inorg. Nuclear Chem.*, **4**, 62 (1957).

(7) N. Saito and T. Sekine, *Nature*, **180**, 753 (1957).

(8) R. C. Vickery, *J. Chem. Soc. (London)*, 2360 (1955).

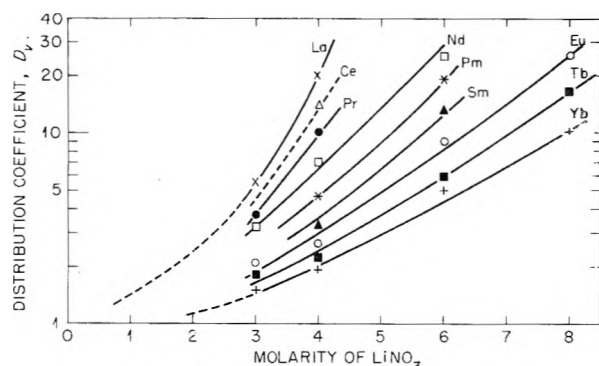


Fig. 1.—Adsorption of rare earths from lithium nitrate solutions ( $2 \times 10^{-3} M HNO_3$ ,  $78^\circ$ ).

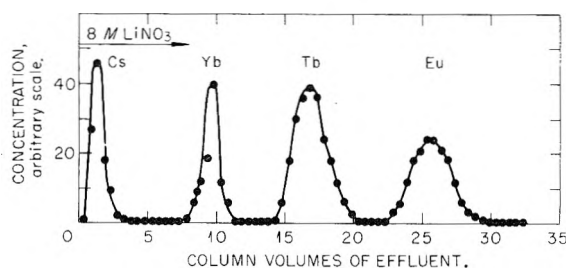


Fig. 2.—Separation of Cs, Yb, Tb and Eu in  $LiNO_3$  solution ( $78^\circ$ ,  $0.25 \text{ cm.}^2 \times 6 \text{ cm.}$  column).

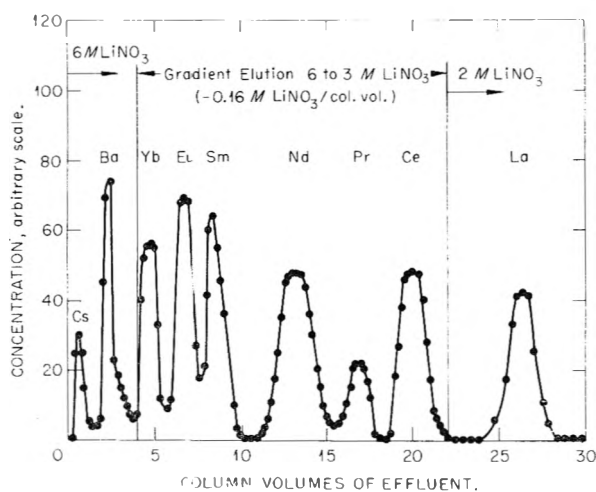


Fig. 3.—Separation of Cs, Ba and several rare earths in  $LiNO_3$  solutions ( $78^\circ$ ,  $0.25 \text{ cm.}^2 \times 10.5 \text{ cm.}$  column).

Of these media, nitrate solutions appeared to warrant more extensive investigation since preliminary equilibration studies at room temperature showed significant differences in the adsorbabilities of the various rare earths, particularly in concentrated  $LiNO_3$  solutions.

### Experimental

A strongly basic quaternary amine resin of the polystyrene-divinylbenzene type (Dowex-1, 10% DVB) was used. It was initially in the chloride form and was converted to the nitrate form by treatment, in a column, with several column volumes of  $2 M$  nitrate solution. The excess electrolyte was removed from the bed by washing with water.

Since the nitrate form of this resin reaches equilibrium relatively slowly,<sup>4</sup> a rather small particle size ( $-325$  mesh) was chosen, and most measurements were carried out at elevated temperature ( $78^\circ$ ) which was maintained by placing the columns inside jackets heated by the vapor of refluxing ethanol. Although rate problems probably could

also have been circumvented with resins of lower cross-linking, the 10% DVB resin was chosen to obtain greater selectivity.

Adsorbabilities were determined by column techniques. Small aliquots of appropriate  $LiNO_3$ - $HNO_3$  solutions containing tracers of the metals were added to the columns (ca.  $0.25 \text{ cm.}^2 \times 4 \text{ cm.}$ ) which had been pretreated with  $LiNO_3$ - $HNO_3$  solutions of the same concentration. The columns were eluted with the same nitrate solutions used in pretreating, and metal concentrations in the effluent were determined radiometrically. From the number of column volumes  $V_{max}$  of effluent at which the metal appeared in maximum concentration, the volume distribution coefficient,  $D_v$  (amount per liter of bed/amount per liter of solution), was computed from the relationship  $D_v = V_{max} - i$  where  $i$  is the fractional interstitial volume ( $i = \text{ca. } 0.4$ ).

Separations were carried out with columns which had a cross sectional area of about  $0.25 \text{ cm.}^2$  and varied in length from 4 to 20 cm. Both stepwise and gradient elution<sup>9</sup> techniques were used in separations. For the gradient elutions, an apparatus similar to that described in the literature<sup>10</sup> was constructed which delivered eluent having an approximately linear concentration gradient. The apparatus consisted of two 50-ml. graduated cylinders filled with nitrate solutions of different concentrations and connected at the bottom through a narrow stopcock. One cylinder had a delivery tube and provision for magnetic stirring. Flow rate was controlled by adjusting the hydrostatic head.

The following radioactive tracers were used:  $Cs^{137}$  (30 y);  $Ba^{140}$  (12.8 d);  $La^{140}$  (40.2 h);  $Ce^{144}$  (285 d);  $Pr^{142}$  (19.1 h);  $Nd^{147}$  (11.6 d);  $Pm^{147}$  (2.6 y);  $Sm^{153}$  (47 h);  $Eu^{156}$  (1.7 y);  $Tb^{160}$  (72 d);  $Yb^{169}$  (32 d);  $Am^{243}$  (8000 y). The tracers were obtained from the ORNL Isotopes Division except  $Sm^{153}$ ,  $Tb^{160}$  and  $Yb^{169}$ , which were prepared by irradiating samples of the appropriate rare earth oxides in the ORNL Low Intensity Training Reactor (LITR). The tracers supplied by the ORNL Isotopes Division were analyzed by them and were all of acceptable radiochemical purity. Those prepared in the LITR were also found to be of satisfactory purity by half-life measurements or by separate column experiments. Since the tracers were of high specific activity, all experiments pertain to resin loadings of less than 1% capacity. Analyses of  $\gamma$ -emitters were carried out with liquid samples and a standard well-type scintillation counter. Samples containing pure  $\alpha$  or  $\beta$ -emitting tracers were evaporated on plates and counted with a Geiger or  $\alpha$ -proportional counter.

### Results and Discussion

1. Adsorption from  $LiNO_3$  Solutions.—The adsorption of rare earths from  $LiNO_3$  solutions is independent of acidity only at low acid concentrations. Thus, in  $4 M LiNO_3$ , the distribution coefficient of La is about 20 and remains constant in the region of nitric acid concentration,  $10^{-2}$  down to at least  $10^{-4} M HNO_3$ . Above  $10^{-2} M HNO_3$ , adsorption of La decreases rapidly with increasing acid concentration. Similar results were obtained with europium and ytterbium. This effect of acidity on adsorbability at constant total ionic strength is reminiscent of the behavior of many elements in chloride solutions,<sup>4</sup> although in nitrate solutions, the acid independent region appears at lower acidities.

A series of adsorption measurements were carried out as a function of  $LiNO_3$  concentration with solutions containing  $0.002 M HNO_3$ , an acid concentration within the acid independent region which, presumably, is also sufficiently high to prevent complicating hydrolytic reactions from occurring. The results are summarized in Fig. 1 where the values of

(9) (a) E. C. Freiling, *J. Am. Chem. Soc.*, **77**, 2067 (1955); (b) W. E. Neric, *This Journal*, **59**, 690 (1955).

(10) See, e. g., (a) C. W. Parr, *Proc. Biochem. Soc.*, 324th Meeting, 1953; (b) R. M. Bock and Nan-Sing Liang, *Anal. Chem.*, **26**, 1543 (1954).



$D_v$  (obtained at 78°) are plotted against  $M$  LiNO<sub>3</sub>. For a given rare earth, the adsorbability rises with  $M$  LiNO<sub>3</sub> and the slope,  $d \log D_v/d M$  LiNO<sub>3</sub>, decreases with increasing atomic number. Surprisingly, the adsorbability of the rare earths at constant  $M$  LiNO<sub>3</sub> decreases with increasing atomic number. However, sufficient data are not available to explain this behavior or to reach unambiguous conclusions on the complexing properties of the rare earths.

In the region 3 to 4  $M$  LiNO<sub>3</sub>, where comparative data are available, the ratio of adsorbability appears to be similar for adjoining rare earths from La to Eu. This ratio (or separation factor,  $S$ ) is about 1.4 and, hence, is comparable to separation factors obtained in the cation-exchange separation of light rare earths ( $S \cong 1.6$ ) with  $\alpha$ -hydroxyisobutyric acid<sup>11</sup> and ethylenediaminetetraacetic acid.<sup>12</sup>

Of the rare earths heavier than Eu, only Tb and Yb were studied. In fairly concentrated LiNO<sub>3</sub> solutions where adsorption of these elements becomes appreciable, ( $D_v > 5$ ) separation factors for the non-adjoining rare earths, Eu-Tb and Tb-Yb, are about 1.5. On the basis of these results, one concludes that separation of the adjoining *trans*-Eu rare earths will be considerably more difficult than of the lighter rare earths as is usually the case in rare earth separations.

**2. Separations.**—The following experiments demonstrate some of the separations which may be achieved with LiNO<sub>3</sub> solutions although it should be recognized that optimal conditions were not necessarily selected.

A mixture of Eu, Tb, Yb and a typical non-adsorbable element (Cs<sup>137</sup>) in 8  $M$  LiNO<sub>3</sub> was added to a 0.25 cm.<sup>2</sup>  $\times$  6 cm. column. Elution was carried out at 78° with 8  $M$  LiNO<sub>3</sub> at a flow rate of 0.4 cm./min. The non-adsorbable element, Cs, appeared immediately in the effluent while Yb, Tb and Eu eluted in separate bands with peak maxima at 10, 17 and 26 column volumes, respectively (Fig. 2).

A gradient elution experiment which illustrates separation of several rare earths from each other, as

(11) (a) G. R. Choppin and R. J. Silva, *J. Inorg. Nuclear Chem.*, **3**, 153 (1956); (b) H. L. Smith and D. C. Huffman, *ibid.*, **3**, 243 (1956).

(12) S. W. Mayer and E. C. Freiling, *J. Am. Chem. Soc.*, **75**, 5647 (1953).

well as from a "non-adsorbed" element (Cs) and a weakly adsorbed element (Ba), is shown in Fig. 3. For this experiment, an aliquot containing a mixture of rare earth tracers, as well as Cs<sup>137</sup> and Ba<sup>140</sup> (in secular equilibrium with La<sup>140</sup>) in 6  $M$  LiNO<sub>3</sub>-0.002  $M$  HNO<sub>3</sub> was added to a 0.25 cm.<sup>2</sup>  $\times$  10.5 cm. column maintained at 78°. Elution was carried out at a flow rate of 0.6 cm./min. with sufficient 6  $M$  LiNO<sub>3</sub>-0.002  $M$  HNO<sub>3</sub> solution to remove Cs<sup>137</sup> and Ba<sup>140</sup>. The Cs<sup>137</sup> appeared almost immediately in the effluent near 0.4 column volumes, while Ba<sup>140</sup>, interestingly, was adsorbed strongly enough to be separated from Cs and appeared in maximum concentration near 2.4 column volumes. Elution was then continued by the gradient technique at approximately the same flow rate with a solution initially 6  $M$  in LiNO<sub>3</sub>. A concentration gradient of about -0.16  $M$  LiNO<sub>3</sub> per column volume was used. The elements, Yb, Eu, Sm, Nd, Pr and Ce eluted in this order in reasonably sharp bands though with some overlapping. After removal of Ce, the eluent was *ca.* 3  $M$  LiNO<sub>3</sub> and only La remained on the column. It was removed with 2  $M$  LiNO<sub>3</sub>. Total separation time was about 7 hours.

In other experiments, it was shown that the parent-daughter nuclides, Ba<sup>140</sup>-La<sup>140</sup>, are easily separated in a few minutes with 3-4  $M$  LiNO<sub>3</sub> and a 1 cm. long column. Lanthanum is adsorbed while Ba passes through; La may be eluted with dilute lithium nitrate or nitric acid.

Adsorbability of one of the actinides, Am(III), was also measured. Strong adsorption ( $D_v > 5$ ) was found above 3  $M$  LiNO<sub>3</sub> and the adsorption function was similar to that of La or Ce. Adsorption of the lighter actinide, Ac(III), however, has been found by Dannon<sup>5</sup> to be significantly different from that of La. Separation of Am(III) from Ac(III) and from most of the rare earths should thus be possible with relatively short columns.

**Acknowledgments.**—The authors are indebted to Dr. K. A. Kraus for helpful suggestions and criticisms. Y.M. wishes to thank the Israel Atomic Energy Commission for a research grant. The generosity of Dr. Waldo E. Cohn of the Biology Division, ORNL, for allowing the work to be done in his Laboratory is warmly acknowledged.

# AN APPLICATION OF IRREVERSIBLE THERMODYNAMICS TO THE STUDY OF DIFFUSION<sup>1</sup>

BY RICHARD W. LAITY

*Frick Chemical Laboratory, Princeton University, Princeton, N. J.*

*Received July 25, 1958*

An attempt is made to show the usefulness of irreversible thermodynamics in permitting the definition of new terms by which the rates of dynamic processes may be characterized. A set of rate constants with which to describe simple mass diffusion is discussed and is shown to be potentially more useful than some of the phenomenological coefficients employed in other treatments of diffusion. The coefficient under discussion represents the proportionality between the thermodynamic force on a substance and its velocity relative to another substance in the mixture, and is therefore termed a "friction coefficient." How such coefficients may be determined for some simple systems is explained, and examples are cited from the literature. It is suggested that these may be more useful quantities than more conventionally defined diffusion coefficients upon which to focus our attention in the search for microscopic models to explain the mechanism of diffusion processes.

Two ways in which the science of thermodynamics has been most useful to the theoretician are: (1) within the framework of its known laws it has made possible all macroscopic correlations among the properties of matter, thus greatly simplifying the task of constructing microscopic models; (2) by defining new terms, *e.g.*, entropy and activity, it has permitted choice of the most useful properties upon which to focus our attention in attempting to build such models. The extension of thermodynamic principles to the study of dynamic processes known as irreversible thermodynamics gives hope of achieving similar success in an area where much progress remains to be made. The principal emphasis in the development of irreversible thermodynamics up to the present time has been on the study of macroscopic correlations, an approach which has proved fruitful in a number of areas. Such work has entailed the definition of new terms, usually known as phenomenological coefficients, by which the rates of various processes and their interdependence can be characterized. As with conventional thermodynamics, however, an endless variety of new terms could be defined with varying degrees of simplicity and utility. Relatively little critical attention has thus far been paid to the problem of defining thermodynamic "rate constants" in the most useful way possible, *i.e.*, the way which might best lend itself to microscopic interpretation.

It is the purpose of this paper to show how a particular method of setting up the phenomenological equations for the description of simple mass diffusion under a concentration gradient leads to the definition of terms which may well prove more useful than the conventionally defined (Fick's Law) diffusion coefficient. The fundamental basis for the treatment under discussion actually was presented in 1945 by Onsager.<sup>2</sup> The significance of this work apparently has not been fully appreciated by subsequent workers, however, so that some clarification and expansion seems in order at this time.

Onsager's treatment starts with the definition of the "dissipation-function"  $F$  for a system of  $N$  components at constant temperature (constant pressure will also be assumed in the present discussion)

$$F = \frac{1}{2} \sum_{i,k} R_{ik}(J_i \cdot J_k) \quad (1)$$

where the vector  $J_i$  represents the local flux of component  $i$  and  $J_k$  is similarly defined. Note that the case  $i = k$  is included, the summation being taken over all possible combinations. The  $R_{ik}$  are thus scalars the significance of which will shortly become apparent. As a part of this definition Onsager incorporates the "convention" that  $R_{ik} = R_{ki}$ . The reason such an option is available is apparent when we consider that  $R_{ik}(J_i \cdot J_k) + R_{ki}(J_k \cdot J_i) = (R_{ik} + R_{ki})(J_i \cdot J_k)$ , so that only the sum ( $R_{ik} + R_{ki}$ ) is important in defining the dissipation-function.

Since the dissipation-function is to represent half the rate at which free energy is dissipated (locally, *i.e.*, within a volume  $dV$ ) by the irreversible flows, Onsager now notes an additional restriction on the  $R_{ik}$ . This is the requirement that there be no dissipation when all the velocities are equal and is written

$$\sum_k R_{ik} c_k = 0 \quad (2)$$

where  $c_k$  is the concentration of component  $k$ . In the subsequent development of the equations of diffusion the relation 2 is not made explicit use of in the Onsager treatment, but is merely allowed to stand by itself in the form shown above. Specific inclusion of this restraint in the derivation gives considerable insight into the nature of the  $R_{ik}$ , however, as will now be shown.

Multiplying each of the equations 2 by  $J_i^2/c_i$  and subtracting from (1) gives

$$2F = \sum_{i,k} R_{ik} J_i (J_k - c_k J_i / c_i) \quad (3)$$

for the restricted form of the dissipation-function. If we now continue following Onsager's variational method for finding the fields of flow  $J_i$  in a system characterized by a set of local gradients of the chemical potential  $\nabla \mu_i$  by maximizing the function

$$-(dZ/dt) - \int F dV$$

where  $Z$  is the free energy of the system as a whole,  $t$  is the time and  $V$  the volume, we find that the condition to be satisfied by the local flows is

$$-\nabla \mu_i = \sum_k R_{ik} (J_k - c_k J_i / c_i) \quad (4)$$

(1) Presented at the National Meeting of the American Chemical Society, Chicago, 1958.

(2) L. Onsager, *Ann. N. Y. Acad. Sci.*, **46**, 241 (1945).

Making use of the fact that a flux can be expressed in the form  $J_i = c_i v_i$ , where  $v_i$  is the local velocity vector, we may rewrite (4) in the form

$$-\nabla \mu_i = \sum_k^N R_{ik} c_k (v_k - v_i) \quad (5)$$

Thus we have obtained the restricted phenomenological equations. Although  $i$  may take any value from 1 to  $N$  in the equations 5, only  $N - 1$  of these equations are independent, since the Gibbs-Duhem equation relates the forces at all points in the system.

A slightly different derivation of equations basically the same as (5) has been employed by A. Klemm,<sup>3</sup> who apparently failed to note that their existence was already implicit in the work of Onsager. Observing that the concentrations can be expressed in the form  $c_i = CX_i$ , where  $C$  is the number of moles of solution per cc. and  $X_i$  the mole fraction of the  $i$ th component, Klemm's equations appear in the form

$$K_i = \sum_k^N r_{ik} X_k (v_i - v_k) \quad (6)$$

where  $K_i$  represents the thermodynamic force on  $i$ . By comparison of (6) with (5) it is apparent that  $r_{ik} = -R_{ik}C$ .

The special virtue of this formulation lies in the way in which the phenomenological coefficients are defined. Since the  $R_{ik}$  depend only on velocity differences, they are independent of the motion of the reference with respect to which the velocities happen to be defined. This is much more satisfactory than some of the awkward artifices that have been employed, such as referring all velocities to the mass average velocity of the solution or arbitrarily taking the velocity of one component to be zero, in defining coefficients whose values depend on the reference chosen. Thus, instead of obtaining "cross-coefficients", *i.e.*,  $L_{ik}$ , where  $i \neq k$ , whose values represent a complex combination of the interactions of  $i$  and  $k$  with each other and with the reference species, or obtaining "rate constants" the magnitudes of which are influenced by such extraneous factors as isotopic mass (as would be true for  $L_{ik}$  dependent on the mass average velocity even in the absence of kinetic isotope effects), the treatment described here gives rise quite naturally to a set of numbers  $R_{ik}$  each of which refers to the specific interaction of just two species. (Note that all coefficients of the type  $R_{ii}$  drop out of equation 5.)

Klemm's use of the term "friction coefficient" to describe the  $R_{ik}$  (or  $r_{ik}$ ) seems particularly appropriate, since it is the proportionality between the velocity of  $i$  relative to  $k$  and the "force" applied to  $i$ , with suitable allowance made for the fraction of  $i$ 's total environment that consists of  $k$ . There is ample precedent for such a name, the  $r_{ik}$  being a generalization to multicomponent systems of the "molecular friction coefficients" discussed by Kirkwood<sup>4</sup> and others. Indeed, in Lord Rayleigh's original prototype upon which the Onsager dissipa-

tion-function is based, the coefficients corresponding to  $R_{ik}$  are true friction coefficients.<sup>5</sup>

The quantities  $R_{ik}$  are readily obtainable in simple systems through the experimental determination of diffusion coefficients. In a system of two components, for example, the equations 5 define only one friction coefficient,  $R_{12}$  and there exists only one independent diffusion coefficient,  $D_{12}$ . This mutual diffusion coefficient is usually defined by the relations

$$\begin{aligned} J_1 &= -D_{12} \nabla c_1 \\ J_1 \bar{V}_1 + J_2 \bar{V}_2 &= 0 \end{aligned} \quad (7)$$

where the  $\bar{V}_i$  are partial molar volumes. The second equation is necessary to fix the reference with respect to which the fluxes are measured. As pointed out by Hartley and Crank, the restriction noted is equivalent to choosing a reference fixed with respect to the cell walls in cases where the partial molar volumes are independent of concentration.<sup>6</sup> An alternative mutual diffusion coefficient,  $D_{12}'$ , more useful to the present discussion, may be defined by the relations

$$\begin{aligned} J_1 &= -D_{12}'(c_1/a_1)\nabla a_1 \\ c_1 v_1 + c_2 v_2 &= 0 \end{aligned}$$

where  $a_1$  is the thermodynamic activity of component 1 and the  $v_i$  are the local velocities at any point in the system. The first equation can also be written in the form

$$v_1 = -D_{12}' \nabla \ln a_1 = -(D_{12}'/RT) \nabla \mu_1 \quad (8)$$

which can be compared with the corresponding equation for  $D_{12}$

$$v_1 = -D_{12} \nabla \ln c_1$$

Note, however, the change of reference for  $D_{12}'$ . Some authors, recognizing that the driving force for diffusion is actually a gradient of the chemical potential, have applied a "thermodynamic correction" of the form (8), while retaining the "volume-fixed" reference (7).<sup>7</sup> This procedure gives rise to a different coefficient for each of the two components. The  $D_{12}'$  defined here might thus be called the "thermodynamic mutual diffusion coefficient." It is related to  $D_{12}$  by

$$D_{12}'(1 + \partial \ln \gamma_1 / \partial \ln X_1) = D_{12} \quad (9)$$

where  $\gamma_i$  is the activity coefficient of either component and  $X_i$  its mole fraction. Now for a system of two components equation 5 reads

(5) R. J. Strutt, *Proc. Math. Soc. London*, **4**, 363 (1873).

(6) G. S. Hartley and K. Crank, *Trans. Faraday Soc.*, **45**, 801 (1949).

(7) See, for example, A. R. Gordon, *J. Chem. Phys.*, **5**, 522 (1937). It should perhaps be noted that the paper contains an error in the expression for the "change in thermodynamic potential of the solute with concentration." In passing from equation 2 to equation 4a the author has implied that

$$c_2 \frac{\partial \mu_2}{\partial c_2} = n_2 \frac{\partial \mu_2}{\partial n_2} (V/n_1 \bar{V}_1)$$

where the  $n_i$  are mole fractions and  $V$  is the molar volume of the solution. The correct relation is

$$c_2 \frac{\partial \mu_2}{\partial c_2} = n_2 \frac{\partial \mu_2}{\partial n_2} (V/\bar{V}_1)$$

English and Dole [*J. Am. Chem. Soc.*, **72**, 3261 (1950)] failed to correct this in making use of the equation, while Gordon repeated the error in a subsequent note [*J. Am. Chem. Soc.*, **72**, 4840 (1950)]. The effect of this error on the calculations contained in these publications is small.

(3) A. Klemm, *Z. Naturforschung*, **8a**, 397 (1953).

(4) J. G. Kirkwood, *J. Chem. Phys.*, **22**, 783 (1954).

$$-\nabla\mu_1 = R_{12}c_2(v_2 - v_1)$$

If the velocity reference is chosen such that  $c_1v_1 + c_2v_2 = 0$ , this becomes

$$-\nabla\mu_1 = -R_{12}v_1(c_1 + c_2)$$

or

$$\nabla\mu_1/R_{12} = v_1/V$$

where  $V$  is the volume of liquid containing one mole of solution. By comparison with (8) we may conclude that

$$R_{12} = -VRT/D_{12}' \quad (10a)$$

The corresponding equation using Klemm's friction coefficient is

$$\tau_{12} = +RT/D_{12}' \quad (10b)$$

The use of  $R_{12}$  might appear preferable due to the smaller variation with concentration expected, since  $D_{12}'$  is apt to decrease with decreasing molar volume. Either form of the friction coefficient will in general be a more complicated function of the composition, however, so that the Klemm formulation (6) will be selected for subsequent discussion here on the basis of its simplicity. From the definition of the dissipation-function it will be observed that the  $R_{ik}$  are negative; hence, the  $\tau_{ik}$  to be discussed here are all positive quantities.

Experimental data recently have become available which demonstrate the concentration dependence of  $\tau_{12}$  in some binary liquid mixtures.<sup>8,9</sup> These data indicate that the variation of  $\tau_{12}$  with concentration is more nearly linear in solutions that approach thermodynamic ideality than in non-ideal solutions. This shows that it may be possible in the case of liquids to define an "ideal" behavior for the friction coefficient, a concept which might enhance its usefulness considerably. Conclusions about the behavior of  $\tau_{12}$  in non-ideal solutions can only be drawn, however, when truly reliable thermodynamic data are available, the parameter  $\partial \ln \gamma_i / \partial \ln X_i$  being very sensitive to the accuracy of the data. Thus, Johnson and Babb's procedure of calculating the required curve for the benzene-ethanol system from the Van Laar equation<sup>10</sup> gives very misleading results. Thermodynamic data reported by Brown and Smith<sup>11</sup> can be used to show that the Van Laar equation gives a very poor approximation to the experimental curve for this system. Application of the experimental curve to the diffusion data indicates that the deviation of  $\tau_{12}$  from a linear concentration dependence is considerably smaller than Johnson and Babb's plot of  $D_{12}'$  would suggest.

A "two-component" system of particular interest is one in which the two species are chemically identical, differing only in isotopic composition. The mutual diffusion coefficient in such a system is called the tracer diffusion coefficient and may generally be identified with the unmeasurable "self-diffusion" coefficient. From the thermodynamic ideality of such a system it follows that

$$\tau_{12} = \tau_{11} = RT/D_{11}' = RT/D_{11}$$

(8) C. S. Caldwell and A. L. Babb, *This Journal*, **60**, 51 (1956).

(9) D. K. Anderson, J. R. Hall and A. L. Babb, *ibid.*, **62**, 404 (1958).

(10) P. A. Johnson and A. L. Babb, *ibid.*, **60**, 14 (1956).

(11) I. Brown and F. Smith, *Australian J. Chem.*, **7**, 264 (1954).

Tracer diffusion coefficients thus may be used to define the coefficients  $R_{ii}$  which dropped out of the dissipation-function in the modified form (3).

Similarly, in systems of two different chemical species it is possible to measure three different friction coefficients:  $\tau_{12}$ ,  $\tau_{11}$  and  $\tau_{22}$ . The connection between  $\tau_{12}$  and  $D_{12}$  already has been pointed out. The relation of the  $\tau_{ii}$  to the corresponding self-diffusion coefficients is derived readily by considering the phenomenological equations 6 for a system of three components

$$\begin{aligned} -\nabla\mu_1 &= \tau_{12}X_2(v_1 - v_2) + \tau_{13}X_3(v_1 - v_3) \\ -\nabla\mu_2 &= \tau_{21}X_1(v_2 - v_1) + \tau_{23}X_3(v_2 - v_3) \end{aligned} \quad (11)$$

Now to find  $\tau_{11}$  we consider component 3 to be chemically identical to component 1. Thus  $\tau_{13} = \tau_{11}$  and  $\tau_{23} = \tau_{21} = \tau_{12}$ . The tracer diffusion coefficient  $D_{11}$  is defined by

$$D_{11} = v_1 / -\nabla \ln c_1 = RT v_1 / -\nabla\mu_1 \quad (12a)$$

$$X_1v_1 + X_3v_3 = 0 \quad (12b)$$

$$\nabla\mu_2 = 0 \quad (12c)$$

The restriction (12c) results from the lack of chemical composition gradients in the system, while the second equation of (12a) is based on the ideality of isotopic solutions. Applying restrictions (12b) and (12c) to equations 11, we may eliminate  $v_2$  and  $v_3$ , which gives

$$v_1 = -\nabla\mu_1 / (X_1'\tau_{11} + X_2\tau_{12}) \quad (13)$$

where  $X_1' = X_1 + X_3$  is the total mole fraction of chemical species 1 in the solution. Now by comparison of (13) with (12a) we see that

$$D_{11}/RT = 1/(X_1'\tau_{11} + X_2\tau_{12}) \quad (14a)$$

By an identical procedure we can, of course, show that

$$D_{22}/RT = 1/(X_2'\tau_{22} + X_1\tau_{12}) \quad (14b)$$

The three friction coefficients in a binary system are thus related in a simple way to diffusion coefficients which can be determined experimentally. First,  $\tau_{12}$  is found at any given concentration from the mutual diffusion coefficient  $D_{12}$  and thermodynamic data by equations 10b and 9. The values of  $D_{11}$  and  $D_{22}$  at the same composition are then substituted into equations 14, along with the value of  $\tau_{12}$  just found, to obtain  $\tau_{11}$  and  $\tau_{22}$  at this concentration.

One conclusion can be drawn from equations 14 and 10b by considering the behavior of  $D_{ii}$  as  $X_i$  approaches zero. It will be seen that at infinite dilution the self-diffusion coefficient of either constituent must have the same value ( $RT/\tau_{12}$ ) as the mutual diffusion coefficient  $D_{12}$  ( $= D_{12}'$  at infinite dilution by Henry's law). Although mechanistic considerations have previously led to the same conclusion, the above derivation is rigorously based on well-established thermodynamic principles combined with the readily acceptable hypothesis that  $\tau_{ii}$  does not become infinite, or, rather, does not increase asymptotically at a rate inversely proportional to  $X_i$ . The diffusion measurements of Johnson and Babb<sup>10</sup> on several liquid systems are consistent with this prediction. The slight discrepancies which appear must be due either to experimental error or to isotope effects in the tracer diffusion measurements.

A study of the data cited above reveals that, in addition to  $r_{12}$ , the  $r_{11}$  appear to show a linear concentration dependence in ideal liquid systems. For only two systems, however, are sufficient data presented by these workers to calculate all three friction coefficients. These are the non-ideal benzene-alcohol systems. The possibility of isotope effects in the measurements was minimized by labeling the molecules with  $C^{14}$  rather than deuterium.<sup>12</sup> The accuracy of the diffusion data combined with available thermodynamic figures is nevertheless sufficient to warrant only qualitative discussion of the concentration dependence of the friction coefficients at 25° and 1 atm. in these systems. We have calculated these for the benzene-ethanol system only, for which the following observations are consistent with the accuracy of the results (taking benzene as component 1 and ethanol as 2).

(1) The value of  $r_{12}$  is lower than that of either  $r_{11}$  or  $r_{22}$  at all concentrations. It ( $r_{12}$ ) shows a negative deviation from linearity, passing through a minimum somewhere between 15 and 30 mole % ethanol.

(2) The agreement among the results reported by Johnson and Babb<sup>10</sup> and those of Partington, Hudson and Bagnall [*Nature* **169**, 583 (1952)], who used deuterium-labeled molecules, appears to refute the suggestion of B. Ottar [*Acta Chem. Scand.*, **9**, 344 (1955)] that deuterium-labeling gives rise to a strong isotope effect in the tracer diffusion of the lower alcohols.

(2) The value of  $r_{11}$ , almost constant in the more concentrated benzene solutions, begins at concentrations below 80 mole % to show a gradually increasing rate of rise with decreasing concentration of benzene, but remains less than the value of  $r_{22}$  except, perhaps, at concentrations below 25 mole %.

(3) The value of  $r_{22}$  shows a similar behavior, remaining nearly constant as pure ethanol is diluted to about 80 mole % below which it rises with decreasing concentration at a steadily increasing rate.

The discussion immediately preceding summarizes the concentration dependence of molecular fraction coefficients in a single binary liquid system of non-electrolytes. A great deal more information of this type, as well as data on the effects of temperature and pressure, is needed before an understanding of the factors determining the values of these quantities can be developed. We nevertheless share with Onsager (ref. 2, p. 247) the feeling that the theory of transport processes may perhaps be most rapidly advanced by focusing our attention on the coefficients of the dissipation-function rather than on more commonly employed rate constants.

A subsequent publication will deal with the extension of this approach to electrolytic systems.<sup>13</sup>

(13) R. W. Laity, *J. Chem. Phys.*, in press.

## PREPARATION OF FINE PARTICLES FROM BIMETAL OXALATES<sup>1</sup>

BY WILLIAM J. SCHUELE

*The Franklin Institute Laboratories, Philadelphia 3, Pennsylvania*

*Received July 31, 1958*

Ferromagnetic and ferrimagnetic fine particles were prepared by suitably heat-treating co-precipitated oxalates of Co-Fe, Ni-Fe and Cu-Fe systems in a wide range of compositions. The particles produced by this method included metals, alloys, ferrites and other oxides. The technique is an excellent method for producing fine particles with a wide range of magnetic properties. Ferrite particles were prepared in a manner much simpler than the standard techniques. The existence of permanent magnetic properties in fine particles of normally "soft" magnetic materials such as the ferrites was in agreement with predictions of the theory of single domain particles. While the experimental work was confined to magnetic materials, the technique also can be useful in the preparation of other fine particle materials.

### Introduction

The specific purpose of the research described in this paper was the development of a method whereby various ferromagnetic materials (metals, alloys, ferrites and oxides) could be prepared in fine particle form.<sup>2</sup> It is well known that ferromagnetic materials in fine particle form exhibit "hard" or permanent magnetic properties, while in large particle form they exhibit "soft" or temporary magnetic properties.<sup>3</sup> Since fine particle materials sinter at lower temperatures than larger particle materials, it was obvious that we could not use a method of preparation which required high temperatures. The usual preparation of a ferrite involves a solid state reaction between the two

metal oxides,<sup>4,5</sup> but since this required the diffusion of the cations over large distances ( $\sim 10^4$  Å.) high temperatures are necessary. It seemed possible to eliminate this long range diffusion problem by starting with the two metals in a solid solution, in which case the ions would have to diffuse only the distance of the lattice spacings or a few ångströms. Wickham<sup>6</sup> and Robin<sup>7</sup> indicated that some of the bimetal oxalates form solid solutions. Since these oxalates could be decomposed thermally at moderate temperatures to yield the metal oxides and easily removed gaseous decomposition products, they were selected as the intermediates in our preparation of fine particle materials. We found, experimentally, that we could form solid

(1) This research was supported by the United States Air Force under Contract No. AF 33(616)-5041, monitored by Aeronautical Research Laboratory, Wright Air Development Center.

(2) Detailed magnetic studies are being made on the products reported here and will appear as a separate paper at a later date.

(3) C. Kittel, *Phys. Rev.*, **70**, 965 (1946).

(4) J. L. Snoek, "Ferromagnetic Materials." Elsevier (Press, Houston, Texas, 1949).

(5) E. W. Gorter, *Compt. rend.*, **230**, 192 (1950).

(6) D. G. Wickham, Tech. Rept. 89, Lab. for Insulation Research, MIT, Cambridge, Mass.

(7) J. Robin, *Bull. soc. chim., France*, 1078 (1953).

solutions of ferrous oxalate with the oxalates of zinc, cobalt, nickel, magnesium and manganese. It is interesting to note that these ions have nearly the same ionic radii as the ferrous ion.<sup>8</sup>

### Experimental

**Preparation and Characterization of the Oxalates.**—The sulfates of the two metals desired in the bimetal oxalate were dissolved in water at 60° in the proper ratio to give 1000 meq. in 1500 ml. of solution. The stoichiometric amount of ammonium oxalate was dissolved in 1500 ml. of water at 60° and added with rapid stirring to the metal ion solution. The precipitate was filtered in a buchner funnel, washed with water and then washed with acetone to speed up drying. Of the systems prepared, three were selected for more extensive study: cobalt ferrous oxalate, nickel ferrous oxalate and copper ferrous oxalate. The Goldschmidt ionic radii for cobalt (0.82) and nickel (0.78) are similar to ferrous ion (0.83) while copper (0.70) is smaller. In each of these systems, oxalates were prepared in one mole quantities of the composition  $A_yFe_{1-y}C_2O_4$ , where A = Cu, Ni or Co and  $y = 0.1, 0.2, 0.3, 0.4, 0.5, 0.6, 0.7, 0.8, 0.9, 1.0$ .

In order to determine whether our samples were solid solutions or just a mixture of the two oxalates, X-ray spectra were taken for each sample. If the two metal oxalates did not form solid solutions, the X-ray spectra would consist of the two separate spectra superimposed. If the bimetal oxalate was formed, the characteristic peaks on the spectra would lie between those of the pure components. Data of the nickel ferrous oxalate system shown in Table I will serve to illustrate this variation of  $d$  values with composition for a solid solution. A similar set was obtained for cobalt ferrous oxalate. However, for the copper ferrous oxalate, solid solution was not obtained and the peaks of both copper and iron oxalates were present in the spectra, the intensity of the respective peaks being proportional to the concentration of the metal oxalate. The X-ray data further supported the idea that similarity of ionic radii greatly aids in the formation of solid solutions.

TABLE I

PRINCIPAL " $d$ " VALUES<sup>a</sup> FOR Ni-Fe OXALATE SYSTEM

NiC <sub>2</sub> O <sub>4</sub>	4.78	3.94	3.01	2.53	2.07	1.94	1.87
Ni <sub>0.9</sub> Fe <sub>0.1</sub> C <sub>2</sub> O <sub>4</sub>	4.78	3.93	3.01	2.53	2.07	1.94	1.87
Ni <sub>0.8</sub> Fe <sub>0.2</sub> C <sub>2</sub> O <sub>4</sub>	4.80	3.92	3.02	2.55	2.08	1.95	1.87
Ni <sub>0.7</sub> Fe <sub>0.3</sub> C <sub>2</sub> O <sub>4</sub>	4.81	3.92	3.03	2.57	2.09	1.95	1.88
Ni <sub>0.6</sub> Fe <sub>0.4</sub> C <sub>2</sub> O <sub>4</sub>	4.83	3.91	3.04	2.58	2.09	1.96	1.88
Ni <sub>0.5</sub> Fe <sub>0.5</sub> C <sub>2</sub> O <sub>4</sub>	4.85	3.90	3.07	2.59	2.10	1.98	1.88
Ni <sub>0.4</sub> Fe <sub>0.6</sub> C <sub>2</sub> O <sub>4</sub>	4.87	3.90	3.11	2.59	2.11	1.99	1.88
Ni <sub>0.3</sub> Fe <sub>0.7</sub> C <sub>2</sub> O <sub>4</sub>	4.89	3.89	3.12	2.60	2.11	2.00	1.88
Ni <sub>0.2</sub> Fe <sub>0.8</sub> C <sub>2</sub> O <sub>4</sub>	4.89	3.89	3.14	2.61	2.12	2.01	1.88
Ni <sub>0.1</sub> Fe <sub>0.9</sub> C <sub>2</sub> O <sub>4</sub>	4.90	3.88	3.15	2.62	2.12	2.02	1.89
FeC <sub>2</sub> O <sub>4</sub>	4.89	3.87	3.16	2.63	2.13	2.02	1.89

<sup>a</sup> Interplanar spacings.

The oxalates were crystalline precipitates whose particle size depended on the metal ions and the ratio of metals involved. The size was determined from measurements of electron micrographs. In the nickel ferrous oxalate system there was a steady decrease in the average particle size as the nickel concentration increased, ranging from 6  $\mu$  for 10% Ni to 1  $\mu$  for 100% Ni. In the cobalt ferrous oxalate system, there was no gradual change as the composition varied. The particles were ellipsoidal, with an average major axis of 4–6  $\mu$ , and an average minor axis of 2–3  $\mu$ . In the copper ferrous oxalate system, two types of particles were obtained, one spherical, the other a parallelepiped. The spherical particles were found to be the copper oxalate and measured about 1  $\mu$  in diameter. The ferrous oxalate particles were about 3  $\mu$  in width and depth, and up to 10  $\mu$  in length.

**Treatment of the Bimetal Oxalates.**—Each of the three oxalate systems was given four treatments: (A) heated in a stream of hydrogen at 390°; (B) heated in its own decomposition products (CO and CO<sub>2</sub>) at 390°; (C) heated in a stream of air at 390°; (D) heated in air at 1100°.

The temperature of 390° was chosen because all the

oxalates in the three systems decompose at some temperature below this and such a temperature was low enough to prevent serious sintering of the products. Treatments A and B constituted reducing conditions, treatments C and D oxidizing conditions.

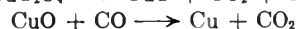
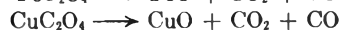
**A. Reduction in Hydrogen.**—Fifteen grams of oxalate was placed in a 21 mm. diameter tube using glass wool plugs to confine the material to the center portion of the tube. The tube then was inserted in a furnace at 390° and hydrogen passed through it for one hour. This effected a reduction to the metals or alloy.

X-Ray spectra for the products of the copper-iron series gave separate peaks for the two metals, the height of the peaks being proportional to the amount of copper or iron present. No alloying of the two metals was detected.

Alloys were obtained for the nickel iron system. A maximum in the saturation magnetization near 20% nickel found experimentally for the fine particle material agrees with that reported in the literature for the bulk alloy.<sup>9</sup>

X-Ray spectra for the cobalt-iron system indicated the production of powder alloys. The X-ray intensity of the characteristic lines for the Co-Fe series are presented in Fig. 1. In the region 0 to 70% cobalt, the X-ray intensity remained essentially constant for the body centered cubic peak. This confirmed the fact that iron and cobalt form a single alloy phase within this composition range. A face centered cobalt phase appeared experimentally in the region of 75% cobalt. This was in excellent agreement with the phase diagram for the bulk iron-cobalt alloy which also indicated that a face-centered cobalt phase should appear in that region.<sup>10</sup> The lattice spacings for the region in which the single phase iron-cobalt alloy exists were in good agreement with the values obtained by Ellis and Greiner for the bulk iron cobalt alloy.

**B. Reduction in CO + CO<sub>2</sub>.**—Fifteen grams of oxalate was packed in a tube which was closed at one end and contained a one hole stopper at the other end. The tube was inserted in a furnace at 390°. As the oxalate decomposed, the gases produced (CO and CO<sub>2</sub>) were passed through tubing into a wash bottle partially filled with water. The progress of the reaction was indicated by the bubbling in the wash bottle. When the decomposition reaction was over, the tube was sealed and permitted to cool. The product was then protected from air by the addition of benzene. This treatment resulted in products consisting of several phases and is the least understood of the four treatments. One would anticipate that the decomposition of the oxalate would proceed according to the equations



X-Ray examination of the products obtained from the copper ferrous oxalate system revealed copper and magnetite lines. The high saturation magnetization values appear to require that about one fourth of the total iron be present as free iron and the remainder as magnetite. Similarly, Franklin, *et al.*,<sup>12</sup> showed that a mixture of magnetite and iron was obtained from the decomposition of ferrous formate. They suggested the disproportionation reaction  $4FeO \rightarrow Fe + Fe_3O_4$ . This would correlate well with our data. However, in our samples careful scans of the X-ray spectra at 0.04°/minute and the highest sensitivity, could not verify the presence of free iron. Its presence in extremely small (100 Å.) particle size is suggested as a possible explanation, since the X-ray lines would be too broad to be detected. This hypothesis was further supported by the fact that the coercive forces of these samples were found to be four to five times greater at -196° than they were at room temperature, which is consistent with the magnetic behavior of very small particles.<sup>12</sup>

(9) R. M. Bozorth, "Ferromagnetism," D. Van Nostrand Co., New York, N. Y. 1951, p. 247.

(10) "Metals Handbook," American Society for Metals, 1948, p. 1192.

(11) W. D. Ellis and E. S. Greiner, *Trans. Am. Soc. Metals*, **29**, 415 (1941).

(12) A. D. Franklin, L. Muldrew and P. J. Flanders, *This Journal*, **59**, 340 (1955).

(13) L. Meel, *Compt. rend.* **228**, 664 (1949); *Ann. Geophys.*, **5**, 99 (1949); *Rev. Mod. Phys.*, **25**, 293 (1953).

(8) L. Pauling, "The Nature of the Chemical Bond," 2nd Ed., Cornell University Press, Ithaca, N. Y., 1940, p. 343–350.

TABLE II  
EXPERIMENTAL AND CALCULATED MOMENTS FOR CuFe AND NiFe OXALATE SYSTEMS HEATED IN AIR

Oxalate system	Moment, calcd.	Heated at 1100°, obsd.	Heated at 390°, obsd.	Oxalate system	Moment, calcd.	Heated at 390° obsd.
Cu <sub>0.1</sub> Fe <sub>0.9</sub> C <sub>2</sub> O <sub>4</sub>	9.0	9.3	40.0	Ni <sub>0.1</sub> Fe <sub>0.9</sub> C <sub>2</sub> O <sub>4</sub>	67.7	67.3
Cu <sub>0.2</sub> Fe <sub>0.8</sub> C <sub>2</sub> O <sub>4</sub>	18.0	19.5	36.8	Ni <sub>0.2</sub> Fe <sub>0.8</sub> C <sub>2</sub> O <sub>4</sub>	59.1	60.8
Cu <sub>0.3</sub> Fe <sub>0.7</sub> C <sub>2</sub> O <sub>4</sub>	27.0	28.8	29.0	Ni <sub>0.3</sub> Fe <sub>0.7</sub> C <sub>2</sub> O <sub>4</sub>	50.5	49.0
Cu <sub>0.4</sub> Fe <sub>0.6</sub> C <sub>2</sub> O <sub>4</sub>	27.0	25.8	16.0	Ni <sub>0.4</sub> Fe <sub>0.6</sub> C <sub>2</sub> O <sub>4</sub>	43.1	42.4
Cu <sub>0.5</sub> Fe <sub>0.5</sub> C <sub>2</sub> O <sub>4</sub>	22.5	23.5	26.5	Ni <sub>0.5</sub> Fe <sub>0.5</sub> C <sub>2</sub> O <sub>4</sub>	36.1	34.9
Cu <sub>0.6</sub> Fe <sub>0.4</sub> C <sub>2</sub> O <sub>4</sub>	18.0	17.1	19.1	Ni <sub>0.6</sub> Fe <sub>0.4</sub> C <sub>2</sub> O <sub>4</sub>	29.2	28.5
Cu <sub>0.7</sub> Fe <sub>0.3</sub> C <sub>2</sub> O <sub>4</sub>	13.5	9.7	13.2	Ni <sub>0.7</sub> Fe <sub>0.3</sub> C <sub>2</sub> O <sub>4</sub>	21.9	22.3
Cu <sub>0.8</sub> Fe <sub>0.2</sub> C <sub>2</sub> O <sub>4</sub>	9.0	8.1	3.6	Ni <sub>0.8</sub> Fe <sub>0.2</sub> C <sub>2</sub> O <sub>4</sub>	14.7	17.2

The interpretation of the nickel-ferrous system is also complicated by the presence of several phases. Additional studies will be necessary to elucidate the composition of these products.

X-Ray spectra obtained from the cobalt-ferrous system indicate the presence of magnetite in the high iron end of the system and CoO and Co in the high cobalt end of the system. The presence of cobalt indicates the reduction of CoO by carbon monoxide.

C. Oxidation in Air at 390°.—Fifteen grams of the oxalate was placed in a tube and held in position with glass wool plugs. The tube was inserted in a furnace at 390° and air passed through the tube for one hour at this temperature.

The products obtained indicated clearly that when the starting material was not a solid solution this temperature was too low to permit the ions to diffuse distances of the particle diameters ( $\mu$ ). Table II presents the calculated and observed moments per gram for the copper-ferrous system at 390 and 1100° and the nickel-ferrous system at 390°. The calculated values for copper are based on the production of stoichiometric copper ferrite with the excess metal present as CuO or  $\alpha$ -Fe<sub>2</sub>O<sub>3</sub>, depending on which ion was present in excess of the ferrite composition.

The nickel ferrous oxalate system, which was a solid solution, produced the ferrites at 390°. The calculated moments for the nickel system were based on the production of nickel ferrite with the excess metal present as NiO or as the magnetic iron oxide  $\gamma$ -Fe<sub>2</sub>O<sub>3</sub>. No consideration was made for the solubility of any phase in the others, but the agreement of experimental values with the calculation on our basis would suggest that such considerations are not required. At present it is not clearly understood why the  $\gamma$ -Fe<sub>2</sub>O<sub>3</sub> is stable in the Ni-Fe system and not in the Cu-Fe and Co-Fe system. There are some indications, however, that certain ions do increase the stability of  $\gamma$ -Fe<sub>2</sub>O<sub>3</sub>.<sup>14</sup>

A possible explanation for the deviation which occurred at the high nickel end is proposed: in the nickel ferrite, the nickel ions tend to occupy the B sites of the spinel structure, while the iron occupies both the B and the A sites.<sup>15</sup> When the number of nickel ions is low, there is a good probability that they occupy only B sites but as the concentration of nickel ions increases the probability of all nickel ions going into the B sites is decreased. The presence of nickel in the A sites increases the moment. An alternate explanation is that in the initial decomposition of the oxalate some of the material was reduced to metallic nickel, and reoxidation was not complete at this relatively low temperature.

The cobalt-iron system also produced the ferrites at 390°. X-Ray spectra for this system were made and the intensity of the characteristic lines vs. composition are plotted in Fig. 2. This plot would also suggest that there is very little mutual solubility of the various phases.

D. Oxidation at 1100°.—The samples were treated as in treatment C. They were then placed in Vycor crucibles and heated in a Lindberg furnace at 1100° for one hour. This treatment produced ferrites in all three systems. This was as expected, since the temperature was high enough to permit diffusion of the ions between particles, even in the Cu-Fe system where no solid solution had been formed. Unfortunately, there has also been considerable sintering of the particles resulting in the loss of the fine particle nature of the product. In all cases, at least two phases

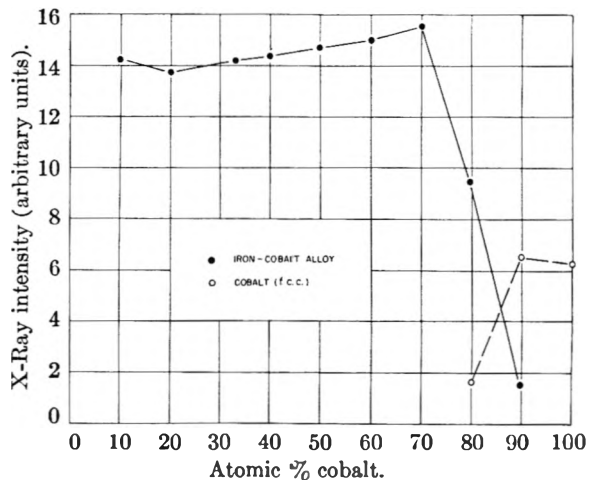


Fig. 1.

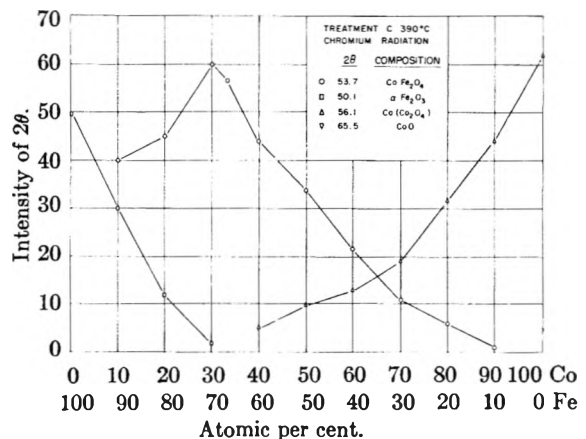


Fig. 2.

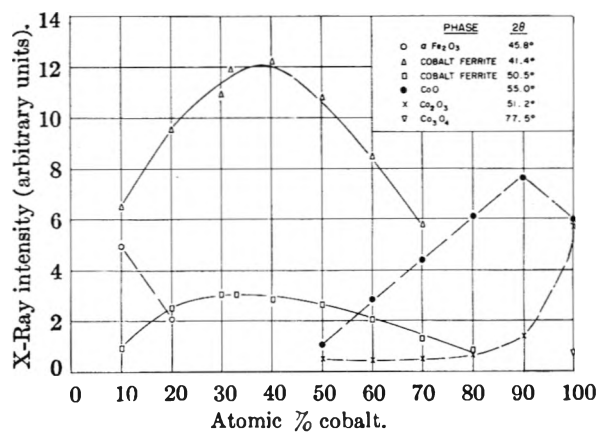


Fig. 3.

(14) P. W. Selwood, "Magnetochemistry," 2nd Ed., Interscience Publishers, New York, N. Y., p. 307.

(15) L. Neel, *Ann. Phys. Paris*, **3**, 127-9 (1948).

were produced, the ferrite and the oxide or oxides of the metal ion present in excess. Figure 3 is a plot of the X-ray intensities of characteristic lines *vs.* composition for the Co-Fe system heated at 1100°. Note that two curves are given for the ferrite and that these are in good agreement with each other.

### Conclusion

Metals, alloys, ferrites, metals in metal oxides and ferrites in metal oxides have been prepared as fine particles by the solid solution oxalate technique. By virtue of their particle size, it was possible to produce the ferrites as magnetically hard substances. Excellent control of the composition of the oxalate was possible because the metal ions were mixed in solution before precipitation. This method offers the possibility of "doping" a sample in the initial precipitation with very small amounts of a foreign metal ion. The low solubility of the oxalates involved eliminated the necessity of making solubility corrections.

General metallurgical techniques for the preparation of alloys in bulk form are well established but not applicable to the preparation of fine particle materials. Some of the techniques useful for powder metallurgy purposes produce particles several microns in diameter. The technique presented in this work permits the production of fine particles down to single domain sizes and should have general application in the production of fine particles of any alloy whose metals have atomic radii of the proper size to form the bimetal oxalate. Because of their unusually small particle size, the alloys prepared by the above method should be of great interest in nuclear and electron magnetic spin resonance measurements as well as the ferromagnetic studies for which they were intended. These alloys also would be useful in the study of the penetration of radio frequency fields into fine particles to determine electron mean free paths.

## USE OF DIFFUSION AND THERMODYNAMIC DATA TO TEST THE ONLAGER RECIPROCAL RELATION FOR ISOTHERMAL DIFFUSION IN THE SYSTEM NaCl-KCl-H<sub>2</sub>O AT 25°

BY PETER J. DUNLOP AND LOUIS J. GOSTING

*Contribution from the University of Wisconsin, Madison, Wisconsin,  
and the Institute of Physical Chemistry, Uppsala, Sweden*

*Received August 4, 1958*

A test of the Onsager reciprocal relation has been made for four compositions of the system NaCl-KCl-H<sub>2</sub>O, using existing data for the diffusion and activity coefficients. The Onsager relation is satisfied within 5% at all four compositions. Significant errors which affect these tests have been considered in detail; for each composition the observed deviation is about half the maximum error which is estimated from uncertainties in the experimental data.

Just as classical thermodynamics provides equations relating certain measurable properties of a system at equilibrium, the thermodynamics of irreversible processes provides equations relating measurable properties of a system which is somewhat removed from equilibrium. Of basic importance to the theory of irreversible processes are the reciprocal relations derived by Onsager<sup>1-4</sup> from the assumption of microscopic reversibility. The Onsager reciprocal relations and their connection with the theory of irreversible processes have been discussed in several monographs (see for example, ref. 5-8) which also list original articles in this field.

For isothermal diffusion in a ternary system there is a single reciprocal relation which provides one restriction on the values of the four diffusion coefficients that can be measured experimentally for

any composition of the system; thermodynamic quantities also appear in this equation. Here we attempt to test this Onsager relation by using data for diffusion at four compositions of the system NaCl-KCl-H<sub>2</sub>O at 25°. The diffusion coefficients used were measured with the Gouy diffusimeter by O'Donnell and Gosting<sup>9</sup> and the activity coefficients employed were derived from isopiestic data reported by Robinson<sup>10</sup> and by Robinson and Stokes.<sup>11</sup> Although the four diffusion coefficients for a few other ternary systems have been measured at one or two compositions<sup>12-16</sup> we will not consider them here. Activity coefficients have been measured only for those systems containing two electrolytes, and of these only the system NaCl-KCl-H<sub>2</sub>O obeys Harned's rule<sup>17-19</sup> ( $\beta_1 = \beta_2 =$

(1) L. Onsager, *Phys. Rev.*, **37**, 405 (1931).

(2) L. Onsager, *ibid.*, **38**, 2265 (1931).

(3) L. Onsager and R. M. Fuoss, *THIS JOURNAL*, **36**, 2689 (1932).

(4) L. Onsager, *Ann. N. Y. Acad. Sci.*, **46**, 241 (1945).

(5) S. R. de Groot, "Thermodynamics of Irreversible Processes," Interscience Publishers, Inc., New York, N. Y., 1951.

(6) K. G. Denbigh, "The Thermodynamics of the Steady State," John Wiley and Sons, Inc., New York, N. Y., 1951.

(7) J. O. Hirschfelder, C. F. Curtiss and R. B. Bird, "Molecular Theory of Gases and Liquids," John Wiley and Sons, Inc., New York, N. Y., 1954.

(8) I. Prigogine, "Introduction to Thermodynamics of Irreversible Processes," Charles C. Thomas, Springfield, Illinois, 1955.

(9) I. J. O'Donnell and L. J. Gosting, a paper presented in a Symposium at the 1957 meeting of the Electrochemical Society in Washington, D. C.; the Symposium papers are to be published as a monograph by John Wiley and Sons, New York, N. Y.

(10) R. A. Robinson, in "Electrochemical Constants," National Bureau of Standards Circular 524, 1953.

(11) Appendix 8.3 of ref. 18.

(12) P. J. Dunlop and L. J. Gosting, *J. Am. Chem. Soc.*, **77**, 5238 (1955).

(13) H. Fujita and L. J. Gosting, *ibid.*, **78**, 1099 (1956).

(14) P. J. Dunlop, *THIS JOURNAL*, **61**, 994 (1957).

(15) P. J. Dunlop, *ibid.*, **61**, 1619 (1957).

(16) F. E. Weir and M. Dole, *J. Am. Chem. Soc.*, **80**, 302 (1958).

(17) H. S. Harned and B. B. Owen, "The Physical Chemistry of Electrolytic Solutions," Third Edition, Reinhold Publ. Corp., New York, N. Y., 1958.



0 in equations 11); therefore, we have chosen it to test the Onsager reciprocal relation. The validity of this relation for some ternary systems has been considered in a recent communication<sup>20</sup> by using estimated, rather than measured, values for the activity coefficients. In this report experimental data are used for all quantities, and the effects of errors in these data are considered in detail. It is believed that our analysis of experimental errors will be helpful in planning further tests of the Onsager reciprocal relation.

### Summary of Equations

The Onsager reciprocal relations consist of equalities between certain fundamental coefficients (usually denoted by  $L_{ij}$  or  $\Omega_{ij}$ ) in equations relating flows to forces. For isothermal diffusion in a ternary solution the flows,  $(J_i)_0$ , of the two solutes ( $i = 1, 2$ ) relative to the solvent (component 0) may be expressed as follows in terms of the chemical potential gradients,  $\partial\mu_i/\partial x$ , of the two solutes<sup>21-23</sup>

$$(J_1)_0 = -(L_{11})_0 \frac{\partial\mu_1}{\partial x} - (L_{12})_0 \frac{\partial\mu_2}{\partial x} \quad (1a)$$

$$(J_2)_0 = -(L_{21})_0 \frac{\partial\mu_1}{\partial x} - (L_{22})_0 \frac{\partial\mu_2}{\partial x} \quad (1b)$$

For these flow equations there is one Onsager reciprocal relation<sup>21-23</sup>

$$(L_{12})_0 = (L_{21})_0 \quad (1c)$$

Here subscripts 0 are used on the  $J_i$  and the  $L_{ij}$  to denote a solvent-fixed frame of reference. These equations are applicable to components in ternary solutions of electrolytes as well as of non-electrolytes.<sup>22</sup> We choose to express the  $(J_i)_0$  as moles per cm.<sup>2</sup> per sec. and the  $\mu_i$  as per mole. The  $(L_{ij})_0$  may be related to diffusion coefficients,  $(D_{ij})_0$ , for the solvent-fixed frame of reference by expressing the chemical potential gradients in equations 1a and 1b in terms of solute concentration gradients.<sup>22,24</sup> If the values of these diffusion coefficients are those corresponding to flows and concentration gradients both expressed in terms of moles of solute, one obtains the equations

$$(L_{11})_0 = [(D_{11})_0\mu_{22} - (D_{12})_0\mu_{21}]/(1000rS) \quad (1d)$$

$$(L_{12})_0 = [(D_{12})_0\mu_{11} - (D_{11})_0\mu_{12}]/(1000rS) \quad (1e)$$

$$(L_{21})_0 = [(D_{21})_0\mu_{22} - (D_{22})_0\mu_{21}]/(1000rS) \quad (1f)$$

(18) R. A. Robinson and R. H. Stokes, "Electrolyte Solutions," Butterworths Scientific Publications, London, 1955.

(19) For a ternary system which obeys Harned's rule, one can evaluate activity coefficients over the entire concentration range if complete data for activity coefficients are available for each solute alone in the solvent and if the thermodynamic constant  $K_\alpha$  (equation 14) has been determined from experiments at one composition of the ternary system. Hence, to the extent that Harned's rule is valid for the system NaCl-KCl-H<sub>2</sub>O, it is possible to evaluate rigorously the activity coefficients at any composition, including the concentration range for which diffusion coefficients are available, even though the activity coefficients for this ternary system have been measured only at the higher concentrations. For the other electrolyte solutions (ref. 12 and 13), also, there is the problem that some of the necessary data are for different concentration ranges; for those systems the situation is more complicated because Harned's rule does not apply.

(20) D. G. Miller, *THIS JOURNAL*, **62**, 767 (1958).

(21) G. J. Hooyman, *Physica*, **22**, 751 (1956).

(22) R. L. Baldwin, P. J. Dunlop, L. J. Gosting, G. Kegeles and J. G. Kirkwood, in preparation.

(23) See equations 4.12.6 and 4.12.7 of ref. 3.

(24) See equations 17 and 18 of ref. 21; equation 18 must be inverted and appropriate changes made in units of the concentrations, the  $D_{ij}$  and the  $L_{ij}$  to obtain equations 1d-1g.

$$(L_{22})_0 = [(D_{22})_0\mu_{11} - (D_{21})_0\mu_{12}]/(1000rS) \quad (1g)$$

where

$$S = \mu_{11}\mu_{22} - \mu_{12}\mu_{21} \quad (1h)$$

and

$$\mu_{ij} = (\partial\mu_i/\partial C_j)_{T,P,C_{k \neq j}} \quad (1i)$$

Here subscripts  $T$ ,  $P$  and  $C_{k \neq j}$  indicate that temperature, pressure and the concentration of the other solute are held constant during the differentiation. We have introduced the factor 1000 $r$  into equations 1d-1g because all concentrations,  $C_j$ , in this paper are expressed as moles per liter instead of moles per cc.; the ratio  $r = 1.000027$  is the number of cubic centimeters in a milliliter and will be taken as unity. Throughout this paper the components H<sub>2</sub>O, NaCl and KCl will be denoted by subscripts 0, 1 and 2, respectively.

**Diffusion Coefficients for the Solvent Frame of Reference.**—The diffusion coefficients which were reported<sup>9</sup> for this system are coefficients in modified forms<sup>12,25</sup> of Onsager's flow equations.<sup>4</sup> These coefficients correspond to a volume-fixed frame of reference (denoted by a subscript V), which becomes identical with the cell frame of reference if the partial molal volumes are independent of concentration; they may be converted to the solvent-fixed reference frame by means of the equations<sup>22,26</sup>

$$(D_{ij})_0 = (D_{ij})_V + \frac{C_i}{C_0\bar{V}_0} \sum_{k=1}^2 \bar{V}_k(D_{ki})_V \quad \left( \begin{matrix} i = 1, 2 \\ j = 1, 2 \end{matrix} \right) \quad (2)$$

Here  $\bar{V}_k$  denotes the partial molal volume of component  $k$ . Values of  $\bar{V}_k$  in ml./mole for the solutes are readily obtained from data for the solution density in g./ml.,  $\rho$ , using the relation (see equation A-7 of the Appendix)

$$\bar{V}_k = \frac{M_k - 1000H_k}{\rho - \sum_{j=1}^2 H_j C_j} \quad (k = 1, 2) \quad (3)$$

Here  $M_k$  is the molecular weight of component  $k$  and

$$H_k = (\partial\rho/\partial C_k)_{T,P,C_{l \neq k}} \quad (3a)$$

The concentration and partial molal volume of the solvent are then obtained from the relations

$$\sum_{i=0}^2 M_i C_i = 1000 \rho \quad (4)$$

and

$$\sum_{i=0}^2 C_i \bar{V}_i = 1000 \quad (5)$$

**Derivatives of the Chemical Potentials.**—To evaluate the derivatives  $\mu_{ij}$  in equations 1d-1h it is necessary to use experimental data for the solute activity coefficients. Because activity coefficients for electrolytes are usually reported for the molality concentration scale, we first relate the  $\mu_{ij}$  to corresponding derivatives for that scale using the relation

(25) R. L. Baldwin, P. J. Dunlop and L. J. Gosting, *J. Am. Chem. Soc.*, **77**, 5235 (1955).

(26) Equation 2 may be obtained from equations 30 and 31 of ref. 21.

$$\mu_{ij} = \sum_{k=1}^2 A_{ik} B_{kj} \quad \left( \begin{array}{l} i = 1,2 \\ j = 1,2 \end{array} \right) \quad (6)$$

where

$$A_{ik} = (\partial \mu_i / \partial m_k)_{T,P,m_l \neq k} \quad (6a)$$

and

$$B_{kj} = (\partial m_k / \partial C_j)_{T,P,C_l \neq j} \quad (6b)$$

The molality  $m_k$  of solute  $k$  in a ternary solution is related to the solute molarities and the solution density  $\rho$  by

$$m_k = C_k / \theta \quad (k = 1,2) \quad (7)$$

where

$$\theta = \rho - \sum_{l=1}^2 M_l C_l / 1000 \quad (7a)$$

An expression for the  $B_{kj}$  is readily obtained by differentiation of equation 7 with respect to  $C_j$

$$B_{kj} = [\partial \delta_{kj} - C_k (H_j - M_j / 1000)] / \theta^2 \quad (8)$$

where  $H_j$  is defined by equation 3a and  $\delta_{kj}$  is the Kronecker delta ( $\delta_{kj} = 1$  if  $k = j$  and  $\delta_{kj} = 0$  if  $k \neq j$ ). The derivative  $A_{ik}$  depends on the solute concentrations and also on the concentration dependence of the activity coefficients. It is evaluated from the expressions for the chemical potentials of the two salts: for this case of two 1-1 electrolytes with a common ion we have  $m_{Na^+} = m_1$ ,  $m_{K^+} = m_2$  and  $m_{Cl^-} = m_1 + m_2$ , so<sup>27</sup>

$$\mu_1 = \mu_1^0 + 2RT \ln \gamma_1 [m_1(m_1 + m_2)]^{1/2} \quad (9a)$$

$$\mu_2 = \mu_2^0 + 2RT \ln \gamma_2 [m_2(m_1 + m_2)]^{1/2} \quad (9b)$$

in which  $R$  and  $T$  are the gas constant per mole and the absolute temperature, respectively. Here  $\gamma_1$  is the mean ionic activity coefficient for the  $Na^+$  and  $Cl^-$  ions for the molal scale; similarly  $\gamma_2$  is the mean ionic activity coefficient for the  $K^+$  and  $Cl^-$  ions. Differentiation of equations 9 with respect to the appropriate solute molalities and conversion from natural logarithms to those for base 10 gives

$$A_{ik} = RT \left[ \frac{\delta_{ik}}{m_i} + \frac{1}{m_1 + m_2} + 4.605 \Gamma_{ik} \right] \quad (10)$$

where

$$\Gamma_{ik} = (\partial \log \gamma_i / \partial m_k)_{T,P,m_l \neq k} \quad (10a)$$

Finally, the derivatives  $\Gamma_{ik}$  may be evaluated by using an extended form of Harned's rule which, for solutions of two 1-1 electrolytes, is written<sup>28</sup>

$$\log \gamma_1 = \log \gamma_{1(0)} - \alpha_1 m_2 - \beta_1 m_2^2 \quad (11a)$$

$$\log \gamma_2 = \log \gamma_{2(0)} - \alpha_2 m_1 - \beta_2 m_1^2 \quad (11b)$$

These equations are applicable when the total solute molality

$$m = m_1 + m_2 \quad (12)$$

is held constant. The coefficients  $\alpha_1$ ,  $\alpha_2$ ,  $\beta_1$  and  $\beta_2$  are independent of  $m_1$  and  $m_2$  for constant  $m$ . The symbols  $\gamma_{1(0)}$  and  $\gamma_{2(0)}$  denote the mean ionic activity coefficients of  $NaCl$  and  $KCl$ , respectively, when each salt is present alone in water as a binary solution at molality  $m$ . According to Robinson,<sup>10</sup> the terms  $\beta_1$  and  $\beta_2$  are zero for the

system  $NaCl-KCl-H_2O$ , but we retain them here to investigate how experimental errors in these quantities may affect tests of the Onsager reciprocal relation. Differentiation of equations 11 with respect to the solute molalities gives the  $\Gamma_{ij}$ , equation 10a

$$\Gamma_{11} = \frac{d \log \gamma_{1(0)}}{dm} - m_2 \frac{d\alpha_1}{dm} - m_2^2 \frac{d\beta_1}{dm} \quad (13a)$$

$$\Gamma_{12} = \frac{d \log \gamma_{1(0)}}{dm} - \alpha_1 - m_2 \frac{d\alpha_1}{dm} - 2m_2\beta_1 - m_2^2 \frac{d\beta_1}{dm} \quad (13b)$$

The derivatives  $\Gamma_{21}$  ( $=\Gamma_{12}$ ) and  $\Gamma_{22}$  may be obtained by interchanging subscripts 1 and 2 in equations 13. For some purposes it is useful to note that

$$\Gamma_{11} + \Gamma_{22} = \Gamma_{12} + \Gamma_{21} + (\alpha_1 + \alpha_2) + 2(m_2\beta_1 + m_1\beta_2) \quad (13c)$$

Because experimental measurements are not yet sufficiently accurate to show any dependence of  $\beta_1$  and  $\beta_2$  on  $m$ ,<sup>29</sup> we now assume that  $d\beta_1/dm = d\beta_2/dm = 0$  so that it is possible to use the relations<sup>30</sup>

$$\alpha_1 + \alpha_2 = K_\alpha - 2m(\beta_1 + \beta_2) \quad (14)$$

$$\alpha_1 - \alpha_2 = 2\Phi - \frac{2}{3}m(\beta_1 - \beta_2) \quad (15)$$

where  $K_\alpha$  is a quantity independent of  $m$  and

$$\Phi = \frac{1}{2.3026m} [\phi_{1(0)} - \phi_{2(0)}] \quad (15a)$$

The osmotic coefficients

$$\phi_{i(0)} = 1 + \frac{1}{m} \int_0^m m \, d \ln \gamma_{i(0)} \quad (i = 1,2) \quad (16)$$

are for the two binary solutions containing electrolytes 1 and 2, respectively, at molality  $m$ . Equations 14 and 15 may then be solved for  $\alpha_1$

$$\alpha_1 = \Phi + \frac{K_\alpha}{2} - \frac{2}{3}m(2\beta_1 + \beta_2) \quad (17)$$

Differentiation of this relation with respect to  $m$  and use of equation 16 yields

$$\frac{d\alpha_1}{dm} = \frac{1}{m} \left[ -2\Phi + \frac{d \log \gamma_{1(0)}}{dm} - \frac{d \log \gamma_{2(0)}}{dm} - \frac{2}{3}m(2\beta_1 + \beta_2) \right] \quad (18)$$

Expressions for  $\alpha_2$  and  $d\alpha_2/dm$  are obtained by interchanging subscripts 1 and 2 in equations 17 and 18 and changing the sign of  $\Phi$ .

Convenient expressions for calculating the  $\Gamma_{ik}$  are obtained by substituting these relations for  $\alpha_1$ ,  $\alpha_2$ ,  $d\alpha_1/dm$  and  $d\alpha_2/dm$  into equations 13 and into the corresponding equations for  $\Gamma_{21}$  and  $\Gamma_{22}$ ; remembering that  $d\beta_1/dm$  and  $d\beta_2/dm$  are assumed to be zero,<sup>29</sup> we obtain

$$\Gamma_{11} = \frac{1}{m} \left[ m_1 \frac{d \log \gamma_{1(0)}}{dm} + m_2 \frac{d \log \gamma_{2(0)}}{dm} + 2m_2\Phi \right] + \frac{2}{3}m_2(2\beta_1 + \beta_2) \quad (19a)$$

$$\Gamma_{22} = \frac{1}{m} \left[ m_1 \frac{d \log \gamma_{1(0)}}{dm} + m_2 \frac{d \log \gamma_{2(0)}}{dm} - 2m_1\Phi \right] + \frac{2}{3}m_1(\beta_1 + 2\beta_2) \quad (19b)$$

(27) These relations may be obtained from equations 2.6-2.9 of ref. 18, using equation 2.12 of that reference to define the mean ionic activity coefficients ( $\gamma_1$  and  $\gamma_2$  in our notation).

(28) See equation 14-8-1 of ref. 17 or equations 15.6 and 15.7 of ref. 18.

(29) See page 431 of ref. 18.

(30) Equation 14 is identical with equation 15.1C of ref. 18 and equation 15 is a special case, with  $z_1 = (m_1/m) = 1$ , of equation 14-8-2 of ref. 17.

TABLE I  
DATA FOR TESTING THE ONSAGER RECIPROCAL RELATION AT  
FOUR COMPOSITIONS OF THE SYSTEM NaCl-KCl-H<sub>2</sub>O AT 25°

	$M_{\text{H}_2\text{O}} \equiv M_0 = 18.0160$	$M_{\text{NaCl}} \equiv M_1 = 58.454$	$M_{\text{KCl}} \equiv M_2 = 74.557$	
$C_1$ (moles/l.)	0.2500 <sub>0</sub>	0.2500 <sub>0</sub>	0.5000 <sub>0</sub>	0.5000 <sub>0</sub>
$C_2$ (moles/l.)	0.2500 <sub>0</sub>	0.5000 <sub>0</sub>	0.2500 <sub>0</sub>	0.5000 <sub>0</sub>
$C_0$ (moles/l.)	54.706	54.300	54.443	54.033
$m_1$ (molality)	0.2536 <sub>6</sub>	0.2555 <sub>8</sub>	0.5097 <sub>6</sub>	0.5136 <sub>4</sub>
$m_2$ (molality)	0.2536 <sub>6</sub>	0.5111 <sub>0</sub>	0.2548 <sub>8</sub>	0.5136 <sub>4</sub>
$m$ (molality)	0.5073 <sub>2</sub>	0.7666 <sub>6</sub>	0.7646 <sub>4</sub>	1.0272 <sub>8</sub>
$\bar{V}_0$ (ml./mole)	18.062	18.058	18.057	18.050
$\bar{V}_1$ (ml./mole)	18.6 <sub>9</sub>	19.1 <sub>2</sub>	19.1 <sub>4</sub>	19.5 <sub>2</sub>
$\bar{V}_2$ (ml./mole)	28.8 <sub>7</sub>	29.3 <sub>6</sub>	29.3 <sub>6</sub>	29.9 <sub>0</sub>
$(D_{11})_v \times 10^{10}$	1.37 <sub>2</sub>	1.34 <sub>2</sub>	1.41 <sub>4</sub>	1.38 <sub>9</sub>
$(D_{12})_v \times 10^6$	-0.00 <sub>6</sub>	-0.00 <sub>1</sub>	-0.01 <sub>2</sub>	-0.01 <sub>0</sub>
$(D_{21})_v \times 10^6$	0.14 <sub>3</sub>	0.20 <sub>3</sub>	0.09 <sub>6</sub>	0.15 <sub>4</sub>
$(D_{22})_v \times 10^6$	1.82 <sub>6</sub>	1.83 <sub>8</sub>	1.82 <sub>4</sub>	1.84 <sub>1</sub>
$(D_{11})_0 \times 10^6$	1.38 <sub>0</sub>	1.35 <sub>1</sub>	1.42 <sub>9</sub>	1.40 <sub>6</sub>
$(D_{12})_0 \times 10^6$	0.00 <sub>3</sub>	0.01 <sub>3</sub>	0.01 <sub>6</sub>	0.01 <sub>8</sub>
$(D_{21})_0 \times 10^6$	0.15 <sub>1</sub>	0.22 <sub>1</sub>	0.10 <sub>4</sub>	0.17 <sub>0</sub>
$(D_{22})_0 \times 10^6$	1.83 <sub>9</sub>	1.86 <sub>6</sub>	1.83 <sub>9</sub>	1.86 <sub>9</sub>
$B_{11}$	1.0194 <sub>3</sub>	1.0271 <sub>9</sub>	1.0294 <sub>5</sub>	1.0375 <sub>6</sub>
$B_{12}$	0.0074 <sub>1</sub>	0.0076 <sub>6</sub>	0.0152 <sub>4</sub>	0.0157 <sub>6</sub>
$B_{21}$	0.0048 <sub>0</sub>	0.0099 <sub>7</sub>	0.0049 <sub>6</sub>	0.0102 <sub>8</sub>
$B_{22}$	1.0220 <sub>6</sub>	1.0375 <sub>2</sub>	1.0271 <sub>4</sub>	1.0430 <sub>3</sub>
$d \log \gamma_{1(0)}/dm$	-0.061 <sub>7</sub>	-0.027 <sub>2</sub>	-0.027 <sub>2</sub>	-0.011 <sub>4</sub>
$d \log \gamma_{2(0)}/dm$	-0.093 <sub>3</sub>	-0.058 <sub>9</sub>	-0.058 <sub>9</sub>	-0.041 <sub>7</sub>
$\Phi$	0.019 <sub>1</sub>	0.017 <sub>4</sub>	0.017 <sub>4</sub>	0.016 <sub>6</sub>
$K_\alpha$	0.016 <sub>8</sub>	0.016 <sub>8</sub>	0.016 <sub>8</sub>	0.016 <sub>8</sub>
$\beta_1$	0	0	0	0
$\beta_2$	0	0	0	0

\* Diffusion coefficients are expressed as cm.<sup>2</sup>/sec.; they correspond to amounts of solute expressed as moles rather than grams.

$$\Gamma_{12} = \Gamma_{21} = \frac{1}{m} \left[ m_1 \frac{d \log \gamma_{1(0)}}{dm} + m_2 \frac{d \log \gamma_{2(0)}}{dm} - (m_1 - m_2) \Phi \right] - \frac{K_\alpha}{2} + \frac{2}{3} [m_1(2\beta_1 + \beta_2) + m_2(\beta_1 + 2\beta_2)] \quad (19c)$$

Equation 13c then becomes

$$\Gamma_{11} + \Gamma_{22} = \Gamma_{12} + \Gamma_{21} + K_\alpha - 2(m_1\beta_1 + m_2\beta_2) \quad (19d)$$

### Tests of the Onsager Reciprocal Relation

In Table I are summarized the data for testing this relation at four compositions of the system NaCl-KCl-H<sub>2</sub>O. The numbers in each column correspond to the composition defined by the molalities in the first two lines of the column. Each solute molality  $m_i$  was calculated from equation 7 by using these linear relations to represent the densities (g./ml.) reported by O'Donnell and Gosting<sup>9</sup>: near  $C_1 = 0.25$  and  $C_2 = 0.25$

$$\rho = 1.01883_0 + 0.0398_1(C_1 - 0.25) + 0.0457_6(C_2 - 0.25) \quad (20a)$$

with an average deviation of  $\pm 0.0011\%$ ; near  $C_1 = 0.25$  and  $C_2 = 0.5$

$$\rho = 1.03016_6 + 0.0393_8(C_1 - 0.25) + 0.0452_6(C_2 - 0.5) \quad (20b)$$

with an average deviation of  $\pm 0.0004\%$ ; near  $C_1 = 0.5$  and  $C_2 = 0.25$

$$\rho = 1.02871_7 + 0.0393_8(C_1 - 0.5) + 0.0452_6(C_2 - 0.25) \quad (20c)$$

with an average deviation of  $\pm 0.0005\%$ ; and near  $C_1 = 0.5$  and  $C_2 = 0.5$

$$\rho = 1.03995_7 + 0.0389_7(C_1 - 0.5) + 0.0447_1(C_2 - 0.5) \quad (20d)$$

with an average deviation of  $\pm 0.0003\%$ . The method of least squares was used to determine the coefficients in these equations. Partial molal volumes  $\bar{V}_i$  of the solutes were obtained by use of equations 3 and 20; the molalities and partial molal volumes of the solvent were calculated from these data by using equations 4 and 5. Values of the measured diffusion coefficients,<sup>9</sup>  $(D_{ij})_v$ , shown in Table I were converted to diffusion coefficients for the solvent frame of reference,  $(D_{ij})_0$ , by substituting the appropriate data into equations 2. The derivatives  $B_{kj}$  were evaluated using equations 7a, 8 and 20.

Thermodynamic data for the binary systems NaCl-H<sub>2</sub>O and KCl-H<sub>2</sub>O at 25° have been tabulated by Robinson and Stokes.<sup>11</sup> From their values for the osmotic coefficients of these systems the values of  $\Phi$  shown in Table I were computed using equation 15a. Their tables also were used to obtain the values shown<sup>31</sup> for  $d \log \gamma_{1(0)}/dm$  and  $d \log \gamma_{2(0)}/dm$ . The values for  $K_\alpha$ ,  $\beta_1$  and  $\beta_2$  are those obtained by Robinson<sup>10</sup> from an analysis of iso-

(31) These values were obtained by plotting on large graphs the data (ref. 11) for  $\log \gamma_{1(0)}$  and  $\log \gamma_{2(0)}$  versus  $m$  for the two binary systems and measuring the slopes at the four required values of  $m$ . For  $m = 1.0272_8$ , values of the slopes were also determined by numerical differentiation (using Newton's interpolation formula) and by differentiation of cubic expressions which had been fitted by the method of least squares to the tabulated data: the three methods yielded slopes which agreed within 0.0007.

TABLE II

SUMMARY OF TESTS OF THE ONSAGER RELATION AT FOUR COMPOSITIONS OF THE SYSTEM NaCl-KCl-H<sub>2</sub>O AT 25°  
 Columns 1-4 summarize tests using experimental data; columns 5 and 6 summarize corresponding calculations using certain approximations for the activity coefficients.

	1	2	3	4	5	6
$C_1$	0.25000	0.25000	0.50000	0.50000	0.50000	0.50000
$C_2$	.25000	.50000	.25000	.50000	0.50000	0.50000
$\Gamma_{11}$	— .0584	— .0251	— .0262	— .0102	(log $\gamma_1 =$ con-	(log $\gamma_1 =$ con-
$\Gamma_{12}$	— .0859	— .0509	— .0520	— .0351	stant and	stant and
$\Gamma_{21}$	— .0859	— .0509	— .0520	— .0351	log $\gamma_2 =$	log $\gamma_2 =$
$\Gamma_{22}$	— .0966	— .0599	— .0610	— .0432	constant)	constant)
$\mu_{11}/(RT)$	5.7617	5.2513	3.2469	2.9896	3	3.0400
$\mu_{12}/(RT)$	1.6522	1.1492	1.1453	0.8920	1	1.0613
$\mu_{21}/(RT)$	1.6325	1.1289	1.1243	0.8703	1	1.0400
$\mu_{22}/(RT)$	5.6009	3.1053	5.1009	2.8513	3	3.0613
$(L_{11})_0 \times RT \times 10^{9a}$	2.609	2.785	4.761	5.150		
$(L_{22})_0 \times RT \times 10^9$	3.498	6.359	3.829	7.016		
$(L_{12})_0 \times RT \times 10^9$	-0.755	-0.989	-1.040	-1.548	-1.689	-1.751
$(L_{21})_0 \times RT \times 10^9$	-0.729	-0.946	-1.006	-1.474	-1.699	-1.735
$\% \Delta_{\text{exp}}^b$	-3.5	-4.4	-3.3	-4.9	0.6	-0.9

<sup>a</sup> The coefficients  $(L_{ij})_0$  reported here are for flow equations expressed in moles of the components; they may be converted to the corresponding coefficients for flow equations expressed in grams of components by multiplying each  $(L_{ij})_0$  by the product  $M_i M_j$ . <sup>b</sup> Calculated by means of equation 21a.

piestic data for the ternary system NaCl-KCl-H<sub>2</sub>O; his value for  $(\alpha_1 + \alpha_2)$  may be identified with  $K_\alpha$ , equation 14, because he found that  $\beta_1 = \beta_2 = 0$  for this system.

The Onsager reciprocal relation may be tested by using the data in Table I to evaluate  $(L_{12})_0$  and  $(L_{21})_0$ . According to equation 1c his relation is confirmed if the values obtained for these two coefficients are equal. For this computation appropriate data from Table I were used to evaluate the  $\Gamma_{ik}$  from equations 19, the  $A_{ik}$  from equation 10 and then the  $\mu_{ij}$  from equation 6. Finally, the values of  $(L_{12})_0$  and  $(L_{21})_0$  were obtained from equations 1e and 1f; they are reported in columns 1-4 of Table II, together with values for some of the intermediate quantities.

The percentage difference

$$\% \Delta_{\text{exp}} = 100 \left\{ \frac{(L_{21})_0 - (L_{12})_0}{[(L_{12})_0 + (L_{21})_0]/2} \right\}_{\text{exp}} \quad (21a)$$

between these values of  $(L_{21})_0$  and  $(L_{12})_0$  are shown in the last line. Values of  $(L_{11})_0$  and  $(L_{22})_0$  are included in Table II to indicate their magnitudes, although they are not needed for testing the Onsager relation.

### Discussion

Columns 1-4 of Table II show that experimental data for this system satisfy the Onsager reciprocal relation for isothermal diffusion within 5%. For these tests to be meaningful, however, it is necessary to consider experimental errors in the several data and their effects on the tests.

That erroneous interpretations may result from the use of some assumed or approximate data in a test of the Onsager relation can be seen by comparison of columns 4-6 of Table II. Column 5 was computed from the same values of  $(D_{ij})_0$  that were used in column 4, but the mean ionic activity coefficients,  $\gamma_1$  and  $\gamma_2$ , corresponding to the molarity concentration scale were arbitrarily assumed to be constant. Column 6 was computed in the same way as column 4, except that  $\gamma_1$  and  $\gamma_2$ , the mean ionic activity coefficients corresponding to the

molality concentration scale, were arbitrarily assumed to be constant. Both of these assumptions fortuitously lead to an apparent excellent "confirmation" of the Onsager relation (within 1%). For the other compositions of this system, however, the arbitrary assumption that activity coefficients  $\gamma_1$  and  $\gamma_2$  are constant does not lead to such good agreement between  $(L_{12})_0$  and  $(L_{21})_0$ ; for two of the compositions these quantities differ by more than 2%.

The only experimental errors which may significantly affect present tests of the Onsager relation (columns 1-4 of Table II) are those in the diffusion coefficients,  $(D_{ij})_0$ , and in the data for activity coefficients. Conversion of the measured diffusion coefficients from a volume-fixed to a solvent-fixed frame of reference by using equation 2 leaves the errors in the diffusion coefficients essentially unchanged. This is because the ratios  $C_i/C_0$  are small and the  $C_i$  and  $\bar{V}_i$  are accurately known; the  $C_i$  are known to about 0.01% and the  $\bar{V}_i$  are probably within 0.3% of the true values. Similarly, when computing the  $\mu_{ij}$  from equation 6, the errors in the  $B_{kj}$  are negligible compared to those in the  $A_{ik}$ .

To show the effects of significant experimental errors on tests of the Onsager relation, we now derive an expression for estimating the expected percentage errors,  $\% \Delta_{\text{est}}$ , in these tests. This expression is valid if, in the absence of experimental errors, the values of  $(L_{12})_0$  and  $(L_{21})_0$  are equal. As a first step the estimated difference between  $(L_{12})_0$  and  $(L_{21})_0$

$$\Delta_{\text{est}} = \delta \{ [(L_{21})_0 - (L_{12})_0] \times RT \times 10^9 \}_{\text{est}} \quad (21b)$$

is expressed in terms of estimated errors,  $\delta(D_{ij})_0$  and  $\delta\Gamma_{ij}$ , in the diffusion coefficients and in the concentration dependences of the logarithms of the activity coefficients. Thus, neglecting products of errors, observing that the  $m_i$  and  $B_{kj}$  may be considered constant, and ignoring the difference between the cubic centimeter and the milliliter, we obtain from equations 1e, 1f, 6 and 10

$$\Delta_{\text{est}} = [(RT)^2/S] \times 10^6 \left\{ \frac{1}{RT} [\mu_{12}\delta(D_{11})_0 - \mu_{11}\delta(D_{12})_0 + \mu_{22}\delta(D_{21})_0 - \mu_{21}\delta(D_{22})_0] + 4.605[E_{11}\delta\Gamma_{11} + E_{12}\delta\Gamma_{12} + E_{22}\delta\Gamma_{22}] \right\} \quad (22)$$

where

$$E_{11} = B_{12}(D_{11})_c - B_{11}(D_{12})_0 \quad (22a)$$

$$E_{12} = B_{22}(D_{11})_0 - B_{21}(D_{12})_0 + B_{12}(D_{21})_0 - B_{11}(D_{22})_0 \quad (22b)$$

$$E_{22} = B_{22}(D_{21})_0 - B_{21}(D_{22})_0 \quad (22c)$$

Errors in the main diffusion coefficients depend predominantly on errors in the cross-term diffusion coefficients when the former are evaluated by the procedure<sup>32</sup> used to obtain the data<sup>9</sup> considered here. It may be shown that

$$\delta(D_{11})_v = F_1\delta(D_{12})_v + F_2\delta(D_{21})_v \quad (23a)$$

$$\delta(D_{22})_v = F_3\delta(D_{12})_v + F_4\delta(D_{21})_v \quad (23b)$$

where the coefficients  $F_1, \dots, F_4$  can be calculated from available data.<sup>33</sup> Into equation 22 we now introduce the good approximations  $\delta(D_{ij})_0 \cong \delta(D_{ij})_v$  and substitute equations 23a and 23b. Equations 19 are then used to express the  $\delta\Gamma_{ij}$  in terms of errors in measured quantities associated with the activity coefficients. Finally we multiply by 100 and divide by the average experimental value,  $\{[(L_{12})_0 + (L_{21})_0]/2\} \times RT \times 10^9$ , to obtain a convenient expression for the estimated percentage error in testing the Onsager relation:

$$\% \Delta_{\text{est}} = 100 \frac{[10(RT)^2/S]}{\left[ \left( \frac{(L_{12})_0 + (L_{21})_0}{2} \right) \times RT \times 10^9 \right]} \sum_{i=1}^8 \psi_i \delta_i \quad (24)$$

where

$$\left. \begin{aligned} \psi_1 &= [\mu_{12}F_1 - \mu_{11} - \mu_{21}F_3]/(RT) \\ \psi_2 &= [\mu_{12}F_2 + \mu_{22} - \mu_{21}F_4]/(RT) \\ \psi_3 &= 4.605 \times 10^6 (m_1/m) [E_{11} + E_{12} + E_{22}] \\ \psi_4 &= 4.605 \times 10^6 (m_2/m) [E_{11} + E_{12} + E_{22}] \\ \psi_5 &= 4.605 \times 10^6 (1/m) [2m_2E_{11} + (m_2 - m_1)E_{12} - 2m_1E_{22}] \\ \psi_6 &= -2.3026 \times 10^6 E_{12} \\ \psi_7 &= 3.070 \times 10^6 [2m_2E_{11} + (2m_1 + m_2)E_{12} + m_1E_{22}] \\ \psi_8 &= 3.070 \times 10^6 [m_2E_{11} + (m_1 + 2m_2)E_{12} + 2m_1E_{22}] \end{aligned} \right\} \quad (24a)$$

The symbols  $\delta_i$  denote errors in the several measured quantities and are defined in Table III in the column headed  $(\delta_i)_{\text{def}}$ . Equation 24 is valid for any composition of a ternary solution of two 1-1 electrolytes with a common ion. To apply it to the system NaCl-KCl-H<sub>2</sub>O the coefficients  $\psi_i$  were calculated for each of the four compositions considered here; these values are listed in Table III. All quantities required for calculation of these  $\psi_i$  are available in Tables I and II except for the  $F_i$ , which were found to be constant within  $\pm 0.01$  for the compositions considered and which

(32) Equations 84-94 of ref. 13.

(33) Relations 23a and 23b, together with expressions for the  $F_1, F_2, F_3$  and  $F_4$ , are obtained by differentiation of equations 82 and 83 of ref. 13 while assuming that  $I_A, S_A, L_A, R_1$  and  $R_2$  are constant. These quantities may be considered constant because they can be determined much more accurately than the cross-term diffusion coefficients. The two resulting equations are then solved for the errors  $\delta(D_{11})_v$  and  $\delta(D_{22})_v$  in terms of  $\delta(D_{12})_v$  and  $\delta(D_{21})_v$ . These cross-term diffusion coefficients are limited in accuracy because they must be obtained from deviations of the refractive index gradient curve from Gaussian shape by using the measured fringe deviations,  $\Omega$  (see equations 38 and 81 of ref. 12 and 13, respectively).

were found to have the values:  $F_1 = F_4 = 0.00$ ,  $F_2 = -0.86$  and  $F_3 = -1.17$ .

We have estimated *maximum* values of the experimental errors,  $\delta_i$ ; they are listed in the second column of Table III under the heading  $(\delta_i)_{\text{exp}}$ . The same values of  $\delta_i$  are used for all four compositions. Values of  $\pm 0.02 \times 10^{-5}$  are assigned to  $\delta_1$  and  $\delta_2$  on the basis of probable errors in the Gouy fringe deviations which were used to calculate  $(D_{12})_v$  and  $(D_{21})_v$ <sup>33</sup>; concentration dependences of the diffusion coefficients and refractive increments cause some error in the  $(D_{ij})_v$ , but these effects have been neglected because of the relatively small concentration differences between the two solutions used in each experiment.<sup>9</sup> The errors shown for  $\delta_3$  and  $\delta_4$  are about 1.5 to 2 times greater than differences between derivatives of the data tabulated by Robinson and Stokes<sup>11</sup> and of some corresponding data reported by other workers.<sup>34-36</sup> The value of  $\pm 0.002$  for  $\delta_5$  corresponds to an assumed error of  $\pm 0.1\%$  in the osmotic coefficient of each binary system for  $m \cong 0.5$ . Two cases are considered for the errors in  $K^a, \beta_1$  and  $\beta_2$ . In case (a) for which  $\beta_1 = \beta_2 = 0$  (i.e., Harned's rule is assumed to be perfectly valid) a value of  $\pm 0.001$  is assigned to  $\delta_6$ . For case (b) the values shown for  $\delta_7$  and  $\delta_8$  are estimates of the probable maximum deviations of  $\beta_1$  and  $\beta_2$  from zero<sup>37</sup>; for this range of  $\beta_1$  and  $\beta_2$ ,  $\delta_6$  is estimated to be  $\pm 0.004$ . From these estimated maximum errors were computed the products,  $\psi_i \delta_i$ , as shown in Table III. Substitution of these products for cases (a) and (b), respectively, into equation 24, and use of data from Table II to evaluate the coefficient of the summation, gives the estimated percentage errors,  $\% \Delta_{\text{est}}$ , shown in the last two lines of Table III.

It is now of interest to compare the  $\% \Delta_{\text{est}}$  in Table III with the  $\% \Delta_{\text{exp}}$  in Table II. For each composition the  $\% \Delta_{\text{est}}$  are approximately twice the value of the  $\% \Delta_{\text{exp}}$ ; these values are not inconsistent because *maximum* expected errors are used for the  $\delta_i$ . The  $\% \Delta_{\text{est}}$  are seen from Table III to be essentially independent of composition over the range of concentrations considered here. The reason for this is apparent from equations 24 if we restrict our consideration to the simple case that  $m_1 = m_2 = m/2$  and if the  $\Gamma_{ik}$  contributes only a small fraction of the  $A_{ik}$ . Then if the concentration range is not too large and if the  $\delta_i$  and  $E_{ij}$  are constant, the contributions to  $\% \Delta_{\text{est}}$  of the several terms depend approximately on composition as follows: those for  $i = 1, 2$  are independent of  $m$ ; those for  $i = 3, \dots, 6$  are proportional to  $m$ ; and those for  $i = 7, 8$  are proportional to  $m^2$ . Because errors  $\delta_1$  and  $\delta_2$  in the diffusion coefficients are considerably larger than other errors, the terms which are independent of  $m$  predominate here;

(34) T. Shedlovsky and D. A. MacInnes, *J. Am. Chem. Soc.*, **59**, 503 (1937).

(35) H. S. Harned and M. A. Cook, *ibid.*, **59**, 1290 (1937).

(36) H. S. Harned and M. A. Cook, *ibid.*, **61**, 495 (1939).

(37) An estimate of  $\beta_1 - \beta_2$  was made by considering possible deviations from linearity of the data plotted in Fig. 18.1 of ref. 10. Assuming that  $d\beta_1/dm = d\beta_2/dm = 0$ , an estimate of  $\beta_1 + \beta_2$  is made by observing linear deviations of  $\alpha_1 + \alpha_2$  (Table 4 of ref. 10) from a constant value. Solution of these expressions for  $\beta_1 - \beta_2$  and for  $\beta_1 - \beta_2$  leads to the estimates shown for  $\delta_7$  and  $\delta_8$ .

TABLE III<sup>a</sup>  
 MAXIMUM ESTIMATED ERRORS FOR TESTS OF THE ONSAGER RECIPROCAL RELATION

$(\delta_i)_{\text{def.}}$	$(\delta_i)_{\text{exp}}$	$\frac{C_1 = 0.25}{C_2 = 0.25}$		$\frac{C_1 = 0.25}{C_2 = 0.5}$		$\frac{C_1 = 0.5}{C_2 = 0.25}$		$\frac{C_1 = 0.5}{C_2 = 0.5}$	
		$\psi_i$	$\psi_i \delta_i$	$\psi_i$	$\psi_i \delta_i$	$\psi_i$	$\psi_i \delta_i$	$\psi_i$	$\psi_i \delta_i$
$\delta_1 = \delta[(D_{12})_V \times 10^5]$	$\pm 0.02$	-3.85	0.077	-3.93	0.079	-1.93	0.039	-1.97	0.039
$\delta_2 = \delta[(D_{21})_V \times 10^5]$	$\pm .02$	4.18	.084	2.12	.042	4.12	.082	2.08	.042
$\delta_3 = \delta\left(\frac{d \log \gamma_1(c)}{dm}\right)$	$\pm .002$	-0.73	.001	-0.47	.001	-0.98	.002	-0.71	.001
$\delta_4 = \delta\left(\frac{d \log \gamma_2(c)}{dm}\right)$	$\pm .002$	-0.73	.001	-0.94	.002	-.49	.001	-.71	.001
$\delta_5 = \delta\Phi$	$\pm .002$	-0.66	.001	-1.45	.003	.07	.000	-.71	.001
$\delta_6 = \delta K_\alpha$	(a)	$\pm .001$	1.07	1.18	.001	.97	.001	1.09	.001
	(b)	$\pm .004$	1.07	1.18	.005	.97	.004	1.09	.004
$\delta_7 = \delta\beta_1$	(a)	0	-0.97	0	-1.46	0	-1.49	0	-1.97
	(b)	$\pm .001$	-0.97	.001	-1.46	.001	-1.49	.001	-1.97
$\delta_8 = \delta\beta_2$	(a)	0	-0.85	0	-1.69	0	-1.01	0	-1.73
	(b)	$\pm .001$	-0.85	.001	-1.69	.002	-1.01	.001	-1.73
$\% \Delta_{\text{est}}$	(a)		$\pm 7.5$		$\pm 8.8$		$\pm 8.0$		$\pm 7.3$
	(b)		$\pm 7.7$		$\pm 9.3$		$\pm 8.3$		$\pm 7.9$

<sup>a</sup> Because the  $\delta_i$  may be either positive or negative, values of  $\psi_i \delta_i$  are reported without regard to sign; the  $\% \Delta_{\text{est}}$  in the last two lines were obtained from equation 24 by assuming that these products all have the same signs. In practice some of the products  $\psi_i \delta_i$  probably have opposite signs, causing some cancellation of errors, and some experimental errors will be less than the assigned values,  $\delta_i$ . Therefore it is not unreasonable that the above values of  $\% \Delta_{\text{est}}$  are about twice the observed differences,  $\% \Delta_{\text{exp}}$ , in Table II.

they may also be expected to predominate even at considerably higher concentrations if the  $\delta_i$  and  $E_{ij}$  remain essentially constant. Therefore it seems that more accurate methods for measuring  $(D_{12})_V$  and  $(D_{21})_V$  must be developed before better tests of the Onsager reciprocal relation can be made with this system. Nevertheless, data for diffusion at appreciably higher electrolyte concentrations would be valuable, even if higher accuracy could not be achieved, because the derivatives  $\Gamma_{ik}$  would then contribute different proportions of the derivatives  $\mu_{ij}$  in a test of the Onsager relation.

No detailed comparisons of the above tests of the Onsager relation with those reported by Miller<sup>20</sup> are possible until the paper giving details of his calculations is available. One difference, already noted, is that he used approximate, rather than measured, data for the activity coefficients; for the system NaCl-KCl-H<sub>2</sub>O he used Harned's rule with  $\alpha_1 = \Phi$ , which is equivalent to assuming that  $K_\alpha = \beta_1 = \beta_2 = 0$ . By using the appropriate value of  $\psi_6$  from Table III we estimate from equation 24 that his approximation, corresponding to  $\delta_6 \equiv \delta K_\alpha = -0.0168$ , would lead to a value of -3.3 instead of -4.9 for  $\% \Delta_{\text{exp}}$  for the case  $C_1 = C_2 = 0.5$  (see Table II). Thus for this system use of the experimental, instead of the assumed, value of  $K_\alpha$  actually increases the difference between  $(L_{12})_0$  and  $(L_{21})_0$ . This emphasizes the fact that good experimental data for all quantities are necessary for rigorous tests of the Onsager reciprocal relation.

**Acknowledgments.**—It is a pleasure to acknowledge the interest and encouragement of Professors J. W. Williams and S. Claesson during the course of this investigation. This work was supported in part by the National Science Foundation, by the Research Committee of the Graduate School of the University of Wisconsin from funds supplied by the Wisconsin Alumni Research Foundation, and by a research grant from the Physical Chemistry Department of the University of Uppsala, Sweden.

## Appendix

**Expressions for the Partial Molal Volumes of Solutes in Multicomponent Systems.**—Consider a solution containing  $q + 1$  components designated by the subscripts  $0, \dots, q$ ; here 0 denotes the solvent. The volume,  $V$ , of the solution is given by

$$V = \sum_{j=0}^q n_j M_j / \rho \quad (\text{A-1})$$

where  $n_j$  is the number of moles of component  $j$  with molecular weight  $M_j$ , and  $\rho$  is the density of the solution in g./ml. Differentiation with respect to  $n_i$  at constant temperature and pressure and use of the expression

$$m_j = \frac{1000 n_j}{n_0 M_0} \quad (\text{A-2})$$

for the molality of component  $j$  yields an expression for the partial molal volume,  $\bar{V}_i$ , of solute  $i$  in ml./mole

$$\bar{V}_i = \frac{1}{\rho^2} \left[ M_{i\rho} - 1000 \left( 1 + \sum_{j=1}^q \frac{M_j m_j}{1000} \right) \left( \frac{\partial \rho}{\partial m_i} \right)_{m_{k \neq i}} \right] \quad (\text{A-3})$$

Equation A-3 may be expressed in terms of molalities by means of the relation

$$\left( \frac{\partial \rho}{\partial m_i} \right)_{m_{k \neq i}} = \sum_{j=1}^q \left( \frac{\partial \rho}{\partial C_j} \right)_{C_{k \neq j}} \left( \frac{\partial C_j}{\partial m_i} \right)_{m_{k \neq i}} \quad (\text{A-4})$$

and the two equations relating molalities to molalities,  $C_i$ ,

$$m_i = \frac{C_i}{\rho - \sum_{j=1}^q M_j C_j / 1000} \quad (\text{A-5})$$

and

$$C_i = \frac{\rho m_i}{1 + \sum_{k=1}^q M_k m_k / 1000} \quad (\text{A-6})$$

After some manipulations one obtains

$$\bar{V}_i = \frac{M_i - 1000H_i}{\rho - \sum_{j=1}^{\xi} H_j C_j} \quad (\text{A-7})$$

where

$$H_i = (\partial\rho/\partial C_i)_{T,P,C_{k \neq i}} \quad (\text{A-8})$$

The derivatives  $H_i$  may be determined readily when the density is known as a function of the solute molarities. Equation A-3 may be employed directly to obtain  $\bar{V}_i$  for solute  $i$  if the density is known as a function of  $m_i$ .

## A THERMOANALYTICAL STUDY OF THE BINARY OXIDANT SYSTEM BARIUM PERCHLORATE-POTASSIUM NITRATE

BY VIRGINIA D. HOGAN AND SAUL GORDON

*Pyrotechnics Chemical Research Laboratory, Picatinny Arsenal, Dover, New Jersey*

*Received August 4, 1958*

A differential thermal analysis and thermogravimetric study of the thermally unstable barium perchlorate-potassium nitrate system revealed that its physico-chemical behavior at elevated temperatures varies widely with composition. Differential thermal analysis first revealed the occurrence of an exothermal, solid state, metathetical reaction which takes place at 325°, predominantly close to the stoichiometric composition. The reaction, which is thermodynamically spontaneous and involves cations of equal crystal radii, was found by X-ray diffraction analysis to go to completion; therefore, the potassium perchlorate-barium nitrate system which is produced must be the stable salt pair. The diversity in the thermal behavior of this system at elevated temperatures can be elucidated satisfactorily on a basis of (a) the physico-chemical properties and reactions characteristic of the four reciprocal salts which are present as a result of the solid state metathesis, and (b) the fusion of an exceedingly potassium nitrate-rich mixture of the original ingredients.

### Introduction

The thermoanalytical techniques of differential thermal analysis and thermogravimetry are versatile experimental tools which are finding increasing application in chemical research. Differential thermal analyses furnish data relative to the evolution or absorption of heat as a result of the high temperature physico-chemical phenomena characteristic of the sample under study, while thermogravimetric curves yield data concerning any physical or chemical reactions accompanied by weight changes that occur at elevated temperatures. A thermoanalytical study of the system potassium perchlorate-barium nitrate utilizing these techniques<sup>1</sup> revealed varied and interesting thermal effects which suggested an investigation of the high temperature phenomena characteristic of the reciprocal system barium perchlorate-potassium nitrate. In common with the potassium perchlorate-barium nitrate system, the system considered here exhibits thermal instability which precludes its study by conventional cooling curve techniques. Therefore, differential thermal analysis and thermogravimetry were employed. The thermal behavior of the barium perchlorate-potassium nitrate system varies widely with the composition of the particular mixture under study. However, this variation in thermogravimetric and differential thermal analysis behavior with composition can be accounted for satisfactorily by assuming the fusion of a eutectic mixture of the ingredients and the occurrence of a metathetical reaction between them, in addition to the physico-chemical reactions of the pure materials.

**Reagents.**—Potassium nitrate, analytical reagent grade (Fisher Scientific Co.); barium perchlorate, Desicchlora (made by G. Frederick Smith Chemical Co. for J. T. Baker Chemical Co.) were used. It was found necessary to prepare the individual samples from reagents freshly dried at 200°. In the presence of moisture, binary mixtures of these salts

apparently undergo a metathetical reaction which destroys the potassium nitrate at the temperature necessary to completely dry barium perchlorate.

**Apparatus and Procedures.**—The differential thermal analysis and thermogravimetric apparatus employed have been described previously.<sup>2</sup> Four gram samples were taken for differential thermal analyses and an equal volume of alumina served as the reference material. In the DTA curves the temperature difference between the sample and reference materials is plotted as a function of the sample temperature. Conventionally, exothermal reactions appear as upward deflections while endothermal reactions appear as downward deflections. Three hundred and fifty milligram samples were used in the thermogravimetric analyses with a range of 200 mg. full-scale for changes in weight. Thermogravimetric curves are plotted as loss in weight as a function of furnace temperature. This furnace temperature was found to be five to thirty degrees higher than the actual sample temperature at the heating rate used. In both thermoanalytical techniques the furnace is set for a linear heating rate of 15° per minute.

### Results and Discussion

Differential thermal analysis and thermogravimetric curves for the ingredients are illustrated in Fig. 1. Differential thermal analysis of pure barium perchlorate reveals one endothermic crystalline transition at 290° and possibly a second at about 365° prior to melting at 490° and vigorously exothermic decomposition at 500°. The accompanying thermogravimetric curve displays a loss in weight equivalent to decomposition to barium chloride at 535°. The DTA curve of pure potassium nitrate exhibits first an endothermic crystalline transition at about 130°. A small exothermic spike at 330° culminates in endothermic fusion at 340°. A slight bubbling reaction starts at about 675°, although no definite thermal reaction is occurring. The bubbling most probably is due to slight impurities which are oxidized and escape as carbon dioxide or oxides of nitrogen. The sample does not begin to decompose visibly until temperatures above 750°. The thermogravimetric curve

(2) V. Hogan, S. Gordon and C. Campbell, *Anal. Chem.*, **29**, 306 (1957).

(1) V. Hogan and S. Gordon, *This Journal*, **62**, 1433 (1958).

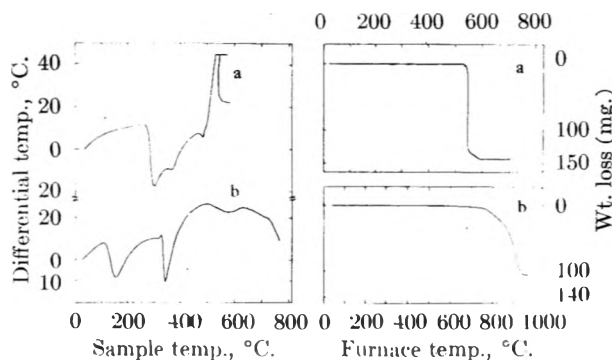


Fig. 1.—Differential thermal analysis and thermogravimetric curves for pure barium perchlorate and pure potassium nitrate: (a) barium perchlorate; (b) potassium nitrate

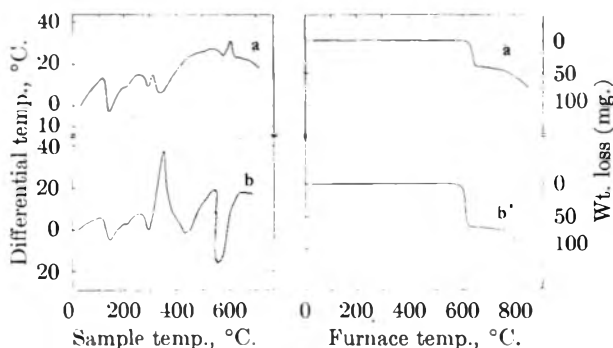


Fig. 2.—Differential thermal analysis and thermogravimetric curves for the system barium perchlorate-potassium nitrate: (a) 30% barium perchlorate-70% potassium nitrate, mole ratio 1:7.8; (b) 50% barium perchlorate-50% potassium nitrate, mole ratio 1:3.3.

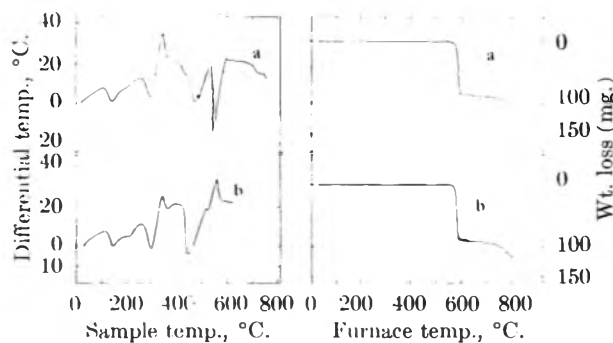
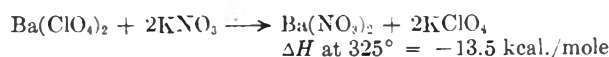


Fig. 3.—Differential thermal analysis and thermogravimetric curves for the system barium perchlorate-potassium nitrate: (a) 62.5% barium perchlorate-37.5% potassium nitrate, mole ratio 1:2; (b) 70% barium perchlorate-30% potassium nitrate, mole ratio 1:1.4.

of potassium nitrate shows a weight loss beginning at about 575° and ending at 960° which corresponds to complete conversion to potassium oxide.

The differential thermal analysis and thermogravimetric behavior of the mixtures, Fig. 2 and 3, vary with the composition. The thermogravimetrically determined temperature at which perchlorate ion loses its oxygen ranges from 560° for 1 to 2 mole ratio barium perchlorate-potassium nitrate to 610° for the 1 to 7.8 composition, compared to 535° for pure barium perchlorate and 600° for pure potassium perchlorate.<sup>1</sup> The DTA curves of the mixtures containing 50% or less potassium nitrate exhibit a sharp exotherm at 325°,

which cannot be attributed to any of the physical or chemical reactions of the pure ingredients, while that of the mixture containing 70% potassium nitrate shows a fusion endotherm at 315° instead of the exotherm at 325°. However, all the DTA and TGA behavior of the mixtures can be satisfactorily elucidated, if one assumes, in addition to the physico-chemical reactions of the pure ingredients, the fusion of a potassium nitrate-rich eutectic mixture of the ingredients and the occurrence of a solid state, metathetical reaction such as



Unfortunately, free energy calculations cannot be made for this reaction because values for neither the free energy of formation nor the entropy of barium perchlorate at any temperature are available in the literature. However, the entropy change necessary to make the free energy change of the above reaction zero, calculated from the heat of reaction is  $-22.5 \text{ cal./degree/mole}$  at 325°. The relative magnitude of the entropy change for a reaction can be estimated qualitatively from the stoichiometry, *i.e.*,  $\Delta S$  will be positive and relatively large where the number of moles of products exceeds the number of moles of reactants; it will be relatively small where the number of moles remains the same; and it will be negative and relatively large where the number of moles of products is less than the number of moles of reactants. The metathetical reaction postulated is of the type which should involve a small entropy change, while the value necessary to make the free energy change zero,  $-22.5 \text{ cal./degree/mole}$ , is relatively large. Therefore, it seems likely that the free energy change in this reaction is negative, meaning that the reaction is thermodynamically spontaneous.

This interpretation is further supported by the previous investigation of the potassium perchlorate-barium nitrate system. The perchlorate and nitrate DTA and thermogravimetric decomposition patterns exhibited by mixtures of potassium nitrate-barium perchlorate containing 50% or less potassium nitrate are similar to those exhibited by barium nitrate-potassium perchlorate samples of corresponding composition where eutectic fusion precedes barium nitrate catalyzed, exothermic or endothermic perchlorate decomposition.<sup>1</sup> The appropriate decomposition is identified easily since perchlorate decomposition involves a vigorous, visible evolution of oxygen, and nitrate decomposition evolves red-brown oxides of nitrogen.

The DTA curves of the mixtures for which this reaction is postulated indicate that it is a solid state phenomenon. In addition, the crystal lattice structures of the high temperature forms, indicated in Table I, are basically the same and involve a simple configuration and spatial symmetry that should facilitate the ionic mobility necessary to effect a solid state metathetical reaction. Differential thermal analysis indicates that barium perchlorate undergoes two transitions, one at 290° and one at 360°. According to the literature, barium perchlorate crystals are hexagonal at room



TABLE I

CRYSTAL STRUCTURE AS A FUNCTION OF TEMPERATURE

Formula	Transition temp., °C.	Crystalline modifications
Ba(ClO <sub>4</sub> ) <sub>2</sub>	360	? <sup>b</sup> → cubic <sup>a</sup>
KClO <sub>4</sub>	300	rhombic → cubic
KNO <sub>3</sub>	128	rhombic → trigonal
Ba(NO <sub>3</sub> ) <sub>2</sub>	...	cubic → (cubic)

<sup>a</sup> See ref. 3. <sup>b</sup> Hexagonal → (?) at nominally 290°.

temperature; above 360° they are body centered cubic.<sup>3</sup> However, the transition indicated by the endotherm at 290° has not yet been identified. This concept is further supported by the similarity of the crystal radii of the cations Ba<sup>++</sup> and K<sup>+</sup>, 1.35 and 1.33 Å., respectively.<sup>4</sup> In a comprehensive review of solid state reactions, including thermodynamic and kinetic considerations, Hedvall and Cohn affirm that reactions of mixtures involving solid phases only are exothermic.<sup>5</sup> More recent data indicate that defects in the crystal lattice are responsible for solid state reactions.<sup>6</sup> To obtain experimental confirmation for the postulated solid state reaction, a finely ground mixture of 2 to 1 mole ratio potassium nitrate-barium perchlorate was heated for 11 hours at 326°, the temperature of the observed exotherm. No visible melting was observed, although the sample was converted from a free flowing powder to a solid, easily crushed lump. X-Ray diffraction analysis of the crushed material revealed that it consisted of barium nitrate and potassium perchlorate. A similar experiment where a larger sample was heated at this temperature for two hours showed the presence of both products and reactants, while a portion heated at 175° showed the presence of only the reactants, barium perchlorate and potassium nitrate. These data show that the reaction goes to completion and therefore potassium perchlorate and barium nitrate must be the stable salt pair in this reciprocal system.

The DTA curve of the 30-70 mixture, Fig. 2, a mole ratio of 1 to 7.8 barium perchlorate-potassium nitrate, displays first the endothermic crystalline transition of potassium nitrate at 130°, followed by an endothermic shoulder at about 200° which is due to moisture absorbed by the barium perchlorate during handling. This effect has been confirmed by comparison with DTA curves of dried and undried barium perchlorate. Then there is a small endothermic peak at about 290° corresponding to the first crystalline transition of barium perchlorate. This is followed by an endotherm starting at about 315° which, since partial melting is observed, may be due to the fusion of a eutectic mixture of the ingredients. A further study of this composition region of the binary system will be undertaken. The completely molten sample exhibits an exothermal trend which culminates in a shallow endotherm at about 575° immediately prior to a weakly exothermal per-

chlorate decomposition at 590°. Nitrate decomposition takes place above 700°. Thermogravimetric analysis of this mixture shows a weight loss equivalent to the loss of oxygen from barium perchlorate at 610° followed by a further more gradual loss above 700° due to nitrate decomposition.

Differential thermal analysis of 50-50 barium perchlorate-potassium nitrate, Fig. 2, a mole ratio of 1 to 3.3, exhibits first the crystalline transition endotherm of potassium nitrate. The endotherm at 290° caused by the first crystalline transition of barium perchlorate culminates in a steep exotherm at 325° due to the exothermal solid state metathesis. By the time the melting point of potassium nitrate, 340°, is reached, the metathesis is well along and the heat of fusion of the excess potassium nitrate (1.3 moles × 2.8 kcal./mole = 3.6 kcal.) is insufficient to influence appreciably the exothermal reaction (13.5 kcal./stoichiometric mole ratio). The sample, which at this point contains barium nitrate, potassium perchlorate and a small excess of molten potassium nitrate, melts during the succeeding broad, ill-defined endotherm which peaks at 440°. Highly endothermic perchlorate decomposition takes place at 560° and nitrate decomposition above 700°. The thermogravimetric curve shows that the loss of oxygen from barium perchlorate occurs at 580° followed, above 700°, by a further gradual loss presumably due to nitrate decomposition.

As shown in Fig. 3, the DTA curve of the 1:2 barium perchlorate-potassium nitrate mixture, 62.5-37.5% by weight, which is stoichiometric for the metathetical reaction displays first the endothermic crystalline transition of potassium nitrate at 130°. Then there is an endothermic peak at 290° corresponding to the first crystalline transition of barium perchlorate culminating, at 325°, in a high sharp exotherm due to the metathetical reaction. This reaction would completely obscure both the melting point of potassium nitrate (340°), and the second transition of barium perchlorate (365°), if they are present at this stage of the reaction. The next thermal phenomenon is a broad multiple endothermic peak extending from 400 to 510° during which the sample, which now consists of barium nitrate and potassium perchlorate, melts. This endotherm corresponds roughly to the eutectic fusion endotherm observed at 465° on the DTA curves for the reciprocal system potassium perchlorate-barium nitrate. It is succeeded by markedly endothermic perchlorate decomposition at 545°. Endothermic nitrate decomposition occurs above 700°. The complementary thermogravimetric analysis indicates loss of oxygen from perchlorate ion at 560° and then a gradual loss above 700° due to nitrate decomposition.

Differential thermal analysis of the 70-30 barium perchlorate-potassium nitrate mixture, Fig. 3, a mole ratio of 1 to 1.4, shows a different combination of effects, since the barium perchlorate is in excess of the amount required for the metathetical reaction. The endothermic crystalline transition of

(3) J. J. Campisi, unpublished results, Picatinny Arsenal.

(4) L. Pauling, "The Nature of the Chemical Bond," Cornell Univ. Press, Ithaca, N. Y., 1944, pp. 343-350.

(5) J. A. Hedvall and G. Cohn, *Kolloid-Z.*, **88**, 224 (1939).

(6) A. L. G. Rees, "Chemistry of the Defect Solid State," John Wiley and Sons, New York, N. Y., 1954.

potassium nitrate is observed at 130°. The endotherm at 290° corresponding to the first crystalline transition of barium perchlorate culminates in the sharp exotherm at 325° caused by the solid state metathesis. All of the potassium nitrate is used up in the reaction and the next break in the curve is a shallow endotherm at 360° corresponding to the second crystalline transition of the excess barium perchlorate. During the endotherm at 410°, the sample, which now consists of barium nitrate, potassium perchlorate and excess barium perchlorate, melts completely. This endotherm is succeeded immediately by exothermic perchlorate decomposition at 535°. The 410° endothermic

fusion and subsequent perchlorate decomposition observed with this sample is similar to that exhibited by potassium perchlorate-barium nitrate mixtures at 465°. This system, however, is inherently more complex since the metathetical reaction occurring in the presence of an excess of one of the reactants results in a ternary system. This in turn may lead to the formation of lower melting eutectics. Nitrate decomposition occurs above 700°. On thermogravimetric analysis the mixture loses an amount of weight equivalent to the decomposition of barium perchlorate to barium chloride at 565°. It undergoes a further loss in weight above 700° due to the decomposition of nitrate ion.

## MAGNETIC SUSCEPTIBILITIES OF THE CUPRIC SALTS OF SOME $\alpha,\omega$ -DICARBOXYLIC ACIDS

BY OSAMU ASAI, MICHIIHIKO KISHITA AND MASAJI KUBO

*Chemical Department, Nagoya University, Chikusa, Nagoya, Japan*

*Received August 4, 1958*

The magnetic susceptibilities of the cupric salts of  $\alpha,\omega$ -dicarboxylic acids,  $\text{HOOC}(\text{CH}_2)_{n-2}\text{COOH}$  with  $n = 2-10$ , were measured by the Gouy method at room temperature. The diamagnetic susceptibilities of the free acids were also measured. From these data, the effective magnetic moments were evaluated per one copper atom of these salts. They are smaller than the theoretical spin-only moment, 1.73 Bohr magnetons, for a single unpaired electron, except that of cupric malonate. The effective magnetic moment plotted against  $n$ , the number of carbon atoms in the acid radicals, shows a zig-zag line: the moment of the cupric salt having an odd  $n$  value is greater than those of the adjacent homologs of even  $n$  values. This alternate dependence upon the number of carbon atoms in a normal chain is striking only for the lower members of this series. An adequate explanation for these experimental results is presented based on the plausible structures of the salt crystals that can be presumed from the geometric configuration of cupric acetate monohydrate as well as of an oxalic acid radical.

### Introduction

Although copper has an odd atomic number, it is usually bivalent. The resulting compounds have an odd number of electrons in their monomeric forms. Accordingly, provided that the ordinary  $LS$  coupling exists, the theoretical spin moment is 1.73 Bohr magnetons for a single unpaired electron and the orbital contributions add to rather than subtract from the spin moment, because the copper atom has a more than half filled 3d subshell.<sup>1</sup> In fact, cupric compounds generally show a magnetic moment of about 1.8 B.M. or slightly more, in magnetically dilute compounds and solutions.<sup>2</sup> Some cupric compounds, however, show smaller effective moments than the theoretical moment. Cupric acetate is one of these compounds showing subnormal magnetic moments that have been most extensively studied. For this compound, the existence of some sort of magnetic coupling between two copper atoms in an isolated pair has been suggested by the decreasing magnetic susceptibility determined by Guha<sup>3</sup> and others<sup>4</sup> as the temperature was lowered as well as by the decreasing intensity of the paramagnetic resonance absorption with de-

creasing temperature observed by Bleaney and Bowers.<sup>5</sup> It was finally confirmed by the X-ray crystal analysis on cupric acetate monohydrate carried out by van Niekerk and Schoening,<sup>6</sup> who revealed that the real unit composing the crystal is a dimeric molecule, in which the Cu-Cu distance, 2.64 Å., is nearly equal to that in metallic copper, 2.551 Å. Here is a means for the structural elucidation of cupric compounds by magnetic measurements. This paper presents the results of magnetochemical study undertaken in order to investigate the structures of the cupric salts of  $\alpha,\omega$ -dicarboxylic acids,  $\text{HOOC}(\text{CH}_2)_{n-2}\text{COOH}$  with  $n = 2-10$ .

**Preparation of Materials.**—One part of commercially available oxalic acid was dissolved in about 50 parts of water. Cupric carbonate was added to the solution until no further evolution of carbon dioxide took place while the solution was warmed gently at 60–70°. The solution was filtered and the filtrate was evaporated. The precipitates of cupric oxalate were separated, washed with water and purified by repeated recrystallization. Cupric malonate, succinate and glutarate were prepared in the same way.

The samples of adipic, pimelic, suberic, azelaic and sebacic acids were furnished from Toyo Rayon Company. Adipic acid (m.p. 149–150°) was prepared by the oxidation of cyclohexanone with nitric acid. The specimen of pimelic acid (m.p. 104–105°) was drawn from Wako Pure Chemicals Company. A sample of suberic acid (m.p. 141–141.5°) was prepared by the method described by Vanino.<sup>7</sup> It was

(1) For example, in a chlorine atom having a more than half filled 3p subshell, the  $^2P_{3/2}$  level is lower than the  $^2P_{1/2}$  level, whereas in an excited sodium atom having a less than half filled 3p subshell,  $^2P_{1/2}$  is lower than  $^2P_{3/2}$ .

(2) P. W. Selwood, "Magnetochemistry," Interscience Publishers Inc., New York, N. Y., 2nd ed., 1956, p. 235. See also the first edition, 1943, p. 100.

(3) B. C. Guha, *Proc. Roy. Soc. (London)*, **A206**, 353 (1951).

(4) B. N. Figgis and R. L. Martin, *J. Chem. Soc.*, 3837 (1956).

(5) B. Bleaney and K. D. Bowers, *Phil. Mag.*, [7] **43**, 372 (1952); *Proc. Roy. Soc. (London)*, **A214**, 451 (1952).

(6) J. N. van Niekerk and F. R. L. Schoening, *Nature*, **171**, 30 (1953); *Acta Cryst.*, **6**, 227 (1953).

(7) L. Vanino, "Handbuch der präparativen Chemie. II. Organischer Teil," Ferdinand Enke, Stuttgart, 1937, p. 135.

decolorized by means of carbon black and subjected to recrystallization several times from water. The final preparation showed a melting point slightly higher than that given by Vanino, 140°, but lower than the highest one found in the literature, 144°. The specimen of azelaic acid (m.p. 106.5–107.5°) was procured from Nippon Ozone Company, in which  $\text{CH}_3(\text{CH}_2)_7\text{CH}=\text{CH}(\text{CH}_2)_7\text{COOH}$  was subjected to ozonolysis to obtain nonanoic acid  $\text{C}_8\text{H}_{17}\text{COOH}$  and azelaic acid. Sebacic acid (m.p. 133–134°) was imported from the United States. These acid samples were purified by recrystallization from water or ethanol. The melting points given above are in good agreement with those found in the literature, except that of the suberic acid preparation. Each of these acids was dissolved in water and the solution of cupric acetate was added to it in excess. The precipitates were washed thoroughly with warm water.

With the increasing chain length, the yield decreased and the available amount did not permit repeated recrystallization as was done for the lower members. In particular, the yield of the suberate was small.

The malonate was blue while other cupric salts assumed a blue color tinged with green. The oxalate, malonate and succinate showed a decrease in weight on heating at 110° for about 12 hours, the water of crystallization calculated therefrom being 1/2, 3 and 2 molecules of water per one atom of copper, respectively. The observed loss in weight on heating was 3.6, 24.5 and 16.4%, respectively, for the oxalate, malonate and succinate, as compared with the theoretical figures, 5.6, 24.6 and 16.6%. The water-free samples were stable and did not take up water again even when they were left to stand in atmospheric air. The absence of water of crystallization in these nine dried cupric salts was confirmed by the examination of their infrared absorption spectra in Nujol mulls over the wave number range covering 3000–3750  $\text{cm}^{-1}$ , where the OH stretching vibrations of water would have appeared.

**Experimental Method and Results.**—Magnetic susceptibilities were determined at room temperature by means of the powder method using a Gouy magnetic balance described in our previous report.<sup>8</sup> From the measured magnetic susceptibility  $\chi_g$  per gram,<sup>9</sup> the molar magnetic susceptibility  $\chi_M$  was calculated for each anhydrous cupric salt as well as its hydrate, if it was available. Measurements were made also of the magnetic susceptibilities of the free acids and the observed values were assumed to be equal to the diamagnetic contributions  $\chi_{\text{dia}}$  from the portions of cupric salts other than copper, the loss of two hydrogen atoms in salt formation being merely the removal of protons leaving electrons on the acid radicals. In the case of oxalic acid, the susceptibility of its dihydrate was determined and the contribution from water molecules was subtracted from it to obtain  $\chi_{\text{dia}}$ . The diamagnetic contribution  $\chi_{\text{dia}}$  of the acid part of each salt was also calculated from Pascal's constants.<sup>10</sup> The difference between the observed and calculated values was so small as to cause no appreciable changes in the final values of the effective moment. Since the available amount of suberic acid was too limited to permit direct measurements, the value calculated from Pascal's constants was used for  $\chi_{\text{dia}}$ .

Allowing for the diamagnetism and assuming the validity of Curie-Langevin law, the effective magnetic moments  $\mu$  per one copper atom were calculated from the molar susceptibilities  $\chi_M$  as

$$\mu = 2.83[(\chi_M - \chi_{\text{dia}})T]^{1/2}$$

The results are shown in Table I.

### Discussion

The effective magnetic moments of these compounds are definitely smaller than the spin-only value for a single unpaired electron, except that of cupric malonate, which has a slightly higher moment than the theoretical value, the difference being attributable to orbital contributions. The ef-

(8) M. Kondo and M. Kubo, *THIS JOURNAL*, **61**, 1648 (1957).

(9) Throughout this article, the data of magnetic susceptibility are given in c.g.s. e.m.u.

(10) In later publications from Pascal's laboratory, the combined value for the two oxygen atoms in carboxylic acid is given as  $-7.95 \times 10^{-6}$ . See also ref. 2, p. 92.

TABLE I

THE MOLAR MAGNETIC SUSCEPTIBILITIES, THE DIAMAGNETIC CONTRIBUTIONS AND THE EFFECTIVE MAGNETIC MOMENTS IN B.M. OF THE COPPER SALTS OF  $\alpha,\omega$ -DICARBOXYLIC ACIDS,  $\text{HOOC}(\text{CH}_2)_{n-2}\text{COOH}$  WITH  $n = 2-10$

Compounds	$T$ (°K.)	$\chi_M \times 10^6$	$\chi_{\text{dia}} \times 10^6$ Obsd.	Calcd.	$\mu$ (B.M.)
Oxalate	288	591	-34	-34	1.20
Malonate	286	1312	-46	-46	1.76
Succinate	299	755	-57	-58	1.40
Glutarate	300	792	-69	-69	1.45
Adipate	289	690	-78	-81	1.33
Pimelate	291	765	-88	-93	1.41
Suberate	288	792	...	-105	1.44
Azelate	290	751	-109	-117	1.41
Sebacate	288	776	-124	-129	1.44
Oxalate·1/2aq	295	623	-41	-41	1.25
Malonate·3aq	296	1513	-85	-85	1.95
Succinate·2aq	298	736	-83	-84	1.40

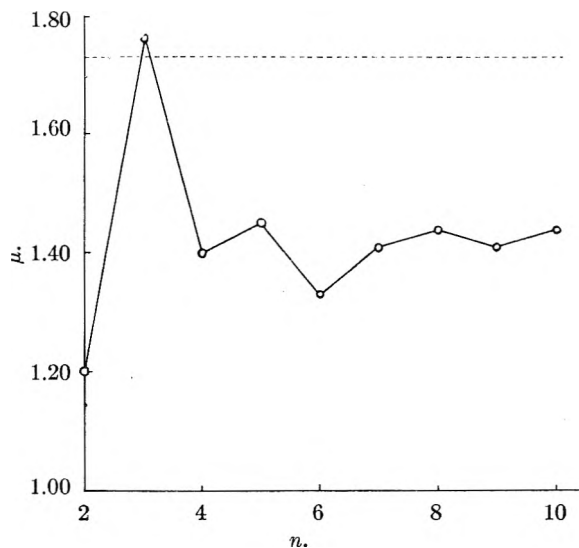


Fig. 1.—Dependence of the effective magnetic moment in B.M. per one copper atom of the anhydrous copper salts of  $\alpha,\omega$ -dicarboxylic acids upon the number of carbon atoms in the acids. The broken line indicates the theoretical spin-only moment, 1.73 B.M., for a single unpaired electron.

fective moment plotted against the number of carbon atoms in the acid molecules gives a zig-zag line as shown in Fig. 1: the cupric salt of a dicarboxylic acid having an odd  $n$ -value shows, in general, a greater effective moment than the neighboring homologs do. This fluctuation is striking only for the lower members of this series and becomes less pronounced with the increasing chain length of acid molecules until it is so small beyond pimelic acid that the alternate dependence upon the chain length is irregular or the existing regularity is masked by experimental errors, etc. The zig-zag shape of the curve of magnetic moments has been observed also for a series of bis-( $N$ -alkylsalicylaldimine)-nickel-(II) complexes by Sacconi, Paoletti and Del Re.<sup>11</sup>

Ploquin<sup>12</sup> has measured the magnetic susceptibilities of various organic salts of bivalent copper, but since his discussion was based on the structure

(11) L. Sacconi, P. Paoletti and G. Del Re, *J. Am. Chem. Soc.*, **79**, 4062 (1957).

(12) J. Ploquin, *Bull. soc. chim. France*, 757 (1951).

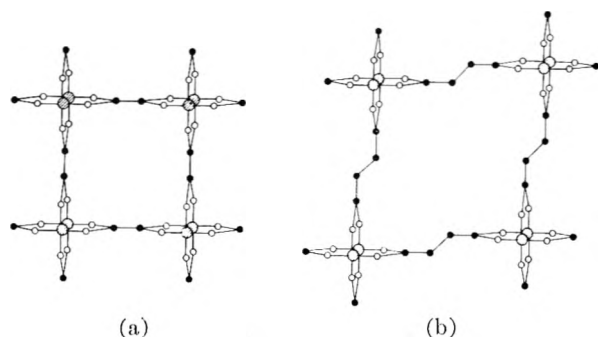
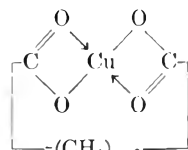


Fig. 2.—Schematic representation of the presumed structures for cupric oxalate (a) and cupric succinate (b). Black circles stand for carbon atoms, white ones for oxygen atoms and shaded ones for copper atoms.



his discussion need not be considered here. The data on some of the cupric salts that are available in tables<sup>13</sup> are not in exact agreement with those of the present study, but qualitatively the agreement is fairly good. In particular, the high magnetic susceptibility for the malonate hydrate is represented in both cases. The tabular values for oxalic, malonic and succinic acids are in complete agreement with the present ones.

The observed magnetic moment, 1.20 B.M., of cupric oxalate is a little smaller than the moment, 1.3–1.4 B.M., of anhydrous and hydrated cupric acetates determined by Figgis and Martin<sup>4</sup> at room temperatures. It is definitely established beyond all doubt by the X-ray crystal analysis carried out by van Niekerk and Schoening<sup>6</sup> that the subnormal magnetic moment of cupric acetate monohydrate is intimately associated with the close distance of approach of two copper atoms in a dimeric molecule,  $\text{Cu}_2(\text{CH}_3\text{COO})_4 \cdot 2\text{H}_2\text{O}$ . According to Bleaney and Bowers,<sup>5</sup> a strong coupling due to exchange forces exists in an isolated pair of copper atoms, leading to the interaction of two electron spins to form a lower diamagnetic singlet state and a higher paramagnetic triplet state, the population in the former state increasing with decreasing temperature at the expense of that in the latter state. Figgis and Martin<sup>4</sup> advanced a theory in which they presumed that cupric acetate monohydrate represented the first case in which a  $\delta$ -bond was the sole direct link between two atoms. The dimer formation of cupric acetate persists in dioxane, in ethanol, and to some extent also in methanol solutions.<sup>14</sup> It is reasonable to suppose that the structure around copper atoms in cupric acetate monohydrate crystals is considerably stable and that the same configuration is realized also in similar compounds that show subnormal moments. The coplanar structure of an oxalate radical has been amply demonstrated by X-ray crystal analysis<sup>15</sup> and electron diffraction<sup>16</sup> by

gas molecules. It is presumed that the oxalate radical in cupric oxalate also assumes a planar configuration. The only conceivable structure of cupric oxalate satisfying these two conditions is a two-dimensional rectangular network shown in Fig. 2a. A fairly compact structure will result, since the space inside each square ring will be effectively occupied by copper atoms protruding from neighboring networks located above and below the square ring in question.

In the case of other salts of the even series, analogous structures are possible as shown schematically in Fig. 2b. The extended zig-zag carbon chain in crystals has been demonstrated by Morrison and Robertson<sup>17</sup> for a number of normal aliphatic carboxylic acids. It should be mentioned in this connection that in the acids of the even series, the grouping of the acid molecules in crystals is characterized by a fairly close lateral approach. However, with the increasing length of carbon chains in the cupric salts, the empty space becomes greater in accordance with the enlarged rings, because the zig-zag chains are not exactly parallel to one another provided that the valency angle of carbon atoms assumes its normal value. If the normal carbon chains favor more or less parallel orientation, as already has been presumed by Herron and Pink<sup>18</sup> for anhydrous cupric laurate and stearate, the empty space will be reduced. At the same time, the resulting stress will cause a strain in the regular structure around the copper atoms and the bonded Cu–Cu distance will increase. As a consequence, the overlap of  $3d_{x^2-y^2}$  bonding orbitals belonging to two copper atoms decreases, leading to the decreased energy separation between the lowest singlet level and the upper triplet level of a pair of copper atoms and to the increase in the magnetic moment.

The copper salts of acids having odd  $n$ -values present a different situation. In the malonate, for instance, the turning of chains at the central carbon atoms renders the formation of structures similar to those shown in Fig. 2 impossible. The normal magnetic moment found for cupric malonate suggests that the atom pairs of copper are not formed in the crystals. The structures of cupric salts of the odd series are open to speculation, but it is likely that they are less simple: the unit cell may be doubled as compared with the salts of even  $n$ -values and possibly the lateral connections are weak as was found for glutaric acid crystals.<sup>19</sup> With the increasing chain length, however, the flexibility of linear chains may permit the approach of two copper atoms, leading to the decrease in the magnetic moment as was actually found in the present experiments.

Thus, the relationship between the observed magnetic moments of these cupric salts and the number of carbon atoms in the acids can be explained in terms of the proposed structures for the

(15) J. M. Robertson and I. Woodward, *J. Chem. Soc.*, 1817 (1936); J. D. Dunitz and J. M. Robertson, *ibid.*, 142 (1947).

(16) S. Shihata and M. Kimura, *Bull. Chem. Soc. Japan*, **27**, 485 (1954).

(17) J. D. Morrison and J. M. Robertson, *J. Chem. Soc.*, 980–987, 993 (1949).

(18) R. C. Herron and R. C. Pink, *ibid.*, 3948 (1955).

(19) J. D. Morrison and J. M. Robertson, *ibid.*, 1001 (1949).

(13) "Selected Constants, No. 7. On Diamagnetism and Paramagnetism," International Union of Pure and Applied Chemistry, Paris, 1957.

(14) M. Kondo and M. Kubo, *This Journal*, **62**, 468 (1958).

salts. It is not intended to insist upon the correctness of the models in every minor detail. For instance, the square ring of the oxalate may not be exactly rectangular and the meandering ring in the proposed crystal structure of succinate may be three-dimensional rather than coplanar as is depicted in Fig. 2. In fact, in cupric acetate monohydrate, the six nearest neighbors of a copper atom that are comprised of four oxygen atoms belonging to four different acetate groups, an adjacent copper atom and a water molecule are known<sup>6</sup> to be located not exactly on the rectangular coordinate

axes, the angles between the planes of adjacent acetate groups being 83 and 97°. In this sense, even the simple octahedral configuration about each of the copper atoms is an approximation. Still, the general features that are embodied in the discussion are adequate to explain the experimental results of the present investigation.

**Acknowledgment.**—Our grateful thanks are due to Dr. K. Hoshino, the director of the Research Laboratories of Toyo Rayon Company for a generous supply of the materials used in the present investigation.

## THE MECHANISM OF THE DECOMPOSITION OF TRICHLOROACETIC ACID IN AROMATIC AMINES

BY LOUIS WATTS CLARK

*Contribution from the Department of Chemistry, Saint Joseph College, Emmitsburg, Md.*

*Received August 7, 1958*

Kinetic data are reported on the decomposition of trichloroacetic acid in five aromatic amines, namely, aniline, *o*-toluidine, *o*-chloroaniline, quinoline and 8-methylquinoline. On the basis of the absolute reaction rate theory it is shown that a transition complex probably is formed between the electrophilic carbonyl carbon atom of the trichloroacetate ion and the unshared pair of electrons on the nucleophilic nitrogen atom of the amine. Inductive, electromeric and steric effects are all consistent with the proposed mechanism. A comparison of corresponding data for the decomposition of malonic acid in the same solvents reveals an astonishing parallelism between the two acids. For the same solvent the enthalpy of activation is lower in each case for the decomposition of trichloroacetic acid than for the decomposition of malonic acid due to the fact that the effective positive charge on the carbonyl carbon atom of the trichloroacetate ion is greater than that on the carbonyl carbon atom of malonic acid. The steric effect of the trichloromethyl group on the trichloroacetate ion is larger in each case than that of the acetic acid moiety of malonic acid.

Studies on the decomposition of trichloroacetic acid in aromatic amines have been in progress for over half a century. Silberstein<sup>1</sup> reported in 1884 that trichloroacetic acid is split into CO<sub>2</sub> and CHCl<sub>3</sub> when warmed with dimethylaniline and similar bases. Goldschmidt and Brauer<sup>2</sup> established the fact that the decomposition of trichloroacetic acid in aniline is a first-order reaction and reported measurements on the velocity at 25 and 45°. Patwardhan and Kappanna<sup>3</sup> studied the decomposition of trichloroacetic acid in aniline solution, as well as in aniline-benzene and aniline-toluene mixtures. They found that the velocity constant is dependent upon the concentration of the aniline and is proportional to the square of the concentration of the aniline molecules. Verhoek<sup>4</sup> measured the rate of decomposition of anilinium trichloroacetate in aniline and found that it increased with time, a fact which he ascribed to changes in the degree of ionization. He found that the reaction velocity is dependent upon the concentration of the trichloroacetate ion. In spite of the large amount of work which already has been carried out on this reaction it appears that the role of the solvent and the mechanism of the reaction have not as yet been explained adequately. It was thought that further insight into this problem might be gained by a comparison of the effects of different amines upon the reaction. Accordingly, experiments have been carried out in this Labora-

tory on the decomposition of trichloroacetic acid in five aromatic amines, namely, aniline, *o*-toluidine, *o*-chloroaniline, quinoline and 8-methylquinoline. The results of this investigation are reported herein.

### Experimental

**Reagents.**—(1) The trichloroacetic acid used in these experiments was reagent grade, better than 99.9% pure. (2) The solvents were reagent grade chemicals which were freshly distilled at atmospheric pressure directly into the reaction flask immediately before the beginning of each decarboxylation experiment.

**Apparatus and Technique.**—The apparatus and technique in this investigation, involving measuring the volume of CO<sub>2</sub> evolved at constant pressure, were the same as those used in studying the decarboxylation of trichloroacetic acid in glycerol.<sup>5-6</sup> The reaction flask was of 100-ml. capacity. Temperatures were controlled to within  $\pm 0.05^\circ$  and were determined by means of a thermometer calibrated by the U. S. Bureau of Standards. In each experiment a 292-mg. sample of trichloroacetic acid (the amount required to produce 40 ml. of CO<sub>2</sub> at STP on complete reaction) was introduced in the usual manner into the reaction flask containing a weighed quantity of solvent saturated with dry CO<sub>2</sub> gas. The system was filled with CO<sub>2</sub> gas to prevent atmospheric oxidation of solvent.

### Results

First-order kinetics were observed for the decarboxylation of trichloroacetic acid in each of the aromatic amines studied. In general, the experiments were carried out using 67.0 g. of solvent; however, no appreciable difference in the specific reaction velocity constant at a fixed temperature could be detected when the quantity of solvent used was varied from 40 to 70 g. Table I gives the val-

(1) H. Silberstein, *Ber.*, **17**, 2664 (1884).

(2) H. Goldschmidt and R. Brauer, *ibid.*, **39**, 109 (1906).

(3) H. W. Patwardhan and A. N. Kappanna, *Z. physik. Chem.*, **A166**, 51 (1933).

(4) F. H. Verhoek, *J. Am. Chem. Soc.*, **56**, 571 (1934).

(5) L. W. Clark, *ibid.*, **77**, 3130 (1955).

(6) L. W. Clark, *This Journal*, **60**, 1150 (1956).

ues of the apparent first-order rate constants for the reaction in the five amines at the various temperatures studied, obtained from the slopes of the experimental logarithmic plots. Arrhenius plots of the data in Table I yielded excellent straight lines in each case. The parameters of the Eyring equation are shown in Table II.

TABLE I  
APPARENT FIRST-ORDER RATE CONSTANTS FOR THE DECARBOXYLATION OF TRICHLOROACETIC ACID IN VARIOUS AMINES

Solvent	Temp. (°C. cor.)	No. of expt.	$k \times 10^4$ (sec. <sup>-1</sup> )
Aniline	66.38	4	2.91 ± 0.02
	71.50	5	5.10 ± .02
	75.59	6	7.81 ± .01
	79.65	3	12.16 ± .01
<i>o</i> -Toluidine	75.28	2	2.42 ± .02
	79.65	3	3.75 ± .03
	82.40	7	4.93 ± .02
	88.02	4	8.45 ± .01
<i>o</i> -Chloroaniline	85.33	2	1.82 ± .01
	93.51	4	3.94 ± .01
	105.32	3	11.91 ± .02
	115.58	2	28.12 ± .03
Quinoline	43.00	2	5.14 ± .01
	52.12	2	14.84 ± .02
	53.00	3	17.27 ± .02
	63.26	2	55.08 ± .02
8-Methylquinoline	52.75	3	9.42 ± .01
	63.10	2	27.83 ± .02
	73.24	2	75.86 ± .03

TABLE II  
KINETIC DATA FOR THE DECARBOXYLATION OF TRICHLOROACETIC ACID IN VARIOUS AMINES

Solvent	$\Delta H^\ddagger$ (cal.)	$\Delta S^\ddagger$ (e.u.)	$\Delta F_{900}^\ddagger$ (cal.)	$k_{920} \times 10^4$ (sec. <sup>-1</sup> )
(1) Aniline	24,500	-2.57	25,440	33
(2) <i>o</i> -Toluidine	23,800	-6.82	26,280	10
(3) <i>o</i> -Chloroaniline	24,370	-8.25	27,190	3
(4) Quinoline	23,980	-2.41	23,100	832
(5) 8-Methylquinoline	22,310	-8.43	25,370	34

### Discussion of Results

Studies on the decarboxylation of malonic acid in various amines<sup>7,8</sup> have confirmed the hypothesis of Fraenkel and co-workers<sup>9</sup> that an activated complex results from the coordination of the electrophilic carbonyl carbon atom of the undissociated diacid with the unshared pair of electrons on the nucleophilic atom of the solvent molecule. A comparison of the kinetic data for the decomposition of malonic acid<sup>7,8</sup> with that for the decomposition of trichloroacetic acid in the same five amines (Table II) reveals an interesting parallelism between the two acids, suggesting the possibility that the decomposition of trichloroacetic acid in these solvents occurs by essentially the same mechanism as does that of malonic acid. Such a comparison is shown in Table III.

In line (1) of Table III we see that, for the decom-

position of both acids,  $\Delta H^\ddagger$  as well as  $\Delta S^\ddagger$  decreases on passing from aniline to *o*-toluidine. The decrease in  $\Delta H^\ddagger$  in the case of malonic acid has been attributed to the increase in the effective negative charge on the nitrogen due to the positive inductive effect of the methyl group.<sup>7</sup> The decrease in  $\Delta S^\ddagger$  for malonic acid has been ascribed to the steric effect of the methyl group in the *ortho* position,<sup>10</sup> hindering the approach of the electrophilic carbonyl carbon atom to the unshared pair of electrons on the nitrogen.<sup>7</sup>

There is likewise a decrease in  $\Delta H^\ddagger$  and  $\Delta S^\ddagger$  in the case of both acids on going from aniline to *o*-chloroaniline (line 2 of Table III). The decrease in  $\Delta H^\ddagger$  for malonic acid in this case has been attributed to the positive electromeric effect of the halogen,<sup>7</sup> the lowering of  $\Delta S^\ddagger$  to the *ortho* effect.<sup>7,10</sup>

For both acids  $\Delta H^\ddagger$  decreases and  $\Delta S^\ddagger$  increases on going from aniline to quinoline (line 3 of Table III). The decrease in  $\Delta H^\ddagger$  for malonic acid<sup>8</sup> has been explained as being due to the fact that quinoline is slightly more basic than aniline ( $K_b$  for aniline is  $3.8 \times 10^{-10}$ , for quinoline  $6.3 \times 10^{-11}$ ).<sup>11</sup> Since the nitrogen atom in quinoline is in a somewhat more open position than it is in aniline, less steric hindrance is encountered by the electrophilic agent in quinoline than in aniline resulting in a larger value of  $\Delta S^\ddagger$ .<sup>8</sup>

For both acids a very large decrease in both  $\Delta H^\ddagger$  and  $\Delta S^\ddagger$  takes place on going from quinoline to 8-methylquinoline (line 4 of Table III). For malonic acid this has been explained on the basis of the positive inductive effect and the strong steric effect of the methyl group in the 8-position on the quinoline nucleus.<sup>8</sup>

Steric effects are produced not only by substituents on the aromatic nucleus but also by groups attached to the carboxyl group of the acid. It would be expected that the trichloromethyl group on the trichloroacetate ion would exert a larger steric effect than would the acetic acid moiety of malonic acid. That this is actually the case is revealed by the data in the last two columns of Table III. The absence of a hydrogen atom on the trichloroacetate ion probably accounts for the fact that  $\Delta S^\ddagger$  is generally somewhat higher for the decomposition of trichloroacetic acid than for that of malonic acid in these liquids.

The effective positive charge on the carbonyl carbon atom of the trichloroacetate ion is greater than that on the carbonyl carbon atom of the undissociated malonic acid, due to the strong -I effects of the three halogens and the resonance of the carboxylate group in the former. In other words, in the same solvent, the attraction between trichloroacetate ions and solvent molecules should be greater than that between malonic acid and solvent molecules. From the principle that an increase in the attraction between two reagents lowers the enthalpy of activation<sup>12</sup> it would be expected that, for the same solvent,  $\Delta H^\ddagger$  should be lower for the de-

(10) L. P. Hammett, "Physical Organic Chemistry," McGraw-Hill Book Co., Inc., New York, N. Y., 1940, p. 204.

(11) Lange's "Handbook of Chemistry," Handbook Publishers, Sandusky, Ohio, 9th edition, 1956, p. 1202.

(12) K. J. Laidler, "Chemical Kinetics," McGraw-Hill Book Co., Inc., New York, N. Y., 1950, p. 138.

(7) L. W. Clark, THIS JOURNAL, 62, 79 (1958).

(8) L. W. Clark, *ibid.*, 62, 500 (1958).

(9) G. Fraenkel, R. L. Belford and P. E. Yankwich, J. Am. Chem. Soc., 76, 15 (1954).

TABLE III

A COMPARISON OF KINETIC DATA FOR THE DECARBOXYLATION OF MALONIC ACID AND TRICHLOROACETIC ACID IN VARIOUS AMINES. CHANGE OF  $\Delta S^\ddagger$  AND  $\Delta H^\ddagger$  WITH CHANGE IN SOLVENT

Change of solvent		$\Delta(\Delta H^\ddagger)$ (cal.)		$\Delta(\Delta S^\ddagger)$ (e.u.)	
From	To	Trichloroacetic acid	Malonic acid	Trichloroacetic acid	Malonic acid
(1) Aniline	<i>o</i> -Toluidine	-700	-1200	-4.25	-2.59
(2) Aniline	<i>o</i> -Chloroaniline	-130	-320	-4.78	-2.47
(3) Aniline	Quinoline	-520	-160	+4.98	+2.09
(4) Quinoline	8-Methylquinoline	-1670	-2300	-10.84	-8.10

composition of the trichloroacetate ion than for that of malonic acid. A comparison of the data (references 7, 8 and Table II) reveals that this is actually true in each case. For the decomposition of trichloroacetic acid in aniline  $\Delta H^\ddagger$  is 2400 cal. lower than for that of malonic acid; in *o*-toluidine

1900 cal. lower; in *o*-chloroaniline 2200 cal. lower; in quinoline 2760 cal. lower; in 8-methylquinoline 2100 cal. lower.

**Acknowledgment.**—The support of this research by the National Science Foundation, Washington, D. C., is gratefully acknowledged.

## IONIZATION OF STRONG ELECTROLYTES. VII. PROTON MAGNETIC RESONANCE AND RAMAN SPECTRUM OF IODIC ACID

By G. C. HOOD, A. C. JONES AND C. A. REILLY

*Shell Development Company, Emeryville, California*

Received August 11, 1958

The proton magnetic resonance shifts and intensities of Raman lines in solutions of iodic acid have been measured and used to calculate degrees of dissociation. The thermodynamic dissociation constant is found to be 0.18 at 30° in good agreement with the results of classical measurements.

The most satisfactory methods for the determination of the degree of dissociation of strong electrolytes are based on measurements of nuclear magnetic resonance (n.m.r.) shifts or measurements of Raman intensities.<sup>1-4</sup> These methods are free of the problem of ionic interaction which is inherent in classical methods. Comparison of the results obtained by the n.m.r. and by the Raman technique showed excellent agreement.<sup>2-6</sup>

The dissociation of iodic acid has now been investigated by both the n.m.r. and the Raman methods. Iodic acid is of special interest since its thermodynamic dissociation constant of about 0.18 is approximately the upper limit of the region where classical methods can also be expected to yield meaningful dissociation constants of univalent electrolytes.<sup>1</sup> Thus a comparison of all methods is possible.

### Experimental

The samples were prepared from reagent grade iodic acid which was not further purified.

Nuclear magnetic resonance shifts were measured at 40 megacycles per second with a Varian Model V-4300 spectrometer equipped with a sample spinner and a field stabilizer. The magnetic field was swept through resonance by injecting a small voltage into the sensing circuit of the field stabilizer.

The shift of the protons in each sample relative to that of water at 30° was determined as described previously.<sup>5</sup> One important modification, however, was the use of two ref-

erence compounds. The shifts in the more concentrated solutions (down to 1.850 molar) were measured directly with respect to that of water. The shifts in the more dilute solutions were so small that they were difficult to measure directly. For these solutions the shifts were measured relative to that of the ring protons in toluene. The shift of these protons from that of water at 30° was determined in separate experiments to be  $65.5 \pm 0.1$  c.p.s. (to lower applied field). The iodic acid shifts relative to water then were calculated. This procedure allowed the determination of shifts with a precision of  $5 \times 10^{-3}$  of the resonance frequency. The magnetic susceptibility per gram  $\chi$  of each solution was determined by means of a Gouy balance. The density  $d$  of each solution also was measured and the bulk magnetic susceptibility then calculated from the relation

$$\kappa = \chi d \quad (1)$$

The Raman spectra of the solutions were obtained with a standard Cary Model 81 recording spectrometer.

**Degrees of Dissociation.**—The assumptions involved in obtaining degrees of dissociation from magnetic resonance measurements have been described previously.<sup>2</sup> The degrees of dissociation were calculated from the shifts according to

$$s = \Delta\nu/40 + g \quad (2)$$

$$g = +2.60(\kappa + 0.700) \times 10^6 \quad (3)$$

$$s/p = \alpha s_1 + (1 - \alpha)s_2 \quad (4)$$

where  $\Delta\nu$  is the measured resonance shifts in c.p.s.,  $g$  is the bulk magnetic shielding correction,  $k$  and  $-0.700 \times 10^6$  are the bulk magnetic susceptibilities of the sample and of water, respectively,  $s$  is the total chemical shift,  $s_1$  is the shift of  $\text{H}_3\text{O}^+$ ,  $s_2$  is the shift of undissociated  $\text{HIO}_3$ ,  $\alpha$  is the degree of dissociation and  $p$  is the stoichiometric mole fraction of hydrogen in  $\text{H}_3\text{O}^+$  on a total hydrogen basis.

The variation of  $s$  with  $p$  (shown in Fig. 1 for lower concentrations) is similar to that of nitric acid.<sup>2</sup> The straight line portion of the curve ( $c > 1.85$ ,  $p > 0.052$ ) is attributed to the equilibria between undissociated monomer and associated species. The curved portion of the curve ( $c < 1.85$ ,  $p < 0.052$ ) is attributed to dissociation. The situation can be seen more readily in Fig. 2 where  $s/p$  is shown as a

(1) O. Redlich, *Chem. Revs.*, **39**, 333 (1946).

(2) H. S. Gutowsky and A. Saika, *J. Chem. Phys.*, **21**, 1688 (1953); G. C. Hood, O. Redlich and C. A. Reilly, *ibid.*, **22**, 2067 (1954); **23**, 2229 (1955).

(3) O. Redlich and G. C. Hood, *Disc. Faraday Soc.*, **24**, 87 (1957).

(4) A. Krawetz, Doctoral Thesis, University of Chicago, 1955.

(5) G. C. Hood and C. A. Reilly, *J. Chem. Phys.*, **27**, 1126 (1957).

(6) O. Redlich, *Monatsh.*, **86**, 329 (1955).

TABLE I  
DISSOCIATION OF IODIC ACID

<i>c</i> , moles/l.	<i>p</i>	Susceptibility corr., <i>g</i> .	Resonance shift, <i>s</i>	Degree of dissociation, $\alpha$ (n.m.r.)	$\log a/c$	$\log K/\beta$	Raman intensity ratio, <i>R</i>	Degree of dissociation, $\alpha$ (Raman)
0.034	0.00094	-0.003	0.012	0.88	-1.710	-0.788	2.30	(0.88)
.076	.00198	-.006	.024	.80	-1.540	-.841	2.18	.86
.104	.00258	-.008	.030	.73	-1.460	-.892	2.00	.81
.160	.00427	-.01	.048	.68	-1.400	-.905	...	...
.362	.0100	-.03	.090	.39	-1.353	-1.138	1.50	.56
.662	.0183	-.05	.14	.22	-1.307	-1.279	1.33	.34
1.020	.0287	-.09	.20	.12	-1.470	-1.415	1.23	.14
1.318	.0380	-.12	.25	.08	...	...	1.22	.10
1.850	.0520	-.20	.31	0	...	...	1.19	0
3.292	.0980	-.27	.57	...	...	...	...	...
5.800	.200	-.40	1.14	...	...	...	...	...
7.53	.311	-.59	1.67	...	...	...	...	...
7.53	.324	-.60	1.70	...	...	...	...	...
0.360			Sodium iodate soln.	...	...	...	3.69	...

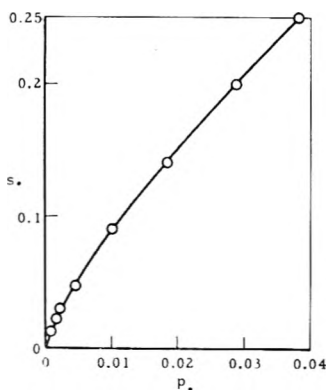


Fig. 1.—Observed chemical shift of iodine acid.

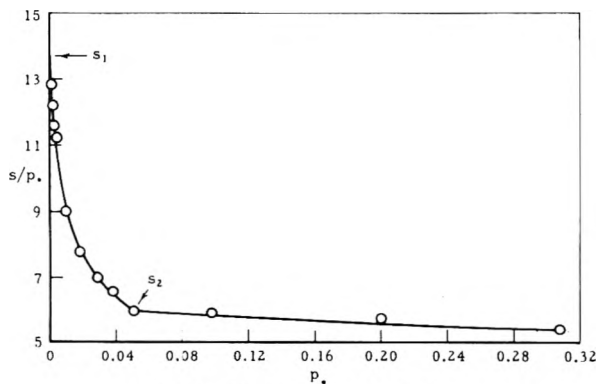


Fig. 2.—Evaluation of *s*<sub>1</sub> and *s*<sub>2</sub>.

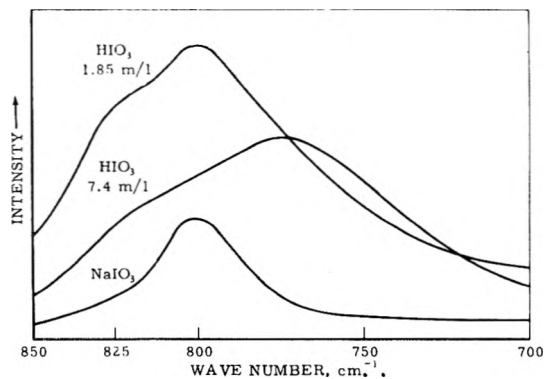


Fig. 3.—Raman spectra of iodic acid and sodium iodate.

function of *p*. This interpretation is substantiated by Raman spectral data which are discussed later.

The value 13.70 was obtained for *s*<sub>1</sub> by utilizing the expression

$$s_1 = \lim_{p \rightarrow 0} s/p \tag{5}$$

This value for the shift of H<sub>3</sub>O<sup>+</sup> is to be compared with the values 13.1, 11.8 and 9.2 determined previously<sup>23</sup> for H<sub>2</sub>SO<sub>4</sub>, HNO<sub>3</sub> and HClO<sub>4</sub> solutions, respectively. The value 3.00 for *s*<sub>2</sub> was taken directly from *s* at *c* = 1.85 where the solution appears to consist predominantly of undissociated monomeric HIO<sub>3</sub> (Table I). A small error in this value is not too serious since the degree of dissociation calculated is not particularly sensitive to *s*<sub>2</sub>.

The experimental data and the degrees of dissociation calculated from equation 4 are given in Table I.

The Raman spectra of concentrated aqueous solutions of iodic acid have bands with Raman shifts of 330, 630 and 780, with a shoulder indicating the presence of a band near 825 cm<sup>-1</sup> (Fig. 3). As the concentration of iodic acid is reduced, the 780 cm<sup>-1</sup> band shifts to 800 cm<sup>-1</sup> and as the concentration is further reduced the intensity at 800 cm<sup>-1</sup> increases relative to the shoulder at 825 cm<sup>-1</sup>. The intensity of the 630 cm<sup>-1</sup> band also decreases more rapidly than linearly with concentration below 1 molar. In the most dilute solutions examined, the spectrum is predominantly a single band at 800 cm<sup>-1</sup>. This band is also observed in solutions of NaIO<sub>3</sub> and may be ascribed to both undissociated acid and iodate ion. The rather weak band at 330 cm<sup>-1</sup> persists in spectra of all acid concentrations as well as in sodium iodate solutions. Typical spectra are given in Fig. 3.

The interpretation of the spectral changes with dilution is that the shift of the band at 780 cm<sup>-1</sup> corresponds to the equilibrium shift of associated iodic acid to undissociated monomer. The subsequent increase in intensity of the 800 cm<sup>-1</sup> band relative to that at 825 cm<sup>-1</sup> corresponds to the dissociation of iodic acid to iodate ion. These observations differ from the older data of Rao<sup>7</sup> in that at no point in the concentration interval from 7.5 to 0.03 molar is the intensity of the 825 cm<sup>-1</sup> band greater than the intensity of the 800 cm<sup>-1</sup> band as Rao reported for 6 to 3 molar solutions.

Calculation of degrees of dissociation from Raman spectra requires quantitative intensity measurements which, unfortunately, are affected by a variety of instrumental factors and sample properties.<sup>8,9</sup> In the present case, the principal sources of error in the relative intensity measurements are the effects of variations in the optical absorption and refractive index of the various solutions. One method of dealing with this situation is to consider that the spectrum of each solution is recorded on a different unknown intensity scale; therefore, although it is not possible to compare the observed intensities from different spectra, the ratios of intensities at given spectral positions may be compared.

(7) N. R. Rao, *Indian J. Phys.*, **16**, 71 (1942).  
 (8) H. J. Bernstein and G. Allen, *J. Opt. Soc. Am.*, **46**, 237 (1955).  
 (9) A. C. Jones, Doctoral Thesis, University of Chicago, 1955.



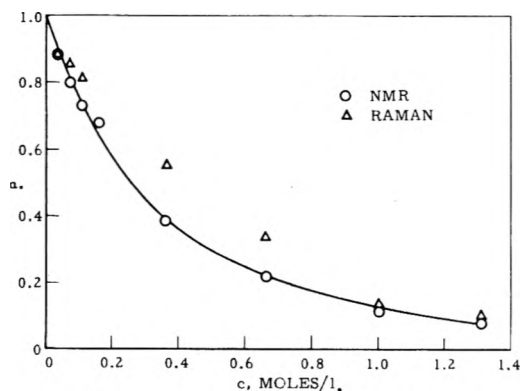


Fig. 4.—Degree of dissociation of iodic acid.

The degrees of dissociation of iodic acid can be computed from the ratio  $R$  of Raman intensities at two spectral positions (300 and 825  $\text{cm}^{-1}$ ) at which the relative contributions from  $\text{HIO}_3$  and from  $\text{IO}_3^-$  differ appreciably. If one assumes that, after the spectrum has been corrected for the presence of water and material which may contribute a flat background component, the remaining observed intensity is due only to the contributions from the species  $\text{HIO}_3$  and  $\text{IO}_3^-$ , then the intensity ratio for a given solution is

$$R = \frac{\gamma_A c_A J_{A300} + \gamma_I c_I J_{I300}}{\gamma_A c_A J_{A825} + \gamma_I c_I J_{I825}} \quad (6)$$

The symbols  $c_A$  and  $c_I$  refer to the concentrations of the undissociated acid  $\text{HIO}_3$  and  $\text{IO}_3^-$ , respectively. The specific Raman scattering coefficient  $J$  represents the intensity of the Raman emission from a solution of unit concentration of the molecular species and at the spectral position designated by the subscripts. The term  $\gamma$  represents the factor to reduce the different intensity scales of the spectra from which the respective  $J$ 's were derived to a common intensity scale, namely, that of the spectrum of the solution under consideration. Since  $c_A/c_I = (1 - \alpha)/\alpha$ , expression (7) is derived easily

$$\frac{1 - \alpha}{\alpha} = \frac{\gamma_I J_{I300} R_A}{\gamma_A J_{A300} R_I} \left( \frac{R_I - R}{R - R_A} \right) \quad (7)$$

The values of  $R_I$  and  $R_A$  were obtained from Raman spectra of solutions of  $\text{NaIO}_3$  and of the undissociated monomer acid, respectively. It has been assumed here, as in the n.m.r. analysis, that  $\text{HIO}_3$  exists as essentially undissociated monomer in the 1.85 molar solution. The ratio of  $\gamma$ 's in equation 7 can only be obtained by the assumption of the value of  $\alpha$  obtained from the n.m.r. method for one solution. The 0.034 molar solution with an  $\alpha$  of 0.88 was used. Having thus obtained the necessary parameters, the degrees of dissociation for the remaining solutions were calculated from the Raman data.

As shown in Table I and Fig. 4, the Raman data are not inconsistent with the n.m.r. data but the difficulties inherent in the Raman method in this case preclude a more quantitative comparison.

**Dissociation Constant.**—The thermodynamic dissociation constant  $K$  was determined from the n.m.r. data by extrapolation of  $\log K\beta$  to zero concentration (Fig. 5)

$$K\beta = a/c(1 - \alpha) \quad (8)$$

The symbol  $\beta$  represents the activity coefficient of undissociated iodic acid,  $a$  is the activity of iodic and  $c$  is the stoichiometric concentration in moles/l. The activities of the solutions were computed from activity coefficients deter-

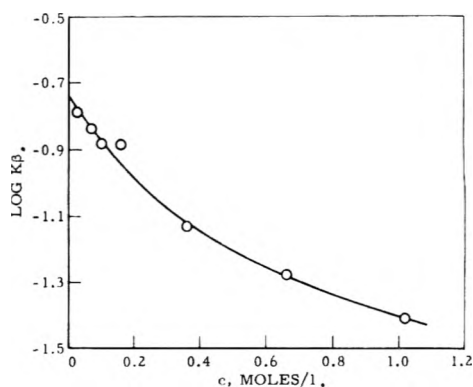


Fig. 5.—Dissociation constant of iodic acid

TABLE II  
DISSOCIATION CONSTANT OF IODIC ACID

Method	Temp., °C.	$K$	Ref.
Freezing point	0	0.262	11
Conductivity	18	.19	11
Conductivity, freezing point	25	.18	12
Conductivity	25	.17	13
Conductivity	25	.1686	14
Solubility	25	.163	15
Indicator	25	.167	16
N.m.r.	30	.18	This investigation

mined from freezing points.<sup>13</sup>

The value of 0.18 determined for  $K$  may be compared with the values obtained by classical methods (Table II).

### Conclusions

The dissociation constant 0.18 determined from n.m.r. data, and supported by Raman data, is in good agreement with previous classical determinations. As suggested earlier,<sup>1</sup> a dissociation constant of this magnitude is probably close to the limit of reliability for classical methods with univalent electrolytes. Previous data have shown that dissociation constants near unity (trifluoroacetic and heptafluorobutyric acids) are not obtainable by classical methods.<sup>2,17,18</sup>

(10) E. Abel, O. Redlich and F. Hersch, *Z. physik. Chem.*, **A170**, 112 (1934).

(11) E. Abel, O. Redlich and F. Hersch, *ibid.*, **A170**, 112 (1934).

(12) V. Rothmund and K. Drucker, *ibid.*, **46**, 827 (1903).

(13) L. Onsager, *Physik Z.*, **28**, 277 (1927).

(14) R. M. Fuoss and C. A. Kraus, *J. Am. Chem. Soc.*, **55**, 476 (1933).

(15) S. Naidich and J. E. Ricci, *ibid.*, **61**, 3268 (1939).

(16) R. von Halban and J. Brill, *Helv. Chim. Acta*, **27**, 1719 (1944); *C. A.*, **60**, 791 (1946).

(17) G. C. Hood and C. A. Reilly, *J. Chem. Phys.*, **28**, 329 (1958).

(18) T. F. Young and A. C. Jones, *Ann. Rev. Phys. Chem.*, **3**, 278 (1952).

# THE THERMAL DECOMPOSITION OF DIMETHYL PEROXIDE: THE OXYGEN-OXYGEN BOND STRENGTH OF DIALKYL PEROXIDES

BY PHILIP L. HANST AND JACK G. CALVERT

Contribution from the McPherson Chemical Laboratory, The Ohio State University, Columbus 10, Ohio

Received August 11, 1958

Dimethyl peroxide was decomposed in a static system at various temperatures and the products measured by infrared absorption spectroscopy. The decomposition is first order and approximately follows the stoichiometry  $2\text{CH}_3\text{OOCH}_3 \rightarrow 3\text{CH}_3\text{OH} + \text{CO}$ . The fact that the decomposition proceeds *via* methoxy radicals was proved by the addition of nitric oxide which led to the formation of methyl nitrite as the only major product. The presence of oxygen did not alter the decomposition seriously, although it did lead to the production of some formic acid and formaldehyde. An Arrhenius plot of the data gave an activation energy ( $\text{CH}_3\text{O}-\text{OCH}_3$  bond strength) of  $35.3 \pm 2.5$  kcal./mole which is in good agreement with the values obtained by other investigators for dimethyl peroxide and some of its homologs. Three sets of published data on the thermal decomposition of diethyl peroxide were combined in a composite Arrhenius plot to give an activation energy of 34.1 kcal./mole. This value is in fair agreement with the activation energies of decomposition of homologous dialkyl peroxides, whereas the values obtained separately in the three investigations are anomalously low.

## Introduction

Investigations of the chemical kinetics of the decomposition of a number of alkyl peroxides are reported in the chemical literature. The activation energy is an important one of the factors which have been determined; the mechanisms indicate that it is the minimum energy necessary to cause the reaction  $\text{ROOR} \rightarrow 2\text{RO}$ , and this energy is a quantity one needs in the calculation of the thermodynamic properties of alkoxy free radicals as well as in the calculation of the strengths of certain other bonds. For example, this activation energy enters importantly into the calculations reported recently by Gray.<sup>1</sup>

Summarized in Table I are some of the above-mentioned results. The most notable aspect of these data is that the activation energies do not appear to be entirely consistent with each other. That is, the values for diethyl peroxide all seem to be low compared to the others. It does not seem likely to us that a change in the hydrocarbon chain length should have such a large effect on this energy. If the effect were real, however, we feel that it should show a more consistent trend. It seemed to us that there could be two possible explanations for the apparent anomaly; either the diethyl values are all too low, or the value of 36.9 for dimethyl peroxide is too high.

In view of these considerations we undertook to measure the decomposition rate of dimethyl peroxide at various temperatures and thus get another check on the activation energy. In our opinion, the anomaly in the above table is satisfactorily corrected by the results of these experiments plus some reconsideration of the data pertaining to diethyl peroxide.

## Experimental Technique

**Thermal Decomposition of Dimethyl Peroxide.**—The decompositions were conducted in a 5-liter Pyrex flask contained in an electrically heated oven. The products of thermal decomposition were analyzed periodically by means of infrared absorption spectroscopy using 10 cm. and 1 meter gas absorption cells on Perkin-Elmer Model 21 double beam spectrophotometer. Air was added to the cells before analysis so that the total pressure was one atmosphere. Concentrations were determined by comparison to reference spectra run on pure compounds under conditions of resolution, pressure broadening and per cent. absorption as near as possible to those existing during the analysis.

A typical experiment was performed as follows. After the oven had come to thermal equilibrium at a temperature indicated by a precision thermometer, dimethyl peroxide was admitted simultaneously to the reaction flask and to the previously evacuated infrared cell. The timing of the run was then started; the initial pressure was read on a mercury manometer at room temperature, and the spectrum of the reactant was recorded. After that, the infrared cell was evacuated, and when the desired time had elapsed, the hot gases were allowed to expand out of the reaction vessel and into the infrared cell where the concentration of unreacted dimethyl peroxide and/or reaction products was measured. This sampling and analysis process was repeated to get the successive points on the curves. It was necessary to correct for the small pressure drop which occurred on expansion by multiplying each measured pressure by the ratio of the pressure at the start of the experiment to the pressure after sampling. The pressure drop was measured for each of the infrared cells in separate calibration runs using tetramethylethylene, which did not decompose at the temperatures used, and was found to be about 6% for the 10 cm. cell and about 23% for the 1 meter cell. In order to apply the correction successively, it was necessary to assume the first-order rate law. The 1 meter cell was used only in a few experiments where a single measurement was made. The temperature usually fluctuated over a range of about  $\pm 0.2^\circ$  during a run, and an average was estimated from periodic readings.

**Preparation of Dimethyl Peroxide.**—The dimethyl peroxide was prepared as follows. Ten cc. (about 0.1 mole) of dimethyl sulfate and 15 cc. (about 0.14 mole) of 30% aqueous

TABLE I

SUMMARY OF PREVIOUS RESULTS ON DECOMPOSITION OF  
DIALKYL PEROXIDES

Compd. dec.	Pre-exponential factor, <i>A</i> (sec. <sup>-1</sup> )	Activation energy (kcal./mole)	Ref.
Dimethyl peroxide	$4.1 \times 10^{16}$	36.9	2
Diethyl peroxide	$5.1 \times 10^{14}$	31.5	3
Diethyl peroxide	$2.1 \times 10^{13}$	31.7	4
Diethyl peroxide	$1.1 \times 10^{12}$	29.9	5
Di- <i>n</i> -propyl peroxide	$2.5 \times 10^{15}$	36.5	6
Di- <i>t</i> -butyl peroxide	$4 \times 10^{14}$	36	7
Di- <i>t</i> -butyl peroxide	$3.2 \times 10^{16}$	39.1	8

(1) P. Gray, *Trans. Faraday Soc.*, **62**, 344 (1956).

(2) Y. Takezaki and C. Takeuchi, *J. Chem. Phys.*, **22**, 1527 (1954).

(3) E. J. Harris and A. C. Egerton, *Proc. Roy. Soc. (London)*, **A168**, 1 (1938).

(4) R. E. Rebert and K. J. Laidler, *J. Chem. Phys.*, **20**, 574 (1952).

(5) K. Moriya, *Rev. Phys. Chem. (Japan)*, Horiba Vol., 143 (1946).

(6) E. J. Harris, *Proc. Roy. Soc. (London)*, **A173**, 126 (1939).

(7) J. Murawski, J. S. Roberts and M. Szwarc, *J. Chem. Phys.*, **19**, 698 (1951).

(8) J. H. Raley, F. F. Rust and W. E. Vaughan, *J. Am. Chem. Soc.*, **70**, 88 (1948).

hydrogen peroxide were placed in a 250-cc. 3-necked flask fitted with a stirrer, a 125-cc. dropping funnel and an outlet tube. From the dropping funnel, 20 cc. (about 0.15 mole) of 40% aqueous potassium hydroxide was added slowly with stirring and cooling in ice. The dropping funnel was then replaced with a tube leading to a nitrogen tank, a very weak flow of nitrogen was started, and the outlet tube was attached to a cold trap immersed in liquid nitrogen. Heat then was applied gently to the flask, until at about 60° the contents began to bubble smoothly, and the reaction then maintained itself. At times, some moderating with the ice-bath was necessary. The dimethyl peroxide vapors were carried in the nitrogen stream into the cold trap. When bubbling in the reaction flask had ceased, the trap containing the product was removed to the vacuum line where the volatile dimethyl peroxide was distilled into a storage bulb. This distillation served to separate the peroxide from any H<sub>2</sub>O, H<sub>2</sub>O<sub>2</sub>, etc., which may have been carried over during the preparation. The infrared spectrum of the final product showed no detectable amounts of possible contaminants. The peroxide was stored as a vapor in a clear bulb at room temperature and showed no appreciable decomposition over periods as long as one week.

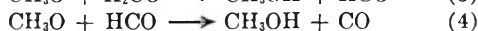
### Discussion

From the data of Fig. 1 it is seen that dimethyl peroxide decomposition is first order in the temperature range used. Takezaki and Takeuchi also found this to be the case.<sup>2</sup> The only major products were methanol and carbon monoxide. Table II shows that although the measurements were somewhat erratic, the products appeared to be in the mole ratio of approximately 3 to 1 in agreement with the over-all reaction

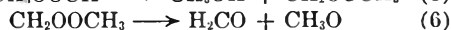
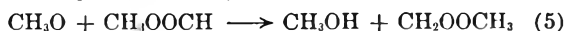


The lack of reproducibility of the measured mole ratios is believed to be due to the fact that the CO band is a very weak one and the spectrometer background noise was somewhat high. Although it was difficult to measure the amount of decomposed dimethyl peroxide accurately because of interference from the methanol, it appeared that the amount used up could be approximately accounted for in the observed products.

The products are assumed to form in the reactions



The possibility of chain decomposition of the dimethyl peroxide through the repeated occurrence of the cycle (5) and (6)



can be eliminated. This follows from the facts that formaldehyde does not build up as a final product of the reaction and the stoichiometry follows closely the relation



It appears that methoxy radicals react with the product formaldehyde in the reaction 3 to the practical exclusion of (5). In other words, the possible chain decomposition of dimethyl peroxide is self-inhibited by the formaldehyde product.

To test the mechanism 1 to 4, dimethyl peroxide was decomposed in the presence of nitric oxide with the results that methanol and CO formation was suppressed, and the only major product was

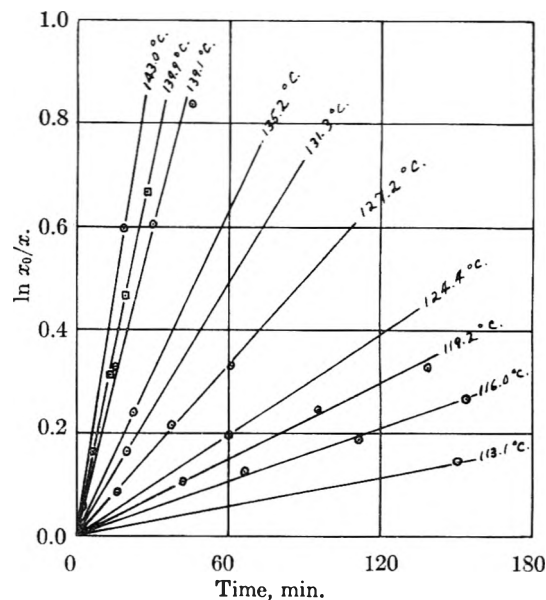


Fig. 1.—Plots of integrated first-order rate law for the thermal decomposition of dimethyl peroxide.

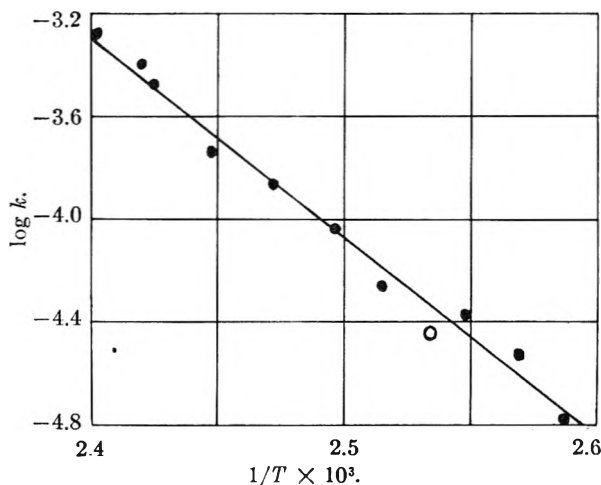


Fig. 2—Arrhenius plot for rate constants of the thermal decomposition of dimethyl peroxide.

methyl nitrite. When it was assumed that the measured amount of methyl nitrite formed was twice the dimethyl peroxide decomposed, a rate constant was obtained which was in good agreement with the rate constants calculated directly from dimethyl peroxide disappearance and from methanol formation. The open circle on the activation energy curve in Fig. 2 was obtained from this experiment with nitric oxide.

The decomposition also was conducted in the presence of oxygen, although no rate constant could be measured in this case. In the presence of the oxygen, the methanol and carbon monoxide still formed to a large extent, but in addition there appeared a small amount of formic acid and apparently a fairly good yield of formaldehyde as indicated by its infrared spectrum and by the formation of a white solid deposit on expansion of the hot gases into the infrared cell. Because of this deposit, no quantitative measurements of products were attempted. It appears likely that the large

TABLE II  
PRODUCTS OF THERMAL DECOMPOSITION OF DIMETHYL PEROXIDE

Temp. (°C.)	Starting CH <sub>3</sub> OOCH <sub>3</sub> (mm. Hg)	Elapsed time (min.)	Pressure of CH <sub>3</sub> OH (mm.)	Pressure of CO (mm.)	P <sub>CH<sub>3</sub>OH</sub> P <sub>CO</sub>
119.7	7.25	130	1.85	0.54	3.4
127.2	30.0	61	12.6	5.0	2.5
135.2	14.3	22	4.6	1.8	2.6
147	3.16	15	1.99	0.6	3.3
147	3.16	45	3.14	1.3	2.4
162	11.5	20	11.4	3.9	2.9
167 (Takezaki and Takeuchi <sup>2</sup> )	23	...	20 to 40	10	2 to 4

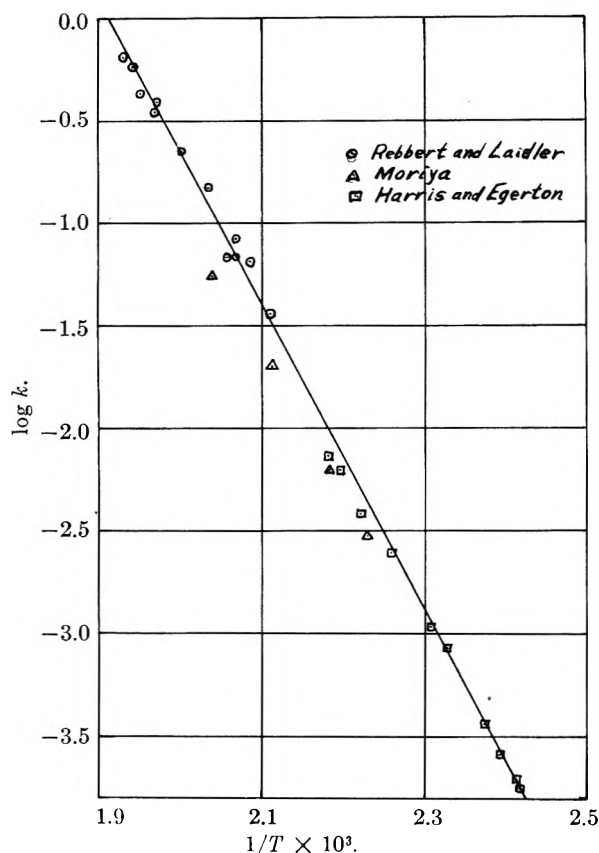


Fig. 3.—Composite Arrhenius plot for rate constants of the thermal decomposition of diethyl peroxide.

amount of formaldehyde in the experiments with added oxygen has its origin in reaction 7

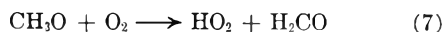


Figure 1 shows the integrated first-order rate law plots for the decomposition at the various temperatures. The measurements at 139.9° (square points) were made on the disappearance of dimethyl peroxide using its infrared band at 8.7  $\mu$ ; all others were made on the rate of formation of methanol using the OH band at 2.7  $\mu$  and assuming the stoichiometry  $2\text{CH}_3\text{OOCH}_3 \rightarrow 3\text{CH}_3\text{OH} + \text{CO}$ . A sample calculation showed that a deviation of as much

as 10% from this stoichiometry would not affect the calculated rate constants significantly.

The logarithms of the rate constants obtained from these curves (slope =  $k$ ) are plotted against  $1/T$  in Fig. 2. The slope of this curve, calculated by the least squares method, leads to an activation energy of  $35.3 \pm 2.5$  kcal./mole, where the uncertainty is twice the statistical standard deviation and represents 95% confidence limits. This value is in satisfactory agreement with the  $36.9 \pm 1.1$  kcal./mole obtained by Takezaki and Takeuchi.<sup>2</sup> The pre-exponential factor calculated from the intercept by least squares is  $1.6 \times 10^{15}$  sec.<sup>-1</sup>. The open circle obtained in the experiment with added nitric oxide was not used in these calculations.

This agreement with the results of Takezaki and Takeuchi emphasized the anomaly of the low values for diethyl peroxide shown in Table I. In view of this, we have checked the results of the three different investigations on diethyl peroxide against each other by making the combined Arrhenius plot shown in Fig. 3. This treatment has the advantage of a wider temperature range than a plot from one of the sets of data alone. The results of the different studies appear to be consistent. The least squares method of calculation applied to this curve gives an activation energy of 34.1 kcal./mole and a frequency factor of  $1.6 \times 10^{14}$  sec.<sup>-1</sup>.

In summary, we suggest the following values as the most reliable estimates of the pre-exponential factors (sec.<sup>-1</sup>) and activation energies (kcal./mole), respectively, for the four peroxides discussed: dimethyl peroxide,  $2.4 \times 10^{15}$ , 36.1 (average of our values and those of Takezaki and Takeuchi<sup>2</sup>); diethyl peroxide,  $1.6 \times 10^{14}$ , 34.1 (values taken from the combined Arrhenius plot, Fig. 3<sup>3,4,5</sup>); di-*n*-propyl peroxide,  $2.5 \times 10^{15}$ , 36.5 (Harris<sup>6</sup>); di-*t*-butyl peroxide,  $4 \times 10^{15}$ , 37.5 (average of values from Murawski, *et al.*,<sup>7</sup> and Raley, *et al.*<sup>8</sup>

**Acknowledgment.**—The authors gratefully acknowledge the financial support received from the United States Public Health Service, National Institutes of Health, Bethesda, Md., and the helpful communication with Dr. M. H. J. Wijnen.

# THE EFFECT OF CONTINUOUSLY CHANGING POTENTIAL ON THE SILVER ELECTRODE IN ALKALINE SOLUTIONS

BY THEDFORD P. DIRKSE AND DALE B. DE VRIES

*Department of Chemistry, Calvin College, Grand Rapids, Michigan*

*Received August 13, 1958*

When a silver wire is oxidized by continuously increasing its potential in alkaline solutions, four reactions take place. It is suggested that the first is due to the formation of  $\text{AgOH}$ . The others are due to the formation of  $\text{Ag}_2\text{O}$ , of  $\text{AgO}$  and of oxygen. The first and second reactions are indistinguishable in solutions having a high pH. The results show that the formation of  $\text{Ag}_2\text{O}$  is not due to the action of oxygen on silver, and the formation of  $\text{AgO}$  does not involve the  $\text{HO}_2^-$  ion.

## Introduction

When silver is electrolytically oxidized in alkaline solutions,  $\text{Ag}_2\text{O}$  is formed, then, at a higher voltage level  $\text{AgO}$  is produced. As the voltage rises still higher oxygen is evolved. There is doubt whether  $\text{Ag}_2\text{O}_3$  is formed in such a treatment. Most of the work that has been carried out in an attempt to understand the mechanism of these processes has been done by the use of a constant current technique.<sup>1-4</sup> The work reported here was carried out in an effort to shed more light on these reactions. This was done by applying a continuously increasing potential to the silver electrode. So far as could be determined, no such work on these reactions has been reported in the literature. Such results cannot be subjected to strict quantitative interpretations because of a variety of variables present, *e.g.*, convection and changing electrode surface area. However, significant qualitative conclusions can be drawn from such data.

## Experimental

The circuit employed in this work was similar to that in polarography. A Sargent Model III polarograph was used as the voltage control. It was equipped with a 0.5 r.p.m. motor to increase the voltage continuously and uniformly. The current, instead of passing through the galvanometer, was fed into a precision resistor and the voltage drop across this resistor was measured by a Brown recording potentiometer. Only relative current values were necessary in this work. An H type cell contained the electrodes. In one branch there was a saturated calomel electrode with a plug of agar and  $\text{KNO}_3$  solution in the cross piece. The other electrode was a silver wire about 2 cm. long fitted in a polystyrene holder. This electrode was the anode in all the runs. Measurements were made at room temperature and 2°. In addition to temperature, the other variables studied were: agitation, potassium hydroxide concentration and dissolved oxygen. Since rather high concentrations of potassium hydroxide were used, corrections were made for junction potentials.<sup>5</sup>

## Results

On Fig. 1 are shown results that are typical of all those that were obtained. One of the first things noted was the presence of another oxidative stage in addition to that of the formation of  $\text{Ag}_2\text{O}$ ,  $\text{AgO}$  and oxygen. This is indicated by peak a on Fig. 1. The formation of  $\text{Ag}_2\text{O}$  takes place at peak b, of  $\text{AgO}$  at c, of oxygen at d. The presence of  $\text{Ag}_2\text{O}$  and  $\text{AgO}$  at the peaks indicated was confirmed by e.m.f.

(1) R. Luther and F. Pokorny, *Z. anorg. allgem. Chem.*, **57**, 290 (1908).

(2) I. A. Denison, *Trans. Electrochem. Soc.*, **90**, 387 (1946).

(3) A. Hickling and D. Taylor, *Disc. Faraday Soc.*, No. 1, 277 (1947).

(4) P. Jones, H. Thirsk and W. F. K. Wynne-Jones, *Trans. Faraday Soc.*, **52**, 1003 (1956).

(5) T. P. Dirkse, *Z. physik. Chem., N.F.*, **5**, 1 (1955).

measurements. The evolution of oxygen was observed visually.

For each reaction, the rise in current indicates an increase in the rate of the reaction and a decrease in the current represents a decrease in the rate of the electrode reaction. For reactions a and b the decrease in rate of reaction is rather gradual and this may correspond to the gradual shutting off of the reaction due to the formation of a film of the reaction product. With reaction c the decrease in rate of reaction was very sudden. This was accompanied also by the formation of a visible film of gas (oxygen) on the surface of the electrode. As soon as this film was broken and bubbles of gas were evolved from the electrode surface, the current rose again, peak d. In some of the runs a vigorous stream of air was passed through the solution during passage of current. However, in general, the nature of the curves was unaffected by such agitation.

The effect of dissolved oxygen was observed by carrying out a run after purified nitrogen had been passed through the electrolyte for some time. Then a similar run was made after air had been bubbled through the electrolyte. It appeared that none of these phenomena was affected by the presence or absence of dissolved oxygen, see Table I. There is a little variation in the potential at which oxygen is evolved but these potentials are at best hardly reproducible in a given system. Thus it appears that none of the reactions noted involves dissolved oxygen. This indicates, *e.g.*, that in the formation of  $\text{Ag}_2\text{O}$  it is not the action of dissolved or liberated oxygen on the silver that is responsible.

TABLE I

EFFECT OF DISSOLVED OXYGEN ON POTENTIALS FOR OXIDATION OF SILVER IN KOH SOLUTIONS AT ROOM TEMPERATURE

mKOH	Soln. satd. with	Minimum potential for			
		Formation of $\text{AgOH}$	Formation of $\text{Ag}_2\text{O}$	Formation of $\text{AgO}$	Formation of $\text{O}_2$
1.0	Air	0.08	0.16	0.43	0.68
1.0	Nitrogen	.08	.16	.43	.66
1.6	Air	.12	.18	.46	.69
1.6	Nitrogen	.12	.18	.46	.68
4.9	Air	.09	.15	.41	.61
4.9	Nitrogen	.08	.15	.41	.65
13.2	Air	...	.16	.42	.57
13.2	Nitrogen	...	.15	.42	.60

The effect of KOH concentration is shown on Fig. 2. The point of interest here is that the lines representing points a', b' and c' on Fig. 1 are parallel. Except at the highest concentration these lines are also approximately parallel to that for oxy-

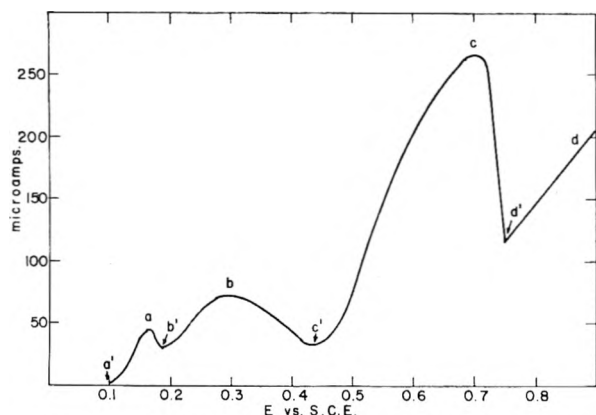


Fig. 1.—Variation of current with voltage for a silver electrode in 1.7% KOH at 2°; no agitation; voltage varied at a rate of 100 mv. per minute.

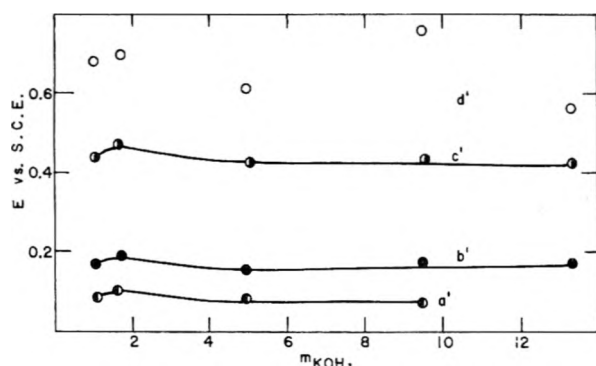
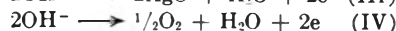
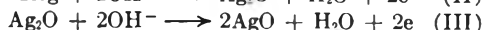


Fig. 2.—Effect of KOH concentration on the anodic processes of silver at room temperature. The letters refer to Fig. 1.

gen evolution. Thus, all of these reactions have the same dependence on hydroxyl ion concentration. This dependence can serve as a means for indicating the mechanisms for these reactions. However, it is slight except at the lower pH values. The reaction for the evolution of oxygen does involve hydroxyl ions in these alkaline solutions. It should be noted that the points on Fig. 2 represent the minimum voltage at which these processes or reactions begin under these conditions.

Since these reactions appear to have the same dependence on the hydroxyl ion concentration, the mechanisms likely also are similar. Reactions I-IV show such similarity and (II), (III) and (IV) are generally accepted as the equilibrium reactions. If these were the rate controlling electrochemical reactions one might expect a greater hydroxyl ion



dependence than is actually observed. However, in the most dilute solutions there is such dependence and as the concentration of KOH increases the number of hydroxyl ions is so large that they are no longer a limiting factor and an increase in concentration does not materially add to the number "available" for reaction. Arguing by analogy, *i.e.*, similarity in variation of voltage with hydroxyl ion concentration, reaction I likely represents the reaction taking place at a in Fig. 1.

The reaction at peak a appears to be something hitherto unreported. It was accompanied in each case by a slight discoloration of the silver electrode. It disappeared at the highest KOH concentration used, or it occurred at a potential so close to that of the formation of  $\text{Ag}_2\text{O}$  that it was not discernible. To investigate this further, the applied voltage was held at that of peak a for some 30 minutes in 5 *m* KOH, and then the potential of the silver electrode was measured against the S.C.E. with a potentiometer. The results are shown in Table II, together with the potentials of the other peaks. Whatever is formed at peak a does give rise to a distinct potential value.

TABLE II  
POTENTIAL OF VARIOUS SILVER PRODUCTS  
IN 5 *M* KOH

Substance	<i>E</i> vs. S.C.E., v.
Ag wire	+0.028
Peak a	+ .052
$\text{Ag}_2\text{O}$	+ .067
AgO	+ .311

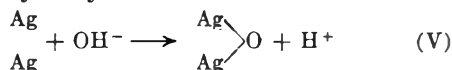
An attempt was also made to determine the X-ray diffraction pattern of this substance. A larger (1 × 4 cm.) sheet silver electrode was held at a voltage of +0.32 v. *vs.* a Hg-HgO electrode in 23% KOH. This voltage corresponded to that of peak a. The Hg-HgO electrode was used in order to eliminate the anions other than  $\text{OH}^-$ , and to eliminate the resistance due to the fritted glass disk and agar plug. Because of the larger silver electrode a larger cell was used and the electrodes were farther apart. Even with this arrangement the current passed was only a few microamps. The silver electrode was held at the potential mentioned for 2 days. During this time the electrode became discolored and the current decreased from 2 microamps to 0. The electrode then was rinsed quickly in distilled water, dried with filter paper and X-rayed. The results, however, were the lines for silver and only silver. In fact, the silver pattern was a better one than that obtained before this treatment. The discolored area also had a smoother appearance under the microscope than did the untreated area. It appears that the "high" points on the silver surface were attacked to form  $\text{Ag}^+$  ions or  $\text{AgOH}$ , and the  $\text{AgOH}$  dissolved in the electrolyte. The discoloration of the electrode, then, was not due so much to a deposit of  $\text{AgOH}$  on the electrode as to the "smoothing" of the electrode surface by this action.

On the basis of the evidence it seems likely that peak a corresponds to reaction I. The similarity in dependence on hydroxyl ion concentration between this reaction and reactions II and III is thus accounted for. The potential set up by the reaction at peak a is then the potential between the silver in the electrode and the dissolved  $\text{AgOH}$  in the electrolyte, whereas that at peak b is the potential between the Ag and the  $\text{Ag}_2\text{O}$  both in the electrode. The  $\text{AgOH}$  likely exists in solution as  $\text{Ag}(\text{OH})_2^-$  or  $\text{AgO}^-$ . As soon as the film of electrolyte next to the surface of the electrode has a certain amount of this species dissolved in it the reaction slows down and the current decreases.

Since KOH solutions absorb  $\text{CO}_2$  very readily it is conceivable that a film of  $\text{Ag}_2\text{CO}_3$  could be formed on the electrode. However, it is unlikely that this happens at peak a because the voltage needed for the formation of such a film in basic solutions is about 130 mv. greater than that required for the formation of  $\text{Ag}_2\text{O}$ .<sup>6</sup> Furthermore, the presence of such a film probably would have been detected in the X-ray diffraction patterns.

If peak a were due solely to the charging of the double layer it is difficult to account for the discoloration of the electrode.

The discussion above, in terms of reactions I-III, has dealt with equilibrium conditions and the potentials for these conditions. The mechanisms of these processes, however, need not correspond to these reactions. The fact that the hydroxyl ion dependence for each of these processes is similar to the others indicates a similarity of mechanisms. The simplest mechanism would involve a single hydroxyl ion. As the potential of the silver becomes more positive it attracts the hydroxyl ions to it and may form  $\text{AgOH}$  or  $\text{AgO}^-$  and  $\text{H}^+$ , the latter immediately combining with another hydroxyl ion to form  $\text{H}_2\text{O}$ . As the potential of the silver becomes still more positive, not only are hydroxyl ions attracted to the silver but the charge on the silver is sufficient to separate the oxygen from the hydrogen in the hydroxyl ion and the  $\text{H}^+$  can then unite



with an  $\text{OH}^-$  ion to form  $\text{H}_2\text{O}$ . This reaction continues until the surface is covered with  $\text{Ag}_2\text{O}$ . The addition of  $\text{O}^-$  ions into the silver lattice also reduces the positive charge on the surface. Consequently, in order to continue the introduction of oxygen into the lattice the potential of the electrode (or the surface) must be increased still further. This can be done by, in effect, removing a second electron from each silver atom. This then, by the same type of action as described above, introduces another  $\text{O}^-$  ion into the lattice forming a surface layer of  $\text{AgO}$ . As the potential becomes increasingly positive the reaction continues but since no more oxygen atoms or ions can be accommodated in the electrode lattice under these conditions, the liberated oxygen is evolved. It is possible also that when the potential of the electrode surface is sufficiently high the  $\text{HO}_2^-$  ion may be formed and decompose to produce the oxygen.

The formation of a layer of  $\text{Ag}_2\text{O}$  also increases the electrical resistance of the electrode surface.<sup>7</sup> As this layer is built up the current passed through the system at a given potential decrease.

While the effect of agitation was very slight, it did modify the voltage necessary to begin all these reactions very slightly, but only in the most dilute solutions used. In those solutions, where the concentration of the hydroxyl ions is so small, the agitation may disturb the migration of these ions to the electrode, necessitating a slightly higher voltage for causing these reactions to begin. This was the effect observed.

(6) W. M. Latimer, "Oxidation Potentials," Prentice-Hall, Inc., New York, N. Y., 1952, 2nd Ed., p. 191.

(7) M. Le Blanc and H. Sachse, *Physik. Z.*, **32**, 887 (1931).

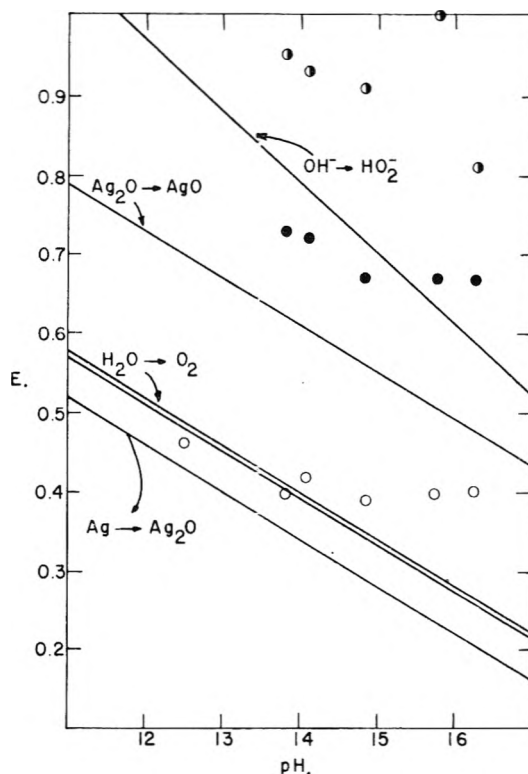


Fig. 3.—Potential-pH diagram for silver and its oxides at 25°C: O, voltages at which formation of  $\text{Ag}_2\text{O}$  begins; ●, voltages at which formation of  $\text{AgO}$  begins; ●, voltages at which oxygen is evolved.

The temperature effect over the range studied is small, but most pronounced at lower KOH concentrations. This may be due to the greater viscosity of such solutions at the lower temperature. As the concentration increases, the viscosity also increases, but no appreciable change in voltage is necessary to start these reactions at the higher concentrations. This may be due to the fact that the effect of higher viscosity is offset by the increased number of hydroxyl ions. Since only a surface film of the oxides is formed in this method there are sufficient hydroxyl ions at the surface for reaction at these higher KOH concentrations and little migration of these ions is necessary.

Further information regarding the mechanisms of these reactions can be obtained by reference to Fig. 3, which is a modification of data published earlier.<sup>8</sup> The lines plotted here represent reversible potentials for the reactions indicated. The pH values were determined by using the data of Akerlof and Bender.<sup>9</sup> The data for the  $\text{HO}_2^-$  ion were obtained from ref. 6, p. 45. The two lines for the evolution of  $\text{O}_2$  represent the variation of potential as the pressure of  $\text{O}_2$  varies from 0.2 to 1.0 atm.

At the lower pH values the formation of  $\text{Ag}_2\text{O}$  from Ag takes place at potentials lower than that for the formation of oxygen. Hence the production of  $\text{Ag}_2\text{O}$  here is not by means of the action of oxygen on silver. At higher pH values the forma-

(8) P. Delahay, M. Pourbaix and P. Van Rysselberghe, *J. Electrochem. Soc.*, **98**, 65 (1951).

(9) G. C. Akerlof and P. Bender, *J. Am. Chem. Soc.*, **70**, 2366 (1948).

tion of  $\text{Ag}_2\text{O}$  does take place at potentials above that for the formation of oxygen but there is no evidence that the mechanism here is different from that at the lower pH values.

Similar reasoning shows that the formation of  $\text{AgO}$  from  $\text{Ag}_2\text{O}$  does not involve the  $\text{HO}_2^-$  ion.

However, the mechanism of the formation of oxygen may involve this ion, but this is a subject that will be dealt with in a later paper.

**Acknowledgment.**—The authors wish to express appreciation to the Research Corporation for a grant which made this work possible.

## THERMODYNAMICS OF AQUEOUS BENZOIC ACID AND THE ENTROPY OF AQUEOUS BENZOATE ION

BY LEVERNE P. FERNANDEZ AND LOREN G. HEPLER

Contribution from Cobb Chemical Laboratory, University of Virginia, Charlottesville, Va.

Received August 14, 1958

Calorimetric investigations of the heats of solution of sodium benzoate in water and dilute acid have been carried out at 10, 25 and 40°. Heats of ionization of aqueous benzoic acid at each of these temperatures have been calculated from the results of these calorimetric experiments. The heats of ionization have been used to calculate the change in heat capacity on ionization. Results of earlier investigations of the ionization constant of aqueous benzoic acid have been combined with our data to give the entropy of ionization and thereby have made it possible for us to derive a thermodynamic equation for the ionization constant of aqueous benzoic acid as a function of temperature. From solubility data in the literature we have calculated the free energy, heat and entropy of solution of benzoic acid. These data have been used with the above mentioned data to calculate the free energies and heats of formation and entropies of aqueous benzoic acid and benzoate ion and the heat of formation of crystalline sodium benzoate (all in the standard state at 298°K.).

Jones and Parton<sup>1</sup> have reported thermodynamic ionization constants of aqueous benzoic acid at several temperatures and have calculated heats of ionization ( $\pm 150$  cal./mole) at several temperatures. Heats of ionization of aqueous benzoic acid also have been determined calorimetrically by Cottrell, *et al.*,<sup>2</sup> at 10, 20 and 30°. These heats are in only fair agreement with those reported by Jones and Parton.<sup>1</sup> The change in heat capacity on ionization ( $\Delta C_p^0$ ) as calculated from these heats<sup>2</sup> is not in agreement with  $\Delta C_p^0$  given by Jones and Parton.<sup>1</sup>

Jones and Parton have also calculated (with incorrect results) from solubility data in the literature the entropy of solution of benzoic acid and have combined this entropy of solution with their entropy of ionization and an old value for the entropy of crystalline benzoic acid to obtain the entropy of aqueous benzoate ion.

We have determined calorimetrically the heat of ionization of aqueous benzoic acid at 10, 25 and 40°. These heats have been used with data from the literature to calculate several free energies and heats of formation and entropies and to derive a thermodynamic equation for the ionization constant of aqueous benzoic acid in the temperature range 10–40°.

### Experimental

The solution calorimeter used in this investigation has been described in detail.<sup>3,4</sup> Because of the small heats with which this investigation was concerned, particular care was used in determining the heat effects associated with stopping the calorimeter stirrer for a few seconds (known  $\pm 0.5$  second) and the simultaneous breaking of the sample bulb attached to the stirrer.

(1) A. V. Jones and H. N. Parton, *Trans. Faraday Soc.*, **48**, 8 (1952).

(2) T. L. Cottrell, G. W. Drake, D. L. Levi, K. S. Tully and J. A. Wolfenden, *J. Chem. Soc.*, 1016 (1948).

(3) C. N. Muldrow, Jr., and L. G. Hepler, *J. Am. Chem. Soc.*, **79**, 4045 (1957).

(4) R. L. Graham and L. G. Hepler, *ibid.*, **78**, 4846 (1956).

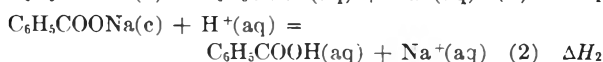
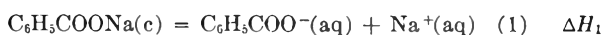
Sodium benzoate, Baker and Adamson U.S.P. grade, was recrystallized at least twice from ethanol-water mixtures. Recrystallized sodium benzoate was dried at 150° and stored in a desiccator. Analysis of this sodium benzoate was by titration with perchloric acid in glacial acetic acid with methyl violet used as indicator.<sup>5</sup> Perchloric acid for this purpose was standardized by titration against potassium acid phthalate in glacial acetic acid.<sup>6</sup> Various samples of sodium benzoate were found to require for neutralization 99.5–99.7% of the calculated amount of  $\text{HClO}_4$ .

Hydrochloric acid solutions were prepared and standardized by common methods.

All of the calorimetric experiments were carried out with 950 ml. of solution in the calorimeter vessel at  $10.0 \pm 0.4^\circ$ ,  $25.0 \pm 0.3^\circ$  or  $40.0 \pm 0.5^\circ$ .

### Results and Calculations

Heats of reactions 1 and 2 at 10, 25 and 40° were measured over a range of concentrations in dilute solution.



Heat and concentration data for the 25° experiments are given in Tables I and II. The standard heats of reaction 1,  $\Delta H_1^0$ , at 10, 25 and 40° were determined graphically ( $\Delta H_1$  plotted *vs.*  $m^{1/2}$ ) by extrapolating the experimental heats to zero concentration dissolved sodium benzoate. In making these extrapolations we were guided by experimental heats of dilution of other electrolytes and by the Debye-Hückel limiting law as well as by our own data. The standard heats of reaction 2,  $\Delta H_2^0$ , at 10, 25 and 40° also were determined graphically by extrapolating to zero concentration. All of these reactions were carried out in such dilute solutions that all heats of dilution were small.

The values we have found for  $\Delta H_1^0$  and  $\Delta H_2^0$  at 10, 25 and 40° are given in Table III. Uncertainties listed in Table III are our estimates of the un-

(5) I. Kashima, *Bull. Natl. Hyg. Lab. (Tokyo)*, **72**, 145 (1954); *C. A.*, **49**, 7186g (1955).

(6) W. Seaman and E. Allen, *Anal. Chem.*, **23**, 592 (1951).



TABLE I

HEAT OF SOLUTION OF SODIUM BENZOATE AT 25°		
Moles C <sub>6</sub> H <sub>5</sub> COONa/ 950 ml.	Moles/liter added NaOH soln.	$\Delta H_1$ (cal./mole C <sub>6</sub> H <sub>5</sub> COONa)
0.00837	0.01039	-526
.01427	.001039	-515
.01538	.001039	-500
.02034	.02558	-526
.02675	.002558	-489
.03390	.001279	-494
.03649	.002558	-498
.03864	.001039	-507

TABLE II

HEAT OF REACTION OF C<sub>6</sub>H<sub>5</sub>COONa(c) WITH HCl (aq) AT 25°

Moles C <sub>6</sub> H <sub>5</sub> COONa/ 950 ml.	HCl, M	$\Delta H_2$ (cal./mole C <sub>6</sub> H <sub>5</sub> COONa)
0.002201	0.03354	-679
.006369	.09777	-637
.007916	.09777	-657
.009033	.02444	-662
.009952	.02444	-630
.01133	.08386	-670
.01195	.04889	-635
.01259	.02444	-662
.01419	.02444	-675
.01938	.08386	-643
.01968	.03354	-643
.01989	.04889	-633
.02047	.09777	-639
.02122	.04889	-645
.02857	.09777	-645

certainties for these reactions at the specified temperatures. These uncertainties include contributions from our experimental measurements and from the extrapolations to infinite dilution.

TABLE III

STANDARD HEATS OF REACTIONS 1 AND 2 AT 10, 25 AND 40°		
Temp. (°C.)	$\Delta H_1^0$ (cal./mole)	$\Delta H_2^0$ (cal./mole)
10	-665 ± 65	-1450 ± 95
25	-565 ± 35	-670 ± 35
40	-240 ± 40	+ 225 ± 40

The ionization of benzoic acid in aqueous solution may be written as in equation 3. We see that  $C_6H_5COOH(aq) = C_6H_5COO^-(aq) + H^+(aq)$  (3)  $\Delta H_3^0 = \Delta H_1^0 - \Delta H_2^0$ , and therefore calculate that  $\Delta H_3^0 = +785 \pm 110$ ,  $+105 \pm 40$  and  $-465 \pm 50$  cal./mole at 10, 25 and 40°, respectively. Because  $\Delta H_3^0$  is the difference in two heats determined in the same way so that systematic errors at least partly cancel, the uncertainty in  $\Delta H_3^0$  is considerably less than the sum (or the square root of the sum of the squares) of the uncertainties in  $\Delta H_1^0$  and  $\Delta H_2^0$ .

Jones and Parton<sup>1</sup> have given an empirical equation for the heat of ionization of aqueous benzoic acid as a function of temperature and have calculated the values for  $\Delta H_3^0$  given in Table IV. We also have listed in Table IV our calorimetric heats of ionization and those of Cottrell, *et al.*<sup>2</sup> The estimates of uncertainties for the heats of ionization determined by Cottrell, *et al.*, and Jones and Par-

ton are theirs. We believe the estimates of Cottrell, *et al.*, may be a bit optimistic.

TABLE IV

HEATS OF IONIZATION OF AQUEOUS BENZOIC ACID (CAL./MOLE)

Temp. (°C.)	Cottrell, <i>et al.</i>	Jones and Parton	Present
10	+622 ± 60		+785 ± 110
20	+295 ± 60	+338 ± 150	
25		+104 ± 150	+105 ± 40
30	-68 ± 60	-143 ± 150	
35		-390 ± 150	
40			-465 ± 50

The thermodynamic equation for the temperature dependence of  $\Delta H^0$ ,  $d\Delta H^0/dT = \Delta C_p^0$ , has been used to evaluate  $\Delta C_p^0$  for the ionization of aqueous benzoic acid. We have plotted all of the  $\Delta H_3^0$  values in Table IV (indicating the uncertainty associated with each  $\Delta H_3^0$  value) vs. the temperature and have concluded that  $\Delta C_p^0 = -40 \pm 4$  cal./mole degree. Neither the equilibrium data nor the calorimetric data are sufficiently accurate to justify considering  $\Delta C_p^0$  to be anything more elaborate than a constant  $\pm 4$  cal./mole degree.

The ionization constant of aqueous benzoic acid has been investigated many times at 25°. On the basis of some of the investigations that appear to be the best, namely, those of Jones and Parton,<sup>1</sup> Brockman and Kilpatrick,<sup>7</sup> Saxton and Meier<sup>8</sup> and Dunsmore and Speakman<sup>9</sup> we have chosen  $6.29 \times 10^{-5}$  for the thermodynamic ionization constant of aqueous benzoic acid at 25°. We, therefore, calculate that the standard free energy of ionization of aqueous benzoic acid is 5732 cal./mole at 298.15°K. and taking  $\Delta H_3^0 = 105$  cal./mole we calculate that the standard entropy of ionization is -18.9 cal./deg. mole.

We know from thermodynamics that  $\Delta H^0 = \Delta H_0 + \Delta C_p^0 T$  and  $\Delta S^0 = \Delta S_0 + \Delta C_p^0 \ln T$  and have evaluated the constants of integration,  $\Delta H_0$  and  $\Delta S_0$ , from our values for  $\Delta H_3^0$  and  $\Delta S_3^0$  at 298°K. and our  $\Delta C_p^0$ . By combining these results with the thermodynamic expressions  $\Delta F^0 = -RT \ln K = \Delta H^0 - T\Delta S^0$ , we have derived equation 4

$$\log K = 54.427 - 2629/T - 20.13 \log T \quad (4)$$

which gives  $\log K$  (ionization constant of benzoic acid) as a function of temperature. We have found that this equation reproduces the experimental equilibrium constants satisfactorily. There is no justification for using a more complicated expression for  $\log K$  (which is equivalent to using  $\Delta C_p^0 = f(T)$ ). Pitzer<sup>10</sup> previously has used and justified an equation of the form of our 4 to represent the temperature dependence of  $\log K$ . Our observations that  $\Delta S^0$  and  $\Delta C_p^0$  of ionization of benzoic acid are -18.9 cal./mole and -40 cal./deg. mole are in accord with Pitzer's<sup>10</sup> generalizations about  $\Delta S^0$  and  $\Delta C_p^0$  of ionization of weak acids.

The free energy and heat of formation and en-

(7) F. G. Brockman and M. Kilpatrick, *J. Am. Chem. Soc.*, **56**, 1483 (1934).

(8) B. Saxton and H. F. Meier, *ibid.*, **56**, 1918 (1934).

(9) H. S. Dunsmore and J. C. Speakman, *Trans. Faraday Soc.*, **50** 236 (1954).

(10) K. S. Pitzer, *J. Am. Chem. Soc.*, **59**, 2365 (1937).

ropy of crystalline benzoic acid are all accurately known.<sup>11</sup> We therefore needed to know the standard free energy, heat and entropy of solution of benzoic acid in water in order to make the fullest use of our thermodynamic data for the ionization of benzoic acid. The solubility of benzoic acid in water has been determined at various temperatures by several investigators<sup>12-14</sup> and these data provide the means of calculating the desired free energy, heat and entropy of solution. The reported solubilities represent the *total* concentration of benzoic acid, dissociated and undissociated, in saturated solution. From these total solubilities and ionization constants at the corresponding temperatures we have calculated the concentrations of undissociated benzoic acid present in the saturated solutions.

Following Jones and Parton<sup>1</sup> we have calculated as a first approximation the standard free energy of solution of benzoic acid in water, as in equation 5, from the relation  $\Delta F^0 = -RT \ln S$



where  $S$  is the concentration of undissociated benzoic acid in the saturated solution. This treatment, which is based on the assumption that the activity coefficient of benzoic acid is unity at each temperature considered, leads to  $\Delta F_5^0 = 2150$  cal./mole,  $\Delta H_5^0 = 6200$  cal./mole and  $\Delta S_5^0 = 13.5$  cal./deg. mole. Jones and Parton<sup>1</sup> erred in this calculation in that they used the wrong total solubility at 35° and transposed two numbers in the 25° solubility given in their paper and used in their calculation.

A more exact treatment has been carried out by Paul<sup>15</sup> who has avoided making the assumption that all activity coefficients are unity. His treatment, based on  $\Delta H_5^0 = 6500$  cal./mole, leads to an activity coefficient of 0.94 for benzoic acid in saturated solution at 25°. This activity coefficient combined with the concentration of undissociated

benzoic acid in saturated solution at 25° gives a value for the activity of benzoic acid in agreement with that found by Kolthoff and Bosch<sup>16</sup> and leads to  $\Delta F_5^0 = 2160$  cal./mole. This free energy with the above heat leads to  $\Delta S_5^0 = 14.5$  cal./deg. mole. We also have carried out a treatment of the solubility data similar to the second method described by Paul<sup>15</sup> and have found values for the free energy, heat and entropy of solution between those already given. We therefore choose  $\Delta F_5^0 = 2160$  cal./mole,  $\Delta H_5^0 = 6400$  cal./mole and  $\Delta S_5^0 = 14$  cal./deg. mole.

We have used our thermodynamic data for the solution and ionization of benzoic acid with Bureau of Standards data of Furukawa, *et al.*,<sup>11</sup> on crystalline benzoic acid to calculate standard free energies and heats of formation and entropies of aqueous benzoic acid and benzoate ion. We also have calculated the heat of formation of crystalline sodium benzoate from our heats of formation of aqueous benzoic acid and benzoate ion and heats of reactions 1 and 2. All of these thermodynamic quantities (298°K.) are given in Table V.

TABLE V  
SUMMARY OF FREE ENERGIES AND HEATS OF FORMATION AND ENTROPIES (298°K.)

Substance	$\Delta F_5^0$ (kcal./ mole)	$\Delta H_5^0$ (kcal./ mole)	$\bar{S}_5^0$ (cal./ deg. mole)
$\text{C}_6\text{H}_5\text{COOH}(aq)$	-56.5	-85.7	54
$\text{C}_6\text{H}_5\text{COO}^-(aq)$	-50.7	-85.6	35
$\text{C}_6\text{H}_5\text{COONa}(c)$		-142.3	

Uncertainties in the free energies given in Table V are less than 0.1 kcal./mole and uncertainties in the heats and entropies are about 0.3 kcal./mole and 1 cal./deg. mole. Almost all of these uncertainties should be attributed to difficulty in the thermodynamic interpretation of the solubility data.

**Acknowledgment.**—It is a pleasure to acknowledge financial support of this research by the National Science Foundation. We also are grateful to R. L. Graham, C. N. Muldrow, Jr., and J. G. Spencer for their assistance with some of the calorimetric experiments.

(11) G. T. Furukawa, R. E. McCoskey and G. T. King, *J. Research Natl. Bur. Standards*, **47**, 256 (1951).

(12) F. Hoffman and K. Langbeck, *Z. physik. Chem.*, **51**, 385 (1905).

(13) G. M. Goeller and A. Osol, *J. Am. Chem. Soc.*, **59**, 2132 (1937).

(14) T. J. Morrison, *Trans. Faraday Soc.*, **40**, 43 (194 ).

(15) M. A. Paul, *J. Am. Chem. Soc.*, **75**, 2513 (1953).

(16) I. M. Kolthoff and W. Bosch, *THIS JOURNAL*, **36**, 1685 (1932).

# EFFECTS OF ELECTROLYTES AND TEMPERATURE ON THE SOLUBILITY OF TRIBUTYL PHOSPHATE IN WATER<sup>1</sup>

BY C. E. HIGGINS, W. H. BALDWIN AND B. A. SOLDANO

*Contribution from the Chemistry Division, Oak Ridge National Laboratory, Oak Ridge, Tennessee*

*Received August 18, 1958*

The solubility of tributyl phosphate in water and electrolyte solutions of variable concentration has been measured at temperatures ranging from 5 to 50° through the use of phosphorus-32 labeled TBP. The Setschenow equation is obeyed over a wide concentration range for all the salts studied. Although the solubility decreases markedly with increasing temperature, the salting coefficient  $k_s$  is almost temperature independent. The linearity and equality of slope of the  $k_s$  vs.  $1/T$  curves for most of the salt systems studied indicates that the term  $\lambda/D_s$  in the limiting Debye-McAulay equation is a constant independent of temperature. Consistent with Rothmund, the changes of  $k_s$  with temperature can be ascribed to a small  $\Delta H$  effect indicative of an invariant of water or the organic. The salting coefficients at 25° for all the electrolytes tested, excepting nitrates, are correlated with the Gurney unitary partial molal electrolyte entropy concept.

The tributyl phosphate<sup>2a</sup> molecule, a large polar basic non-electrolyte<sup>2b</sup> with a highly local specificity for one molecule of water<sup>3</sup> is an interesting and useful solvent for the investigation of aqueous organic-salt interactions. Its low solubility in water (~0.4 g. per liter at 25°) considerably reduces the complications that may arise in the interpretation of its activity coefficients in aqueous solutions. The development of synthetic techniques for the labeling of TBP<sup>4,5</sup> with radioactive phosphorus-32 has facilitated the investigation of the physical chemical behavior of such aqueous systems.

Concerning the problem of studying the effects of salts on the solubility of TBP in aqueous solutions, the general techniques, theories and thermodynamics employed in such ternary phase problems have been ably summarized in two excellent review articles.<sup>6,7</sup>

Only a small amount of data, however, is available relative to the salting out characteristics of tributyl phosphate in aqueous solutions. Moreover, the available data pertain, for the most part, solely to nitrate systems at one temperature,<sup>5,8,9</sup> a highly understandable factor when one realizes that most of the emphasis on TBP has been in the area of practical separations. A rather detailed study using a large variety of electrolytes at several temperatures was therefore deemed essential.

Our ultimate objective, however, was to determine what common factors existed between the salting out behavior of TBP in dilute aqueous

solutions and the usual conditions under which this solvent is employed: namely, all TBP containing a varying amount of hydrated electrolytes. This latter phase of the present study will be considered in Part II<sup>3</sup> of this work.

## Experimental

**Materials.**—All reagents were C.P. grade. Solutions of hydrobromic and hydriodic acids were made from freshly distilled acids.

Standardization of solutions (both before and after equilibration) was made by electrometric titration with a Fisher Titrimeter. Acids were analyzed with standard sodium hydroxide, silver nitrate was standardized against dry potassium chloride, and the halide solutions were titrated with standard silver nitrate.

Tributyl phosphate-P<sup>32</sup> (TBP-P<sup>32</sup>) was prepared in 85% yield by the ester interchange between redistilled tributyl phosphate and anhydrous phosphoric acid-P<sup>32</sup> as reported elsewhere.<sup>4b</sup> The TBP-P<sup>32</sup> used for practically all the determinations had a specific activity of 40 to 50  $\mu$ c. per millimole at the start and was discarded after decaying to about 3  $\mu$ c./mmole. Before testing with electrolyte solutions each batch of TBP-P<sup>32</sup> was water washed at 25° until constant activity in the aqueous phase was obtained. The first washes were higher in activity than those of subsequent equilibrations. Usually only four or five equilibrations were necessary. However, some TBP-P<sup>32</sup> batches required more washes than others. Equilibration of the labeled ester with 1 M sodium hydroxide for several hours, followed by water washes, effectively reduces the number of passes required to attain constant activity in the aqueous phase.

**Equilibration.**—A rate of solubility attainment study showed that equilibrium was reached in 5 to 10 minutes when the samples were tumbled at 20 r.p.m. in the constant temperature bath at 25°. In all solubility tests the equilibration mixture (one-half to one ml. water washed TBP-P<sup>32</sup> plus 10 ml. of electrolyte solution in glass stoppered mixing cones of about 15-ml. capacity) was adjusted to the temperature of the bath, stoppered and tumbled in the bath at the desired temperature for one-half to one hour.

**Phase Separation.**—It was found experimentally that solubility could be measured with a higher degree of accuracy by allowing the tubes to stand upright in the bath for one hour to effect phase separation. The settling technique was adopted rather than that of centrifugation since the latter technique invariably resulted in an increase in the temperature of the solution, thereby upsetting the solution equilibrium. Samples at 25° centrifuged 5, 10 and 30 minutes had temperatures of 27, 29 and 33°, respectively, with corresponding solubilities of 400, 386 and 350 mg. TBP per liter of water compared with the 422 mg. per liter found at 25° using the settling technique.

Excellent phase separation was ensured through the use of sample tubes thoroughly cleaned in hot sulfuric acid. In ordinary cleaned glassware TBP droplets clung to the walls.

The aqueous (bottom) layer was removed with a 15-ml. pipet having a drawn out tip. The sample containers and transfer pipets were adjusted to the temperature of the bath before transfer of the sample. In most cases the samples were stored in stoppered tubes in the bath overnight to ensure complete separation before analysis.

(1) This paper is based on work performed for the United States Atomic Energy Commission at the Oak Ridge National Laboratory operated by Union Carbide Corporation.

(2) (a) Tri-*n*-butyl phosphate, hereafter called TBP, is an ester having the structure  $\begin{array}{c} \text{O} \\ | \\ \text{C}_4\text{H}_9\text{OPOC}_4\text{H}_9 \\ | \\ \text{O} \\ | \\ \text{C}_4\text{H}_9 \end{array}$ . (b) W. Gordy and S. C. Stanford, *J. Chem. Phys.*, **9**, 204 (1941).

(3) W. H. Baldwin, C. E. Higgins and B. A. Soldano, *THIS JOURNAL*, **63**, 118 (1959).

(4) (a) W. H. Baldwin and C. E. Higgins, *J. Am. Chem. Soc.*, **74**, 2431 (1952). (b) C. E. Higgins and W. H. Baldwin, *J. Org. Chem.*, **21**, 1156 (1956).

(5) J. Kennedy and S. S. Grimley, AERE-CE/R-1283, Dec. 1, 1953. Decl. Apr. 2, 1957.

(6) P. M. Gross, *Chem. Revs.*, **13**, 91 (1933).

(7) F. A. Long and W. F. McDevit, *ibid.*, **51**, 119 (1952).

(8) L. L. Burger and R. C. Forsman, HW-20936, Apr. 2, 1951. Decl. Mar. 2, 1957.

(9) K. Alcock, S. S. Grimley, T. V. Healy, J. Kennedy and H. A. C. McKay, *Trans. Faraday Soc.*, **52**, 39 (1956).

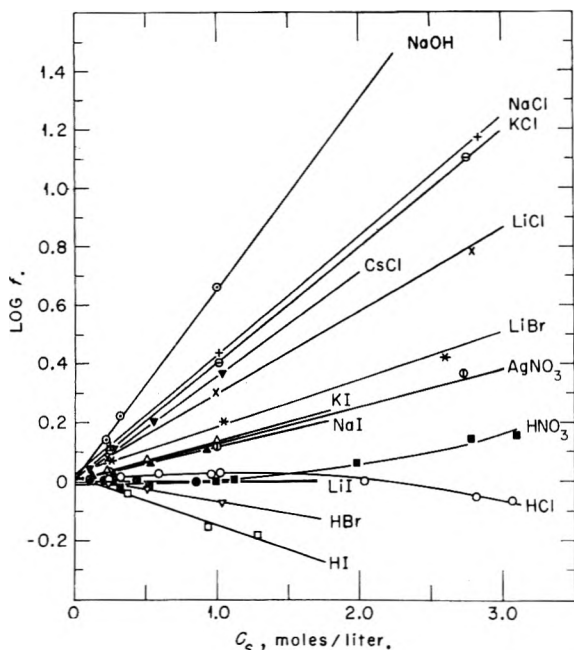


Fig. 1.—Effect of electrolytes on the activity coefficients of tributyl phosphate at 25°.

**TBP Solubility Determinations.**—The solubility of TBP in water and several electrolyte solutions was measured simultaneously at each temperature. Temperatures of 5, 13, 25 and  $50 \pm 0.2^\circ$  were employed. The equilibration and separation technique described above was repeated with fresh portions of the same strength stock solution enough times (usually five) that the last three passes resulted in electrolyte samples which contained the same amount of activity. These samples also were analyzed for electrolyte concentration, which was the same as that of the stock solution.

In the electrolyte studies the solubility was measured in the concentrated solutions first; the TBP-P<sup>32</sup> then was washed with water and given the consecutive pass treatment with a lower concentration of the same electrolyte. Immediate re-equilibration at 13° of saturated solutions from the 5° solubility determinations resulted in the same solubilities as when the regular method was employed at 13°, except for the case of sodium hydroxide.

The solubility values reported were shown to be uninfluenced by hydrolysis of the TBP. Samples neutralized with sodium hydroxide were extracted three times with excess volumes of carbon tetrachloride, followed by re-assay of the aqueous for activity. At 25° only sodium hydroxide was an offender of consequence. In a 1 M NaOH solution which had stood overnight 18% of the activity was non-extractable into CCl<sub>4</sub>. However, most of the hydrolysis was shown to have occurred on TBP-P<sup>32</sup> in solution since only 2% was non-extractable into CCl<sub>4</sub> after the equilibration and one hour settling period. Hydrolysis at 50° by NaOH was so pronounced that it was impossible to ascertain the true solubility of TBP. Hydrolysis of the TBP by electrolytes was of the order NaOH  $\ll$  HI < LiI < HCl < HNO<sub>3</sub>. A 3 M HCl solution containing TBP-P<sup>32</sup> (0.37 g./liter) which stood overnight at 50° hydrolyzed only 5% of the TBP-P<sup>32</sup>.

**Activity Assay.**—The amount of tributyl phosphate in the aqueous phase was determined by counting a dilution of an aliquot containing sufficient activity in the solution counter previously described.<sup>10</sup> The specific activity of the labeled ester was measured at the same time for comparison. (S in mg. TBP per liter of aqueous solution was equal to the activity per liter of aqueous divided by the activity per mg. of dry TBP-P<sup>32</sup>.) Duplicate samples of the distilled TBP-P<sup>32</sup> were weighed and diluted to a known volume with 50% dioxane. Suitable aliquots were counted in solutions of the same composition as the aqueous samples assayed.

At 25° the determination of activity in the electrolyte

solutions was performed on known volumes. At the other temperatures a known weight of solution was counted and the activity per liter of electrolyte was obtained by the use of density curves for each electrolyte at each temperature.

### Results

The solubility of tributyl phosphate in water ( $S_0$ ) at temperatures from 3.4 to 50° is listed in Table I. The values listed are the averages of at least two separate determinations and at 25°  $S_0$  is the average of thirty measurements made on seven batches of TBP-P<sup>32</sup> at different times. The largest average deviation of a single determination from the mean occurred in the 25° measurements and was  $\pm 1.8\%$ . On a molar basis the solubility of TBP in water drops from 0.0040 M at 3.4° to 0.0011 at 50°, with a value of 0.0016 M at 25°.

TABLE I

THE SOLUBILITY OF TBP IN WATER

Temp., °C.	3.4	4.0	5.0	13.0	25.0	50.0
$S_0$ , mg. TBP/l.	1075	1012	957	640	422	285

The values of  $S_0$  presented here are somewhat higher than those reported by Alcock, *et al.*,<sup>9</sup> presumably because they used a centrifugation separation technique. Since  $S_0$  decreases with rising temperature the temperature increase from centrifugation would decrease the solubility of TBP and thereby possibly account for lower reported values.

The values of molar activity coefficient  $f$  of TBP in electrolyte solutions reported here have been obtained from equation 1 as described by

$$f = \frac{S_0}{S} \quad (1)$$

McDevit and Long,<sup>11</sup> where  $S_0$  is the molar solubility of TBP in pure water and  $S$  is the molar solubility of TBP in a given concentration of electrolyte. Activity coefficients for each equilibrium electrolyte concentration ( $C_s$ ) at 25° are listed in Table II. Salting coefficients ( $k_s$ ) at 5, 13, 25 and 50° are found in Table III. The constant  $k_s$  is the slope obtained from the curve resulting from the plot of  $\log f$  vs. electrolyte concentration  $C_s$  in moles per liter. The curves for each electrolyte at 25° are shown in Fig. 1, depicting the fit of the data to the Setschenow<sup>6</sup> equation in all

$$\log f = k_s C_s \quad (2)$$

cases except those of nitric and hydrochloric acids, which do behave in the dilute range, however.

The lack of linearity in the HNO<sub>3</sub> and HCl curves beyond 1 M concentrations indicates specific interaction between the organic and these electrolytes. Since the form of the Setschenow equation we are employing presupposes an absence of specific interaction it is probable, at least in the case of nitric acid, that the values of  $k_s$  would be thereby affected. To minimize this possibility we have, in the case of acids, weighed the points in the dilute concentration range. This does not completely assure that the resultant values of  $k_s$  are free of the above-mentioned complication. On the other hand it will be shown that the values

(10) C. E. Higgins and W. H. Baldwin, *Anal. Chem.*, **27**, 1780 (1955).

(11) W. F. McDevit and F. A. Long, *J. Am. Chem. Soc.*, **74**, 1773 (1952).

TABLE II  
 ACTIVITY COEFFICIENTS OF TRIBUTYL PHOSPHATE IN AQUEOUS SOLUTIONS, 25°

Electrolyte	$C_s$	$f$	$C_s$	$f$	$C_s$	$f$	$C_s$	$C_s$	$C_s$	$\log f / C_s = k_s$	$V_s - \bar{V}_s^0$ , ml./mole <sup>a</sup>
NaOH	0.216	1.38	0.315	1.66	1.00	4.52				0.65	24.5
NaCl	.250	1.32	1.01	2.73	2.84	14.8				.408	12.5
KCl	.246	1.26	1.01	2.52	2.75	12.6				.398	10
CsCl	.104	1.10	0.283	1.27	0.559	1.59	1.03	2.30		.353	7.5
LiCl	.236	1.20	0.992	2.00	2.79	6.07				.284	9
LiBr	.259	1.17	1.05	1.59	2.60	2.61				.161	
KI	.228	1.08	0.503	1.17	1.00	1.37				.133	
AgNO <sub>3</sub>	.245	1.07	1.00	1.30	2.72	2.31				.128	
NaI	.120	1.03	0.266	1.07	0.526	1.15	0.930	1.28		.116	8.0
HCl	.240	1.02	0.319	1.04	0.591	1.06	0.947	1.05		.020	2.5
	1.02	1.07	2.03	0.995	2.81	0.890	3.07	0.856			
HNO <sub>3</sub>	0.255	1.00	0.307	0.950	0.522	0.954	0.994	0.997		.015	
	1.11	1.02	1.98	1.16	2.78	1.39	3.09	1.43			
LiI	0.108	1.01	0.215	0.993	0.433	1.01	0.850	0.993		.000	
HBr	.230	0.984	0.513	0.946	1.03	0.841				-.078	
HI	.368	0.917	0.93	0.700	1.28	0.657				-.16	

<sup>a</sup> From McDevit and Long, reference 11.

 TABLE III  
 SALTING COEFFICIENTS  $k_s$  FOR TRIBUTYL PHOSPHATE IN ELECTROLYTE SOLUTIONS AS A FUNCTION OF TEMPERATURE

Electrolyte	5°	13°	25°	50°
NaOH	0.66	0.66	0.65	
NaCl	.430	.427	.408	0.393
KCl	.420	.415	.398	.384
CsCl			.353	
LiCl	.303	.300	.284	.280
LiBr	.174	.177	.161	.156
KI			.133	
AgNO <sub>3</sub>	.165	.152	.128	.114
NaI			.116	
HCl	.050	.077	.020	-.047
HNO <sub>3</sub>	.122	.085	.015	-.046
LiI			.000	
HBr			-.078	
HI			-.16	

of  $k_s$  for acids, with the exception of HNO<sub>3</sub>, have the same temperature dependence as do those of the alkali halides. Likewise it will be shown in the subsequent paper<sup>3</sup> that, with the exception of the nitrates, all the acids and salts behave in a similar fashion in a situation where one would expect the greatest specific interaction—namely, high salt concentration in TBP itself. Finally the similarity in the water pickup of the acids,<sup>3</sup> again excepting nitric acid, reinforces our conviction that our treatment does give a reasonable estimate of  $k_s$ .

A total of fourteen monovalent electrolytes was employed at 25° (Table II and Fig. 1). Sodium hydroxide salted out TBP the most ( $k_s = 0.65$ ) while HI salted in the most ( $k_s = -0.16$ ). The salting factor  $k_s$  for each electrolyte decreased in the order NaOH > NaCl > KCl > CsCl > LiCl > LiBr > KI > AgNO<sub>3</sub> > NaI > HCl > HNO<sub>3</sub> > LiI > HBr > HI. Both hydrobromic and hydriodic acids caused salting in. Upon comparing the salting parameter  $k_s$  for TBP with that for benzene<sup>11,12</sup> in the

same electrolytes it can be seen that a much greater spread and larger values are found using TBP. For example,  $k_s$  in sodium chloride is twice that found for benzene and is four times greater in cesium chloride, while in hydrochloric acid the value is less, reflecting in part the large difference in size between the two molecules. The molar volumes of benzene and TBP at 25° are 89.4 and 274 ml. per mole, respectively.

Although large differences in solubility occurred at varying temperatures ( $S_0 = 957$  mg./l. at 5° down to 285 mg./l. at 50°) relatively little change in  $k_s$  was noted for a particular electrolyte over the temperature range involved. Table III summarizes the values of  $k_s$  obtained from plots of  $\log f$  vs.  $C_s$  at each temperature. As the temperature rose  $k_s$  decreased somewhat, *i.e.*, in sodium chloride  $k_s$  varied from 0.43 at 5° to 0.39 at 50°. For the halide salts the spread was 6 to 10%. A larger spread was noted in the case of nitrates, 31% for silver nitrate, and the largest differences were displaced by nitric acid, with  $k_s$  decreasing from 0.12 at 5° to a salting-in  $k_s$  of  $-0.046$  at 50°. These results also can be seen in Fig. 2, in which is plotted  $k_s$  vs.  $1/T$  for several electrolytes. The halide salts all have practically the same slope whereas the slopes for silver nitrate and the acids are steeper.

### Discussion

At the present two limiting theories exist as aids in interpreting the salting out data. One recently proposed for neutral type solutes is that of McDevit and Long<sup>11</sup> and is expressed by

$$k_s = \frac{\bar{V}_s^0(V_s - \bar{V}_s^0)}{2.3\beta_0 RT} \quad (3)$$

where  $\beta_0$  is the compressibility of water,  $\bar{V}_s^0$  is the partial molar volume of the non-electrolyte solute,  $\bar{V}_s^0$  is the partial molar volume of the electrolyte,  $V_s$  is the melted volume of the electrolyte, and  $k_s$  is the salting coefficient in infinitely dilute solution.

The essential idea behind this equation is that the salts exert a pressure on the water, thereby affecting

(12) J. H. Saylor, A. I. Whitten, I. Claiborne and P. M. Gross, *J. Am. Chem. Soc.*, **74**, 1778 (1952).

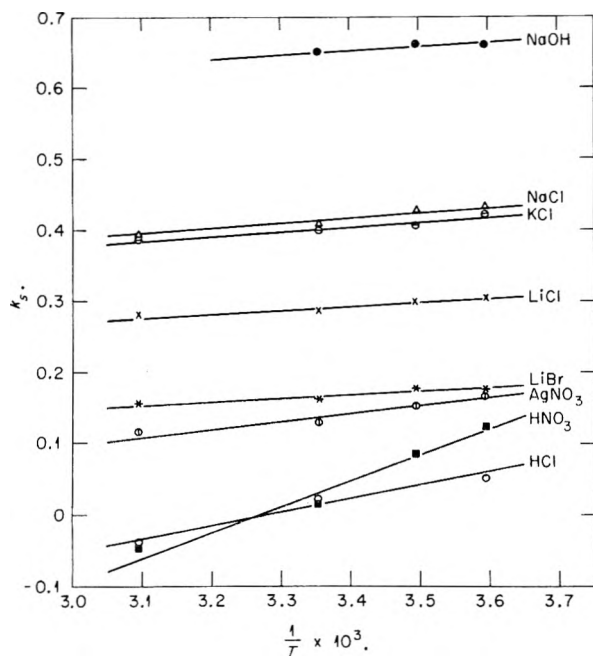


Fig. 2.—Effect of temperature on salting coefficients  $k_s$  for tributyl phosphate in electrolyte solutions.

the solubility of the neutral solute. In addition to predicting salting in as well as salting out, the equation suggests that the problems of ternary systems are, in part, the same ones involved in the nature of the partial molar volumes of salts in water alone. For benzene type compounds and especially for non-polar compounds smaller than benzene this equation has achieved a measure of success and appears to offer a base on which to account for the other forces that affect salting in.

The other approach, originally proposed by Debye and McAulay,<sup>13</sup> is based upon the ion atmosphere concept as applied to ternary systems at infinite dilution where

$$\log f = \lambda n' \frac{\sum \nu_i z_i^2 \epsilon^2}{2D_0 r k T} \quad (4)$$

in which  $f$  is the activity coefficient,  $n'$  is the number of salt molecules per cc.,  $\nu_i$  = the number of ions of one kind in the molecule,  $z_i$  = the valence of the ion,  $\epsilon$  is the charge on the electron,  $D_0$  is the dielectric constant of water,  $k$  = Boltzmann's constant, and  $r$  is an idealized empirical radius ascribed to the salt. The term  $\lambda$  is the effect of the organic solute on the dielectric constant lowering of water and is defined by the expression  $D = D_0(1 - \lambda n)$  where  $D$  is the dielectric constant of the solution containing  $n$  molecules of non-electrolyte per cc. From equation 2

$$k_s = \frac{\log f}{C_s}$$

and therefore equation 4 becomes

$$k_s = \frac{\lambda N \sum \nu_i z_i^2 \epsilon^2}{2,000 D_0 r k T} \quad (5)$$

where  $N$  is Avogadro's number.

TBP can be considered a Lewis-type base. It was therefore desirable to determine which of the two above approaches offered the most aid in

interpreting our results. Although Long, *et al.*, claimed no generality in their approach since it is strictly applicable only to small non-electrolyte molecules, it was nevertheless of interest to test its applicability to our system.

Consistent with equation 3 one notes that the considerably larger volume of TBP is reflected in values of  $k_s$  several times larger than those found for benzene. As for the dependence of  $k_s$  on the term  $(V_s - \bar{V}_s^0)$ , however, our results were only to a first approximation consistent with equation 3. See Table II.

It was the temperature results, however, which indicated that TBP could not be considered to fit within the framework of the Long approach. As pointed out by Long and McDevit,<sup>8</sup> differentiation of equation 3 approximates the temperature coefficient

$$\frac{dk_s}{dT} \cong - \frac{\bar{V}_s^0}{2.3RT} \frac{d\bar{V}_s^0}{dT} \quad (6)$$

or the temperature dependence of  $k_s$  does involve the quantity  $dV^1/dT$ , the size of which varies widely for most salts. Moreover,  $dV^1/dT$  decreases rapidly with temperature. It can be noted from Fig. 2 that all the halide salts showed virtually identical temperature dependence. In view of these findings it appeared that the limiting case represented by the Debye-McAulay equation (eq. 5) might be of greater interpretative advantage.

Part of the difficulty with this limiting approach lies in the lack of information on  $\lambda$ , the effect of the organic on the dielectric constant of water—especially as a function of temperature. Moreover, the  $r$  values are empirical in nature, although one can with some safety assume that these values of  $r$  are temperature independent.

With this assumption in mind equation 5 was applied to Fig. 2. The linearity and more importantly the equality of slope of the halide salt systems portrayed implies that for those systems  $\lambda/D_0 = c$ , where  $c$  is a constant independent of temperature. However, the uncertainties mentioned above caused us to look elsewhere for further interpretation of our data. Thus a thermodynamic approach was investigated.

The standard free energy change per mole for transferring TBP from a solution in pure water to one in which there is added electrolyte is given by the expression

$$\Delta F = RT \ln f_i/f_i^0 \quad (7)$$

where  $f_i$  and  $f_i^0$  are the molar activity coefficients of TBP in electrolyte solution and water, respectively. Differentiating to obtain the temperature coefficient of  $f$  results in the relationship

$$\frac{d \ln f_i/f_i^0}{dT} = - \frac{\Delta H}{RT^2} \quad (8)$$

which Rothmund<sup>14</sup> applied to a variety of non-electrolytes and found a  $\Delta H$  close to zero. Integrating equation 8 we obtain

$$2.3 \log f_i/f_i^0 = \frac{\Delta H}{RT} + C \quad (9)$$

(13) P. Debye and J. McAulay, *Physik. Z.*, **26**, 22 (1925).

(14) V. Rothmund, "Löslichkeit und Löslichkeitsbeeinflussung," Barth, Leipzig, 1907; *Chem. Revs.*, **51**, 119 (1952).

and applying equation 9 to the halide salt curves in Fig. 2 we obtain a value for  $\Delta H$  of 300 cal. for TBP in water. This result is the same for all the salts that retain the same temperature slope, and therefore is probably indicative of an invariant of water or the organic.

If for the term  $2.3 \log f_i/j_i^0$  in equation 9 we substitute its equivalent from equation 7,  $\Delta F/RT$ , we obtain

$$\frac{\Delta F}{RT} = \frac{\Delta H}{RT} + C \quad (10)$$

Since  $\Delta F = \Delta H - T\Delta S$ , equation 10 becomes

$$\frac{\Delta F}{RT} = \frac{\Delta H}{RT} - \frac{\Delta S}{R} \quad (11)$$

or

$$2.3k_s C_s = \frac{\Delta H}{RT} - \frac{\Delta S}{R} \quad (12)$$

where we have a form of the Setschenow equation, its thermal dependence (where  $\Delta H$  is independent of temperature, small, and the same for the halide salts studied), and identification of the intercept term,  $C$ , from the  $k_s$  vs.  $1/T$  plot, with entropy. The entropy term in equation 12, then, is the dominant one. Hence it becomes important to correlate the salting coefficients within the entropy concept.

Entropy is a measure of the extent of disorder in a system. In recent years there has arisen a considerable emphasis on structure order-disorder phenomena and the role they play in aqueous solutions.<sup>15</sup> Frank<sup>16</sup> has used it as a basis for interpreting the effects of temperature on organo-aqueous systems. Recently Bergen and Long<sup>17</sup> qualitatively discussed the role of this mechanism in salting studies.

The advantage of the Gurney approach lies in the extensive systematization that he achieved in correlating many properties of electrolytes within the elementary partial molal entropy concept of salts. For example, he was able to link the temperature coefficients for ionic mobility, the effects of salts on the viscosity of water, the so-called  $B$  term that characterizes short range interactions in solution, all within the entropy concept originally pioneered by Latimer. Earlier, Dole<sup>18</sup> proposed a correlation between the viscosity  $B$  term and thermodynamic heats of dilution for strong electrolytes. What Gurney did was to show that the partial molal entropies of ions as determined by Latimer<sup>19</sup> formed two linear lines, one for anions and one for cations, when plotted against the primary  $B$  term which determines the effect of salt concentration on the viscosity of water. He developed arguments to show that such a term would essentially account for the effects of salts on the primary hydration sphere of water and thereby lead

(15) R. W. Gurney, "Ionic Processes in Solution," McGraw-Hill Book Co., New York, N. Y., 1953.

(16) H. S. Frank and M. W. Evans, *J. Chem. Phys.*, **13**, 507 (1945).

(17) R. L. Bergen, Jr., and F. A. Long, *THIS JOURNAL*, **60**, 1131 (1956).

(18) M. Dole, unpublished work; presented before the 85th meeting of the American Chemical Society Washington, D. C., March 29, 1933.

(19) W. M. Latimer, K. S. Pitzer and W. V. Smith, *J. Am. Chem. Soc.*, **60**, 1829 (1938).

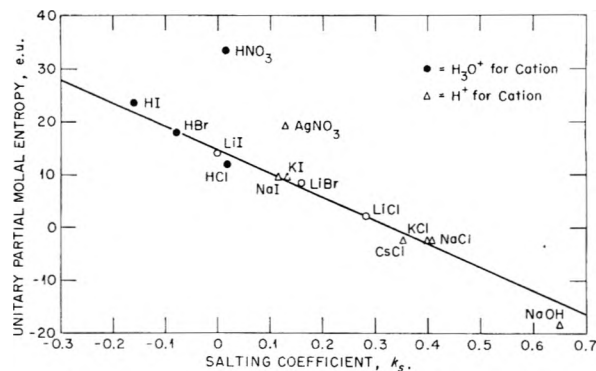


Fig. 3.—The relationship of the salting parameter  $k_s$  to the unitary partial molal entropy of the added electrolyte in aqueous solution at 25°.

to order and disorder in water. Gurney then further normalized his ionic entropies, all related by Latimer to  $H^+$ , so that all the cations and anions fell on the same straight line when plotted against the viscosity  $B$  terms. He then developed arguments to the effect that on such a scale not only relative differences between cations but also differences between cation and anion were significant. Finally he showed that the partial molal entropies of salts in water all contained a constant or cratic term which reflected simply the number of moles of water in 1,000 grams of water. He then subtracted this 8 entropy units from his normalized entropy values and thereby obtained a series of *unitary* entropy values for both cations and anions that should determine true structural effects in water.

In view of this extensive empirical correlation, it was of interest to determine to what extent the Gurney approach could be applied to the problem of salt effects on a Lewis type basic non-electrolyte. We take advantage of the findings pointed out by Long<sup>7</sup> to the effect that basic type non-electrolytes are largely sensitive to anion effects and rather insensitive to cations, with the cation effect extending no further than the  $H^+$  and  $Li^+$  ions, both very small cations.

Our test treatment consists in then making two assumptions: (1) the  $H^+$  in mineral acids tested will be considered to behave like a hydronium ion and (2) all the cations beyond  $Li^+$  behave as if they were protons ( $H^+$ ) (or essentially a dimensionless unit charge). Then using the unitary values listed in Table XXX of Gurney<sup>15</sup> we have compared (Fig. 3) the resultant entropies for each electrolyte against all the corresponding salting coefficients. It is apparent that order-disorder effects do dominate the absolute magnitude of the  $k_s$  values and furthermore that proton migration as reflected in the emphasis of  $H^+$  ion plays a dominant role in this phenomenon relative to Lewis type bases. It may be of some significance to point out that the value of the entropy term for  $k_s = 0$  is 14.5 e.u. This value agrees closely with the total partial molal entropy of  $H_3O^+$  and  $OH^-$  ions as determined by Gurney (ref. 15, p. 178).

We have emphasized the various effects of temperature, order-disorder and salt effects on TBP

for one reason. As conducted in this phase of our program we have a small amount of TBP dissolved in a large amount of water. We intend in the next paper to reverse the situation and determine the affinity of monohydrated TBP for selfsame salts when all the water except that of *primary hydration* of ions is absent. Our aim is to thereby determine which types of salt-water-organic in-

teractions are common to both ranges and to determine whether or not the various types of interactions can be separated.

**Acknowledgment.**—The authors wish to thank Dr. G. E. Boyd for many specific, constructive criticisms and his general encouragement. We also wish to thank Professor G. Scatchard for a helpful discussion.

## THE DISTRIBUTION OF MONOVALENT ELECTROLYTES BETWEEN WATER AND TRIBUTYL PHOSPHATE<sup>1</sup>

BY W. H. BALDWIN, C. E. HIGGINS AND B. A. SOLDANO

*Contribution from the Chemistry Division, Oak Ridge National Laboratory, Oak Ridge, Tennessee*

*Received August 18, 1958*

Equilibrium conditions have been measured for the distribution of electrolytes between water and tributyl phosphate and for the water in the tributyl phosphate. Two classes of extraction behavior have been noted depending upon whether or not water accompanies the electrolyte into the tributyl phosphate. The standard state free energy change has been shown to have a linear relationship with the Gurney unitary partial molal entropy.

It was of interest to investigate the interactions involved in the distribution of salts between water and various organic solvents. An excellent thermodynamic study of extraction of uranyl nitrate by various solvents has been made by Glueckauf, *et al.*<sup>2</sup> The nature of tributyl phosphate (TBP) solutions containing many different nitrates has been studied by Healy and McKay.<sup>3</sup> In our study special emphasis was placed on TBP and on univalent electrolytes which are not usually considered extractable by this solvent. This approach was undertaken with the view that investigation of difficultly extracted species might also give fundamental information on the solvent extraction mechanism. There was an indication, moreover, that Gurney's<sup>4</sup> unitary entropy concept for ion hydration in aqueous salt solutions may be closely identified with the salting out behavior of TBP in aqueous solutions.<sup>5</sup> Since any distribution study of the affinity of TBP for salts involves an empirical disposition of the "primary ion hydration" problem, any links established between the factors governing the solvent-salt behavior of TBP and the previously discussed salting coefficients  $k_s$  should be useful in shedding further light on the Gurney unitary entropy concept. The latter approach is intentionally vague as to the number of waters involved in the ion co-sphere. It does, in common with the Debye-McAulay<sup>6</sup> approach, however, clearly demonstrate the electrostatic nature of ion-solvent interactions.

In a limited sense, moreover, a simple empirical thermodynamic frame is desired that would permit

the systematization of TBP-electrolyte behavior not only for those salts that are normally poorly extracted by TBP but also those that readily enter TBP.

### Experimental

**Chemicals.**—Tributyl phosphate was purified by washing with sodium hydroxide solution and then with distilled water. The dissolved water was removed in the first fraction when the tributyl phosphate was distilled. The anhydrous fraction (b.p. 118° at 2–3 mm. pressure;  $n_D^{20}$  1.4220) was used for the subsequent experiments. Reagent grade chemicals were employed to prepare stock solutions in distilled water. The hydrobromic and hydriodic acid solutions were prepared from the constant boiling mixtures distilled immediately before use, thus eliminating free halogen contamination.

**Equilibration.**—Approximately 3-g. portions of purified, anhydrous tributyl phosphate (without diluent, weighed on an analytical balance) were added to 10-ml. aliquots (volumetric pipet) of standardized aqueous electrolyte solutions of varying concentration. Glass stoppered centrifuge cones of 15-ml. capacity were used for most of these tests. Close fitting stoppers were employed without grease. The cones containing the two phases were tumbled end over end 20 times per minute in a water-bath (held at  $25 \pm 0.2^\circ$ ) for times varying from 0.5 to 24 hours.

**Phase Separation.**—After equilibration the tubes were held upright in the same bath for two hours to allow the phases to separate. The lower, aqueous, phase was removed with a very fine capillary pipet controlled with a syringe in order to make a very sharp boundary separation between the organic and aqueous layers. The remaining organic phase, a solution of tributyl phosphate, water and electrolyte, was then reweighed in the tube.

**Analysis.**—All analyses were performed in duplicate or triplicate. Gravimetric samples (0.3 to 1.5 g.) of the organic solutions were obtained by the use of weight pipets. Volumetric aliquots were taken of the aqueous phases.

Water in the organic phase was determined with the Karl Fischer reagent using the null point method to detect the end-point. The reagent was standardized against a synthetic solution of water in methanol. This was prepared by adding a known quantity of water to methanol which had been dehydrated by reaction with magnesium turnings and distilled. In addition, the Karl Fischer reagent was standardized against tributyl phosphate that had been equilibrated with excess water at 25°. Two standards were used to ensure reliability of the results obtained with the Karl Fischer technique. A standard aqueous methanol solution constitutes the usual procedure. The second

(1) This paper is based on work performed for the United States Atomic Energy Commission at the Oak Ridge National Laboratory operated by Union Carbide Corporation.

(2) E. Glueckauf, H. A. C. McKay and A. R. Mathieson, *Trans. Faraday Soc.*, **47**, 437 (1951).

(3) T. V. Healy and H. A. C. McKay, *ibid.*, **52**, 633 (1956).

(4) R. W. Gurney, "Ionic Processes in Solution," McGraw-Hill Book Co., Inc., New York, N. Y., 1953.

(5) C. E. Higgins, W. H. Baldwin and B. A. Soldano, *THIS JOURNAL*, **63**, 113 (1959).

(6) P. Debye and J. McAulay, *Physik Z.*, **26**, 22 (1925).



standardization serves both as a check upon the first standard and the feasibility of the method in the presence of tributyl phosphate. The check procedure is based upon the well known behavior of tributyl phosphate to dissolve exactly one mole of water per mole of tributyl phosphate under the above described conditions.

Electrolyte concentration in each phase was determined by titration. The organic samples were added to ~200 ml. of distilled water and shaken vigorously or stirred vigorously with a magnetic stirrer during the analysis. Acids were titrated to the phenolphthalein end-point with standardized, carbonate-free sodium hydroxide. The halide salts were determined by titration to the sharp inflection using standardized silver nitrate and a Fisher Titrimeter equipped with calomel and silver electrodes. In all cases the material balances for total electrolyte in both aqueous and organic phases after equilibration checked within 0.5% of the amount originally introduced in the pipetted 10 ml. of stock solution.

### Experimental Results

The largest distribution coefficients are shown by nitric acid (Fig. 1) with the hydrogen halides being extracted next most effectively. The order among the hydrogen halides was  $\text{HI} > \text{HBr} > \text{HCl}$ , with the larger anion being extracted better. It is evident that the concentration of acid in tributyl phosphate approaches 1:1 in all cases with a suggestion in the case of  $\text{HNO}_3$  that at higher concentrations the ratio of acid to solvent exceeds 1:1.

The order of extractability among the halides is maintained among the lithium salts (*i.e.*,  $\text{LiI} > \text{LiBr} > \text{LiCl}$ ).

The effect of the cation (where the anion remained the same) followed the order  $\text{HX} > \text{LiX} > \text{NaX} > \text{KX} > \text{CsX}$ .

Water (Fig. 2) plays an important role in the distribution of electrolytes into tributyl phosphate. Nitric acid, on going into the solvent, displaced water so that the concentration of water in tributyl phosphate was decreased in comparison to the equilibrium conditions in the absence of electrolytes. In contrast, however, the halogen acids carried water along into the tributyl phosphate so that approximately  $4\text{H}_2\text{O}$  were present per  $\text{HX}$ . At the higher concentrations it appears that water was being forced from the tributyl phosphate again. The effect of cation on the amount of water carried into tributyl phosphate can be summarized in the order  $\text{H} > \text{Li} > \text{Na} > \text{K}$ .

Judging from the distribution of water into the tributyl phosphate along with the electrolyte, two mechanisms are evident. The first system is that one in which the electrolytes are extracted along with water. Superimposed upon this fact, however, is the effect of the anion. Among the cations that are represented by the alkali metals the smaller ones are the most highly hydrated and are extracted better.<sup>7</sup>

The second extraction mechanism is represented by nitric acid. Here, the extraction coefficients were the highest among the electrolytes tested but water does not accompany the nitric acid into the tributyl phosphate. Compound formation is essential for the extraction of nitric acid. In addition to a higher extraction coefficient and the exclusion of water, the nitric acid enters tributyl phosphate in a mole ratio slightly greater than 1:1.

### Discussion

The physical-chemical behavior of solvent ex-

(7) R. Spence, *Proc. Roy. Soc. (London)*, **243**, 1 (1957).

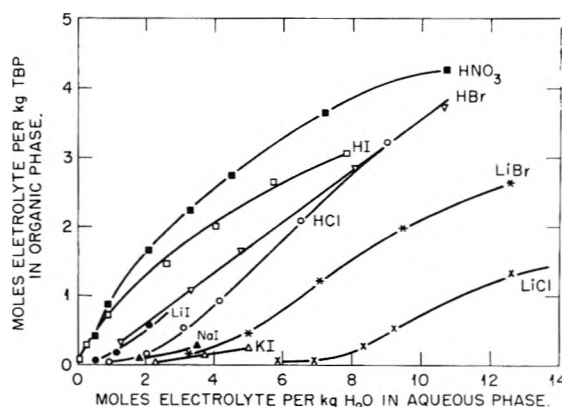


Fig. 1.—Distribution of electrolytes in TBP as a function of electrolyte concentration in the aqueous phase.

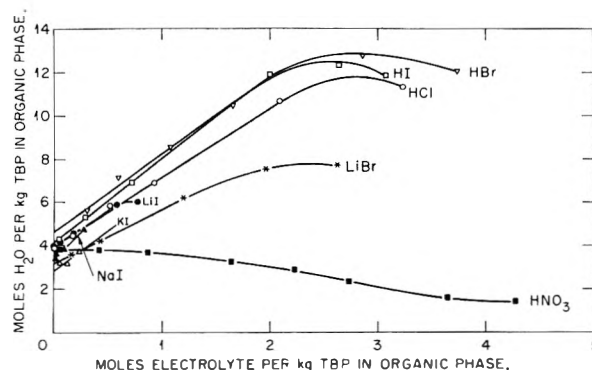


Fig. 2.—Relative hydration of the electrolytes in the organic phase.

tractants of the TBP type can in the first approximation be characterized by two classes: (1) Class I, consisting in the main of mineral salts of the halogen acids (*i.e.*,  $\text{NaCl}$ ) that are usually excluded in any practical extraction process. The behavior of this class will be strongly affected by hydration phenomenon. (2) Class II, consisting of salts characterized by a high affinity for TBP based upon a specific TBP-salt complex formation, for example: nitric acid.

In any two-phase distribution of salts involving an aqueous and organic phase three basic problems become apparent. (1) What operational mathematical formalism shall be employed to codify the data? (2) How shall the "hydration" of the salts be treated? (3) How shall the thermodynamic behavior of the hydrated salt in the organic phase be handled?

The first problem one faces is that involving a decision on the type of empirical equation most suitable for handling the activities of the mineral salts in the organic phase, since at equilibrium the chemical potential of the salt in both the organic and aqueous phases must be equal. Preliminary attempts to apply the Flory-Huggins<sup>8</sup> equation to the hydrated salt-organic solvent systems indicated that not only was the entropy term of negligible importance but that the use of volume fractions appeared to offer no significant gain in representation. At the same time, the added calculation complexi-

(8) J. H. Hildebrand and R. L. Scott, "The Solubility of Nonelectrolytes," 3d ed., Reinhold Publ. Corp., New York, N. Y., 1950.

ties soon suggested that the usual equilibrium approach was most suitable and had the added advantage of simplicity. No uniqueness is implied but a formulation was required that reflected the behavior patterns with a limited number of resultant constants. Thus we *a priori* assumed, as have others,<sup>2,9</sup> that the following equilibrium could be postulated

$$K = \frac{[\text{Electrolyte}] [a_w]^n}{[\text{Electrolyte-organic}]} \quad (1)$$

where

[Electrolyte] = activity of the electrolyte in water  
 $[a_w]$  = activity of water in the aqueous phase  
 $n$  = primary hydration no. of the cation using expl. values for  $n$   
 [Electrolyte-organic] = activity of the hydrated electrolyte in the organic solvent

This equation can then be transposed into

$$2 \log (m\gamma^{\pm}) + n \log a_w = \log K + \log m_a + am_a \quad (2)$$

where

$m$  = molality of the electrolyte in the aqueous phase  
 $\gamma^{\pm}$  = mean ionic activity coefficient of the aqueous electrolyte  
 $\log K$  = proportional to the standard state change in free energy associated with the hydrated salt's changing environment from aqueous electrolyte to electrolyte in the organic solvent  
 $m_a$  = molality of salt in the anhydrous organic solvent  
 $a$  = empirical constant characteristic of each system  
 $\delta = 2 \log (m\gamma^{\pm}) + n \log a_w - \log m_a$

In the last term of equation 2,  $am_a$ , we have assumed that the logarithm of the activity coefficient of the salt in the organic phase can be approximated by a simple linear term in molality. No attempt has been made to refine the term any further since the  $a$  term in organics includes the same co-volume

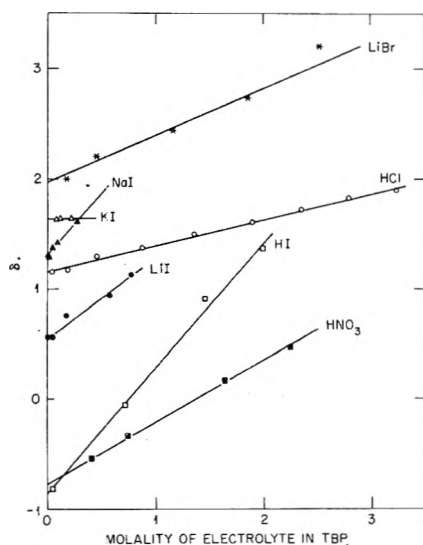


Fig. 3.—The applicability of equation 2 to the representation of the distribution coefficients between TBP and water. The term  $\delta$  is the expression  $2 \log (m\gamma^{\pm}) + n \log a_w - \log m_a$  in equation 2.

effects, ion pair formation and electrostriction contributions that go to make up the extremely complex linear  $B$  term employed for activity coefficients in concentrated aqueous solutions.

(9) N. Bjerrum and E. Larsson, *Z. physik. Chem.*, **A127**, 358 (1927).

Our procedure, therefore, was to show that equation 2 with the empirical  $\log K$  and the  $a$  term could reasonably represent the distribution of salts from water to TBP over an extended concentration range, provided experimentally measured hydration numbers were employed in equation 2. Activity coefficients were obtained from the works of Harned and Owen,<sup>10a</sup> Robinson and Stokes<sup>10b</sup> and supplemental data for HBr from Bierman and Yamasaki.<sup>10c</sup>

**Primary Hydration.**—The exponential dependence of equation 2 on the hydration number  $n$  requires that in the present method of representation we consider the problem of "hydration," since for Class I especially it is usually a hydrated salt that is transferred into the TBP phase.

The method employed in our treatment was that of comparing the molality of salt in TBP against the total amount of water as determined by the Karl Fischer method. In most cases for Class I type, the water content proved to be an almost linear function of the salt concentrations (Fig. 2) except at the highest molalities. As to the specific hydration numbers for the salts, the dual class trend persisted.

For Class II (*i.e.*,  $\text{HNO}_3$ ), the introduction of  $\text{HNO}_3$  into the organic phase results in an ever increasing removal of water. As the salt concentration in TBP is increased the value of  $n$  drops continuously from an initial value of 1 to 0. This indicates that  $\text{HNO}_3$  not only does not introduce any hydration water but that it replaces the one equivalent of  $\text{H}_2\text{O}$  initially bound by the pure TBP and water mixture. This behavior is consistent with the postulation that TBP forms a strong complex with nitric acid, thereby replacing the one water of hydration on TBP. It should be noted that these two classes of behavior retain a similar pattern when the distribution coefficients also are considered.

Class I salts (*i.e.*, LiCl, HCl, etc.) on the other hand retain primary hydration numbers consistent with those proposed by Bockris,<sup>11</sup> Glueckauf,<sup>12</sup> and Bell<sup>13</sup> to account for strong short range ion hydration effects in aqueous solution alone (Table II).

As for the actual hydration numbers obtained in this study one notes (Table II, col. 6) that the values vary from  $n = 5$  to  $n = 0$ . Interestingly, the values of  $n$  for the three halogen acids show no significant deviation from values of  $n = 3$  to 4, whereas the values for the lithium salts vary widely with anion type.

No pretense is made in our treatment that our  $n$  represents an intrinsic property of salt-water interactions but it is of some interest to compare our values of  $n$  with those obtained by Bockris and Glueckauf (Table II). In a comparative study of different methods of determining the very strong

(10) (a) H. S. Harned and B. B. Owen, "The Physical Chemistry of Electrolytic Solutions," Reinhold Publ. Corp., New York, N. Y., 1943. (b) R. A. Robinson and R. H. Stokes, "Electrolyte Solutions," Academic Press, New York, N. Y., 1955. (c) W. J. Biermann and R. S. Yamasaki, *J. Am. Chem. Soc.*, **77**, 241 (1955).

(11) J. O'M. Bockris, *Quart. Rev. Chem. Soc. London*, **3**, 173 (1949).

(12) E. Glueckauf and G. P. Kitt, *Proc. Roy. Soc. (London)*, **A228**, 322 (1955).

(13) R. P. Bell, *Endeavour*, **17**, 31 (1958).

TABLE I  
COMPARATIVE SALT BEHAVIOR IN TRIBUTYL PHOSPHATE AS  
REPRESENTED BY EQUATION 2

Salt	log $K$	$\alpha$
HI	-0.85	1.10
HNO <sub>3</sub>	-0.78	0.57
HBr	0.50	1.00
LiI	0.54	0.78
HCl	1.15	0.24
NaI	1.32	1.00
KI	1.54	0.0
LiBr	1.98	.42
LiCl	2.95	.0
CsCl	3.64	.0

TABLE II  
PRIMARY HYDRATION NUMBERS

Ion	Method			Elec- trolyte	Method	
	Mo- bilities, etc. <sup>a</sup>	Iso- piestic <sup>b</sup>	Com- pressi- bilities <sup>c</sup>		TBP extrac- tion <sup>d</sup>	Extrapd. hydra- tion no. of TBP, moles H <sub>2</sub> O/kg. TBP <sup>e</sup>
H <sup>+</sup>		3.9				
Li <sup>+</sup>	4	3.3	4	NaI	4.9	3.4
Na <sup>+</sup>	3	1.5	5	KI	3.7	2.8
K <sup>+</sup>	2	0.6	5	HI	3.9	4.1
Rb <sup>+</sup>	1	0		HBr	3.6	4.6
F <sup>-</sup>	3		4	HCl	3.1	4.1
Cl <sup>-</sup>	2		2	LiI	3.6	3.9
Br <sup>-</sup>			1	LiBr	2.5	3.1
I <sup>-</sup>	0.7		1	LiCl	1.6	1.6
				CsCl	0	

<sup>a</sup> Ref. 11. Mean of mobility, entropy, compressibility and density determinations of  $n$ . <sup>b</sup> Ref. 12. <sup>c</sup> Ref. 13. <sup>d</sup> Slope of lines plotted in Fig. 2. <sup>e</sup> Intercept of water axis (Fig. 2) at zero electrolyte concentration.

interactions of cations and water, Bockris essentially averaged the results from mobility, entropy, density and compressibility methods as representing the best indicators of very strong salt-water interactions. There exists a rough first-order agreement in our experimental values of  $n$  and those postulated by Bockris (Table II) as indicating strong primary hydration.

It is apparent that our Class I salts relative to TBP involve the strong primary hydration interactions but any "true" hydration number is a function of the system studied. In any event, only experimentally measured values of  $n$  were employed in our thermodynamic treatment of the organo-organic-salt distribution problem.

One other point should be considered, specifically the limiting water content at zero salt concentration in TBP. This limiting intercept of a salt concentration vs. H<sub>2</sub>O plot, whose slope is the value of  $n$  (Fig. 2, Table II), varied in magnitude from 3 to 4.6 moles of H<sub>2</sub>O per 1,000 g. of pure TBP (Table II). This figure approximates the value of 3.76 equivalents of H<sub>2</sub>O per 1,000 g. of pure TBP.

The moisture behavior of these Class I salts appears to preclude the formation of any strong TBP-salt interaction of the nitrate type and suggests that the organic phase, TBP, is behaving as a rather efficient organic reagent useful in the study of aqueous salt behavior. In a later section we shall explore this possibility.

**Standard Free Energy Change for Salt Distribution in TBP.**—The affinity of TBP for salts remains consistent with the hydration behavior of Classes I and II. Nitric acid (Class II) retains the highest affinity of the salts studied for TBP. This is consistent with a process wherein a water molecule is removed from the TBP and a strong TBP-nitric acid complex is formed.

As for the Class I salts, these are normally considered to be excluded in any practical TBP extraction process. One notes that those systems which are most strongly hydrated (*i.e.*, HCl as compared to CsCl), Table II, retain the highest affinity in Class I for TBP. This suggests, therefore, that the mode of pickup in this class might be related to the hydration number of the salt, and a consideration of the standard state free energy change required to move hydrated salts from water into the monohydrated TBP might lead to information on the nature of the binding force.

The empirical equation 2 has led to interpretative results at least consistent with the "hydration" concept characteristic of aqueous salt solutions alone. It is of interest therefore to consider the nature of the log  $K$  term in equation 2. Our aim is to determine the usefulness of such a term in the interpretation of the behavior of the previously discussed Classes I and II.

This term, or more properly its free energy counterpart

$$\Delta F^0 = RT \ln K_0 \quad (3)$$

represents the standard free energy change that arises from removing a hydrated salt from an aqueous salt solution and placing it into the monohydrated TBP organic solvent. Similar two-phase equilibria have been divided by Bjerrum<sup>9</sup> into two steps: one involving the change in the electrical free energy of the hydrated salt due to changes in the dielectric constant, and a second which involves any specific unhydrated salt-organic interaction.

Since the hydration concept is essentially a device to circumvent the highly difficult problem of accounting for very short range ion-water electrical interactions, thereby avoiding any discussion of a so-called microscopic dielectric constant, we shall seek to determine the feasibility of applying our two class concept to  $\Delta F^0$  as a substitute for the more rigorous Bjerrum interpretation. Converting the values of log  $K$ , Table I, into values of  $\Delta F^0$  one obtains values ranging from about 5,000 cal. for CsCl to negative values, especially in Class II (*i.e.*, HNO<sub>3</sub>). Our goal of dividing  $\Delta F^0$  into a hydration phenomenon and one involving specific interactions would be furthered if it could be shown that log  $K$  had a connection with the salting out coefficients measured in the previous study,<sup>5</sup> since we were able to show in that case a connection between  $k_s$  and the Gurney unitary entropy concept as applied to strong ion hydration effects in aqueous salt solutions alone.

There is indeed, Fig. 4, a suggestion that log  $K$  and  $k_s$  involve the same type of interactions. It should be emphasized that the  $k_s$  values are obtained in a system that is essentially all salt and water and a negligible amount of TBP. On the other hand,

the  $\log K$  term arises under conditions wherein the system is almost entirely the monohydrated TBP and varying amounts of hydrated salts.

One notes that all the bromide and chloride systems fall on the same general line (Fig. 4) whereas the specific systems suspected of strong interaction (*i.e.*, iodides and nitrates) fall on lines of increasingly steeper slopes. If one divides the standard free energy change into two parts, one can interpret the bromide-chloride systems as representing a general limiting case wherein the monohydrated organic-salt interaction is the same for all salts (not very likely), or that the limiting slope solely represents a hydration-hydrogen bond formation situation. Deviations from this limiting case then could be considered as a measure of the specific salt-organic compound interaction. In the absence of any specific organic-salt interaction, therefore (as exemplified by  $\text{HNO}_3$ ), the TBP system might serve as a useful probe in studying the ion hydration problem. This point is reinforced (Fig. 5) by the linear relationship of the unitary entropy changes (as used in the previous paper<sup>5</sup>) for salt in water alone as compared with the  $\log K$  term. These results can be represented by the equation

$$\log K = 3.3 - 0.18 \Delta S_w \quad (4)$$

or

$$\Delta F = 4500 \text{ cal./mole} - T(0.8\Delta S_w) \quad (5)$$

Since  $\Delta F = \Delta H - T\Delta S$ , this value of 4500 might presumably be identified with  $\Delta H$ . Over 80% of the unitary entropy behavior of aqueous salt behavior in water alone appears to be retained in any hydrated salt linkage with TBP. Pauling<sup>14</sup> has calculated the heat required for a single hydrogen bond formation in water at about 4500 cal. This is suggestive that Class I interactions might involve the process of making or breaking a hydrogen bond between the hydrated salt and the monohydrated TBP. In the case of the mineral acids, the existence of approximately complete hydration of the  $\text{H}^+$  ion precludes the necessity of additional work in the formation of a bond with the TBP. On the other hand,  $\text{CsCl}$ 's relative freedom from any hydration therefore leads to energy requirements approaching 5 kcal.

TABLE III

COMPARATIVE BEHAVIOR OF NITRIC ACID AS DETERMINED BY DILUENT AND STRUCTURE OF SOLVENT

Organic phase	Log $K$	$\alpha$
TBP (undiluted)	-0.78	0.57
TBP (0.2 $M$ in $n$ -hexane)	- .03	.30
Dibutyl butylphosphonate <sup>a</sup> (0.2 $M$ in $n$ -hexane)	- .55	.29
Dibutyl phenylphosphonate <sup>a</sup> (0.2 $M$ in $n$ -hexane)	- .19	.30

<sup>a</sup> W. H. Baldwin and J. E. Savolainen, unpublished data.

Turning to the more general problem of the affinity of salts for TBP, Fig. 4 shows a natural division between the limiting Class I wherein ion hydration effects are paramount and Class II wherein specific interactions or compound-formation dominate and hydration phenomena assume a far smaller

(14) Linus Pauling, "The Nature of the Chemical Bond," Cornell Univ. Press, Ithaca, N. Y., 1944, p. 304.

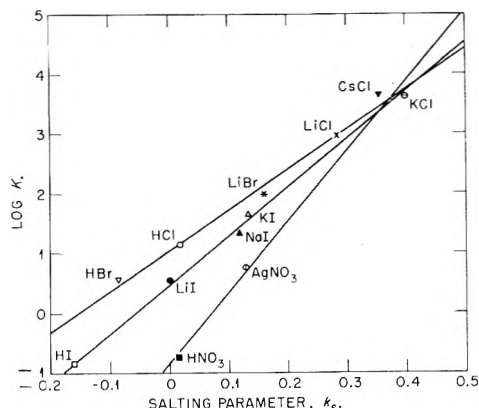


Fig. 4.—Relationship of the standard free energy change (actually  $RT \ln K_0$ ) in the TBP phase to the salting coefficients,  $k_s$  for highly dilute solutions of TBP in water.

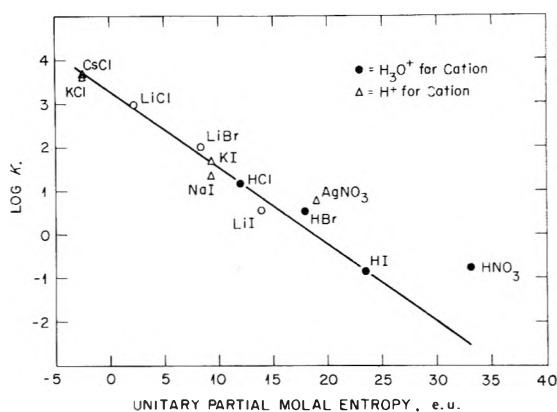


Fig. 5.—Relationship of  $\log K$  to the Gurney unitary partial molal entropies<sup>4</sup> for the electrolytes.

role. This difference in behavior, as previously pointed out, also was reflected in the water desorption behavior of the  $\text{HNO}_3$ .

Since any practical separation involves an organic diluent, it is of some interest to consider its effect on selectivity. As expected, the values of  $\log K$  are more negative (better affinity) in the class of no diluent (Table I) as compared to those using a 0.2  $M$  solution of TBP in hexane (Table III). Significantly, the work of Baldwin and Savolainen,<sup>15</sup> a study involving equivalent concentrations of analogs of TBP in a diluent (hexane), not only shows the same values for  $\alpha$  independent of structure, but serve to emphasize that structural changes in the extractant reflect their effects on selectivities in the change of the standard free energy term.

Finally, this constancy in the empirical  $\alpha$  term with diluent and its change in the case of no diluent highlight the importance of the diluent and its concentration in effecting sharp separations by the solvent extraction technique.

We conclude this discussion by suggesting that Class I, Fig. 4, represents a limiting case of hydrated salt-monohydrated TBP interaction, and that the characteristics of these systems are primarily determined by aqueous solution, ion hydration effects.

On the other hand, deviations from this line

(15) W. H. Baldwin and J. E. Savolainen, unpublished data.

should prove useful in characterizing the magnitude of the specific organic-non-hydrated salt in-

teraction that is present in any actual, practical separations process.

## NOTES

### THE EFFECT OF TEMPERATURE ON THE PHASE EQUILIBRIUM OF POLYPHOSPHATES

By W. J. DIAMOND<sup>1</sup>

Research Laboratories, Whirlpool Corporation, St. Joseph, Michigan  
Received June 13, 1958

Quimby<sup>2</sup> reported the phase equilibrium diagram for the  $\text{Na}_5\text{P}_3\text{O}_{10}\text{-Ca}^{++}$  system in aqueous solution at 60° as determined by J. A. Gray and K. A. Lemmerman. Previously, Topley<sup>3</sup> had determined the dissociation constant of the soluble calcium triphosphate complex at 25°. The excellent agreement between these values suggested negligible temperature effect on stability of the complex.

Examination of the Quimby curve suggested that the two phase regions should be more properly labeled suspension and chelate solution. When so designated, it was predicted that washing phenomena such as soil removal, redeposition, and rinsability would be influenced by the phase regions. Before investigating this proposition, it was necessary to determine the phase boundaries of the common sodium polyphosphates at the temperatures encountered in laundering.

Tripolyphosphate and tetrapolyphosphate were selected because of their use in most detergents. Hexametaphosphate was investigated because of its common use as a water softening agent in laundering even though it is not an ingredient of any common packaged detergent.

Temperatures of 20, 40 and 57° were selected to cover the range of most laundry processes. Polyphosphate concentrations were limited to 4 mmoles/l. which is the normal upper limit for home laundering.

#### Experimental

Fresh polyphosphate solutions were prepared daily using distilled water. The tripolyphosphate and hexametaphosphate were secured from Westvaco Mineral Products Division of Food Machinery and Chemical Company. The former analyzed 96.24%  $\text{Na}_5\text{P}_3\text{O}_{10}$ .<sup>4</sup> The latter had an average chain length of 14 and was 99% polymerized. Fisher C.P. tetrasodium pyrophosphate  $\text{Na}_4\text{P}_2\text{O}_7 \cdot 10\text{H}_2\text{O}$  was considered as 100% pure in all calculations. Fisher U.S.P.  $\text{CaCl}_2 \cdot 2\text{H}_2\text{O}$  was used for preparation of 0.01 *M* stock solution.

Two hundred ml. of test solution was required for each experiment. The required quantity of polyphosphate solution was measured into a beaker and warmed to the

test temperature in a constant temperature bath. In a second beaker, calcium chloride solution and distilled water were heated. When both solutions were at temperature, the tripolyphosphate was added to the calcium chloride solution and mixed for one minute. Turbidity readings were made at several intervals during a period of 15 minutes with a Fisher Nefluorophotometer. Between readings, the mixture was kept in the constant temperature bath.

#### Discussion

Gray and Lemmerman's results for tripolyphosphate at 60° are generally confirmed by these experiments. The relatively minor discrepancies at low tripolyphosphate concentration can be attributed to the slightly different temperatures (57° was the limit of the constant temperature bath used in these experiments) and the time limit of 15 minutes for these experiments in contrast to their equilibrium time. The divergence between the two curves appears to increase at higher tripolyphosphate concentrations. Further, these experiments failed to detect any deviation from linearity as reported by Quimby. In Fig. 1, the

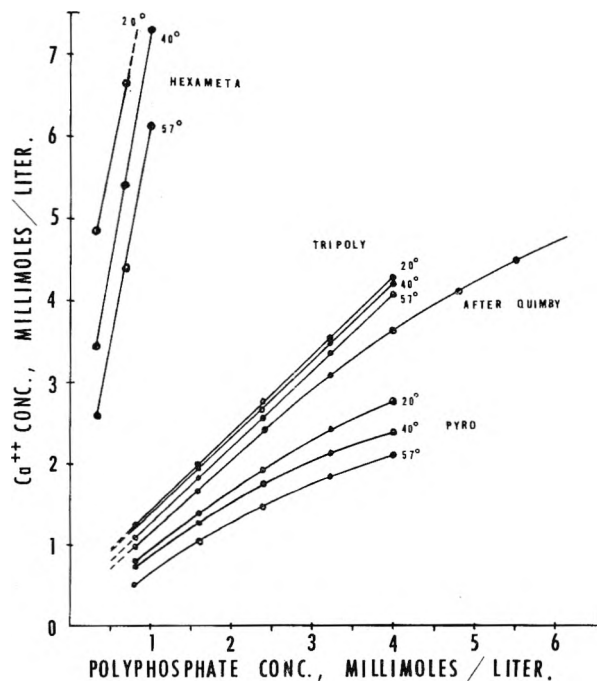


Fig. 1.—Phase boundaries for sodium polyphosphate- $\text{Ca}^{++}$  systems.

phase boundary for the tripolyphosphate-calcium reaction can be expressed by similar equations

$$[\text{Ca}^{++}] = [\text{Na}_5\text{P}_3\text{O}_{10}] + 0.15 \text{ at } 57^\circ \quad (1)$$

$$[\text{Ca}^{++}] = [\text{Na}_5\text{P}_3\text{O}_{10}] + 0.30 \text{ at } 40^\circ \quad (2)$$

(1) The Brunswick Balke Collender Corporation, Muskegon 82 Michigan.

(2) O. T. Quimby, *THIS JOURNAL*, **58**, 603 (1954).

(3) B. Topley, *Quant. Revs.*, **3**, 354 (1949).

(4) L. E. Netherton, A. R. Wreath and D. N. Bernhart, *Anal. Chem.*, **27**, 860 (1955).

$$[\text{Ca}^{++}] = [\text{Na}_5\text{P}_3\text{O}_{10}] + 0.45 \text{ at } 20^\circ \quad (3)$$

Since most of the non-linear portion of this curve is beyond the practical range of tripolyphosphate in detergents, no attempt was made to explain the differences. The phase boundary is only slightly affected by temperature over the range 20 to 57°.

The tetrasodium pyrophosphate phase boundary is definitely temperature sensitive as shown in Fig. 1. Furthermore, these curves show a definite tendency to curve down as the tetrasodium pyrophosphate is increased. On a molar basis, the tripolyphosphate is approximately twice as effective as tetrasodium pyrophosphate for chelating  $\text{Ca}^{++}$  at 57° and at either 1 or 4 mmoles/l. of polyphosphate. However, at intermediate concentrations, the ratio decreases to as low as 1.66. At 20° and all concentrations, the tripolyphosphate is 1.50 to 1.60 times as effective as the tetrasodium pyrophosphate.

The temperature effect for hexametaphosphate (Fig. 1) was so great that accurate determination of the phase boundary by neofluorometry readings in an instrument without temperature control was difficult. The magnitude of the error in these readings is therefore probably greater than in the tripoly or pyrophosphate measurements.

### Conclusions

Temperature has little effect on the phase boundary of the Ca-tripolyphosphate system in aqueous solution. The influence of temperature on both the sodium pyrophosphate-Ca ion system and the sodium hexametaphosphate-Ca ion system is substantial. As temperature is increased, lower concentrations of  $\text{Ca}^{++}$  are required to form a suspension with a given quantity of the polyphosphates. For the experimental conditions reported herein, the phase boundary is a linear function of  $\text{Ca}^{++}$  with both tripolyphosphate and hexametaphosphate. The  $\text{Ca}^{++}$ -tetrasodium pyrophosphate phase boundary is not a linear relationship.

Quantitatively, the superior chelation capabilities of tripolyphosphate to pyrophosphate vary on a molar basis from 2:1 at 57° and 5 mmoles/l. of polyphosphate to 1.5:1 at 20° and 0.8 mmole/l. of polyphosphate. On a molar basis, the Westvaco hexametaphosphate is more effective than tripolyphosphate for chelating  $\text{Ca}^{++}$  at all temperatures. The effectiveness is not influenced by concentration.

## THE RELATIVE ACIDITY OF $\text{H}_2\text{O}^{18}$ AND $\text{H}_2\text{O}^{16}$ COÖRDINATED TO A TRIPROTONIC ION

By H. R. HUNT AND H. TAUBE

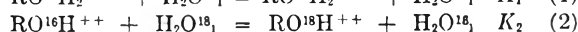
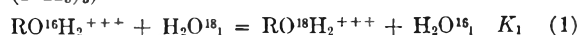
Contribution from the George Herbert Jones Laboratory of the University of Chicago, Chicago, Ill.

Received August 1, 1968

The interpretation<sup>1</sup> of experiments on the fractionation of the isotopes of oxygen in  $(\text{NH}_3)_5\text{CoOH}_2^{+++}$  when this ion reacts with  $\text{Cr}^{++}$  required the measurement of the relative acidities

(1) R. K. MURMENN, H. Taube and F. A. Poscy, *J. Am. Chem. Soc.*, **79**, 262 (1957).

of  $(\text{NH}_3)_5\text{CoO}^{16}\text{H}_2^{+++}$  and  $(\text{NH}_3)_5\text{CoO}^{18}\text{H}_2^{+++}$ . The ratio of the dissociation constants in question can be determined by measuring the equilibrium constants for reactions 1 and 2 (R represents  $\text{Co}(\text{NH}_3)_5$ )



It can be seen that the ratio

$$\frac{K_1}{K_2} = \frac{(\text{RO}^{18}\text{H}_2^{+++})(\text{RO}^{16}\text{H}^{++})}{(\text{RO}^{16}\text{H}_2^{+++})(\text{RO}^{18}\text{H}^{++})} = \frac{K_a^{18}}{K_a^{16}}$$

where  $K_a$  represents the quotients

$$\frac{(\text{ROH}^{++})(\text{H}^+)}{(\text{ROH}_2^{+++})}$$

for the particular isotopic forms of oxygen in question.  $K_1$  is fairly accurately<sup>2</sup> known (and has been redetermined in the course of present work), so that the measurement of  $K_2$  was the principal goal of the present investigation. The temperature coefficient of  $K_1$  also was determined.

### Experimental

A difficulty in the determination of  $K_2$  arises from the circumstance that whereas the exchange equilibrium is established less rapidly as a greater proportion of the aquo salt is converted to the hydroxo, decomposition reactions become more rapid. Early efforts to measure  $K_2$  by allowing sufficient time for exchange equilibrium to be established gave irreproducible and unreasonable results. The method we adopted for the present series of experiments involved fixing the initial values of  $N_R/N_W$  (these symbols refer to the mole fraction of  $\text{O}^{18}$  in the cation and in solvent, respectively) to cover a range wide enough to bracket the equilibrium value. The initial direction of the change of the ratio for each solution was determined and it was assumed that these point to the equilibrium values. A method such as this will work if the initial rate of change in the ratio  $N_R/N_W$  caused by approach to exchange equilibrium is greater than that caused by fractionation effects accompanying net reaction. The principal net change appears to be the production of cobaltic oxide, and this reaction appears furthermore to be autocatalytic. No significant change in the absorption spectrum of the solutions used for the experiments summarized in Table II occurs in 36 hours; the half-time for the exchange reaction under the conditions of the experiments is 46 hours. It is felt, therefore, that the results obtained, within the limits of accuracy of the work, are a dependable measure of the value of  $K_2$ .

The preparation of the salts and the method of isotopic analysis have been described elsewhere.<sup>3</sup> In the isotopic analysis of the solutions which contained a mixture of  $\text{ROH}_2^{+++}$  and  $\text{ROH}^{++}$ , the  $\text{ROH}^{+++}$  is first converted to  $\text{ROH}_2^{+++}$  by acidifying, and the oxygen-isotopic composition of the entire cobaltic salt in solution is determined.

### Results

Table I contains a report of the results on a determination of the equilibrium constant  $K_1$  at 25.2 and 44.7°.

TABLE I  
EQUILIBRIUM CONSTANT FOR WATER EXCHANGE OF THE  
AQUO ION

$N \times 10^4$ for Solvent	$N \times 10^4$ at equilibrium for salt (25.2°)	$N \times 10^4$ at equilibrium for salt (44.7°)
2.1245	2.1663	2.1604
2.1244	2.1661	2.1617
2.1242	2.1652	2.1609
2.1244	2.1659	2.1610

$$K_1 \text{ at } 25.2^\circ = 1.0196$$

$$\text{at } 44.7^\circ = 1.0173$$

(2) A. C. Rutenberg and H. Taube, *J. Chem. Phys.*, **20**, 825 (1952).  
(3) H. R. Hunt and H. Taube, *J. Am. Chem. Soc.*, **80**, 2642 (1958).

An earlier and less careful set of experiments yielded for  $K_1$  at 25.0° the values 1.0194 and 1.0207. The value 1.019 at 27° has been reported in the literature.<sup>2</sup>

Two series of experiments were performed to determine  $K_2$ . For each set, enough base was added to change 30% of the total complex to the hydroxo form. The initial concentration of the salt  $\text{RH}_2\text{O}(\text{ClO}_4)_3$  was approximately 0.025 *M*.

Table II presents the results of the most recent and most complete set of experiments on the measurements of  $K_2$ . Four separate experiments constitute the set; for each experiment the ratio of the mole fraction of  $\text{O}^{18}$  in the total water coordinated to the ion ( $N_R$ ) compared to that for the solvent water ( $N_W$ ) is recorded at three different times, beginning with the ratio which was initially fixed by adjusting the isotopic composition of the water relative to the salt. The initial value of  $N_R$  and the values of  $N_W$  as recorded are the averages of two independent determinations. The average deviations from the mean for these determinations was found to be 1 part in 3000, with the deviation for the salt being slightly greater than for the bulk water. In an earlier set of experiments the sampling was done after exchange proceeded for 23.9 hr. These experiments are not reported in detail, but the results are referred to in the Discussion.

TABLE II

EXPERIMENTS ON THE DETERMINATION OF  $K_2$  (AT 25°;  $\Sigma\text{R(III)} = 0.025M$ ; 30% OF AQUO ION CONVERTED TO  $\text{ROH}^{++}$ )

I		II		III		IV	
Time, hr.	$N_R/N_W$	Time, hr.	$N_R/N_W$	Time, hr.	$N_R/N_W$	Time, hr.	$N_R/N_W$
0	1.0182	0	1.0132	0	1.0074	0	1.0029
15.1	1.0185	15.0	1.0149	14.9	1.0097	14.2	1.0061
36.2	1.0172	36.2	1.0140	36.2	0.0101	36.3	1.0079

### Discussion

In principle it should be possible to treat the data of Table II using the known value of  $t_{1/2}$  for the exchange and calculating for each value of  $N_R/N_W$  after time zero the corresponding value of this ratio at infinite time. When this is done, the set of values obtained for an exchange time of 15 hours give for  $N_R/N_W$  at infinite time a set which group about an average of 1.209; those at 36 hr. give for the same ratio an average of 1.0150. The difference between the two averages seems too great to be accounted for by random error (the average deviation for the 1st set is 0.0012 and for the second is 0.006), but the cause of the difference is not known with certainty. It is possible that net changes do occur which are accompanied by isotopic fractionation effects, even though the spectra did not change significantly. In any event, it seems safer to use the data in the less sophisticated way: simply examining the initial directions and magnitudes of the changes for the ratios  $N_R/N_W$ .

For experiments II, III and IV of Table II,  $N_R/N_W$  certainly increases with time, for experiment I it remains constant or decreases slightly.

On this basis,  $N_R/N_W$  for the equilibrium mixture can be set between 1.0132 (the initial value for experiment II) and 1.0183 (the initial value for experiment I), and considerably closer to the latter value than to the former. On this basis,  $1.0170 \pm 0.00075$  for  $N_R/N_W$  at equilibrium is a safe choice. An earlier set of experiments brackets  $N_R/N_W$  at equilibrium between 1.0153 and 1.0194 with  $1.0165 \pm 0.001$  as the indicated value. Since for a solution which contains  $\text{ROH}_2^{+++}$  and no  $\text{ROH}^{++}$ ,  $N_R/N_W$  at equilibrium is 1.0196, and when 30% of the  $\text{Co(III)}$  is present as  $\text{ROH}^{++}$ , the equilibrium ratio is 1.0170, for a sample completely converted to  $\text{ROH}^{++}$ , the equilibrium ratio is calculated as  $1.008 \pm 0.001$ . This then is the value we report for  $K_2$  (and is substantially the value used in the interpretation of oxygen isotope effects in the  $\text{Cr}^{++}-\text{ROH}_2^{+++}$  system).

A value of 1.035 can be calculated for the relative acidities of  $\text{H}_2\text{O}^{16}$  and  $\text{H}_2\text{O}^{18}$ , using the known<sup>4</sup> partition function ratio for  $\text{H}_2\text{O}^{16}/\text{H}_2\text{O}^{18}$ , and calculating the corresponding ratio for  $\text{O}^{16}\text{H}^-/\text{O}^{18}\text{H}^-$ . For this calculation,  $3603 \pm 4 \text{ cm.}^{-1}$  was used as the fundamental vibration frequency for  $\text{OH}^-$  in solution.<sup>5</sup> It is interesting that the difference in acidity is so considerably reduced from 1.035 to  $1.008 \pm 0.001$  by the coordination of the water to the metal ion. The principal reason for the change in relative acidity when  $\text{H}_2\text{O}$  is coordinated to a metal ion is likely this. The force constant associated with the binding of oxygen to the metal ion will be considerably greater for  $\text{OH}^-$  than it is for  $\text{H}_2\text{O}$ ; thus the oxygen isotope discrimination associated with the loss of a proton from  $\text{H}_2\text{O}$  is partly compensated for by the enhanced oxygen isotope discrimination exerted by  $\text{Co}^{+++}$  when it acts on  $\text{OH}^-$  in place of  $\text{H}_2\text{O}$ .

The only point in connection with the redetermination of  $K_1$  which merits special comment concerns the temperature coefficient of this equilibrium constant. From the data in Table I,  $\Delta H$  is calculated as  $-22 \text{ cal.}$ ,  $\Delta F$  as  $-11.6 \text{ cal.}$  and  $\Delta S$  as  $-0.035 \text{ e.u. mole}^{-1}$ . The value of  $\Delta H$  is in the expected direction. The principal source of the isotopic discrimination lies in the bonds formed by the water molecules; the force constant for this vibration is greater when  $\text{H}_2\text{O}$  is bound to  $\text{Co(III)}$  than it is when  $\text{H}_2\text{O}$  is bound to  $\text{H}_2\text{O}$ , hence the sign of  $\Delta H$ , and of  $\Delta F$ , is as expected. For comparison, the values for the equilibrium are here-

$$1/6 \text{ Al}(\text{H}_2\text{O}^{16})_6^{+++} + \text{H}_2\text{O}^{18} = 1/6 \text{ Al}(\text{O}^{18}\text{H})_6^{+++} + \text{H}_2\text{O}^{16}$$

with recorded:  $\Delta H = -53$ ,  $\Delta F = -14.6$  and  $\Delta S = -0.13 \text{ e.u.}$  These are calculated from Feder's data<sup>6</sup> on the effect which aluminum salts exert on the relative fugacities of  $\text{H}_2\text{O}^{18}$  and  $\text{H}_2\text{O}^{16}$  in solvent water.

**Acknowledgment.**—This work was supported by the Office of Naval Research under contract N6-ori-02026.

(4) H. C. Urey, *J. Chem. Soc.*, 562 (1947).

(5) J. L. Thompson and J. R. Nielsen, *Phys. Rev.*, **37**, 1669 (1931).

(6) H. M. Feder, Ph.D. Dissertation, University of Chicago, 1954.

## KINETICS OF ELECTRON TRANSFER BETWEEN COBALTOUS AND COBAL TIC AMMINES

BY EVAN APPELMAN, MICHAEL ANBAR AND HENRY TAUBE

*George Herbert Jones Chemical Laboratory, University of Chicago,*

*Chicago, Illinois*

*Received August 8, 1958*

In ammoniacal cobaltous solutions there exists a labile equilibrium among all possible species  $\text{Co}(\text{NH}_3)_n^{++}$  and  $\text{Co}(\text{NH}_3)_n\text{OH}^+$  in which  $n$  ranges from zero through six.<sup>1</sup> These species exchange electrons only very slowly with the hexammine cobaltic ion,<sup>2</sup> presumably due to the absence of a low energy mechanism by which the electron can be transferred through the proton shell surrounding the cobaltic ion. If an acidopentammine cobaltic ion is used instead of the hexammine, the acido group ought to provide such a transfer mechanism by forming the symmetrical bridged activated complex<sup>3</sup>  $(\text{NH}_3)_5\text{Co}^*\text{XCo}(\text{NH}_3)_5$ . Exchange has been reported to take place between cobaltous species and aquopentammine cobaltic ion in strongly ammoniacal solution,<sup>4</sup> and we have undertaken a detailed study of the reaction.

### Experimental

Aquopentammine cobaltic perchlorate was prepared as described elsewhere<sup>5</sup> and a  $\text{Co}^{60}(\text{II})$  solution of high specific activity was obtained from the Health Physics group of the University of Chicago. All other chemicals were commercial products of reagent grade.

To prevent air oxidation of the cobaltous amines, most reactions were carried out in rubber-capped serum bottles under a static nitrogen atmosphere. Samples for radioanalysis were withdrawn by a hypodermic syringe and needle and were delivered into a nearly saturated solution of mercuric chloride in concentrated hydrochloric acid cooled to its freezing point. This quenched the exchange and precipitated the cobalt(III) as  $\text{Co}(\text{NH}_3)_5\text{H}_2\text{OHgCl}_5$ .<sup>6</sup> The precipitate was filtered, washed with alcohol and ether, air-dried, mounted on an aluminum card and counted in an end-window, methane-flow  $\beta$ -proportional counter. Corrections were made for variations in self-absorption among the samples. In a few preliminary experiments a different procedure was used. Mixtures were outgassed and sealed under vacuum. For analysis they were frozen, broken open and acidified, thawed and saturated with ammonium thiocyanate. The cobalt(II) was then extracted into an ethyl ether-*n*-amyl alcohol mixture as the thiocyanate complex,<sup>6</sup> and the remaining aqueous solution of cobalt(III) was counted in a glass-jacketed, thin-walled Geiger counter. Tests indicated separation-induced exchange to be negligible in either procedure.

In all cases the radioactive tracer was added in the cobaltous form.

All reaction mixtures were protected from exposure to light and were discarded if any precipitate was observed.

Blanks were run to determine the extent of oxidation by residual oxygen and the appropriate corrections, amounting to 5–10% of the sample activity, were made.

Reactions were followed at least to 50% exchange in all but the very slowest systems, in a few of which the exchange was only 20–30% completed at the end of the run. In

some of the fastest systems the reaction was followed to 97% exchange.

Samples for spectroanalysis were quenched in hydrochloric acid and their absorption spectra measured between 3200 and 10,000 Å., in a Beckman Model DU spectrophotometer.

TABLE I<sup>a</sup>

Expt. no.	Total <sup>b</sup> NH <sub>3</sub>	Free NH <sub>3</sub>	Co <sup>++c</sup> × 10 <sup>4</sup>	ROH <sup>++d</sup> × 10 <sup>3</sup>	Rate × 10 <sup>4</sup> M/hr.	k × 10 <sup>-6</sup> , M <sup>-1</sup> hr. <sup>-1</sup>
1 <sup>e</sup>	0.23	0.163	0.31	42	1.32	0.87
2 <sup>f</sup>	.52	.167	1.42	42	5.6	.72
3 <sup>g</sup>	.34	.164	.75	21	1.30	.70
4 <sup>h</sup>	.35	.174	.62	79	5.5	.70
5	.33	.158	.85	42	3.1	.88
6 <sup>i</sup>	.35	.171	.66	42	3.0	.75
7	.69	.47	.0153	43	10.6	.71
8 <sup>j</sup>	.69	.47	.0153	42	10.5	.71
9	.167	.052	16.5	41	.62	2.4
10 <sup>k</sup>	.167	.052	16.5	40	.37	1.5
11	.092	.020	88	39	.39	36
12 <sup>l</sup>	.095	.020	88	36	.22	22
13 <sup>m</sup>	.33	.150	.48	43	.75	.48
14 <sup>k</sup>	.33	.154	.63	43	1.52	.65
15 <sup>l</sup>	.33	.161	1.07	42	5.8	1.19
16 <sup>m</sup>	.33	.165	1.41	41	13.0	1.82

<sup>a</sup> All concentrations are moles/liter ( $M$ ). The bulk electrolyte was a mixture of  $\text{NaNO}_3$  and  $\text{NH}_4\text{NO}_3$  such that the total ionic strength was 2.28, with  $\text{ClO}_4^-$  present at concentrations between 0.13 and 0.35  $M$ . Unless otherwise specified, temp. = 35.5°,  $\text{NH}_4^+ = 0.94 M$ , total  $\text{Co}(\text{II}) = 0.0535 M$ , and total  $\text{Co}(\text{III}) = 0.043 M$ . <sup>b</sup> Total  $\text{NH}_3 = \text{free NH}_3 + \text{NH}_3$  complexed by  $\text{Co}(\text{II})$ . <sup>c</sup> Distribution of  $\text{Co}(\text{II})$  species was calculated from equilibrium data on  $\text{Co}(\text{II})$  amines<sup>1</sup> by neglecting formation of hydroxocobaltous ions and assuming that substitution of  $\text{Na}^+$  did not alter the equilibria. The mean number of  $\text{NH}_3$ 's bonded to a  $\text{Co}^{++}$  varied from 4.1 at the highest  $\text{NH}_3$  concentrations to 1.4 at the lowest. <sup>d</sup>  $R = \text{Co}(\text{NH}_3)_5^{+++}$ . Correction has been made for the small fraction of  $\text{Co}(\text{III})$  remaining as  $\text{RH}_2\text{O}^{+++}$ , using the acid dissociation constants of  $\text{NH}_4^+$  and  $\text{RH}_2\text{O}^{+++}$  in these media.<sup>1</sup> <sup>e</sup>  $\text{Co}(\text{II}) = 0.0214 M$ . <sup>f</sup>  $\text{Co}(\text{II}) = 0.107 M$ . <sup>g</sup>  $\text{Co}(\text{III}) = 0.0210 M$ . <sup>h</sup>  $\text{Co}(\text{III}) = 0.080 M$ . <sup>i</sup>  $\text{NH}_4^+ = 1.83 M$ . <sup>j</sup> 15.65°. <sup>k</sup> 25.0°. <sup>l</sup> 44.4°. <sup>m</sup> 55.2°.

### Results and Discussion

After a week at 45°, exchange in a mixture 0.01  $M$  in acid and 0.04  $M$  each in  $\text{Co}(\text{II})$  and aquopentammine  $\text{Co}(\text{III})$  has proceeded less than 0.4% toward completion. This agrees with the absence of exchange in the  $\text{Co}^{++}-\text{Co}(\text{NH}_3)_5\text{Cl}^{+++}$  system.<sup>6</sup>

In ammoniacal solutions the reaction followed the exponential equation for homogeneous exchange.<sup>7</sup> The principal results appear in Table I. In addition, compatible results were obtained in the few experiments in which the  $\text{Co}(\text{III})$  was radioassayed in solution, and an experiment in an all-perchlorate medium indicated nitrate ion to have no great specific effect on the reaction.

After exchange in a mixture similar to expt. 7 had proceeded to 80% of completion, the absorption spectrum of an acidified sample could be quantitatively matched by summing the spectrum of a solution containing cobaltous ion with that of a solution containing aquopentammine cobaltic ion, indicating that no net reaction had taken place.

The values of " $k$ " in the last column of the table

(7) G. Friedlander and J. Kennedy, "Nuclear and Radiochemistry," John Wiley and Sons, Inc., New York, N. Y., 1955, p. 316.

(1) J. Bjerrum, "Metal Ammine Formation in Aqueous Solution," P. Haase and Son, Copenhagen, Denmark, 1941, pp. 286–295.

(2) W. B. Lewis, C. D. Coryell and J. W. Irvine, *J. Chem. Soc.*, S386 (1949).

(3) H. Taube and H. Myers, *J. Am. Chem. Soc.*, **76**, 2103 (1954).

(4) K. McCallum, "Brookhaven Conf. on Isotopic Exchange Reactions and Chemical Kinetics" (Chem. Conf. No. 2), BNL-C-8, (1948), p. 128.

(5) A. C. Rutenberg and H. Taube, *J. Chem. Phys.*, **20**, 825 (1952).

(6) J. Flagg, *J. Am. Chem. Soc.*, **63**, 557 (1941).



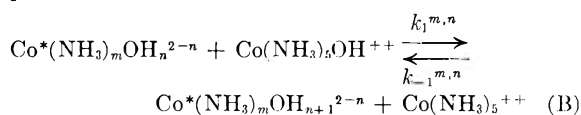
were calculated from the rate law

$$\text{exchange rate} = k(\text{Co}^{++})(\text{Co}(\text{NH}_3)_5\text{OH}^{++})(\text{NH}_3)^5 \quad (\text{A})$$

From the first five experiments we conclude that the reaction is first order in  $\text{Co}^{++}$  and in  $\text{Co}(\text{NH}_3)_5\text{OH}^{++}$ . Comparison of 8 with 7, and of 6 with 5, shows that at ammonia concentrations above 0.16  $M$  the rate is independent of acidity. Comparison of 7 and 8 with 1-6 shows that between ammonia concentrations of 0.16 and 0.47  $M$  the reaction is closely fifth order in ammonia. At lower ammonia concentrations (expts. 9-12) the reaction is much more rapid than is predicted by rate law (A), and for such conditions paths of lower order in ammonia presumably are involved. In the range 0.02 to 0.05  $M$  ammonia, the order with respect to ammonia is between one and two. In this range an inverse dependence on acidity of somewhat less than first order is indicated.

A plot of  $\ln(k/T)$  versus  $1/T$  for expts. 5 and 13-16 shows a slight positive curvature at the high temperature end, giving a  $\Delta H^\ddagger$  which rises from 5.1 kcal. at the four lower temperatures to 7.5 kcal. between the two highest. From the lower value we calculate a  $\Delta S^\ddagger$  of  $-31.5$  e.u.

Thus, although at the highest ammonia concentrations exchange may proceed primarily through the symmetrical activated complex  $(\text{NH}_3)_5\text{Co}^*\text{OHC}(\text{NH}_3)_5^{++}$ , lowering of the ammonia concentration brings out activated complexes containing less than 5 ammonia molecules for each  $\text{Co}^{++}$ . Symmetrical activated complexes can be formulated using less than five ammonia complexes for each  $\text{Co}^{++}$ . However, these would require multiple bridging and bridging through the ammonia, and in the limit would still require 2 ammonia molecules for each  $\text{Co}^{++}$ . Such bridging seems very unlikely, and in any case the observation that the order of the reaction with respect to ammonia concentrations does fall below two is not accommodated by such mechanisms. An alternative suggestion is that unsymmetrical activated complexes play a role. Taking account also of the observation that at low ammonia the reaction rate increases with alkalinity, the reaction may be represented by the parallel reactions



with  $n$  equal to zero or one and  $m$  taking all values from zero through 5. Since under the conditions of our experiments  $\text{Co}(\text{NH}_3)_5\text{OH}^{++}$  is stable with respect to the lower ammine complex,<sup>1</sup> the mechanism requires that  $\text{Co}(\text{II})$  bring about the rapid (compared to rate of electron transfer) transformation of the lower amines to the pentammine complex. The direct test of this feature of the mechanism has not yet been made, but there is no evidence from preparative procedures that the reactions in question are rapid enough.

For the reaction:  $\text{Co}^{++} + 5\text{NH}_3 = \text{Co}(\text{NH}_3)_5^{++}$ ,  $K_{\text{eq}} = 4.79 \times 10^{-5}$  in our media at  $35.5^\circ$  with  $\Delta H = -10.5$  kcal. and  $\Delta S = -8.0$  e.u. We may then rewrite rate law (A)

$$\text{exchange rate} = k'(\text{Co}(\text{NH}_3)_5^{++})(\text{Co}(\text{NH}_3)_5\text{OH}^{++}) \quad (\text{C})$$

At  $35.5^\circ$ , and with ammonia greater than 0.15  $M$ ,  $k' = 1.6 (M)^{-1}(\text{hr.})^{-1}$ ,  $\Delta H^\ddagger = 15.6$  kcal., and  $\Delta S^\ddagger = -23.5$  e.u. At  $45^\circ$   $k'$  becomes 2.2, in sharp contrast to the corresponding constant for the  $\text{Co}(\text{NH}_3)_6^{++}-\text{Co}(\text{NH}_3)_6^{+++}$  exchange, to which an upper limit of  $0.003 (M)^{-1}(\text{hr.})^{-1}$  has been set at this temperature.<sup>2</sup>

**Acknowledgments.**—We gratefully acknowledge the extensive aid and encouragement given by Dr. John W. Cahn during the early part of this work, and we wish to thank Professor Nathan Sugarman for providing our proportional counter. This research was supported by the Office of Naval Research under Contract N 6-ori-02026.

## THERMODYNAMICS OF THE MERCURY REDUCTION OF TITANIUM TETRAFLUORIDE

By JOHN N. BLOCHER, JR. AND ELTON H. HALL

Contribution from Battelle Memorial Institute, Columbus, Ohio

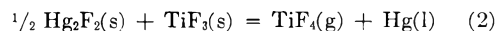
Received August 8, 1958

As part of a program to determine the thermodynamic properties of the titanium halides, the authors have studied the mercury reduction of titanium tetrafluoride by the technique previously employed with the bromide system.<sup>1</sup> The reagents were triple-distilled mercury and titanium tetrafluoride twice sublimed *in vacuo* as described earlier.<sup>2</sup>

Two independent determinations of the equilibrium pressure as a function of temperature gave the data shown in Fig. 1 which are represented by the equation of the full line

$$\log P_{\text{atm}} = -5574/T - 1.86 \log T + 14.62 \quad (1)$$

The coefficient of the  $\log T$  term ( $\Delta C_p/R$ ) was evaluated from an estimate of  $\Delta C_p = -3.7$  for the reaction



to which the equilibrium pressures were tentatively assigned. For the calculation of  $\Delta C_p$ , the heat capacity at  $298.2^\circ\text{K}$ . of  $\text{Hg}(\text{l}) = 6.65$  cal./mole/deg. was taken from Circular 500, National Bureau of Standards, and that of  $\text{TiF}_4(\text{g}) = 19.8$  cal./mole/deg. was calculated from the estimated vibrational frequencies in reference 2. The heat capacities of  $\text{Hg}_2\text{F}_2(\text{s}) = 22.5$  cal./mole/deg. and  $\text{TiF}_3(\text{s}) = 18.9$  cal./mole/deg. were estimated by comparison of published values<sup>3-5</sup> for the fluorides and chlorides of Al, Mg, Ti and Hg.

From equation 1 are calculated

$$\begin{aligned} \Delta F_{298}^0 &= 11.84 \text{ kcal./mole} \\ \Delta H_{298}^0 &= 24.4 \text{ kcal./mole} \\ \Delta S_{298}^0 &= 42.1 \text{ e.u.} \end{aligned}$$

Although X-ray diffraction patterns of the reaction product showed only  $\text{Hg}_2\text{F}_2$  and some poorly de-

(1) E. H. Hall and J. M. Blocher, Jr., *J. Electrochem. Soc.*, **105**, 40 (1958).

(2) E. H. Hall, J. M. Blocher, Jr., and I. E. Campbell, *ibid.*, **105**, 275 (1958).

(3) Circular 500, National Bureau of Standards.

(4) F. D. Rossini, *et al.*, "Properties of Titanium Compounds and Related Substances," ONR Report ACR-17, Office of Naval Research (1956).

(5) K. K. Kelly, U. S. Bureau of Mines Bulletin 476 (1949).

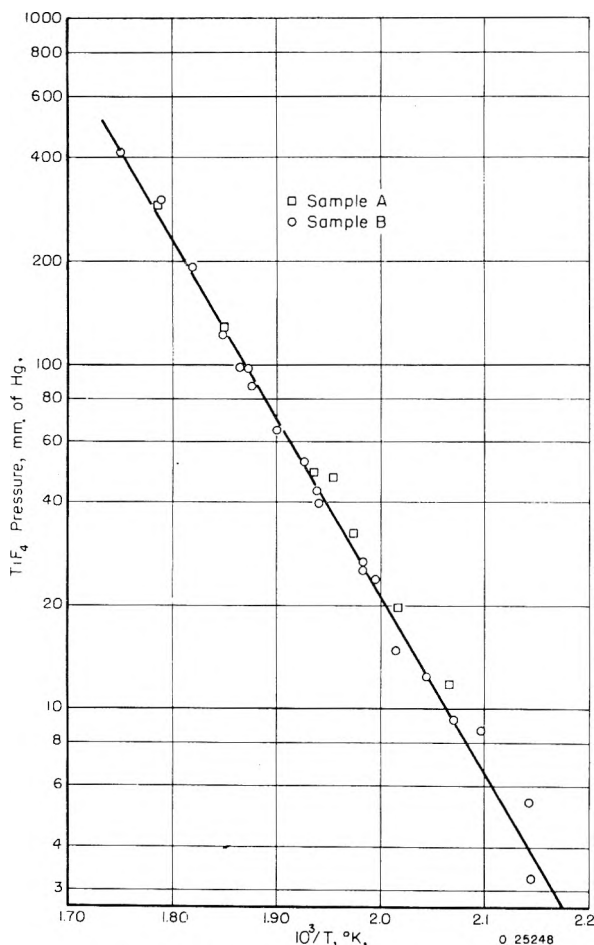


Fig. 1.—Mercury reduction of  $\text{TiF}_4$ .

lined lines not characteristic of  $\text{TiF}_3$ ,<sup>6</sup> it should be noted that the entropy change is close to that (44.7 e.u.) for the corresponding bromide system,<sup>1</sup> and that (also 44.7 e.u.) calculated from data in references 3 and 4, for the chloride system. Thus, if the titanium-bearing reaction product is not  $\text{TiF}_3(\text{s})$ , but a solid solution or complex, it is thermodynamically very similar. Therefore, the above heat of reaction is assigned to equation 2 with a probable uncertainty of  $\pm 3$  kcal.

E. J. Prosen and his associates of the National

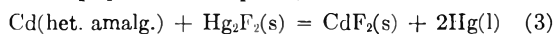
(6) (a) K. S. Vorres and F. B. Dutton, *J. Am. Chem. Soc.*, **77**, 2019 (1955).

(b) Titanium trifluoride prepared at Battelle by the titanium reduction of  $\text{TiF}_4$  gave an X-ray pattern differing somewhat from that of Vorres and Dutton and unlike that of the mercury reduction product.

Bureau of Standards have planned to measure the heat of formation of  $\text{TiF}_4$ . However, these results are not yet available for combination with the present data to give the heat of formation of  $\text{TiF}_3$ . In the meantime, the difference

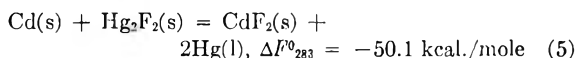
$$\Delta H_{\text{f TiF}_4(\text{s})}^0 - \Delta H_{\text{f TiF}_3(\text{s})}^0$$

may be of interest to those studying the extractive metallurgy of titanium in fluoride systems. For the purpose of this calculation, the cell data of Koerber and De Vries<sup>7</sup> are used. They obtained  $E_{293}^0 = 1.0337$  v., and  $\Delta F_{293}^0 = -47.7$  kcal./mole (the 44.7 in their paper is a misprint) for the reaction



Combination of this value with I.C.T. data<sup>8</sup> for  $\text{Cd}(\text{s}) = \text{Cd}(\text{het. amalg.})$ ,  $\Delta F_{293}^0 = -2.45$  kcal./mole (4)

gives



From data on  $\text{CdF}_2(\text{s})$  on reference 3 ( $\Delta H_{\text{f } 298}^0 = -164.9$  kcal./mole and  $\Delta F_{\text{f } 298}^0 = -154.8$  kcal./mole) and the close approximation  $\Delta F_{293}^0 = \Delta H_{298}^0 - T\Delta S_{298}$ , we calculate

$$\Delta F_{\text{f } 293}^0 \text{ CdF}_2(\text{s}) = -155.3 \text{ kcal./mole} \quad (6)$$

whence, (6 - 5)

$$\Delta F_{\text{f } 293}^0 \text{ Hg}_2\text{F}_2(\text{s}) = -105.2 \text{ kcal./mole} \quad (7)$$

From Latimer's tables,<sup>9</sup> the entropy of  $\text{Hg}_2\text{F}_2(\text{s})$  is estimated to be  $S_{298-2}^0 = 41.8$  e.u. which when combined with the entropies of  $\text{Hg}(\text{l})$  and  $\text{F}_2(\text{g})$  from reference 3, and the above  $\Delta F^0$  value (7) gives

$$\Delta H_{\text{f } 293}^0 \text{ Hg}_2\text{F}_2(\text{s}) \cong \Delta H_{\text{f } 298-2}^0 \text{ Hg}_2\text{F}_2(\text{s}) = -117.6 \text{ kcal./mole}$$

Combination of this value with the present equilibrium data of equation 1 and the heat of sublimation of  $\text{TiF}_4(\text{s})$  ( $\Delta H_{298-2}^0 = 22.9$  kcal./mole) from reference 2, gives

$$\Delta H_{\text{f } 298-2}^0 \text{ TiF}_4(\text{s}) - \Delta H_{\text{f } 298-2}^0 \text{ TiF}_3(\text{s}) = -57.3 (\pm 3) \text{ kcal.}$$

This value confirms the  $-55$  kcal. estimate of Brewer.<sup>10</sup>

The authors are indebted to the Office of Naval Research for their support of this research under Contract No. Nonr-1120(00).

(7) G. G. Koerber and T. De Vries, *J. Am. Chem. Soc.*, **74**, 5008 (1952).

(8) "International Critical Tables," Vol. VII, McGraw-Hill Book Co., New York, N. Y., 1930, p. 256.

(9) W. M. Latimer, *J. Am. Chem. Soc.*, **73**, 1480 (1951).

(10) L. Brewer, L. A. Bromley, P. W. Gilles and N. H. Lofgren, Paper No. 6, Vol. IV-19B, National Nuclear Energy Series, L. L. Quill, Ed. McGraw-Hill Book Co., New York, N. Y., 1950.

Number 6 in  
*Advances In Chemistry Series*

compiled by  
L. H. Horsley and coworkers at the  
*Dow Chemical Company*

## AZEOTROPIC DATA

Contains a 41-page formula index, 107 charts, a 247-page table of binary systems, and a 17-page table of ternary systems.

329 pages—cloth bound—\$5.00 per copy

*order from:*

Special Issue Sales  
American Chemical Society  
1155 Sixteenth Street, N.W.  
Washington 6, D. C.

Number 9 in  
*Advances In Chemistry Series*

edited by the staff of  
*Industrial and Engineering Chemistry*

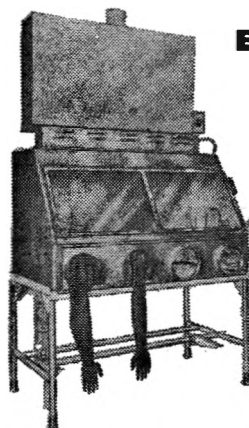
## FIRE RETARDANT PAINTS

Discusses theory of flame-proofing, effectiveness of fire-retardant paints, practical aspects of formulation, and testing. Aircraft coating and flame-resistant mastics are also covered.

94 pages—paper bound—\$2.50 per copy

*order from:*

Special Issue Sales  
American Chemical Society  
1155 Sixteenth Street, N. W.  
Washington 6, D. C.



**BLICKMAN**

## FUME HOOD

for safe  
handling of  
hazardous  
materials

Developed originally for handling bacteria and viruses, this all-stainless steel fume hood is equipped with a micro-biological filter canister incinerator. Polished, seamless, crevice-free construction with rounded corners makes cleaning and decontamination easy and sure. Many convenience features; units 4, 5, 6 or 8 feet long, with or without stand or filter canister. Write for illustrated folder describing 22 different kinds of enclosures for safe handling of hazardous materials. S. Blickman, Inc., 9001 Gregory Avenue, Weehawken, New Jersey.

**BLICKMAN**  
**SAFETY ENCLOSURES**

Look for this symbol of quality 

## COLLECTIVE NUMERICAL PATENT INDEX

to

## Volumes 31-40 of CHEMICAL ABSTRACTS

- Contains more than 143,000 entries, classified by countries in numerical order.
- Classification by patent number is an enormous timesaver.
- Index references give volume, page and location of patent abstract in CHEMICAL ABSTRACTS.
- Cloth bound, 182 pages, 7 1/2" x 10" overall, 8 columns of listings per page covering all patents abstracted in CHEMICAL ABSTRACTS from 1937-46, inclusive.

PRICE \$10.00 POSTPAID

Send orders and inquiries to:  
Special Issue Sales

**American Chemical Society**  
1155 Sixteenth St., N.W., Washington 6, D. C.

---

FOR EASIER, SURER ACCESS  
TO RECORDED INFORMATION  
IN CHEMICAL ABSTRACTS

*Place Your Order to One Or  
More Of The ACS Indexes*

---

## **27-Year Collective Formula Index to Chemical Abstracts**

Over half a million organic and inorganic compounds listed and thoroughly cross referenced for 1920-1946. In 2 volumes of about 1000 pages each.

Paper bound \$80.00

Cloth bound \$85.00

## **10-Year Numerical Patent Index to Chemical Abstracts**

Over 143,000 entries classified by countries in numerical order with volume and page references to Chemical Abstracts for 1937-1946. Contains 182 pages.

Cloth bound \$6.50

## **Decennial Indexes to Chemical Abstracts**

Complete subject and author indexes to Chemical Abstracts for the 10-Year periods of 1917-1926, 1927-1936, and 1937-1946.

<b>2nd Decennial Index (1917-1926)</b>	<b>Paper bound</b>	<b>\$100.00</b>
<b>3rd Decennial Index (1927-1936)</b>	<b>Paper bound</b>	<b>150.60</b>
<b>4th Decennial Index (1937-1946)</b>	<b>Paper bound</b>	<b>120.60</b>

*(Foreign postage on the Decennial Indexes is extra)*

order from: **Special Issue Sales**  
**American Chemical Society**  
1155 Sixteenth Street, N.W.  
Washington 6, D.C.

40-  
14.8